Defining sources of nutrient limitation for tumors

by

Mark Robert Sullivan

B.S. Molecular Biology and Chemistry
University of Pittsburgh (2013)

Submitted to the Department of Biology
in Partial Fulfillment of the Requirements for the Degree of

DOCTOR OF PHILOSOPHY

at the

MASSACHUSETTS INSTITUTE OF TECHNOLOGY

June 2019

Signature of Author.....
Department of Biology
April 30, 2019

Certified by .....
Matthew G. Vander Heiden
Associate Professor of Biology
Thesis Supervisor

Accepted by.....
Amy E. Keating
Professor of Biology
Co-Director, Biology Graduate Committee

Defining sources of nutrient limitation for tumors

by

Mark Robert Sullivan

Submitted to the Department of Biology on April 30, 2019 in Partial Fulfillment of the Requirements for the Degree of Doctor of Philosophy in Biology

ABSTRACT

Tumor growth requires that cancer cells accumulate sufficient biomass to grow and divide. To accomplish this, tumor cells must acquire various nutrients, and growth slows if these metabolites are not obtained in sufficient quantities. Importantly, the metabolic demands of cancer cells can be different from those of untransformed cells, and nutrient accessibility in tumors is different than in normal tissues. Thus, tumor survival and growth may be limited by different metabolic factors than those that are necessary to maintain non-cancerous cells. This dissertation examines sources of nutrient limitation in tumors. We study the role of the amino acid serine in tumor growth and show that endogenous serine availability restrains growth of breast tumors. We also demonstrate that breast cancer and melanoma can overcome physiological serine limitation by upregulating expression of the serine synthesis pathway enzyme phosphoglycerate dehydrogenase (PHGDH). To further study amino acid and nucleotide metabolism in tumor growth, we examine the role of the enzyme methionine synthase (MTR) in tumor progression. MTR is involved in both methionine synthesis and folate metabolism and may be important for tumor progression. We find that MTR is required to maintain intracellular levels of both S-adenosyl methionine and nucleotides, but not methionine. We observe that MTR is dispensable for growth in standard culture media, but essential in media containing the folate source available in blood. Further, MTR is essential for folate metabolism and tumor growth *in vivo*. The conditional requirement for MTR depending on the source of extracellular folate highlights the importance of understanding which nutrients are available to tumors *in vivo*, as nutrient accessibility can determine whether a given metabolite or pathway is limiting for tumor growth. To define the nutrient environment present in tumors, we quantitatively profile the metabolites present in tumor interstitial fluid (TIF). We find that the nutrients available to tumors in TIF differ from those present in circulation. Further, by comparing TIF nutrient levels between murine cancer models, we find that tumor type, anatomical location and animal diet affect local nutrient availability. Together, these studies provide new insight into sources of nutrient limitation in tumors.

Thesis supervisor: Matthew G. Vander Heiden
Title: Associate Professor of Biology

ACKNOWLEDGEMENTS

This dissertation was only made possible by the constant advice and support that I received from many people over the last few years. I first want to thank my advisor Matthew Vander Heiden for his enthusiasm and unconditional support. Matt gave me great license to explore the areas of biology that I found most exciting and encouraged me to build my own approach to experimentation and scientific thought. His willingness to allow me that freedom but to also express incredible enthusiasm and always offer his help and support has provided me with an ideal environment to generate ideas and has been invaluable to my growth as a scientist. I feel fortunate to have joined Matt's lab, and I will always be grateful to him for the positive and productive experience I have had there.

I would like to thank my thesis committee, Jacqueline Lees and Jing-Ke Weng. Jackie and Jing-Ke have provided me with many useful discussions about both my project and my career and have always been willing to give me a different perspective to consider. I'd also like to thank Marcia Haigis for taking the time to serve as my outside committee member.

I would like to acknowledge all of the members of the Vander Heiden lab past and present for helping to foster such a friendly and collaborative environment. I've been lucky to overlap with almost every person who has been a part of the Vander Heiden lab to this point, and it has been incredible to have such thoughtful, helpful people surrounding me as I've progressed through my PhD. I feel that I was able to learn something from nearly every person that I've shared time with in the lab, and I've constantly enjoyed all of their company. I particularly want to thank Katie Mattaini; Katie recruited me to the lab, served as my first mentor, and handed off an amazing project for me to work on. Most importantly, Katie is a lovely human being who has consistently served as a role model for me. I'd like to thank Aaron Hosios for teaching me about essentially every topic imaginable, from how to approach science to how to be an effective teacher. Aaron is an incredible font of knowledge and has always been willing to give his time to help me learn. Much of the work described in this dissertation was derived from ideas generated by Aaron, and I could not be more grateful for his constant support and friendship. I also owe a lot to Alex Muir. For the last few years of my PhD, Alex and I have discussed at length just about every idea that either of us has generated, scientifically or philosophically. Those discussions have been essential to my growth as a scientist and as a person. Alex's thoughtfulness and wit have enriched my lab experience greatly, and I'm very thankful for his friendship. I want to thank Dan Gui for his scientific insight, but also for countless games of basketball together. I'd like to thank Laura Danai; nobody gives better advice, scientifically or personally, and nobody else makes lab as enjoyable as Laura. I'd like to thank Anna Nguyen for always brightening everyone's day in lab and for her help maintaining mice, no matter how much dander they had. I also want to thank Emily Dennstedt; Emily's enthusiasm is infectious and her technical skills were vital for much of the work described in this dissertation. I want to thank Allison Lau for being the best baymate I could have asked for, for her scientific and career advice, and for always stepping up her cake-making game on my birthday. I'd like to thank Zhaoqi Li for always having creative ideas and for many helpful

conversations. I want to thank Caroline Lewis for being an original part of team serine, but also for her constant help with mass spectrometry. I'd also like to thank Alicia Darnell, who has helped me with her thoughtful approach to science and editing. All of the members of the Vander Heiden lab, not just those that I have mentioned here, have taught me so much, and I truly could not have asked for a better set of people to work with.

I had the opportunity to work with two incredible undergraduates during my PhD. Emma Gong worked in the lab throughout most of her time as an undergraduate, and it was such a rewarding experience to watch her develop. Emma's ability to cut to the heart of a topic and identify the important questions always pushed me to be the best mentor and scientist that I could be. I was also fortunate to work with Montana Reilly, who is one of the most intelligent, hard-working people that I know. Much of the work in this dissertation would not have been possible without Montana's contributions. Beyond their abilities as scientists, Emma and Montana are both a joy to work with and I always look forward to talking with them. They are two of the brightest people that I know, and I am excited to see what they do next.

I would like to thank my undergraduate advisor Karen Arndt, as well as Kristin Klucevsek, the graduate student who served as my first scientific mentor. I learned so much in the Arndt lab about how to approach science, and the lessons that I learned in that environment have been critical throughout my time in graduate school.

Finally, I'd like to thank my parents, Katie, Lauren, and my friends both in and out of lab for their constant love and support. I am very fortunate to have all of you.

TABLE OF CONTENTS

CHAPTER ONE: Introduction

A version of this chapter has been submitted for publication at *Critical Reviews in Biochemistry and Molecular Biology.*

INTRODUCTION TO CANCER METABOLISM

Proliferation requires that cells accumulate sufficient biomass to grow and divide. Cancer cells within tumors must acquire a variety of nutrients, and tumor growth slows or stops if necessary metabolites are not obtained in sufficient quantities. For most proliferating cells, survival and proliferation rate can be dictated by nutrient availability (Vander Heiden and DeBerardinis 2017). This effect can be mediated by a lack of substrate availability necessary to produce the macromolecules needed for biomass accumulation, or may affect critical signaling pathways that respond to nutrient levels and are required to orchestrate the processes needed for cell growth and proliferation (Torrence and Manning 2018). Regardless of mechanism, proliferation is reduced when the intracellular levels of some nutrients fall below a certain threshold. This threshold is dictated by two terms: cellular demand for that nutrient and the ability of the cell to access that nutrient or its precursors from the environment (Figure 1). Both of these terms are affected by a multitude of cell-intrinsic and cell-extrinsic factors. As a result, proliferating cells in different tumors and tissues are not universally limited by the availability of the same nutrients. Understanding which nutrients are most limiting for specific cells and determining the contexts that dictate those limitations is critical to find metabolic treatments for cancer that

take advantage of tumor-specific nutrient requirements and effectively starve malignancies without substantially damaging normal tissues.

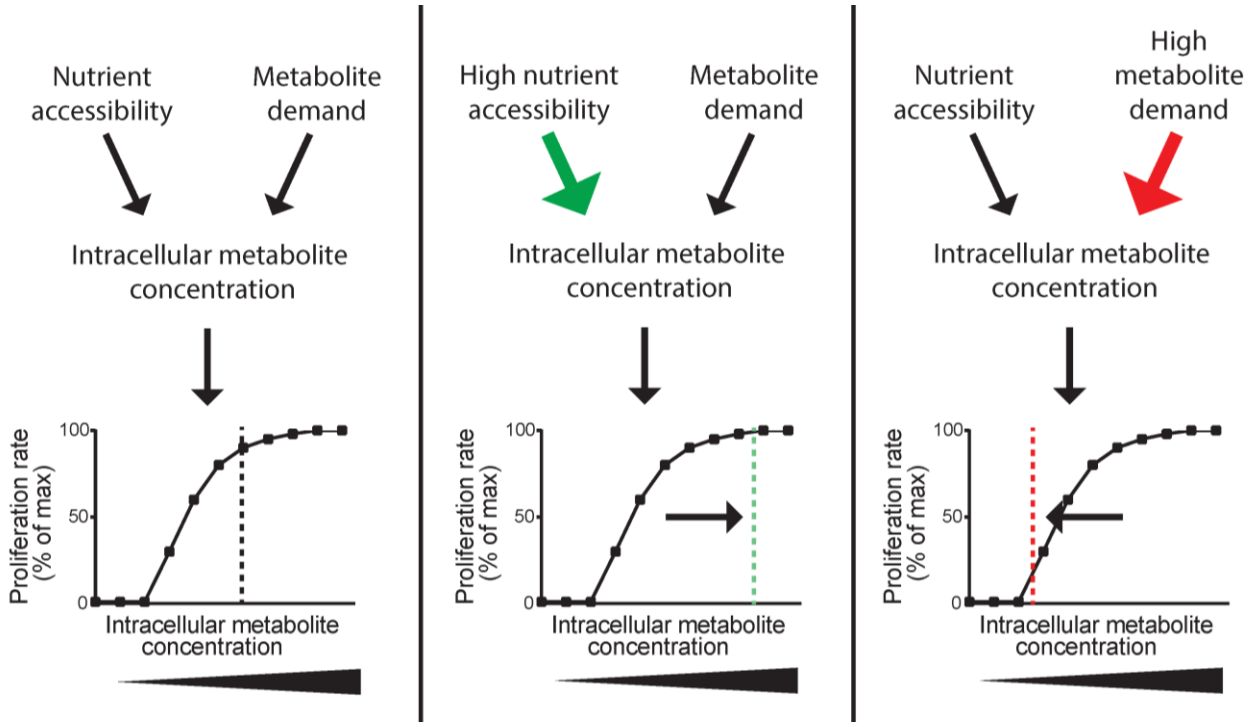

Figure 1. Nutrient limitation is determined by the combined effects of demand and accessibility. Tumor survival and proliferation is influenced by the intracellular concentrations of many metabolites. This intracellular concentration is dictated by the rate of consumption of the metabolite (demand) as well as the rate of metabolite acquisition (accessibility).

NUTRIENT DEMAND

The demand for specific nutrients by cancer cells in tumors is determined by the complex interplay of many factors that influence metabolic pathway use (Figure 2). Here we will examine key variables that affect nutrient demand, including tumor-promoting mutations, chromosomal abnormalities, cancer-specific phenotypic programs, and tissue of origin.

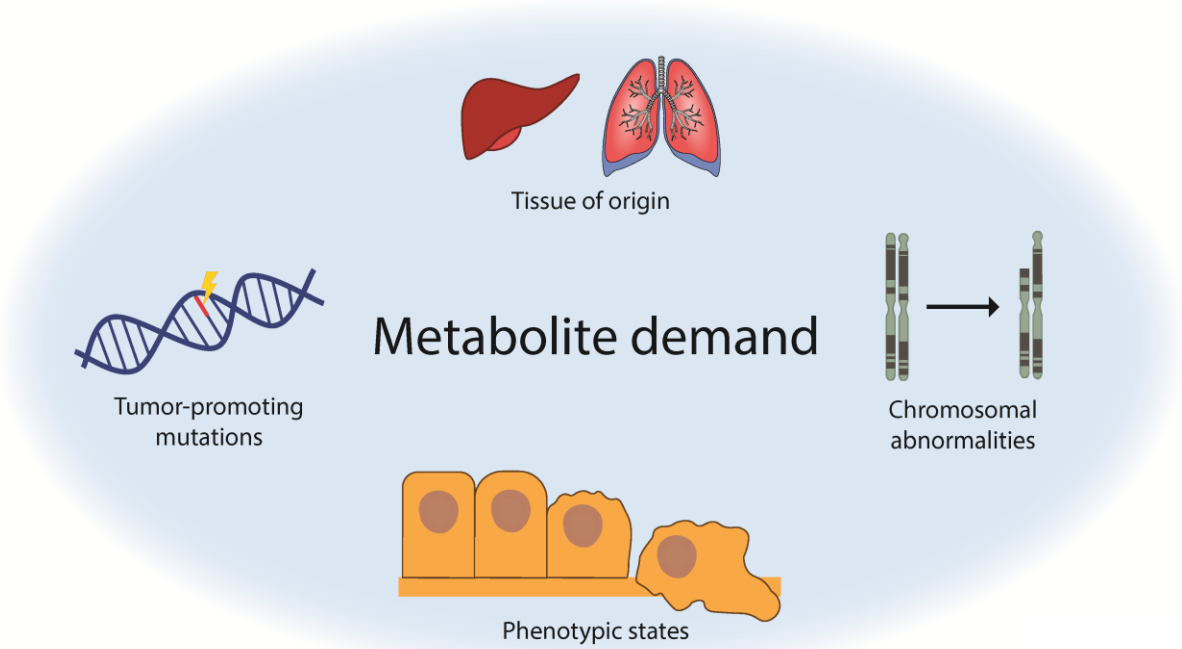

Figure 2. Metabolite demand of cancer cells is determined by several cell-intrinsic factors. These variables include the presence of specific tumor-promoting mutations, chromosomal abnormalities, phenotypic states, and the tissue of origin of the tumor.

Demands imposed by mutations that drive tumor progression

Tumorigenesis is driven by genetic alterations (Hanahan and Weinberg 2011). Many of these genetic changes occur in growth-promoting signaling pathways that also activate metabolic pathways to enable biomass production. Genetic changes in cancer can also occur directly in the metabolic pathways that carry out reactions important for biomass accumulation and can alter the metabolic demands of a cell. Comprehensive descriptions of the metabolic changes that occur due to specific oncogenic mutations are explored in-depth elsewhere (Cairns et al. 2011; Nagarajan et al. 2016); here, we discuss representative examples of tumor-promoting genetic changes found in many cancers and highlight how these genetic changes impact nutrient demand in the tumor.

MYC and its upstream activators

MYC is a transcription factor that regulates the expression of a broad range of genes required for proliferation; when dysregulated, *MYC* can thus act as an oncogene (Wolpaw and Dang 2018). Alterations leading to constitutive MYC expression occur frequently in cancer, and *MYC* is the third-most commonly amplified gene across all cancers studied in The Cancer Genome Atlas (Zack et al. 2013). Constitutive *MYC* expression can occur through somatic gene amplification (Zack et al. 2013) or as a result of mutations in upstream signaling pathways such as the mitogen activated protein kinase (MAPK) pathway (Wolpaw and Dang 2018). Thus, common mutations in proto-oncogenes that are a part of the MAPK pathway, such as *KRAS* and *BRAF*, yield similar metabolic effects as MYC activation (Dang et al. 2009; Bryant et al. 2014; Santana-Codina et al. 2018). When active, MYC serves to stimulate broad metabolic remodeling (Nikiforov et al. 2002; Liu YC et al. 2008; Dang et al. 2009) that can alter the metabolic demands of the tumor. One prominent example is that constitutive MYC expression generates a higher requirement for consumption of the amino acid glutamine in cultured cells (Yuneva et al. 2007). This effect may be driven by MYC-associated expression of xCT, a cell-surface transporter that takes cystine into the cell while exporting glutamate (Ji et al. 2018). In the presence of environmental cystine, high expression of xCT leads to rapid export of glutamate, which imposes a need for increased glutamine consumption in order to replenish glutamate levels (Muir et al. 2017; Sayin et al. 2017). Thus, altered metabolism in tumors with constitutive MYC activity can create new demands for certain metabolites, such as glutamine.

TP53

The most commonly mutated tumor suppressor gene in cancer is *TP53*; at least 50% of tumors display some sort of alteration in the *TP53* gene (Ciriello et al. 2013). The *TP53* gene product, p53, is a protein with myriad functions as a transcription factor and as a cytosolic protein (Kastenhuber and Lowe 2017). Among its many functions, p53 allows cells to adapt to nutrient deprivation (Kruiswijk et al. 2015). For instance, in response to stress conditions, p53 downregulates glycolysis through multiple mechanisms including direct inhibition of glucose transporters (Schwartzenberg-Bar-Yoseph et al. 2004) and induction of glycolysis inhibitors such as TIGAR (Bensaad et al. 2006). Metabolic genes downstream of p53 can also play a role in triggering p53-induced cell death (Jiang L et al. 2015). p53 can directly or indirectly influence expression of genes involved in lipid metabolism, amino acid transport and synthesis, and other metabolic pathways (Puzio-Kuter 2011), making it difficult to predict *a priori* exactly how nutrient demands are altered by p53 loss. Further complicating the effect of p53 on nutrient demand, specific mutations of *TP53* can have different effects on tumor metabolism (Humpton et al. 2018; Schofield et al. 2018). Additional study of the complex changes caused by loss of *TP53* will shed light the specific metabolic demands that are altered by this critical tumor suppressor.

KEAP1/NFE2L2 axis

Another common alteration that occurs in cancer with implications for nutrient demand is the activation of *NFE2L2*, which encodes the transcription factor NRF2 that is involved in the

cellular response to oxidative stress (Venugopal and Jaiswal 1996; Itoh et al. 1997; Raghunath et al. 2018). NRF2 activity can also be induced by loss of function mutations in *KEAP1*, which encodes a ubiquitin ligase that regulates NRF2 levels by targeting it for proteasomal degradation (Itoh et al. 1999; Kobayashi et al. 2004). NRF2 activation leads to increased expression of genes involved in the response to oxidative stress, which includes such processes as xenobiotic detoxification and glutathione synthesis (Raghunath et al. 2018). Further, NRF2 activation leads to induction of ATF4, a transcription factor involved in the response to both nutrient deprivation and endoplasmic reticulum stress (He et al. 2001). As a result, NRF2 activation yields ATF4-dependent metabolic remodeling, including induction of *de novo* serine synthesis (DeNicola et al. 2015) and increased expression of xCT (Romero et al. 2017; Sayin et al. 2017) resulting in an increased dependence on glutamine metabolism as described above. Thus, alteration of the KEAP1/NRF2 signaling axis leads to metabolic changes that modify cellular demands for some amino acids. These examples typify characteristic alterations to metabolic demand created by oncogenic mutations. Given the pleiotropic, complex effects of tumor-promoting mutations, further work to develop a more thorough understanding of the metabolic consequences of these mutations is warranted.

Metabolic demands driven by chromosomal abnormalities

The tumor-promoting mutations described above activate pathways that coopt normal physiology to satisfy the metabolic requirements of cell growth and proliferation. Thus, cancer

cells and some untransformed, proliferating cells may share metabolic alterations that allow them to adapt to the metabolic demands imposed by growth signaling pathway activation (Fendt 2017). However, some tumor-promoting mutations occur through loss of large chromosomal segments, which can result in deletion of genes in regions adjacent to tumor suppressors. These large deletions sometimes include metabolic genes, which can affect metabolic pathway use (Muller et al. 2015). Beyond specific focal deletions of chromosomal regions, many cancers exhibit large-scale changes in chromosome number, known as aneuploidy (Sansregret and Swanton 2017), that can create tumor cell characteristics that are not recapitulated in normal tissues (Knouse et al. 2014). Because these events are not associated with a physiological metabolic program, they may create unique nutrient demands for cancer that differ from those found in all other normal cells.

Collateral mutation of metabolic genes: CDKN2A and MTAP

The most commonly deleted chromosomal locus across cancers is 9p21, due to the presence of the tumor suppressor gene *CDKN2A* in that region (Beroukhim et al. 2010; Zack et al. 2013). *CDKN2A* codes for two proteins, $p16^{INK4A}$ and $p14^{ARF}$ (Duro et al. 1995; Mao et al. 1995; Quelle et al. 1995; Stone et al. 1995), each of which is a tumor suppressor (Serrano et al. 1993; Serrano et al. 1995; Stott et al. 1998). *CDKN2A* deletions of are often accompanied by deletion of surrounding genes (Zhang H et al. 1996), including the enzyme methylthioadenosine phosphorylase (*MTAP*), which is responsible for metabolizing methylthioadenosine that is produced as a byproduct of polyamine synthesis (Pegg and Williams-Ashman 1969a, 1969b; Carrera et al. 1984; Pegg 2009). Deletion of *MTAP* as a consequence of *CDKN2A* loss leads to

dysfunctional salvage of methylthioadenosine. As methylthioadenosine accumulates, it inhibits the protein arginine methyltransferase PRMT5, rendering cancer cells particularly sensitive to knockdown of PRMT5 and related proteins (Marjon et al. 2016; Mavrakis et al. 2016). *MTAP* deletion also causes global changes in metabolism that may be caused by altered epigenetic state or by perturbed methionine metabolism (Sanderson et al. 2018); in either case, *MTAP* deleted cells may exhibit differential nutritional demands that they must meet through adaptation of other metabolic pathways.

Collateral mutation of metabolic genes: SMAD4 and ME2

Another tumor suppressor that is commonly deleted in cancer is *SMAD4* (Hahn et al. 1996). SMAD4 is a part of the TGF-β signaling pathway, and *SMAD4* deletion can promote tumor progression in a variety of cancers, particularly pancreatic ductal adenocarcinoma (Bardeesy et al. 2006; Zhao et al. 2018). Among the genes located proximal to *SMAD4* is malic enzyme 2 (*ME2*) (Dey et al. 2017), a mitochondrial enzyme that is one of three isoforms responsible for interconversion of malate and $NAD(P)^+$ with pyruvate, NAD(P)H, and CO_2 (Moulder et al. 1945; Hsu 1982; Taroni et al. 1987). Loss of ME2 has been suggested to limit both NADPH production and lipid synthesis in cancer (Jiang P et al. 2013), and cancer cells with ME2 deletion become sensitive to depletion of malic enzyme 3 (ME3) (Dey et al. 2017). This suggests that the demand to produce NADPH through other metabolic pathways must be increased in *SMAD4/ME2* deleted tumors. Understanding how cancers cope with ME2 loss could identify metabolic liabilities to target therapeutically in *SMAD4*-deleted cancers.

Beyond focal deletions involving tumor suppressors, some larger chromosomal regions are consistently lost in specific cancers (Beroukhim et al. 2010; Zack et al. 2013; Cai et al. 2016). These losses can also eliminate expression of metabolic genes (Boots-Sprenger et al. 2013; Muller et al. 2015; Branzoli et al. 2019) and create potential therapeutic targets (Muller et al. 2012; Lin et al. 2018). Further examination of how metabolic pathways are affected by chromosomal segment deletions has the potential to uncover novel metabolic demands for certain cancers, and may uncover cancer-specific auxotrophies.

Aneuploidy

Aneuploidy produces a broad range of stresses affecting nearly every facet of biology (Zhu et al. 2018). One of the changes that occurs in aneuploid cells is widespread remodeling of metabolism (Sheltzer 2013; Zhu et al. 2018) For instance, aneuploidy results in increased levels of ceramide lipid species, rendering aneuploid cells more dependent on pathways that normalize ceramide levels (Tang et al. 2017). Similarly, in yeast, aneuploidy imposes an increased demand for certain sphingolipid species, and increases demand for the amino acid serine, which is required for *de novo* sphingolipid synthesis (Hwang et al. 2017). These findings illustrate how abnormal chromosome number and chromosomal rearrangements can alter nutrient demand, and may represent a targetable type of metabolic remodeling that is specific to cancer cells.

Nutrient demands determined by cellular programs that are important in some cancers

In addition to genetic changes that can alter metabolic demands, cancer cells often exhibit phenotypic changes that impact metabolism. Some prominent examples of phenotypes observed across cancers include the epithelial to mesenchymal transition (EMT) (Brabletz et al. 2018), adoption of stem-cell like properties (Batlle and Clevers 2017), and the development of drug resistance (Brown et al. 2014; Mansoori et al. 2017). Cells that have undergone EMT, cancer cells with stem-like properties, and drug resistant cancer cells all exhibit altered metabolism, frequently driven by expression of the same genes (Morandi et al. 2017). For example, each of these states is characterized by high expression of the enzyme dihydropyrimidine dehydrogenase (DPYD), which degrades the nucleobases uracil and thymine into dihydropyrimidines (Mani et al. 2008; Li et al. 2013; Shaul et al. 2014). Increased activity of DPYD alters levels of dihydropyrimidines relative to uracil and thymine (Shaul et al. 2014), and suggests that these cells may have an increased demand for consumption of these nucleobases. Some cellular programs alter nutrient demand in ways that impose increased requirements for certain enzymes. For instance, drug resistant cells have an increased demand for the amino acid cysteine and the tripeptide glutathione; as a result, these cells are highly dependent on pathways that prevent lipid peroxidation and ferroptotic cell death (Hangauer et al. 2017). Broadly, the various phenotypic states adopted by tumors can result in different metabolic demands that affect which nutrients are limiting for tumor growth or survival.

Metabolic demands dictated by tumor tissue of origin

Beyond genetic changes and phenotypic states of tumors, some nutrient demands are shaped by the cell or tissue type from which a tumor arose (Hu et al. 2013; Gaude and Frezza 2016). Thus, these characteristics may not be shared across all tumor types, even those driven by the same oncogenes. For instance, tissue of origin can determine the extent to which tumors are dependent on particular amino acids, including non-essential amino acids such as glutamine (Yuneva et al. 2012), as well as essential nutrients such as branched chain amino acids (Mayers et al. 2016). In the case of branched chain amino acids, tumors arising from lung require the enzyme required to catabolize branched chain amino acids, while tumors arising from the pancreas do not (Mayers et al. 2016). This discrepancy in the requirement for branched chain amino acid transamination may be to fulfill differential demands for products of branched chain amino acid breakdown, such as acquisition of nitrogen or production of the amino acid glutamate. Thus, tissue of origin can be an important determinant of nutrient demand in tumors.

NUTRIENT ACCESSIBILITY

In order to meet varying metabolic demands, tumor cells must be able to acquire relevant nutrients from their environment. Thus, as alluded to above, the second factor that determines which nutrients are limiting for cancer cell proliferation is the accessibility of nutrients in the tumor. Accessibility of nutrients is itself affected by two variables: cell-extrinsic metabolite availability in the environment and cell-intrinsic ability to obtain and effectively use those metabolites (Figure 3).

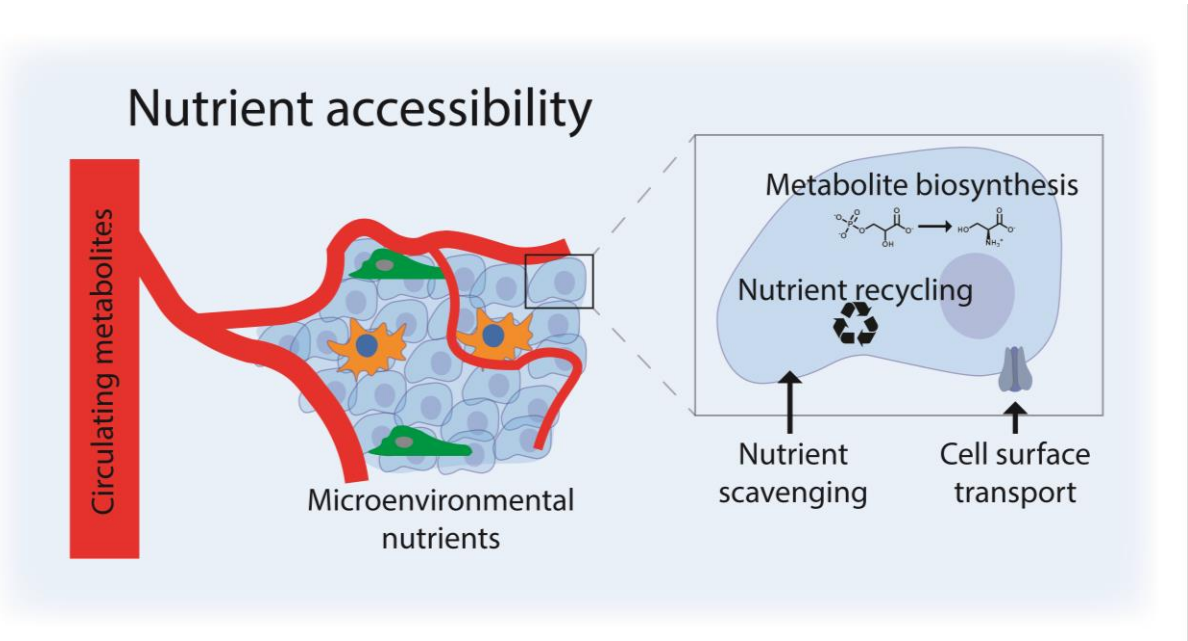

Figure 3. Nutrient accessibility to cells within tumors is driven by both cell-extrinsic and cell-intrinsic variables. Circulating metabolite levels and local microenvironmental nutrient levels determine nutrient accessibility to cells within the tumor, and cell surface transport, scavenging, recycling, and *de novo* metabolite synthesis influence the intracellular levels of metabolites that can be used by the cells.

Circulating nutrient levels

Diet

Nutrient availability to the tumor is dependent on the abundance of circulating metabolites in the blood. The macronutrient content of diet can lead to complex changes in circulating nutrient levels. For instance, consuming diets with varying caloric content and different calorie sources can alter the lipid profile in blood (Raeini-Sarjaz et al. 2001; Appel et al. 2005; Ma et al. 2006). Further, depletion or supplementation of certain nutrients in the diet can lead to a concomitant change in circulating nutrient abundance. In the most extreme example, the circulating levels of nutrients that cannot be synthesized by humans are strongly influenced by diet (Fitzpatrick et al. 2012). As a result, dietary vitamin levels can impact tumor growth,

because although vitamins are typically not consumed by enzymatic reactions, each newly formed cancer cell must be able to obtain a sufficient supply of vitamins to support its enzymatic reactions. For example, dietary folic acid supplementation was noted to exacerbate childhood leukemia in the 1940s (Farber et al. 1947; Farber et al. 1948), and can accelerate the development of murine breast tumors (Hansen et al. 2017). However, given the pleiotropic effects of vitamin deprivation on overall animal health, dietary levels of folic acid have been reported to both positively and negatively affect the risk of developing tumors in humans (Ulrich 2007; Lamm et al. 2015; Ashkavand et al. 2017).

The dietary content of some non-essential nutrients can also influence circulating levels of those metabolites. Feeding mice a diet lacking the amino acids serine and glycine results in lower serine levels in circulation (Maddocks et al. 2013). Reduced serine accessibility in this setting can slow tumor growth without grossly affecting animal health (Maddocks et al. 2013; Maddocks et al. 2017), consistent with tumors having a high demand for serine that they are not able to meet given a diminished accessibility of serine in the circulation. This principle can also be applied more generally in fasted animals. Long-term fasting broadly alters circulating metabolite levels (Broer S and Broer 2017), shifting nutrient accessibility in a manner that decreases tumor proliferation (Lee et al. 2012; Sun et al. 2017). Thus, both broad and specific dietary manipulations can alter nutrient accessibility in tumors.

Hormonal control of metabolism

Circulating nutrient levels are not solely determined by the diet. Instead, complex hormonal mechanisms influence the levels of some nutrients in blood. Perhaps the most well-studied example of hormonal regulation of metabolism is in the control of circulating glucose levels. Glucose levels in the blood are tightly regulated by the action of the hormones insulin and glucagon. Insulin stimulates glucose uptake in many cell types and broadly functions to clear glucose from circulation (Wilcox 2005). Conversely, glucagon stimulates glucose release into the bloodstream from hepatic glycogen stores and *de novo* glucose synthesis through the process of gluconeogenesis (Han et al. 2016). Glucose is not the only metabolite regulated by hormones. In fact, it has long been recognized that endocrine signaling influences the concentrations of amino acids in blood (Friedberg and Greenberg 1947). As a result, circulating amino acid levels are largely held within a certain range of concentrations independent of the composition of diet. Systemic metabolism does not fully control circulating amino acid levels, as within this normal range, amino acid levels can fluctuate over the course of the day in response to normal feeding and fasting, and certain amino acids such as serine, glycine, and alanine vary over a wider range than other amino acids (Broer S and Broer 2017). However, consistent with the importance of hormonal regulation of amino acid levels, derangement of whole-body metabolism in obesity or cancer alters circulating levels of branched chain amino acids (Newgard et al. 2009; Mayers et al. 2014). Beyond regulation of metabolite levels, hormonal processes mediate the effects of dietary and environmental perturbations on circulating nutrient levels. For instance, fasting has been shown to inhibit leukemia progression by altering expression of leptin receptor (Lu et al. 2017), a protein which binds to the hormone leptin and

is involved in maintenance of whole-body energy homeostasis (Kelesidis et al. 2010). Thus, in addition to directly setting the circulating levels of many metabolites, hormonal mechanisms may also mediate the effects of diet and other environmental factors on nutrient accessibility in tumors.

Influence of the microbiome on systemic metabolite levels

Systemic metabolism can be influenced by the actions of the gut microbiome. The microbiome carries out many metabolic reactions, and can affect which nutrients in the diet end up in circulation, or produce metabolites that do not directly reflect the content of diet (LeBlanc et al. 2013; Fujisaka et al. 2018). Microbiome composition may also affect systemic metabolism, as fecal microbiota transplants are sufficient to predictably alter non-fasting glucose levels in mice (Ussar et al. 2015). Thus, the behavior of the microbiome appears to also influence tumor nutrient accessibility.

Fluctuating metabolite levels due to circadian rhythms

Nutrient availability in circulation is not constant throughout the day. In fact, circadian rhythms exhibit a profound effect on the plasma levels of metabolites, with some nutrients displaying greater than 2.5 fold differences in circulating concentration throughout the day (Dallmann et al. 2012; Masri and Sassone-Corsi 2018). In contrast, some metabolites largely do not fluctuate throughout the day (Dallmann et al. 2012). Given the variability in circadian fluctuation between nutrients, certain metabolites could be less accessible and thus more limiting for tumor growth at particular times during the day. For this reason, it may be advantageous for

tumors to reprogram circadian metabolism to promote more favorable nutrient accessibility. Indeed, lung adenocarcinoma has been observed to alter hepatic circadian rhythms in a way that alters whole-body metabolism (Masri et al. 2016). For these reasons, when examining nutrient accessibility with the goal of understanding metabolic limitations on tumors, it is important to consider the effects that circadian rhythms have on circulating metabolite levels.

Nutrient levels in the tumor microenvironment

Though systemic metabolism can impact blood nutrient levels, tumors do not have straightforward access to all of the nutrients present in circulation. The delivery of nutrients to tumor cells is complicated by altered vasculature and competition for metabolites between various cells within the tumor microenvironment. Here we examine some of the factors in the local tumor microenvironment that alter nutrient accessibility.

Tumor vascularization and lymphatics

In contrast to normal tissues, tumors have irregularly spaced, poorly functioning blood vessels (Fukumura et al. 2010). As a result, tumors may not be able to efficiently exchange nutrients and waste products with the circulation. Further compounding the abnormal vasculature is the presence of dysfunctional lymphatics in tumors. Lymphatic ducts are responsible for returning fluid and metabolites that drain from a tissue into the blood (Wiig and Swartz 2012). Solid tumors are typically highly compressed and, as a result, can be deficient in functional lymphatics. This further increases tumoral interstitial pressure, which inhibits nutrient uptake from the blood (Fukumura et al. 2010; Wiig and Swartz 2012). As a result, the accessibility of

nutrients to the tumor depends both on the extent of vascularization and the effectiveness of the blood vessels present in the tumor.

Competition for nutrients between cell types in the tumor microenvironment

Once nutrients are delivered to the local tumor microenvironment, all cells within the tissue, including stromal and immune cells compete for nutrients within the tumor. For example, some immune cells important for restricting tumor growth, such as activated T cells, acquire metabolic characteristics that are similar to tumor cells and are often driven by the same transcriptional programs that exist in cancer (Wang et al. 2011; Le Bourgeois et al. 2018). Thus, these cells compete with tumor cells for the same nutrients. Beyond competition, some immune cells degrade or sequester critical nutrients in the tumor microenvironment (Lyssiotis and Kimmelman 2017). For instance, myeloid derived suppressor cells (MDSCs) deplete the amino acids arginine, tryptophan, and cystine from the tumor microenvironment beyond their own metabolic needs (Kumar et al. 2016). Degradation of these nutrients has an immunosuppressive effect that can favor tumor progression; however, tumors must also cope with this altered nutrient availability.

Nutrient sharing between cell types in the tumor microenvironment

Stromal cells in the tumor microenvironment can also alter nutrient accessibility in a way that is favorable to cancer cells (Lyssiotis and Kimmelman 2017). For example, primary chronic lymphocytic leukemia (CLL) cells have a limited ability to uptake the amino acid cystine due to low expression of the cystine-glutamate antiporter xCT. Bone marrow stromal cells that are

present in the CLL niche, in contrast, are capable of importing cystine using xCT and then excreting cysteine, the reduced form of cystine that can be transported using the ASC family of amino acid transporters (Barker and Ellory 1990; Zhang W et al. 2012). This allows the CLL cells to take up cysteine, providing increased access to a crucial amino acid. Further examples of how cell populations within a tumor might exchange nutrients in a symbiotic relationship are also prominent in the literature (Sonveaux et al. 2008; Tardito et al. 2015; Sousa et al. 2016; Yang et al. 2016).

Uptake of nutrients

Rather than relying upon local delivery or microenvironmental production of specific metabolites, tumor cells can increase the accessibility of nutrients by more effectively taking up metabolites from their environment. For instance, xCT deficient CLL cells mentioned above would not have to rely upon stromal cells to produce reduced cysteine if they were more capable of oxidized cystine uptake. To more effectively acquire metabolites, cancer cells can modulate nutrient uptake using a variety of mechanisms; here we examine some of the adaptations that tumors utilize to better obtain nutrients and therefore increase the accessibility of metabolites from the environment.

Cell surface transporters

Most nutrients are transported into cells through transmembrane proteins, and transport can be either equilibrative or coupled to an energy consuming process to concentrate the nutrient in cells (Glatz et al. 2010; Hediger et al. 2013; Szablewski 2013; Perez-Escuredo et al. 2016;

Young 2016; Inoue 2017). Many nutrient transport proteins are upregulated in cancer, and there has been a renewed interest in understanding nutrient transport phenomena in cancer (Cesar-Razquin et al. 2015; Krall et al. 2016; Broer A et al. 2018; Cha et al. 2018; Ladanyi et al. 2018; Tajan et al. 2018; Todenhofer et al. 2018). One of the most well-known cancer phenotypes is the avid uptake of glucose, a phenomenon that is at least partially driven by increased expression of GLUT family glucose transporters (Szablewski 2013). This increased capacity for glucose transport may increase glucose accessibility to tumors.

In some cases, transporter expression has less predictable effects on nutrient uptake, and therefore availability. The uptake of amino acids occurs through a series of transmembrane transporters with overlapping amino acid specificities (Hediger et al. 2013; Kandasamy et al. 2018). Many of these transporters are obligate amino acid exchangers, which take up one amino acid and excrete a second. These amino acid exchangers are unable to facilitate net uptake of amino acids, but are instead able to shift the relative ratios of various intracellular amino acids. Multiple studies have shown that knocking down expression of amino acid exchangers such as ASCT2 can hinder cancer growth (van Geldermalsen et al. 2016; Cormerais et al. 2018), suggesting that the redistribution of intracellular and extracellular amino acids can affect tumor proliferation. However, the specific effects of increased expression of amino acid exchangers on nutrient accessibility are difficult to predict due to the complex and redundant interactions between amino acid transporters. Further, amino acid transporter activity will be affected by the intracellular and extracellular levels of multiple amino acids. Many studies of amino acid exchange involve non-physiological conditions wherein cells are loaded with high levels of an amino acid of interest and then efflux of that amino acid and uptake of others are

observed. Thus, further work to understand the functions of each transporter when physiological concentrations of amino acids are present is warranted.

Nutrient uptake from extracellular polymers and macromolecules

Not all nutrient acquisition is mediated by the uptake of free metabolites through cell-surface transporters; instead, some metabolites are scavenged from extracellular polymers. One such nutrient is glutathione, a tripeptide that is present at ~10 μM in circulation (Pastore et al. 1998). Glutathione contains the amino acids cysteine, glutamate, and glycine, and can be a source of these amino acids (Orlowski and Meister 1970); however, tumor cells must first degrade glutathione into its amino acid components for uptake through cell-surface transporters. This process requires the expression of γ-glutamyl transferases (GGTs), extracellular membrane proteins that degrade glutathione in the environment. GGT expression is upregulated in some tumors (Hanigan et al. 1999) and downregulated in others (Priolo et al. 2018), suggesting that tumors may differ in their ability to degrade and utilize glutathione as a source of amino acids. Recent work has suggested that glutathione breakdown may serve additional functions (Boysen 2017), but the ability of cells to express GGT and utilize extracellular glutathione as a nutrient source likely plays a role in determining the accessibility of certain amino acids to tumors.

Some cancer cells are able to take up larger macromolecules. For instance, certain tumors are able to consume whole protein from the environment through integrin-mediated scavenging (Finicle et al. 2018), receptor-mediated endocytosis (Merlot et al. 2014; Finicle et al. 2018) or by non-specific uptake involving macropinocytosis (Recouvreux and Commisso 2017; Finicle et al. 2018). The ability to effectively utilize extracellular protein as an amino acid source

can increase the effective accessibility of amino acids for cells within tumors (Finicle et al. 2018). Nutrient scavenging can also be used to take up molecules other than protein to support cellular metabolic processes (Kim et al. 2018). Beyond taking up macromolecules from the environment, some cells can even invade and consume neighboring cells through the process of entosis, allowing for replenishment of nutrients (Overholtzer et al. 2007; Krajcovic et al. 2013; Hamann et al. 2017). Though this process is likely a response to low nutrient levels rather than an active strategy of obtaining nutrients under basal conditions, it provides another path for cancer cells to increase nutrient accessibility.

Nutrient recycling

In addition to altered nutrient uptake, some tumors are able to modulate metabolite accessibility by breaking down macromolecules into their constituent parts through the process of autophagy (Kimmelman and White 2017; Wyant et al. 2017; An and Harper 2018). Autophagy can alter intracellular metabolite levels in response to starvation (Guo et al. 2016), but recycling of nutrients in this way cannot provide a net source of new metabolites for tumor cells. Recycling processes do not lead to net metabolite consumption, and are therefore unable to directly fuel cell growth; however, nutrient recycling can be important as a mechanism to alter nutrient accessibility to allow tumors to preserve levels of critical nutrients during transient periods of deprivation, and thus can affect cancer cell survival. This effect on nutrient availability may explain, in part, why impairment of autophagy can hinder tumor growth (Kimmelman and White 2017).

Altered nutrient biosynthesis

For those metabolites that can be produced by tumors, *de novo* synthesis represents an important method to modulate nutrient availability. The synthesis of many classes of metabolites, including amino acids (Liu W et al. 2012; Mattaini et al. 2016) and lipids (Long et al. 2018), is upregulated in tumors and may represent a method for tumors to bypass low environmental nutrient accessibility in some tissue contexts. Often, the increased rate of *de novo* metabolite synthesis is necessary to maintain tumor proliferation, suggesting that the improved nutrient availability resulting from increased biosynthesis is required to meet the nutrient demands of the cell. For instance, many tumors upregulate the enzymes of the serine synthesis pathway, which converts the glycolytic intermediate 3-phosphoglycerate into serine through a three-step process (Adams 2007; Locasale et al. 2011; Possemato et al. 2011; Nilsson et al. 2012; DeNicola et al. 2015; Ben-Sahra et al. 2016; Samanta et al. 2016). The altered availability of nutrients due to upregulation of serine synthesis can promote tumor growth (Possemato et al. 2011; DeNicola et al. 2015; Pacold et al. 2016). However, biosynthesis of one nutrient inevitably generates a metabolic cost elsewhere. For instance, for each molecule of serine synthesized by a cancer cell, the cell must consume ½ glucose, 2 NAD^+, and convert 1 glutamate into 1 α-ketoglutarate. Thus, altered nutrient biosynthesis can affect the allocation of metabolic resources to other pathways, not just the end product of a biosynthetic pathway. As a result, variability in biosynthetic rates can be an important determinant of nutrient availability for tumors.

CONCLUSIONS

Restricting tumor growth by targeting metabolic pathways or nutrients that are limiting for proliferation remains an attractive therapeutic strategy. However, to successfully target metabolism in this fashion, we must continue to develop a better understanding of what is limiting for tumor growth and the factors that determine these limitations. Both the demand for a metabolite and its accessibility to cancer cells within a tumor will define what is limiting, and each of these terms is determined by a complex mix of tumor-intrinsic and tumor-extrinsic factors that must be considered when studying cancer metabolism. Critically, these variables often represent factors that are unique to specific tumor types. Thus, the altered demand and accessibility of nutrients in tumors may render them specifically vulnerable to inhibition of certain metabolic pathways or deprivation of particular nutrients. Better understanding the complex interplay between these factors will be essential to turn these unique characteristics of cancers into specific, effective therapies.

REFERENCES

Adams CM. 2007. Role of the transcription factor ATF4 in the anabolic actions of insulin and the anti-anabolic actions of glucocorticoids. J Biol Chem. 282(23):16744-16753.

An H, Harper JW. 2018. Systematic analysis of ribophagy in human cells reveals bystander flux during selective autophagy. Nat Cell Biol. 20(2):135-143.

Appel LJ, Sacks FM, Carey VJ, Obarzanek E, Swain JF, Miller ER, 3rd, Conlin PR, Erlinger TP, Rosner BA, Laranjo NM et al. 2005. Effects of protein, monounsaturated fat, and carbohydrate intake on blood pressure and serum lipids: results of the OmniHeart randomized trial. JAMA. 294(19):2455-2464.

Ashkavand Z, O'Flanagan C, Hennig M, Du X, Hursting SD, Krupenko SA. 2017. Metabolic Reprogramming by Folate Restriction Leads to a Less Aggressive Cancer Phenotype. Mol Cancer Res. 15(2):189-200.

Bardeesy N, Cheng KH, Berger JH, Chu GC, Pahler J, Olson P, Hezel AF, Horner J, Lauwers GY, Hanahan D et al. 2006. Smad4 is dispensable for normal pancreas development yet critical in progression and tumor biology of pancreas cancer. Genes Dev. 20(22):3130-3146.

Barker GA, Ellory JC. 1990. The Identification of Neutral Amino-Acid-Transport Systems. Exp Physiol. 75(1):3-26. English.

Batlle E, Clevers H. 2017. Cancer stem cells revisited. Nat Med. 23(10):1124-1134.

Ben-Sahra I, Hoxhaj G, Ricoult SJH, Asara JM, Manning BD. 2016. mTORC1 induces purine synthesis through control of the mitochondrial tetrahydrofolate cycle. Science. 351(6274):728-733. English.

Bensaad K, Tsuruta A, Selak MA, Vidal MN, Nakano K, Bartrons R, Gottlieb E, Vousden KH. 2006. TIGAR, a p53-inducible regulator of glycolysis and apoptosis. Cell. 126(1):107-120.

Beroukhim R, Mermel CH, Porter D, Wei G, Raychaudhuri S, Donovan J, Barretina J, Boehm JS, Dobson J, Urashima M et al. 2010. The landscape of somatic copy-number alteration across human cancers. Nature. 463(7283):899-905.

Boots-Sprenger SH, Sijben A, Rijntjes J, Tops BB, Idema AJ, Rivera AL, Bleeker FE, Gijtenbeek AM, Diefes K, Heathcock L et al. 2013. Significance of complete 1p/19q co-deletion, IDH1 mutation and MGMT promoter methylation in gliomas: use with caution. Mod Pathol. 26(7):922-929.

Boysen G. 2017. The Glutathione Conundrum: Stoichiometric Disconnect between Its Formation and Oxidative Stress. Chem Res Toxicol. 30(5):1113-1116.

Brabletz T, Kalluri R, Nieto MA, Weinberg RA. 2018. EMT in cancer. Nat Rev Cancer. 18(2):128-134.

Branzoli F, Pontoizeau C, Tchara L, Di Stefano AL, Kamoun A, Deelchand DK, Valabregue R, Lehericy S, Sanson M, Ottolenghi C et al. 2019. Cystathionine as a marker for 1p/19q codeleted gliomas by in vivo magnetic resonance spectroscopy. Neuro Oncol.

Broer A, Fairweather S, Broer S. 2018. Disruption of Amino Acid Homeostasis by Novel ASCT2 Inhibitors Involves Multiple Targets. Front Pharmacol. 9:785.

Broer S, Broer A. 2017. Amino acid homeostasis and signalling in mammalian cells and organisms. Biochem J. 474(12):1935-1963.

Brown R, Curry E, Magnani L, Wilhelm-Benartzi CS, Borley J. 2014. Poised epigenetic states and acquired drug resistance in cancer. Nat Rev Cancer. 14(11):747-753.
Bryant KL, Mancias JD, Kimmelman AC, Der CJ. 2014. KRAS: feeding pancreatic cancer proliferation. Trends Biochem Sci. 39(2):91-100.
Cai Y, Crowther J, Pastor T, Abbasi Asbagh L, Baietti MF, De Troyer M, Vazquez I, Talebi A, Renzi F, Dehairs J et al. 2016. Loss of Chromosome 8p Governs Tumor Progression and Drug Response by Altering Lipid Metabolism. Cancer Cell. 29(5):751-766.
Cairns RA, Harris IS, Mak TW. 2011. Regulation of cancer cell metabolism. Nat Rev Cancer. 11(2):85-95.
Carrera CJ, Eddy RL, Shows TB, Carson DA. 1984. Assignment of the gene for methylthioadenosine phosphorylase to human chromosome 9 by mouse-human somatic cell hybridization. Proc Natl Acad Sci U S A. 81(9):2665-2668.
Cesar-Razquin A, Snijder B, Frappier-Brinton T, Isserlin R, Gyimesi G, Bai X, Reithmeier RA, Hepworth D, Hediger MA, Edwards AM et al. 2015. A Call for Systematic Research on Solute Carriers. Cell. 162(3):478-487.
Cha YJ, Kim ES, Koo JS. 2018. Amino Acid Transporters and Glutamine Metabolism in Breast Cancer. Int J Mol Sci. 19(3).
Ciriello G, Miller ML, Aksoy BA, Senbabaoglu Y, Schultz N, Sander C. 2013. Emerging landscape of oncogenic signatures across human cancers. Nat Genet. 45(10):1127-1133.
Cormerais Y, Massard PA, Vucetic M, Giuliano S, Tambutte E, Durivault J, Vial V, Endou H, Wempe MF, Parks SK et al. 2018. The glutamine transporter ASCT2 (SLC1A5) promotes tumor growth independently of the amino acid transporter LAT1 (SLC7A5). J Biol Chem. 293(8):2877-2887.
Dallmann R, Viola AU, Tarokh L, Cajochen C, Brown SA. 2012. The human circadian metabolome. Proc Natl Acad Sci U S A. 109(7):2625-2629.
Dang CV, Le A, Gao P. 2009. MYC-induced cancer cell energy metabolism and therapeutic opportunities. Clin Cancer Res. 15(21):6479-6483.
DeNicola GM, Chen PH, Mullarky E, Sudderth JA, Hu Z, Wu D, Tang H, Xie Y, Asara JM, Huffman KE et al. 2015. NRF2 regulates serine biosynthesis in non-small cell lung cancer. Nat Genet. 47(12):1475-1481.
Dey P, Baddour J, Muller F, Wu CC, Wang H, Liao WT, Lan Z, Chen A, Gutschner T, Kang Y et al. 2017. Genomic deletion of malic enzyme 2 confers collateral lethality in pancreatic cancer. Nature. 542(7639):119-123.
Duro D, Bernard O, Della Valle V, Berger R, Larsen CJ. 1995. A new type of p16INK4/MTS1 gene transcript expressed in B-cell malignancies. Oncogene. 11(1):21-29.
Farber S, Cutler EC, Hawkins JW, Harrison JH, Peirce EC, 2nd, Lenz GG. 1947. The Action of Pteroylglutamic Conjugates on Man. Science. 106(2764):619-621.
Farber S, Diamond LK, Mercer RD, Sylvester RF, Wolff JA. 1948. Temporary remissions in acute leukemia in children produced by folic acid antagonist, 4-aminopteryl-glutamic acid (aminopterin). New England Journal of Medicine. 238(23):787-793.
Fendt SM. 2017. Is There a Therapeutic Window for Metabolism-Based Cancer Therapies? Front Endocrinol (Lausanne). 8:150.

Finicle BT, Jayashankar V, Edinger AL. 2018. Nutrient scavenging in cancer. Nat Rev Cancer. 18(10):619-633.
Fitzpatrick TB, Basset GJ, Borel P, Carrari F, DellaPenna D, Fraser PD, Hellmann H, Osorio S, Rothan C, Valpuesta V et al. 2012. Vitamin deficiencies in humans: can plant science help? Plant Cell. 24(2):395-414.
Friedberg F, Greenberg DM. 1947. Endocrine regulation of amino acid levels in blood and tissues. J Biol Chem. 168(2):405-409.
Fujisaka S, Avila-Pacheco J, Soto M, Kostic A, Dreyfuss JM, Pan H, Ussar S, Altindis E, Li N, Bry L et al. 2018. Diet, Genetics, and the Gut Microbiome Drive Dynamic Changes in Plasma Metabolites. Cell Rep. 22(11):3072-3086.
Fukumura D, Duda DG, Munn LL, Jain RK. 2010. Tumor microvasculature and microenvironment: novel insights through intravital imaging in pre-clinical models. Microcirculation. 17(3):206-225.
Gaude E, Frezza C. 2016. Tissue-specific and convergent metabolic transformation of cancer correlates with metastatic potential and patient survival. Nat Commun. 7:13041.
Glatz JF, Luiken JJ, Bonen A. 2010. Membrane fatty acid transporters as regulators of lipid metabolism: implications for metabolic disease. Physiol Rev. 90(1):367-417.
Guo JY, Teng X, Laddha SV, Ma S, Van Nostrand SC, Yang Y, Khor S, Chan CS, Rabinowitz JD, White E. 2016. Autophagy provides metabolic substrates to maintain energy charge and nucleotide pools in Ras-driven lung cancer cells. Genes Dev. 30(15):1704-1717.
Hahn SA, Schutte M, Hoque ATMS, Moskaluk CA, daCosta LT, Rozenblum E, Weinstein CL, Fischer A, Yeo CJ, Hruban RH et al. 1996. DPC4, a candidate tumor suppressor gene at human chromosome 18q21.1. Science. 271(5247):350-353. English.
Hamann JC, Surcel A, Chen R, Teragawa C, Albeck JG, Robinson DN, Overholtzer M. 2017. Entosis Is Induced by Glucose Starvation. Cell Rep. 20(1):201-210.
Han HS, Kang G, Kim JS, Choi BH, Koo SH. 2016. Regulation of glucose metabolism from a liver-centric perspective. Exp Mol Med. 48:e218.
Hanahan D, Weinberg RA. 2011. Hallmarks of cancer: the next generation. Cell. 144(5):646-674.
Hangauer MJ, Viswanathan VS, Ryan MJ, Bole D, Eaton JK, Matov A, Galeas J, Dhruv HD, Berens ME, Schreiber SL et al. 2017. Drug-tolerant persister cancer cells are vulnerable to GPX4 inhibition. Nature. 551(7679):247-250.
Hanigan MH, Gallagher BC, Townsend DM, Gabarra V. 1999. Gamma-glutamyl transpeptidase accelerates tumor growth and increases the resistance of tumors to cisplatin in vivo. Carcinogenesis. 20(4):553-559.
Hansen MF, Jensen SO, Fuchtbauer EM, Martensen PM. 2017. High folic acid diet enhances tumour growth in PyMT-induced breast cancer. Br J Cancer. 116(6):752-761.
He CH, Gong P, Hu B, Stewart D, Choi ME, Choi AM, Alam J. 2001. Identification of activating transcription factor 4 (ATF4) as an Nrf2-interacting protein. Implication for heme oxygenase-1 gene regulation. J Biol Chem. 276(24):20858-20865.
Hediger MA, Clemencon B, Burrier RE, Bruford EA. 2013. The ABCs of membrane transporters in health and disease (SLC series): introduction. Mol Aspects Med. 34(2-3):95-107.
Hsu RY. 1982. Pigeon liver malic enzyme. Mol Cell Biochem. 43(1):3-26.

Hu J, Locasale JW, Bielas JH, O'Sullivan J, Sheahan K, Cantley LC, Vander Heiden MG, Vitkup D. 2013. Heterogeneity of tumor-induced gene expression changes in the human metabolic network. Nat Biotechnol. 31(6):522-529.
Humpton TJ, Hock AK, Maddocks ODK, Vousden KH. 2018. p53-mediated adaptation to serine starvation is retained by a common tumour-derived mutant. Cancer Metab. 6:18.
Hwang S, Gustafsson HT, O'Sullivan C, Bisceglia G, Huang X, Klose C, Schevchenko A, Dickson RC, Cavaliere P, Dephoure N et al. 2017. Serine-Dependent Sphingolipid Synthesis Is a Metabolic Liability of Aneuploid Cells. Cell Rep. 21(13):3807-3818.
Inoue K. 2017. Molecular Basis of Nucleobase Transport Systems in Mammals. Biol Pharm Bull. 40(8):1130-1138.
Itoh K, Chiba T, Takahashi S, Ishii T, Igarashi K, Katoh Y, Oyake T, Hayashi N, Satoh K, Hatayama I et al. 1997. An Nrf2 small Maf heterodimer mediates the induction of phase II detoxifying enzyme genes through antioxidant response elements. Biochemical and Biophysical Research Communications. 236(2):313-322. English.
Itoh K, Wakabayashi N, Katoh Y, Ishii T, Igarashi K, Engel JD, Yamamoto M. 1999. Keap1 represses nuclear activation of antioxidant responsive elements by Nrf2 through binding to the amino-terminal Neh2 domain. Gene Dev. 13(1):76-86. English.
Ji X, Qian J, Rahman SMJ, Siska PJ, Zou Y, Harris BK, Hoeksema MD, Trenary IA, Heidi C, Eisenberg R et al. 2018. xCT (SLC7A11)-mediated metabolic reprogramming promotes non-small cell lung cancer progression. Oncogene. 37(36):5007-5019.
Jiang L, Kon N, Li T, Wang SJ, Su T, Hibshoosh H, Baer R, Gu W. 2015. Ferroptosis as a p53-mediated activity during tumour suppression. Nature. 520(7545):57-62.
Jiang P, Du W, Mancuso A, Wellen KE, Yang X. 2013. Reciprocal regulation of p53 and malic enzymes modulates metabolism and senescence. Nature. 493(7434):689-693.
Kandasamy P, Gyimesi G, Kanai Y, Hediger MA. 2018. Amino acid transporters revisited: New views in health and disease. Trends Biochem Sci. 43(10):752-789.
Kastenhuber ER, Lowe SW. 2017. Putting p53 in Context. Cell. 170(6):1062-1078.
Kelesidis T, Kelesidis I, Chou S, Mantzoros CS. 2010. Narrative review: the role of leptin in human physiology: emerging clinical applications. Ann Intern Med. 152(2):93-100.
Kim SM, Nguyen TT, Ravi A, Kubiniok P, Finicle BT, Jayashankar V, Malacrida L, Hou J, Robertson J, Gao D et al. 2018. PTEN Deficiency and AMPK Activation Promote Nutrient Scavenging and Anabolism in Prostate Cancer Cells. Cancer Discov. 8(7):866-883.
Kimmelman AC, White E. 2017. Autophagy and Tumor Metabolism. Cell Metab. 25(5):1037-1043.
Knouse KA, Wu J, Whittaker CA, Amon A. 2014. Single cell sequencing reveals low levels of aneuploidy across mammalian tissues. Proc Natl Acad Sci U S A. 111(37):13409-13414.
Kobayashi A, Kang MI, Okawa H, Ohtsuji M, Zenke Y, Chiba T, Igarashi K, Yamamoto M. 2004. Oxidative stress sensor Keap1 functions as an adaptor for Cul3-based E3 ligase to regulate proteasomal degradation of Nrf2. Mol Cell Biol. 24(16):7130-7139.
Krajcovic M, Krishna S, Akkari L, Joyce JA, Overholtzer M. 2013. mTOR regulates phagosome and entotic vacuole fission. Mol Biol Cell. 24(23):3736-3745.
Krall AS, Xu S, Graeber TG, Braas D, Christofk HR. 2016. Asparagine promotes cancer cell proliferation through use as an amino acid exchange factor. Nat Commun. 7:11457.

Kruiswijk F, Labuschagne CF, Vousden KH. 2015. p53 in survival, death and metabolic health: a lifeguard with a licence to kill. Nat Rev Mol Cell Biol. 16(7):393-405.
Kumar V, Patel S, Tcyganov E, Gabrilovich DI. 2016. The Nature of Myeloid-Derived Suppressor Cells in the Tumor Microenvironment. Trends Immunol. 37(3):208-220.
Ladanyi A, Mukherjee A, Kenny HA, Johnson A, Mitra AK, Sundaresan S, Nieman KM, Pascual G, Benitah SA, Montag A et al. 2018. Adipocyte-induced CD36 expression drives ovarian cancer progression and metastasis. Oncogene. 37(17):2285-2301.
Lamm N, Maoz K, Bester AC, Im MM, Shewach DS, Karni R, Kerem B. 2015. Folate levels modulate oncogene-induced replication stress and tumorigenicity. EMBO Mol Med. 7(9):1138-1152.
Le Bourgeois T, Strauss L, Aksoylar HI, Daneshmandi S, Seth P, Patsoukis N, Boussiotis VA. 2018. Targeting T Cell Metabolism for Improvement of Cancer Immunotherapy. Front Oncol. 8:237.
LeBlanc JG, Milani C, de Giori GS, Sesma F, van Sinderen D, Ventura M. 2013. Bacteria as vitamin suppliers to their host: a gut microbiota perspective. Curr Opin Biotechnol. 24(2):160-168.
Lee C, Raffaghello L, Brandhorst S, Safdie FM, Bianchi G, Martin-Montalvo A, Pistoia V, Wei M, Hwang S, Merlino A et al. 2012. Fasting cycles retard growth of tumors and sensitize a range of cancer cell types to chemotherapy. Sci Transl Med. 4(124):124ra127.
Li LH, Dong H, Zhao F, Tang J, Chen X, Ding J, Men HT, Luo WX, Du Y, Ge J et al. 2013. The upregulation of dihydropyrimidine dehydrogenase in liver is involved in acquired resistance to 5-fluorouracil. Eur J Cancer. 49(7):1752-1760.
Lin Y-H, Satani N, Hammoudi N, Ackroyd JJ, Khadka S, Yan VC, Georgiou DK, Sun Y, Zielinski R, Tran T et al. 2018. Eradication of ENO1-deleted Glioblastoma through Collateral Lethality. bioRxiv. doi: http://dx.doi.org/10.1101/331538.
Liu W, Le A, Hancock C, Lane AN, Dang CV, Fan TW, Phang JM. 2012. Reprogramming of proline and glutamine metabolism contributes to the proliferative and metabolic responses regulated by oncogenic transcription factor c-MYC. Proc Natl Acad Sci U S A. 109(23):8983-8988.
Liu YC, Li F, Handler J, Huang CR, Xiang Y, Neretti N, Sedivy JM, Zeller KI, Dang CV. 2008. Global regulation of nucleotide biosynthetic genes by c-Myc. PLoS One. 3(7):e2722.
Locasale JW, Grassian AR, Melman T, Lyssiotis CA, Mattaini KR, Bass AJ, Heffron G, Metallo CM, Muranen T, Sharfi H et al. 2011. Phosphoglycerate dehydrogenase diverts glycolytic flux and contributes to oncogenesis. Nat Genet. 43(9):869-874.
Long J, Zhang CJ, Zhu N, Du K, Yin YF, Tan X, Liao DF, Qin L. 2018. Lipid metabolism and carcinogenesis, cancer development. Am J Cancer Res. 8(5):778-791.
Lu Z, Xie J, Wu G, Shen J, Collins R, Chen W, Kang X, Luo M, Zou Y, Huang LJ et al. 2017. Fasting selectively blocks development of acute lymphoblastic leukemia via leptin-receptor upregulation. Nat Med. 23(1):79-90.
Lyssiotis CA, Kimmelman AC. 2017. Metabolic Interactions in the Tumor Microenvironment. Trends Cell Biol. 27(11):863-875.

Ma YS, Li YF, Chiriboga DE, Olendzki BC, Hebert JR, Li WJ, Leung K, Hafner AR, Ockene IS. 2006. Association between carbohydrate intake and serum lipids. Journal of the American College of Nutrition. 25(2):155-163. English.

Maddocks ODK, Athineos D, Cheung EC, Lee P, Zhang T, van den Broek NJF, Mackay GM, Labuschagne CF, Gay D, Kruiswijk F et al. 2017. Modulating the therapeutic response of tumours to dietary serine and glycine starvation. Nature. 544(7650):372-376.

Maddocks ODK, Berkers CR, Mason SM, Zheng L, Blyth K, Gottlieb E, Vousden KH. 2013. Serine starvation induces stress and p53-dependent metabolic remodelling in cancer cells. Nature. 493(7433):542-546.

Mani SA, Guo W, Liao MJ, Eaton EN, Ayyanan A, Zhou AY, Brooks M, Reinhard F, Zhang CC, Shipitsin M et al. 2008. The epithelial-mesenchymal transition generates cells with properties of stem cells. Cell. 133(4):704-715.

Mansoori B, Mohammadi A, Davudian S, Shirjang S, Baradaran B. 2017. The Different Mechanisms of Cancer Drug Resistance: A Brief Review. Adv Pharm Bull. 7(3):339-348.

Mao L, Merlo A, Bedi G, Shapiro GI, Edwards CD, Rollins BJ, Sidransky D. 1995. A novel p16INK4A transcript. Cancer Res. 55(14):2995-2997.

Marjon K, Cameron MJ, Quang P, Clasquin MF, Mandley E, Kunii K, McVay M, Choe S, Kernytsky A, Gross S et al. 2016. MTAP Deletions in Cancer Create Vulnerability to Targeting of the MAT2A/PRMT5/RIOK1 Axis. Cell Rep. 15(3):574-587.

Masri S, Papagiannakopoulos T, Kinouchi K, Liu Y, Cervantes M, Baldi P, Jacks T, Sassone-Corsi P. 2016. Lung Adenocarcinoma Distally Rewires Hepatic Circadian Homeostasis. Cell. 165(4):896-909.

Masri S, Sassone-Corsi P. 2018. The emerging link between cancer, metabolism, and circadian rhythms. Nat Med. 24(12):1795-1803.

Mattaini KR, Sullivan MR, Vander Heiden MG. 2016. The importance of serine metabolism in cancer. J Cell Biol. 214(3):249-257.

Mavrakis KJ, McDonald ER, 3rd, Schlabach MR, Billy E, Hoffman GR, deWeck A, Ruddy DA, Venkatesan K, Yu J, McAllister G et al. 2016. Disordered methionine metabolism in MTAP/CDKN2A-deleted cancers leads to dependence on PRMT5. Science. 351(6278):1208-1213.

Mayers JR, Torrence ME, Danai LV, Papagiannakopoulos T, Davidson SM, Bauer MR, Lau AN, Ji BW, Dixit PD, Hosios AM et al. 2016. Tissue of origin dictates branched-chain amino acid metabolism in mutant Kras-driven cancers. Science. 353(6304):1161-1165.

Mayers JR, Wu C, Clish CB, Kraft P, Torrence ME, Fiske BP, Yuan C, Bao Y, Townsend MK, Tworoger SS et al. 2014. Elevation of circulating branched-chain amino acids is an early event in human pancreatic adenocarcinoma development. Nat Med. 20(10):1193-1198.

Merlot AM, Kalinowski DS, Richardson DR. 2014. Unraveling the mysteries of serum albumin-more than just a serum protein. Front Physiol. 5:299.

Morandi A, Taddei ML, Chiarugi P, Giannoni E. 2017. Targeting the Metabolic Reprogramming That Controls Epithelial-to-Mesenchymal Transition in Aggressive Tumors. Front Oncol. 7:40.

Moulder JW, Vennesland B, Evans EA. 1945. A study of enzymatic reactions catalyzed by pigeon liver extracts. J Biol Chem. 160:305-325.

Muir A, Danai LV, Gui DY, Waingarten CY, Lewis CA, Vander Heiden MG. 2017. Environmental cystine drives glutamine anaplerosis and sensitizes cancer cells to glutaminase inhibition. Elife. 6.

Muller FL, Aquilanti EA, DePinho RA. 2015. Collateral Lethality: A new therapeutic strategy in oncology. Trends Cancer. 1(3):161-173.

Muller FL, Colla S, Aquilanti E, Manzo VE, Genovese G, Lee J, Eisenson D, Narurkar R, Deng P, Nezi L et al. 2012. Passenger deletions generate therapeutic vulnerabilities in cancer. Nature. 488(7411):337-342.

Nagarajan A, Malvi P, Wajapeyee N. 2016. Oncogene-directed alterations in cancer cell metabolism. Trends Cancer. 2(7):365-377.

Newgard CB, An J, Bain JR, Muehlbauer MJ, Stevens RD, Lien LF, Haqq AM, Shah SH, Arlotto M, Slentz CA et al. 2009. A branched-chain amino acid-related metabolic signature that differentiates obese and lean humans and contributes to insulin resistance. Cell Metab. 9(4):311-326.

Nikiforov MA, Chandriani S, O'Connell B, Petrenko O, Kotenko I, Beavis A, Sedivy JM, Cole MD. 2002. A Functional Screen for Myc-Responsive Genes Reveals Serine Hydroxymethyltransferase, a Major Source of the One-Carbon Unit for Cell Metabolism. Molecular and Cellular Biology. 22(16):5793-5800.

Nilsson LM, Forshell TZ, Rimpi S, Kreutzer C, Pretsch W, Bornkamm GW, Nilsson JA. 2012. Mouse genetics suggests cell-context dependency for Myc-regulated metabolic enzymes during tumorigenesis. PLoS Genet. 8(3):e1002573.

Orlowski M, Meister A. 1970. The gamma-glutamyl cycle: a possible transport system for amino acids. Proc Natl Acad Sci U S A. 67(3):1248-1255.

Overholtzer M, Mailleux AA, Mouneimne G, Normand G, Schnitt SJ, King RW, Cibas ES, Brugge JS. 2007. A nonapoptotic cell death process, entosis, that occurs by cell-in-cell invasion. Cell. 131(5):966-979.

Pacold ME, Brimacombe KR, Chan SH, Rohde JM, Lewis CA, Swier LJ, Possemato R, Chen WW, Sullivan LB, Fiske BP et al. 2016. A PHGDH inhibitor reveals coordination of serine synthesis and one-carbon unit fate. Nat Chem Biol. 12(6):452-458.

Pastore A, Massoud R, Motti C, Lo Russo A, Fucci G, Cortese C, Federici G. 1998. Fully automated assay for total homocysteine, cysteine, cysteinylglycine, glutathione, cysteamine, and 2-mercaptopropionylglycine in plasma and urine. Clin Chem. 44(4):825-832.

Pegg AE. 2009. Mammalian polyamine metabolism and function. IUBMB Life. 61(9):880-894.

Pegg AE, Williams-Ashman HG. 1969a. On the role of S-adenosyl-L-methionine in the biosynthesis of spermidine by rat prostate. J Biol Chem. 244(4):682-693.

Pegg AE, Williams-Ashman HG. 1969b. Phosphate-stimulated breakdown of 5'-methylthioadenosine by rat ventral prostate. Biochem J. 115(2):241-247.

Perez-Escuredo J, Van Hee VF, Sboarina M, Falces J, Payen VL, Pellerin L, Sonveaux P. 2016. Monocarboxylate transporters in the brain and in cancer. Biochim Biophys Acta. 1863(10):2481-2497.

Possemato R, Marks KM, Shaul YD, Pacold ME, Kim D, Birsoy K, Sethumadhavan S, Woo HK, Jang HG, Jha AK et al. 2011. Functional genomics reveal that the serine synthesis pathway is essential in breast cancer. Nature. 476(7360):346-350.

Priolo C, Khabibullin D, Reznik E, Filippakis H, Ogorek B, Kavanagh TR, Nijmeh J, Herbert ZT, Asara JM, Kwiatkowski DJ et al. 2018. Impairment of gamma-glutamyl transferase 1 activity in the metabolic pathogenesis of chromophobe renal cell carcinoma. Proc Natl Acad Sci U S A. 115(27):E6274-E6282.

Puzio-Kuter AM. 2011. The Role of p53 in Metabolic Regulation. Genes Cancer. 2(4):385-391.

Quelle DE, Zindy F, Ashmun RA, Sherr CJ. 1995. Alternative reading frames of the INK4a tumor suppressor gene encode two unrelated proteins capable of inducing cell cycle arrest. Cell. 83(6):993-1000.

Raeini-Sarjaz M, Vanstone CA, Papamandjaris AA, Wykes LJ, Jones PJH. 2001. Comparison of the effect of dietary fat restriction with that of energy restriction on human lipid metabolism. American Journal of Clinical Nutrition. 73(2):262-267. English.

Raghunath A, Sundarraj K, Nagarajan R, Arfuso F, Bian J, Kumar AP, Sethi G, Perumal E. 2018. Antioxidant response elements: Discovery, classes, regulation and potential applications. Redox Biol. 17:297-314.

Recouvreux MV, Commisso C. 2017. Macropinocytosis: A Metabolic Adaptation to Nutrient Stress in Cancer. Front Endocrinol (Lausanne). 8:261.

Romero R, Sayin VI, Davidson SM, Bauer MR, Singh SX, LeBoeuf SE, Karakousi TR, Ellis DC, Bhutkar A, Sanchez-Rivera FJ et al. 2017. Keap1 loss promotes Kras-driven lung cancer and results in dependence on glutaminolysis. Nat Med. 23(11):1362-1368.

Samanta D, Park Y, Andrabi SA, Shelton LM, Gilkes DM, Semenza GL. 2016. PHGDH Expression Is Required for Mitochondrial Redox Homeostasis, Breast Cancer Stem Cell Maintenance, and Lung Metastasis. Cancer Res. 76(15):4430-4442.

Sanderson SM, Mikhael P, Dai Z, Locasale JW. 2018. Environmental factors shape methionine metabolism in p16/MTAP deleted cells. bioRxiv. doi: https://doi.org/10.1101/313288.

Sansregret L, Swanton C. 2017. The Role of Aneuploidy in Cancer Evolution. Cold Spring Harb Perspect Med. 7(1).

Santana-Codina N, Roeth AA, Zhang Y, Yang A, Mashadova O, Asara JM, Wang X, Bronson RT, Lyssiotis CA, Ying H et al. 2018. Oncogenic KRAS supports pancreatic cancer through regulation of nucleotide synthesis. Nat Commun. 9(1):4945.

Sayin VI, LeBoeuf SE, Singh SX, Davidson SM, Biancur D, Guzelhan BS, Alvarez SW, Wu WL, Karakousi TR, Zavitsanou AM et al. 2017. Activation of the NRF2 antioxidant program generates an imbalance in central carbon metabolism in cancer. Elife. 6.

Schofield HK, Zeller J, Espinoza C, Halbrook CJ, Del Vecchio A, Magnuson B, Fabo T, Daylan AEC, Kovalenko I, Lee HJ et al. 2018. Mutant p53R270H drives altered metabolism and increased invasion in pancreatic ductal adenocarcinoma. JCI Insight. 3(2).

Schwartzenberg-Bar-Yoseph F, Armoni M, Karnieli E. 2004. The tumor suppressor p53 down-regulates glucose transporters GLUT1 and GLUT4 gene expression. Cancer Res. 64(7):2627-2633.

Serrano M, Gomez-Lahoz E, DePinho RA, Beach D, Bar-Sagi D. 1995. Inhibition of ras-induced proliferation and cellular transformation by p16INK4. Science. 267(5195):249-252.

Serrano M, Hannon GJ, Beach D. 1993. A new regulatory motif in cell-cycle control causing specific inhibition of cyclin D/CDK4. Nature. 366(6456):704-707.
Shaul YD, Freinkman E, Comb WC, Cantor JR, Tam WL, Thiru P, Kim D, Kanarek N, Pacold ME, Chen WW et al. 2014. Dihydropyrimidine accumulation is required for the epithelial-mesenchymal transition. Cell. 158(5):1094-1109.
Sheltzer JM. 2013. A transcriptional and metabolic signature of primary aneuploidy is present in chromosomally unstable cancer cells and informs clinical prognosis. Cancer Res. 73(21):6401-6412.
Sonveaux P, Vegran F, Schroeder T, Wergin MC, Verrax J, Rabbani ZN, De Saedeleer CJ, Kennedy KM, Diepart C, Jordan BF et al. 2008. Targeting lactate-fueled respiration selectively kills hypoxic tumor cells in mice. J Clin Invest. 118(12):3930-3942.
Sousa CM, Biancur DE, Wang X, Halbrook CJ, Sherman MH, Zhang L, Kremer D, Hwang RF, Witkiewicz AK, Ying H et al. 2016. Pancreatic stellate cells support tumour metabolism through autophagic alanine secretion. Nature. 536(7617):479-483.
Stone S, Jiang P, Dayananth P, Tavtigian SV, Katcher H, Parry D, Peters G, Kamb A. 1995. Complex structure and regulation of the P16 (MTS1) locus. Cancer Res. 55(14):2988-2994.
Stott FJ, Bates S, James MC, McConnell BB, Starborg M, Brookes S, Palmero I, Ryan K, Hara E, Vousden KH et al. 1998. The alternative product from the human CDKN2A locus, p14ARF, participates in a regulatory feedback loop with p53 and MDM2. EMBO J. 17(17):5001-5014.
Sun P, Wang H, He Z, Chen X, Wu Q, Chen W, Sun Z, Weng M, Zhu M, Ma D et al. 2017. Fasting inhibits colorectal cancer growth by reducing M2 polarization of tumor-associated macrophages. Oncotarget. 8(43):74649-74660.
Szablewski L. 2013. Expression of glucose transporters in cancers. Biochim Biophys Acta. 1835(2):164-169.
Tajan M, Hock AK, Blagih J, Robertson NA, Labuschagne CF, Kruiswijk F, Humpton TJ, Adams PD, Vousden KH. 2018. A Role for p53 in the Adaptation to Glutamine Starvation through the Expression of SLC1A3. Cell Metab. 28(5):721-736 e726.
Tang YC, Yuwen H, Wang K, Bruno PM, Bullock K, Deik A, Santaguida S, Trakala M, Pfau SJ, Zhong N et al. 2017. Aneuploid Cell Survival Relies upon Sphingolipid Homeostasis. Cancer Res. 77(19):5272-5286.
Tardito S, Oudin A, Ahmed SU, Fack F, Keunen O, Zheng L, Miletic H, Sakariassen PO, Weinstock A, Wagner A et al. 2015. Glutamine synthetase activity fuels nucleotide biosynthesis and supports growth of glutamine-restricted glioblastoma. Nat Cell Biol. 17(12):1556-1568.
Taroni F, Gellera C, Di Donato S. 1987. Evidence for two distinct mitochondrial malic enzymes in human skeletal muscle: purification and properties of the NAD(P)+-dependent enzyme. Biochim Biophys Acta. 916(3):446-454.
Todenhofer T, Seiler R, Stewart C, Moskalev I, Gao J, Ladhar S, Kamjabi A, Al Nakouzi N, Hayashi T, Choi S et al. 2018. Selective Inhibition of the Lactate Transporter MCT4 Reduces Growth of Invasive Bladder Cancer. Mol Cancer Ther. 17(12):2746-2755.
Torrence ME, Manning BD. 2018. Nutrient Sensing in Cancer. Annual Review of Cancer Biology. 2(1):251-269.

Ulrich CM. 2007. Folate and cancer prevention: a closer look at a complex picture. American Journal of Clinical Nutrition. 86(2):271-273. English.
Ussar S, Griffin NW, Bezy O, Fujisaka S, Vienberg S, Softic S, Deng L, Bry L, Gordon JI, Kahn CR. 2015. Interactions between Gut Microbiota, Host Genetics and Diet Modulate the Predisposition to Obesity and Metabolic Syndrome. Cell Metab. 22(3):516-530.
van Geldermalsen M, Wang Q, Nagarajah R, Marshall AD, Thoeng A, Gao D, Ritchie W, Feng Y, Bailey CG, Deng N et al. 2016. ASCT2/SLC1A5 controls glutamine uptake and tumour growth in triple-negative basal-like breast cancer. Oncogene. 35(24):3201-3208.
Vander Heiden MG, DeBerardinis RJ. 2017. Understanding the Intersections between Metabolism and Cancer Biology. Cell. 168(4):657-669.
Venugopal R, Jaiswal AK. 1996. Nrf1 and Nrf2 positively and c-Fos and Fra1 negatively regulate the human antioxidant response element-mediated expression of NAD(P)H:quinone oxidoreductase1 gene. Proc Natl Acad Sci U S A. 93(25):14960-14965.
Wang R, Dillon CP, Shi LZ, Milasta S, Carter R, Finkelstein D, McCormick LL, Fitzgerald P, Chi H, Munger J et al. 2011. The transcription factor Myc controls metabolic reprogramming upon T lymphocyte activation. Immunity. 35(6):871-882.
Wiig H, Swartz MA. 2012. Interstitial fluid and lymph formation and transport: physiological regulation and roles in inflammation and cancer. Physiol Rev. 92(3):1005-1060.
Wilcox G. 2005. Insulin and insulin resistance. Clin Biochem Rev. 26(2):19-39.
Wolpaw AJ, Dang CV. 2018. MYC-induced metabolic stress and tumorigenesis. Biochim Biophys Acta Rev Cancer. 1870(1):43-50.
Wyant GA, Abu-Remaileh M, Wolfson RL, Chen WW, Freinkman E, Danai LV, Vander Heiden MG, Sabatini DM. 2017. mTORC1 Activator SLC38A9 Is Required to Efflux Essential Amino Acids from Lysosomes and Use Protein as a Nutrient. Cell. 171(3):642-654 e612.
Yang L, Achreja A, Yeung TL, Mangala LS, Jiang D, Han C, Baddour J, Marini JC, Ni J, Nakahara R et al. 2016. Targeting Stromal Glutamine Synthetase in Tumors Disrupts Tumor Microenvironment-Regulated Cancer Cell Growth. Cell Metab. 24(5):685-700.
Young JD. 2016. The SLC28 (CNT) and SLC29 (ENT) nucleoside transporter families: a 30-year collaborative odyssey. Biochem Soc Trans. 44(3):869-876.
Yuneva MO, Fan TW, Allen TD, Higashi RM, Ferraris DV, Tsukamoto T, Mates JM, Alonso FJ, Wang C, Seo Y et al. 2012. The metabolic profile of tumors depends on both the responsible genetic lesion and tissue type. Cell Metab. 15(2):157-170.
Yuneva MO, Zamboni N, Oefner P, Sachidanandam R, Lazebnik Y. 2007. Deficiency in glutamine but not glucose induces MYC-dependent apoptosis in human cells. J Cell Biol. 178(1):93-105.
Zack TI, Schumacher SE, Carter SL, Cherniack AD, Saksena G, Tabak B, Lawrence MS, Zhsng CZ, Wala J, Mermel CH et al. 2013. Pan-cancer patterns of somatic copy number alteration. Nat Genet. 45(10):1134-1140.
Zhang H, Chen Z, Savarese TM. 1996. Codeletion of the genes for p16INK4, methylthioadenosine phosphorylase, interferon-α1, interferon-β1, and other 9p21 Markers in Human Malignant Cell Lines. Cancer Genet Cytogenet. 86:22-28.

Zhang W, Trachootham D, Liu J, Chen G, Pelicano H, Garcia-Prieto C, Lu W, Burger JA, Croce CM, Plunkett W et al. 2012. Stromal control of cystine metabolism promotes cancer cell survival in chronic lymphocytic leukaemia. Nat Cell Biol. 14(3):276-286.

Zhao M, Mishra L, Deng CX. 2018. The role of TGF-beta/SMAD4 signaling in cancer. Int J Biol Sci. 14(2):111-123.

Zhu J, Tsai HJ, Gordon MR, Li R. 2018. Cellular Stress Associated with Aneuploidy. Dev Cell. 44(4):420-431.

CHAPTER TWO: Increased serine synthesis provides an advantage for tumors arising in tissues where serine levels are limiting

Mark R. Sullivan[1,2], Katherine R. Mattaini[1,2], Emily A. Dennstedt[1,2], Anna A. Nguyen[1,2], Montana F. Reilly[1,2], Katrina Meeth[3], Alexander Muir[1,2], Alicia M. Darnell[1,2], Marcus W. Bosenberg[3,4], Caroline A. Lewis[5], Matthew G. Vander Heiden[1,2,6,7]

[1]Koch Institute for Integrative Cancer Research and [2]Department of Biology, Massachusetts Institute of Technology, Cambridge, Massachusetts 02139, USA
[3]Department of Pathology, Yale University School of Medicine, New Haven, CT, USA
[4]Department of Dermatology, Yale University School of Medicine, New Haven, CT, USA
[5]Whitehead Institute for Biomedical Research, Cambridge, MA 02139, USA
[6]Dana-Farber Cancer Institute, Boston, Massachusetts 02215, USA
[7]Broad Institute, Cambridge, Massachusetts 02139, USA

A version of this chapter has been published previously and is reprinted with permission from Elsevier:

Sullivan, M.R., Mattaini, K.R., Dennstedt, E.A., Nguyen, A.A., Sivanand, S., Reilly, M.F., Meeth, K., Muir, A., Bosenberg, M.W., Lewis, C.A., Vander Heiden, M.G., Increased Serine Synthesis Provides an Advantage for Tumors Arising in Tissues Where Serine Levels Are Limiting. *Cell Metabolism*, https://doi.org/10.1016/j.cmet.2019.02.015 (2019).

ABSTRACT

Tumors exhibit altered metabolism compared to normal tissues. Many cancers upregulate expression of serine synthesis pathway enzymes, and some tumors exhibit copy number gain of the gene encoding the first enzyme in the pathway, phosphoglycerate dehydrogenase (*PHGDH*). However, whether increased serine synthesis promotes tumor growth and how serine synthesis benefits tumors is controversial. Here we demonstrate that increased PHGDH expression promotes tumor progression in mouse models of melanoma and breast cancer, human tumor types that exhibit PHGDH copy number gain. We measure circulating serine levels and find that PHGDH expression is necessary to support cell proliferation at lower physiological serine concentrations. Increased dietary serine or high PHGDH expression are sufficient to increase intracellular serine levels and support faster tumor growth. Together, these data suggest that physiological serine availability restrains tumor growth and argues that tumors arising in serine-limited environments acquire a fitness advantage by upregulating serine synthesis pathway enzymes.

INTRODUCTION

Altered metabolism was one of the earliest observed characteristics of cancer. Initial studies demonstrated an increased role of glucose metabolism in tumor progression, but more recent work has highlighted the importance of amino acid, nucleotide, and lipid metabolism in cancer (Pavlova and Thompson, 2016). Identifying metabolic pathways limiting for tumor growth may provide insight into targeting metabolism for cancer therapy (Vander Heiden and DeBerardinis, 2017). One approach to find metabolic pathways important for specific tumors is

to identify enzymes that are upregulated in tumors relative to their tissue of origin. Some tumors highly express enzymes in the serine synthesis pathway (Newman and Maddocks, 2017). Phosphoglycerate dehydrogenase (PHGDH) catalyzes the first step in serine synthesis (Figure 2A), and PHGDH protein levels are upregulated by factors associated with tumor progression including NRF2 (DeNicola et al., 2015), c-MYC (Nilsson et al., 2012), ATF4 (Adams, 2007; DeNicola et al., 2015), HIF-1α (Samanta et al., 2016), mTORC1 (Ben-Sahra et al., 2016), and the lysine methyltransferase G9A (Ding et al., 2013), while PHGDH expression can be repressed by the tumor suppressor p53 (Ou et al., 2015). PHGDH also exhibits gene copy number gain in several tumor types, including melanoma and triple negative breast cancer (Locasale et al., 2011; Possemato et al., 2011). Disrupting serine synthesis can be detrimental for some tumors, as decreasing PHGDH expression impairs the growth of subcutaneous lung cancer (DeNicola et al., 2015) and breast cancer (Pacold et al., 2016; Possemato et al., 2011) xenografts. However, PHGDH knockdown does not affect tumors growth in a different breast cancer model (Chen et al., 2013), arguing that serine synthesis pathway activity is only required in some contexts. What selects for high PHGDH expression and how this benefits tumor growth is poorly understood.

Though many cells express high levels of serine synthesis pathway enzymes and synthesize serine, serine is also the second most highly consumed amino acid in cultured cells (Hosios et al., 2016), reflecting its central role in biosynthetic reactions. Serine is a proteinogenic amino acid and is utilized to synthesize glycine (Newman and Maddocks, 2017) and cysteine (DeNicola et al., 2015). Serine also supports ceramide and sphingolipid synthesis and is a component of phospholipid head groups (Mullen et al., 2012; Vance and Tasseva,

2013). In addition, serine donates one-carbon units for folate-dependent reactions (Labuschagne et al., 2014), including thymidine and purine nucleotide base synthesis (Lane and Fan, 2015). Folate-derived one-carbon units can also regenerate S-adenosyl methionine to support DNA, RNA, protein, phospholipid, and polyamine methylation (Chiang et al., 1996). Given these central biosynthetic roles, many cells do not tolerate serine deprivation (DeNicola et al., 2015; Labuschagne et al., 2014; Ma et al., 2017), and some tumors are sensitive to dietary serine withdrawal (Maddocks et al., 2017; Maddocks et al., 2013).

Beyond supplying serine, serine synthesis pathway activity may provide additional advantages to cells. PHGDH knockdown or inhibition inhibits proliferation of some cancer cells in culture in a manner that cannot be rescued by exogenous serine (Locasale et al., 2011; Mullarky et al., 2016; Pacold et al., 2016; Possemato et al., 2011). One explanation for this phenomenon is that serine synthesis provides a means to obtain α-ketoglutarate (Hwang et al., 2016; Possemato et al., 2011), a TCA cycle intermediate and cofactor for dioxygenases involved in regulation of gene expression and adaptation to hypoxia (Hausinger, 2004). PHGDH can also be a source of D-2-hydroxyglutarate (Fan et al., 2015), which also can affect dioxygenase activity (Ye et al., 2018). Further, in yeast, serine synthesis pathway enzymes are part of a complex containing one-carbon metabolism enzymes, suggesting potential non-enzymatic scaffolding roles for these proteins (Li et al., 2015). Which, if any, of these potential benefits of increased serine synthesis pathway enzyme expression are important in tumors is unknown.

To determine whether increased PHGDH expression promotes tumor progression, and to ascertain why tumors might benefit from increased PHGDH levels, we utilized a mouse model that mimics PHGDH copy number gain (Mattaini et al., 2018). In autochthonous mouse

models of melanoma and breast cancer, we find that increased PHGDH expression promotes tumor progression. Furthermore, we find that increased PHGDH expression maintains serine at a level that is not limiting for tumor growth, suggesting that endogenous serine limitation restrains the growth of some tumors and that cancers arising in low-serine tissues will gain a fitness advantage from increased serine synthesis.

RESULTS

PHGDH expression cooperates with mutant Braf to promote melanoma formation

Increased levels of PHGDH are insufficient to promote tumor initiation (Mattaini et al., 2018). However, PHGDH expression may cooperate with other genetic events to promote tumor growth. To examine this possibility, we first focused on melanoma, a tumor type in which PHGDH copy number gain is observed (Locasale et al., 2011; Possemato et al., 2011). In melanoma, activating *Braf* mutations occur in up to 60% of tumors (Chin, 2003). To determine whether PHGDH expression can cooperate with mutant *Braf* to promote melanoma in mice, we utilized a *PHGDH*^{tetO} allele that allows for doxycycline-inducible expression of human *PHGDH* (Mattaini et al., 2018). The *PHGDH*^{tetO} allele was crossed to mice bearing a *Braf* ^{V600E} conditional allele (*Braf*^{CA}*)* and *Tyr-CreER* allele that enables mutant *Braf* ^{V600E} activation in melanocytes when exposed to tamoxifen (Dankort et al., 2009). *Braf* activation alone does not drive tumor formation in this model (Dankort et al., 2009), but promotes melanoma formation when combined with some other genetic alterations (Damsky et al., 2015). To activate PHGDH expression in *Braf*^{CA}; *Tyr-CreER*; *PHGDH*^{tetO} mice, animals were bred to also harbor a *R26-M2rtTA* that drives transgene expression in most mouse tissues upon exposure to doxycycline

(Zambrowicz et al., 1997). Increased PHGDH expression dependent on both doxycycline and the presence of a *PHGDH*^{tetO} allele is observed in the skin and other tissues in these mice (Mattaini et al., 2018). When fed a doxycycline containing diet to increase PHGDH expression, 13 percent of *Braf*^{CA}; *Tyr-CreER*; *PHGDH*^{tetO}; *R26-M2rtTA* mice formed tumors, while no littermate mice with melanocytic *Braf* activation that lack a *PHGDH*^{tetO} allele developed tumors (Figure 1A). The observed tumors appeared histologically to be melanomas, and expressed the melanoma marker Sox10 (Figure 1B), suggesting that PHGDH expression can cooperate with *Braf* activation to drive melanoma formation with low penetrance.

PHGDH expression accelerates melanoma growth

To examine the role of PHGDH in melanoma growth and progression, *PHGDH*^{tetO}; *R26-M2rtTA* mice were crossed to a mouse melanoma model initiated by *Braf* activation and *Pten* deletion in melanocytes (*Braf*^{CA}; *Tyr-CreER*; *Pten*$^{fl/fl}$) (Dankort et al., 2009). To confirm that the *PHGDH*^{tetO} allele was expressed in this model, we leveraged the fact that the *PHGDH*^{tetO} transgene encodes human *PHGDH* (huPHGDH) that can be distinguished from endogenous mouse *Phgdh* (msPHGDH). Tumors with the *PHGDH*^{tetO} allele express huPHGDH as well as endogenous msPHGDH, while control tumors express msPHGDH but not huPHGDH (Figure 1C). Consistent with this result, tumors from *PHGDH*^{tetO} mice exhibit increased PHGDH protein expression (Figure 1D) using an antibody that recognizes human and mouse PHGDH with equal affinity (Mattaini et al., 2018). The *PHGDH*^{tetO} allele did not alter the histological appearance of melanomas that formed (Figure 1E) or plasma serine levels (Figure 2B), but did decrease the

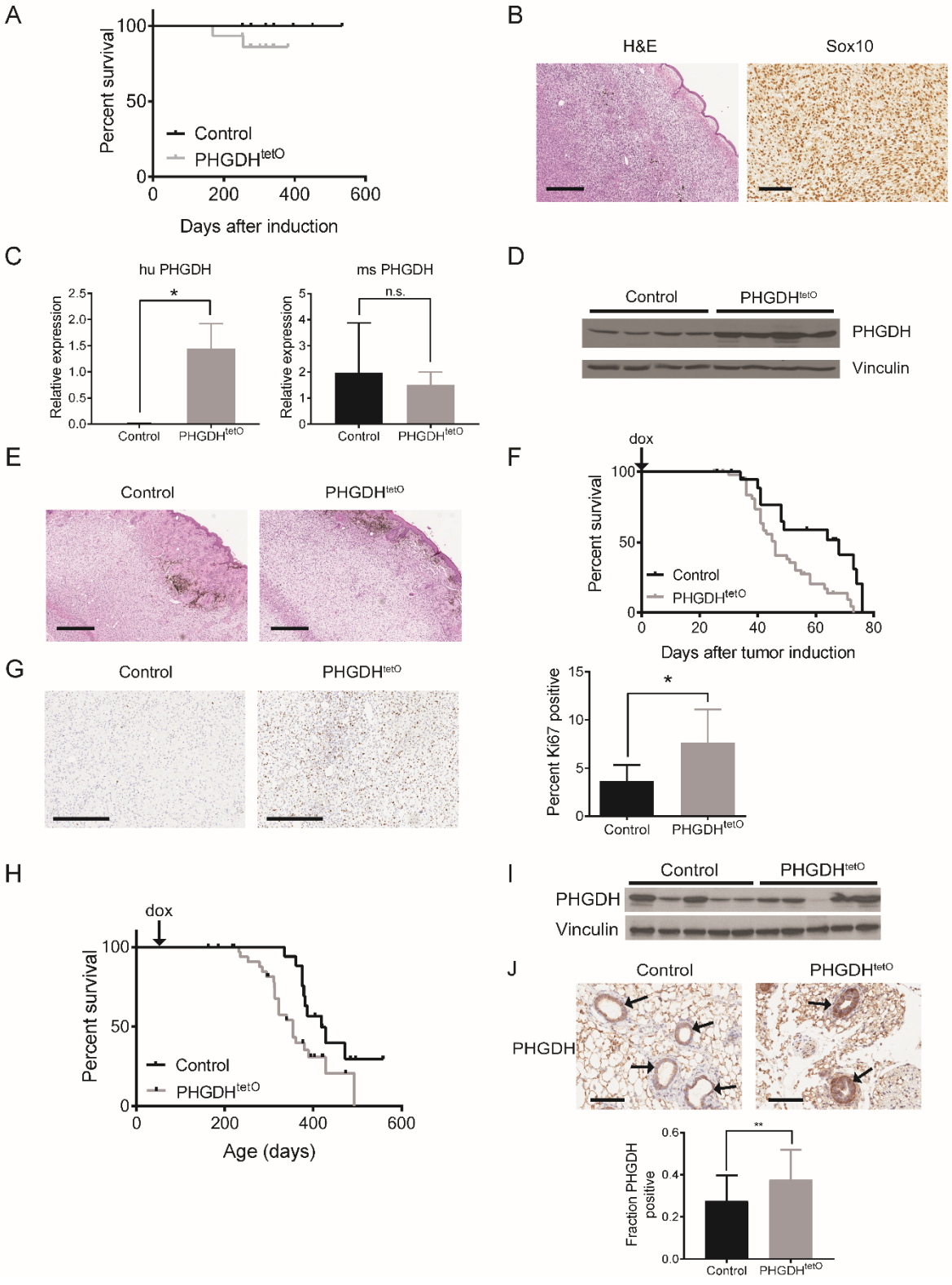
A
Percent survival
100
50
0
Control
PHGDH tetO
0
200
400
600
Days after induction
B
H&E
Sox10
C
hu PHGDH
ms PHGDH
Relative expression
*
n.s.
Control
PHGDH tetO
D
Control
PHGDH tetO
PHGDH
Vinculin
E
Control
PHGDH tetO
F
dox
Percent survival
Control
PHGDH tetO
Days after tumor induction
G
Control
PHGDH tetO
Percent Ki67 positive
H
dox
Percent survival
Control
PHGDH tetO
Age (days)
I
Control
PHGDH tetO
PHGDH
Vinculin
J
Control
PHGDH tetO
PHGDH
Fraction PHGDH positive
**

Figure 1. PHGDH expression promotes melanoma and breast cancer. (A) Kaplan-Meier plot showing survival of control or PHGDH expressing (PHGDH^{tetO}) mice with mutant Braf expression in melanocytes. N=14 for Control, N=15 for PHGDH^{tetO} **(B)** Representative hematoxylin and eosin (H&E) and Sox10 immunohistochemistry staining of a tumor derived from a *Braf^{CA}*; *Tyr-CreER; PHGDH^{tetO}*; *Rosa26-M2rtTA* mouse. H&E image, 4x magnification, scale bar = 500 µm; Sox10 image, 20X magnification, scale bar = 100 µm. **(C)** Species specific RT-qPCR for human (huPHGDH) and mouse (msPHGDH) PHGDH in *Braf^{CA} Pten $^{-/-}$* melanomas from *Braf^{CA}*; *Pten$^{fl/fl}$*; *Tyr-CreER* mice without (control) or with (PHGDH^{tetO}) increased PHGDH expression as above. The difference in huPHGDH expression is significant (p = 0.0368) and the difference in msPHGDH expression is not significant (p = 0.7127) by unpaired, two-tailed Welch's t tests. n=3 tumors for each genotype. **(D)** Western blot analysis of PHGDH expression in control or PHGDH^{tetO} *Braf^{CA} Pten$^{-/-}$* tumors. **(E)** Representative H&E image of *Braf^{CA}*; *PTEN $^{-/-}$* tumors with normal (Control) or increased (PHGDH^{tetO}) PHGDH expression. 4x magnification, scale bar = 500 µm. **(F)** Kaplan-Meier plot showing survival of control or PHGDH expressing (PHGDH^{tetO}) mice bearing *Braf^{CA}*; *Pten $^{-/-}$* melanomas. Doxycycline (dox) diet started on the day of tumor induction (arrow). Difference in survival is significant (p = 0.012) by a stratified Cox proportional hazards model. n=13 for control mice, n=36 for PHGDH^{tetO} mice **(G)** Representative immunohistochemistry assessing Ki67 in control and PHGDH expressing (PHGDH^{tetO}) *Braf^{CA}*; *Pten$^{-/-}$* tumors. 10x magnification, scale bar = 300 µm. The difference in Ki67 staining was significant (p = 0.0358) by an unpaired, two-tailed Welch's T test. **(H)** Kaplan-Meier plot showing survival of control or PHGDH expressing (PHGDH^{tetO}) *BRCA$^{fl/fl}$*; *Trp53$^{+/-}$*; *MMTV-Cre* mice with breast tumors. Difference in survival is significant (p = 0.0269) by a Mantel-Cox log-rank test. n=10 for control mice and n=22 for PHGDH^{tetO} mice. **(I)** Western blot analysis of PHGDH expression in control or *PHGDH^{tetO}* breast tumors arising in *BRCA$^{fl/fl}$*; *Trp53$^{+/-}$*; *MMTV-Cre* mice. **(J)** Representative PHGDH immunohistochemistry staining of mammary glands from 7-week old *MMTV-rtTA* (Control) and *PHGDH$^{tetO/+}$; MMTV-rtTA* (PHGDH^{tetO}) mice fed a doxycycline diet for 1 week prior to harvesting mammary tissue. Arrows indicate mammary ducts. 20x magnification, scale bar = 100 µm. *PHGDH^{tetO}* mice exhibited a significant increase in the fraction of cells with high PHGDH expression (p=0.0025) by an unpaired, two-tailed Welch's t test.
Mean +/- SD is shown for all panels.

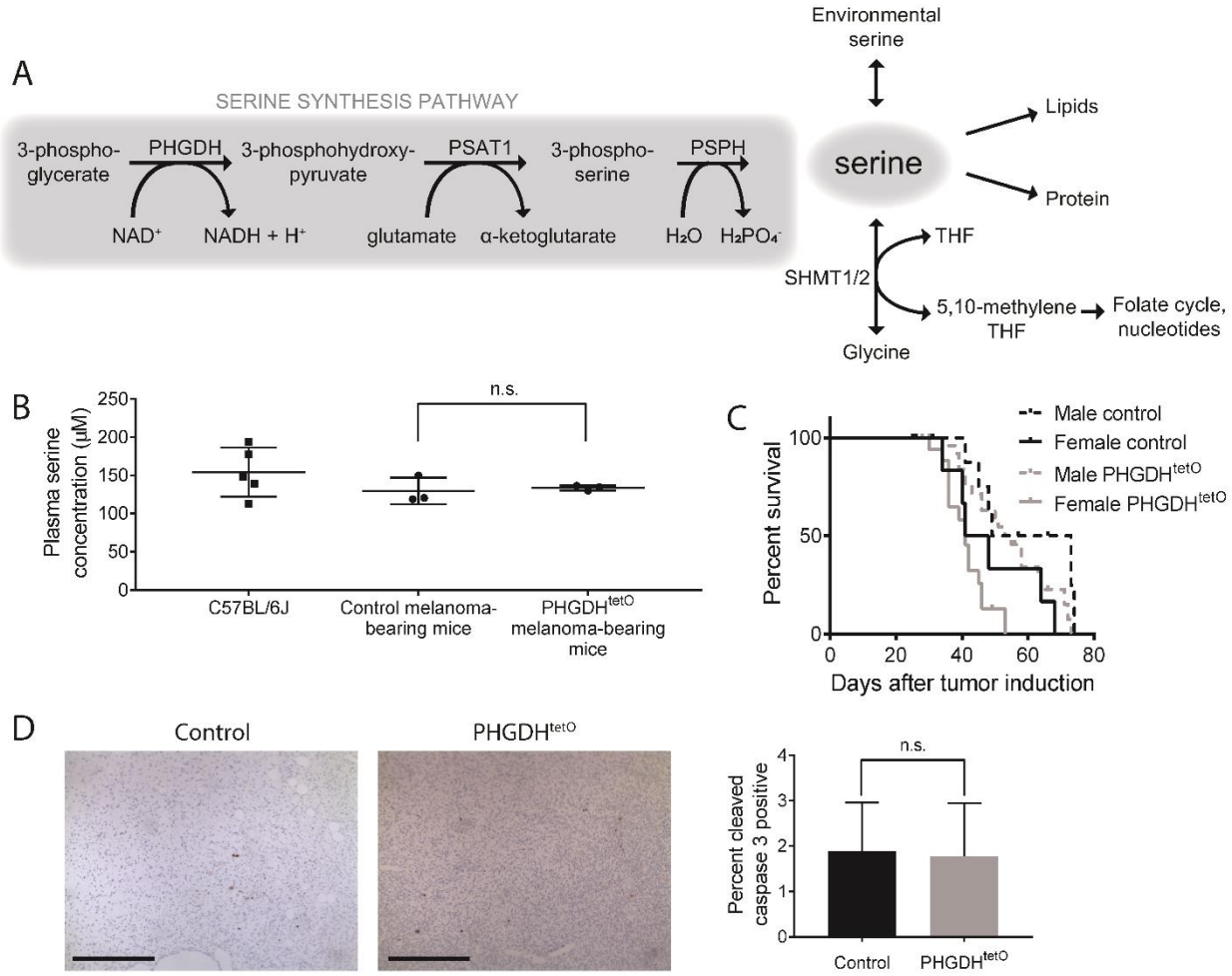

Figure 2. PHGDH expression does not alter circulating serine levels or apoptotic cell death in *Braf*^{CA}; *PTEN* $^{-/-}$ melanoma-bearing mice. (A) Schematic showing the serine synthesis pathway from glucose and how serine contributes to biomass in cells. PHGDH, phosphoglycerate dehydrogenase; PSAT1, phosphoserine amino transferase 1; PSPH, phosphoserine phosphatase; SHMT1/2, serine hydroxymethyltransferase 1/2; THF, tetrahydrofolate. **(B)** Plasma serine concentration in C57BL/6J mice, control *Braf*^{CA}; *PTEN* $^{-/-}$ mice bearing melanomas, and PHGDH^{tetO} *Braf*^{CA}; *PTEN* $^{-/-}$ mice bearing melanomas as measured by GC/MS. Plasma from tumor bearing mice was collected 1 month after tumor induction. There is no statistically significant difference in plasma serine concentration between control and PHGDH^{tetO} tumor bearing mice based on an unpaired, two-tailed Welch's t test with a p-value of 0.7330. n = 3 mice for control and PHGDH^{tetO} mice and n = 5 for C57BL/6J mice. **(C)** Kaplan-Meier plot showing survival of control and PHGDH expressing (PHGDH^{tetO}) mice bearing *Braf*^{CA}; *PTEN* $^{-/-}$ tumors as described in Figure 1, with survival of animals separated by gender. **(D)** Representative immunohistochemistry staining and quantitation of cleaved caspase 3 (CC3) in the same *Braf*^{CA}; *PTEN* $^{-/-}$ melanomas analyzed in Figure 1H that arose in mice without (control) or with (PHGDH^{tetO}) a PHGDH transgene. Images were obtained at 10x magnification, scale bar = 300 μm. CC3 staining was quantitated by scoring 300 cells as CC3 positive or negative for each of 5 tumors of each genotype. No statistically significant difference was observed based on a Welch's t test that yielded a p value of 0.9094. Values represent the mean +/- SD.

median time for tumors to reach 1 cm^3 from 68 to 46 days (Figure 1F). Increased PHGDH expression accelerated melanoma in both male and female mice, which exhibit different tumor growth kinetics in this model (Figure 2C). This phenotype was driven at least in part by increased cell proliferation, as tumors with the *PHGDH^{tetO}* allele displayed increased staining for the proliferative marker Ki67 compared to control mice (Figure 1G), while no difference in staining for a marker of apoptosis, cleaved caspase 3, was observed (Figure 2D). Together, these data suggest that increased PHGDH expression can accelerate melanoma growth.

PHGDH expression accelerates breast cancer

PHGDH copy number gain is also observed in triple-negative breast cancer (Locasale et al., 2011; Possemato et al., 2011). To determine whether PHGDH expression plays a tumorigenic role in this cancer, the *PHGDH^{tetO}* allele was crossed to a triple negative breast cancer model induced by mammary specific *Brca1* deletion in *Trp53* heterozygous mice (*BRCA$^{fl/fl}$; Trp53$^{+/-}$; MMTV-Cre*) (Xu et al., 1999). In addition, to confirm that any role of PHGDH can be attributed to PHGDH expression in the tissue where the cancer arises, increased PHGDH expression was limited to mammary epithelial cells with a mammary specific *MMTV-rtTA* allele (Whisenhunt et al., 2006). *PHGDH^{tetO}* breast tumors reached 1 cm^3 faster than control tumors, suggesting that PHGDH expression can also promote breast tumor progression (Figure 1H). Interestingly, PHGDH expression in end stage tumors is variable, and *PHGDH^{tetO}* tumors do not exhibit increased PHGDH expression compared to control tumors (Figure 1I), even though *PHGDH^{tetO}* mice express huPHGDH derived from the *PHGDH^{tetO}* transgene (Figure 3A). Additionally, end stage *PHGDH^{tetO}* tumors do not display differential staining of Ki67 or cleaved caspase 3 (Figure 3B-C). One possible explanation is that increased PHGDH expression is

selected for in both *PHGDH*^{tetO} and control tumors, and earlier PHGDH expression from the transgene contributes to earlier tumor outgrowth in this more protracted cancer model. To confirm that PHGDH expression is elevated early in *PHGDH*^{tetO} mice, mammary glands from 7 week old *PHGDH*^{tetO}*;MMTV-rtTA* and control *MMTV-rtTA* mice were stained for PHGDH. PHGDH expression was increased in mammary epithelial cells in *PHGDH*^{tetO} mice compared to control mice (Figure 1J). Together, these data suggest that the *PHGDH*^{tetO} allele provides an advantage to tumors prior to end stage, when *PHGDH*^{tetO} tumors exhibit similar PHGDH expression as control tumors.

Breast cancer cell lines are dependent on PHGDH to produce serine

To determine whether PHGDH plays a role throughout breast tumor progression, we generated cell lines from end stage control tumors, which express PHGDH at levels similar to tumors from *PHGDH*^{tetO} mice, and knocked down PHGDH expression using CRISPR interference (CRISPRi) (Figure 4A). PHGDH loss decreased serine synthesis pathway activity as assessed by ^{13}C-labeled glucose incorporation into serine (Figure 4B), but had no effect on proliferation of these cells in culture (Figure 4C). This result could suggest that PHGDH is not required for proliferation of these cancer cells; however, it is also possible that PHGDH expression is beneficial specifically in the breast tumor environment. One difference between the cell culture and breast tumors environments is serine availability. The serine concentration in RPMI-1640 culture media is 285 μM.

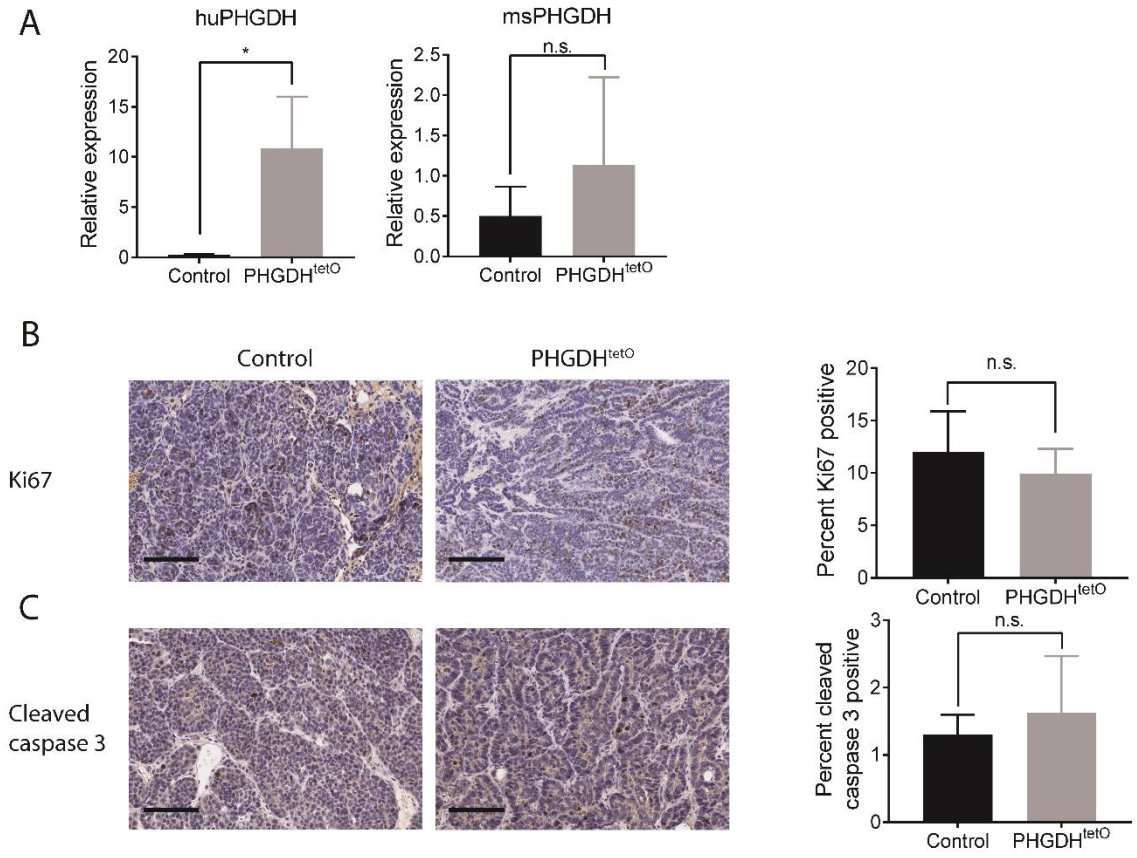

Figure 3. End stage *BRCA$^{fl/fl}$*; *Trp53$^{+/-}$* breast tumors have similar rates of proliferation and apoptosis regardless of PHGDH^{tetO} status. (A) Species specific RT-qPCR for human (huPHGDH) and mouse (msPHGDH) PHGDH in *BRCA$^{fl/fl}$*; *Trp53$^{+/-}$* breast tumors described in Figure 4. The difference in huPHGDH expression is statistically significant with p = 0.0497 by an unpaired, two-tailed Welch's t test, and the difference in msPHGDH expression is not statistically significant, with p = 0.1101 by an unpaired, two-tailed Welch's t test. n=10 tumors per genotype **(B)** Representative immunohistochemistry staining for Ki67 in control and PHGDH^{tetO} *BRCA$^{fl/fl}$*; *Trp53$^{+/-}$* breast tumors. Images were obtained at 20x magnification, scale bar = 100 µm. Ki67 staining in an area of 1.5 mm by 0.7 mm was quantitated for 5 tumors of each genotype, and no statistically significant difference was observed based on a Welch's t test that yielded a p value of 0.6598. **(C)** Representative immunohistochemistry staining for cleaved caspase 3 (CC3) in control and *PHGDH^{tetO}*; *BRCA$^{fl/fl}$*; *Trp53$^{+/-}$* breast tumors. Images were obtained at 20x magnification, scale bar = 100 µm. CC3 staining was quantitated by scoring 300 cells as CC3 positive or negative for each of 5 tumors of each genotype. No statistically significant difference was observed based on a Welch's t test that yielded a p value of 0.7345. For all panels, the values represent the mean +/- SD.

In contrast, the maximal serine concentration available to tumors is likely bounded by the amount of serine in plasma, and could be further affected by impaired nutrient delivery (Farnsworth et al., 2014), as serine concentrations in the center of tumors are lower than in the outer regions (Pan et al., 2016). To determine whether serine availability could plausibly be

limiting for tumor growth under physiological conditions, the plasma serine concentration of fed C57BL/6J mice was measured, since C57BL/6J mice are the strain most similar to those used for the autochthonous melanoma and breast cancer models in this study. Plasma serine levels ranged from 92-314 μM (Figure 4D), values similar to the range of 53-262 μM reported for human plasma (Trabado et al., 2017). We examined whether culturing cells in the range of serine concentrations found in plasma affects proliferation of control and PHGDH-knockdown cells, and found that increased PHGDH expression provides a proliferative advantage only at lower serine concentrations (Figure 4E). These results suggest that serine availability could be an endogenous limitation for proliferation in some tissues with low serine availability.

Serine levels fluctuate in fed mice

The variability in plasma serine levels observed in both mouse and humans suggests that mammals do not actively maintain a constant serine levels in the blood; indeed, plasma serine concentrations in rats shift with diet (Kalhan et al., 2011). Another complication is that many mammals, including mice, do not continuously feed throughout the day (Anlinker and Mayer, 1956). Thus, fluctuations in plasma serine levels between meals, in addition to circadian effects on metabolic gene expression affecting nutrient levels in blood (Feng and Lazar, 2012), could lower serine in some tissues to levels where PHGDH expression might provide an advantage for proliferation. To characterize how plasma serine in mice varies with normal feeding patterns, plasma amino acid levels were measured over the course of a day in C57BL/6J and NOD.Cg-*Prkdc*^{scid} *Il2rg*^{tm1Wjl}/SzJ (NSG) mice that were either fed *ad libitum* or fasted. Serine levels were highest during daylight hours, and fell to fasting levels at 8 AM and 5 PM (Figure 4F).

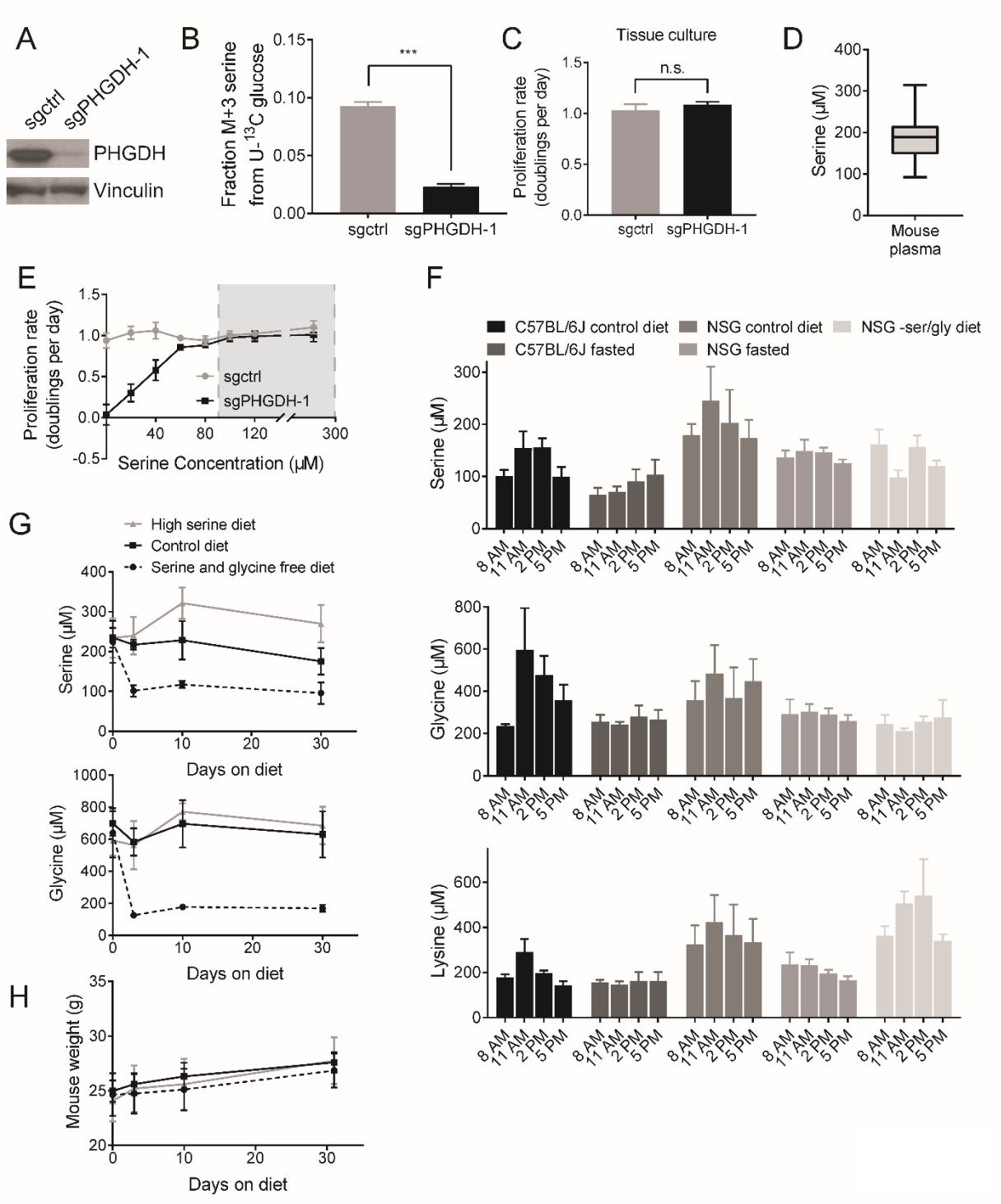
A
sgctrl
sgPHGDH-1
PHGDH
Vinculin
B
Fraction M+3 serine from U-13C glucose
0.15
0.10
0.05
0.00
***
sgctrl
sgPHGDH-1
C
Tissue culture
Proliferation rate (doublings per day)
1.5
1.0
0.5
0.0
n.s.
sgctrl
sgPHGDH-1
D
Serine (μM)
400
300
200
100
0
Mouse plasma
E
Proliferation rate (doublings per day)
1.5
1.0
0.5
0.0
-0.5
sgctrl
sgPHGDH-1
40
80
120
300
Serine Concentration (μM)
F
C57BL/6J control diet
NSG control diet
NSG -ser/gly diet
C57BL/6J fasted
NSG fasted
Serine (μM)
300
200
100
0
Glycine (μM)
800
600
400
200
0
Lysine (μM)
600
400
200
0
8 AM
11 AM
2 PM
5 PM
G
High serine diet
Control diet
Serine and glycine free diet
Serine (μM)
400
300
200
100
0
0
10
20
30
Days on diet
Glycine (μM)
1000
800
600
400
200
0
Days on diet
H
Mouse weight (g)
35
30
25
20
Days on diet

Figure 4. Physiological serine concentrations approach a range that is limiting for cell proliferation in culture. **(A)** Western blot showing CRISPRi-mediated knockdown of PHGDH expression in cells derived from an autochthonous breast tumor arising in a *BRCA*$^{fl/fl}$; *Trp53*$^{+/-}$; *MMTV-Cre* mouse. Cells with sgRNA targeting PHGDH (sgPHGDH-1) or a non-targeting sgRNA (sgctrl) are shown. **(B)** Fraction of ^{13}C-labeled serine (fully labeled, M+3) in control (sgctrl) or PHGDH knockdown (sgPHGDH-1) cells cultured in U-^{13}C glucose. The difference in the fraction of labeled serine between the cell types is significant ($p < 0.0001$) by an unpaired, Welch's t test. (**C)** Proliferation rate of control (sgctrl) and PHGDH knockdown (sgPHGDH-1) cells. There is no significant change in proliferation rate by unpaired, two-tailed Welch's t test ($p = 0.2820$). **(D)** Serine concentration in plasma of C57BL/6J mice collected at 11 AM. n=60 mice. **(E)** Proliferation rate of control (sgctrl) and PHGDH knockdown (sgPHGDH-1) breast cancer cells cultured in media containing the indicated amounts of serine. Grey box indicates the range of plasma serine concentrations measured in **(D)**. **(F)** Plasma serine, glycine, and lysine concentrations measured in the indicated mouse strains fed ad lib on a control diet, fasted starting at 5 AM, or fed a serine and glycine free diet for one week prior to measurement. Plasma was collected at the specified times. n=5 mice on each diet. **(G)** Plasma serine and glycine concentrations in C57BL/6J mice fed a serine and glycine free diet, a control diet, or a high serine diet for the indicated time. Plasma was collected at 11 AM. n=5 mice on each diet. **(H)** Mouse weight for animals fed a serine and glycine free diet, a control diet, or a high serine diet for the indicated time. n=5 mice on each diet.
Mean +/- SD is shown for all panels.

This pattern was also observed for other non-essential amino acids such as glycine as well as essential amino acids such as lysine (Figure 4F). These results indicate that serine levels available to tumors fluctuate and likely fall to near fasting levels for periods of the day, further suggesting that serine may be limiting for tumor growth in some contexts.

Diet can modulate plasma serine availability

In order to examine whether changes in serine availability can affect the rate of tumor growth, we sought to modulate the amount of serine that cancer cells can access in tumors. Previous work has shown that plasma serine levels can be diminished by a serine and glycine deficient diet, which slows the growth of certain tumor types (Maddocks et al., 2017; Maddocks et al., 2013). Glycine is removed from these diets because glycine and serine can be interconverted, and glycine deprivation ensures that animals are not able to synthesize serine from dietary glycine (Maddocks et al., 2017; Maddocks et al., 2013). Feeding mice an amino acid defined diet lacking both serine and glycine (Table 1) stably lowered plasma serine and glycine levels for at least 30 days on the diet (Figure 4G). Mice fed a serine and glycine free diet also display lower levels of plasma serine and glycine over the course of the day compared to control mice (Figure 4F). Conversely, plasma lysine levels are similar in mice fed either a control diet or a serine and glycine free diet (Figure 4F), suggesting that normal amino acid homeostasis is not globally altered. Serine levels can also be increased through dietary manipulation, as mice fed a high serine diet (Table 1) have higher serine levels in the plasma with no changes in glycine (Figure 4G). Neither of these diets altered mouse body weight (Figure 4H) or produced gross abnormalities in mouse behavior or appearance. Further, the serine and glycine free diet and the high serine diet stably hold plasma serine concentrations at the low and high end of the

Table 1. Nutrient composition of serine diets.

Nutrient	Serine and glycine free diet (g/kg)	Control diet (g/kg)	High serine diet (g/kg)
L-Alanine	3.5	3.5	3.5
L-Arginine HCl	12.1	12.1	12.1
L-Asparagine	6.0	6.0	6.0
L-Aspartic Acid	3.5	3.5	3.5
L-Cystine	3.5	3.5	3.5
L-Glutamic Acid	40.0	40.0	40.0
Glycine	0	23.3	23.3
L-Histidine HCl, monohydrate	4.5	4.5	4.5
L-Isoleucine	8.0	8.0	8.0
L-Leucine	12.0	12.0	12.0
L-Lysine HCl	18.0	18.0	18.0
L-Methionine	8.2	8.2	8.2
L-Phenylalanine	7.5	7.5	7.5
L-Proline	3.5	3.5	3.5
L-Serine	0	3.5	20.0
L-Threonine	8.2	8.2	8.2
L-Tryptophan	1.8	1.8	1.8
L-Tyrosine	5.0	5.0	5.0
L-Valine	8.0	8.0	8.0
Sucrose	100.0	100.0	100.0
Corn Starch	407.88	381.18	364.58
Maltodextrin	150.0	150.0	150.0
Soybean Oil	80.0	80.0	80.0
Cellulose	50.0	50.0	50.0
Mineral Mix, AIN-93M-MX (94049)	35.0	35.0	35.0
Calcium Phosphate, monobasic, monohydrate	8.2	8.2	8.2
Vitamin Mix, AIN-93-VX (94047)	13.0	13.0	13.0
Choline Bitartrate	2.5	2.5	2.5
TBHQ, antioxidant	0.02	0.02	0.02

normal physiological range, respectively. Thus, these diets can be used to examine the effects on tumor growth of having circulating serine levels that are at the high and low ends of the normal physiological range.

PHGDH provides serine to promote breast tumor growth in the mammary fat pad

To test whether PHGDH overcomes serine limitation in the breast microenvironment, cells from autochthonous breast tumors with or without PHGDH knockdown were orthotopically implanted into the mammary fat pads of NSG mice. The cells with PHGDH knockdown should retain lower serine synthesis pathway activity in tumors (Pacold et al., 2016). Under normal dietary serine conditions, tumors from control cells that express PHGDH (Figure 6A) grew more rapidly than tumors from PHGDH knockdown cells (Figure 5A). These data argue that PHGDH expression can promote tumor growth in the mammary fat pad. Tumors derived from control cells that express PHGDH were largely insensitive to dietary serine alterations (Figure 5B). In contrast, sgPHGDH tumors grew more slowly on a serine and glycine free diet (Figure 5C), suggesting that tumors with low PHGDH expression are sensitive to environmental serine levels. A second sgPHGDH cell line that had incomplete PHGDH knockdown (Figure 6A) was also sensitive to serine and glycine deprivation, but did not grow more rapidly on a high serine diet, suggesting that intermediate levels of PHGDH may be sufficient to sustain maximal growth on a control diet, but not on a serine and glycine free diet (Figure 6B). sgPHGDH tumors on a high serine diet grow at a similar rate to control tumors on a control diet, suggesting that the high serine diet was able to fully compensate for low PHGDH expression. Consistent with the idea that PHGDH helps tumors overcome serine limitation, serine and glycine levels were lower in sgPHGDH tumors than control tumors, while levels of

essential amino acids such as valine and leucine were unchanged (Figure 5D-E, Figure 6C). Though this result is consistent with altered serine availability in tumors depending on PHGDH expression level, it is important to note that these tumors had different proliferation rates, and thus may have consumed serine at different rates. Thus, steady state tumor serine levels may not fully reflect serine availability. Serine synthesis pathway activity can also produce α-ketoglutarate and 2-hydroxyglutarate, but levels of α-ketoglutarate and 2-hydroxyglutarate were similar in sgPHGDH and control tumors (Figure 5F-G). Together, these data argue that a major effect of increased PHGDH activity in these cancers is to buffer against fluctuations in serine availability, insulating tumor cells from the effects of serine limitation.

Serine availability may not be the same in all tissues. For instance, unlike breast tumors, tumors growing in the pancreas are not sensitive to dietary serine limitation (Maddocks et al., 2017). Consistent with the possibility that differences in serine levels could contribute to this phenomenon, the total tissue serine content is lower in the mammary fat pad than in other tissues, including pancreas (Figure 6E). Total tissue serine content includes both intracellular and extracellular serine and may not reflect differences in serine availability in the environment; nevertheless, to directly test whether tissue site affects dependence on PHGDH, cells derived from autochthonous breast tumors with or without PHGDH knockdown were implanted into the pancreata of NSG mice. Consistent with the pancreas being a more serine-replete environment than the mammary fat pad, mice with control or PHGDH knockdown cells implanted in the pancreas both succumb to pancreatic tumor burden with no statistically significant differences in survival (Figure 6F), suggesting that environmental serine availability may determine whether PHGDH expression promotes tumor growth.

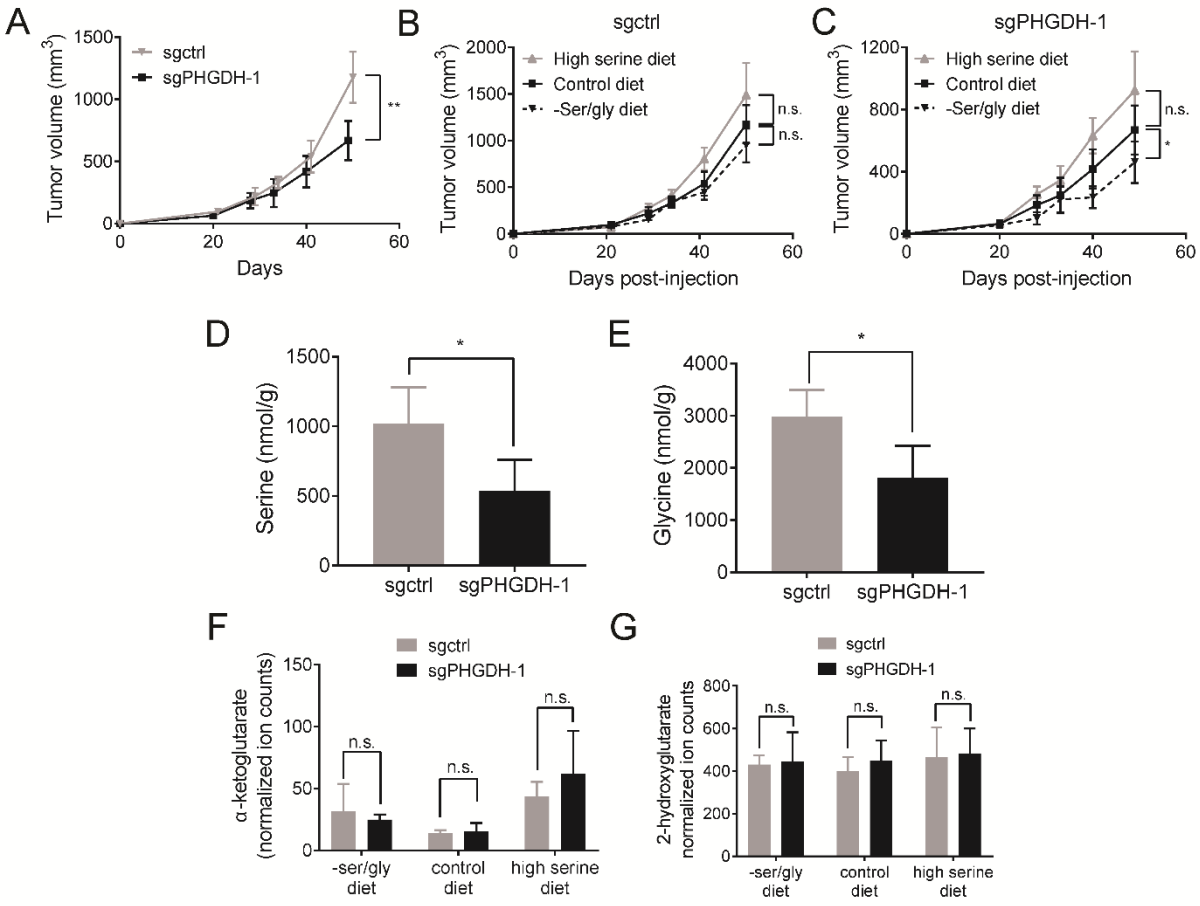
A
Tumor volume (mm3)
sgctrl
sgPHGDH-1
**
Days
B
sgctrl
High serine diet
Control diet
-Ser/gly diet
n.s.
n.s.
Tumor volume (mm3)
Days post-injection
C
sgPHGDH-1
High serine diet
Control diet
-Ser/gly diet
n.s.
*
Tumor volume (mm3)
Days post-injection
D
Serine (nmol/g)
*
sgctrl
sgPHGDH-1
E
Glycine (nmol/g)
*
sgctrl
sgPHGDH-1
F
α-ketoglutarate (normalized ion counts)
sgctrl
sgPHGDH-1
n.s.
n.s.
n.s.
-ser/gly diet
control diet
high serine diet
G
2-hydroxyglutarate normalized ion counts
sgctrl
sgPHGDH-1
n.s.
n.s.
n.s.
-ser/gly diet
control diet
high serine diet

Figure 5. PHGDH expression overcomes serine limitation in tumors growing in the mammary fat pad. (A) Breast cancer cells from a breast tumor arising in a *BRCA*$^{fl/fl}$; *Trp53*$^{+/-}$; *MMTV-Cre* mouse with either a non-targeting sgRNA (sgctrl) or an sgRNA targeting PHGDH (sgPHGDH-1) were injected into the mammary fat pad of female NSG mice fed a control diet. Tumor size over time is shown. Tumor size at the final time point is significantly different based on an unpaired, two-tailed Welch's t test (p = 0.0027). n=5 tumors per genotype. **(B)**-**(C)** Breast cancer cells from a breast tumor arising in *BRCA*$^{fl/fl}$; *Trp53*$^{+/-}$; *MMTV-Cre* mice with either a non-targeting sgRNA (sgctrl) **(B)** or an sgRNA targeting PHGDH (sgPHGDH-1) **(C)** were injected into the mammary fat pad of female NSG mice fed the indicated diets. Mice were fed the indicated diets starting the day that the cells were injected, and tumor size over time is shown. n=5 tumors per genotype. In **(B)**, by comparing all three diet conditions, there was no significant correlation between increased dietary serine and increased tumor volume by an ANOVA test for trend (p=0.0770). There was no significant difference in final tumor volume between mice fed –ser/gly, control, or high serine diets based on unpaired, two-tailed Welch's t tests for –ser/gly versus control (p=0.0986) and for control versus high serine diet (p=0.1217). In **(C)**, by comparing all three diet conditions, there was a significant correlation between increased dietary serine and increased tumor volume by an ANOVA test for trend (p = 0.0022). There was a significant difference in final tumor volume between mice fed –ser/gly and control diets based on an unpaired, two-tailed Welch's t test (p=0.0559). **(D)** Serine amount in control tumors (sgctrl) compared to PHGDH knockdown tumors (sgPHGDH-1). sgctrl tumors display a significant increase in serine concentration based on an unpaired, two-tailed Welch's t test (p=0.032). n=4 tumors per genotype. **(E)** Glycine amount in control tumors (sgctrl) compared to PHGDH knockdown tumors (sgPHGDH-1). sgctrl tumors display a significant increase in glycine concentration based on an unpaired, two-tailed Welch's t test (p=0.0332). n=4 tumors per genotype **(F)** Amount of α-ketoglutarate in control (sgctrl) and PHGDH knockdown (sgPHGDH-1) mammary fat pad orthotopic tumors in mice fed either a –ser/gly diet, a control diet, or a high serine diet as measured by LC/MS. No significant change in α-ketoglutarate levels were detected between sgctrl and sgPHGDH-1 tumors as determined by unpaired, two-tailed Welch's t tests (p=0.5917, 0.6834, and 0.2908, respectively). **(G)** Amount of 2-hydroxyglutarate in control (sgctrl) and PHGDH knockdown (sgPHGDH-1) mammary fat pad orthotopic tumors in mice fed either a –ser/gly diet, a control diet, or a high serine diet as measured by LC/MS. No significant change in 2-hydroxyglutarate levels were detected between sgctrl and sgPHGDH-1 tumors as determined by unpaired, two-tailed Welch's t tests (p=0.8387, 0.4603, and 0.8368, respectively). n=4 tumors per genotype.
Mean +/- SD is shown for all panels.

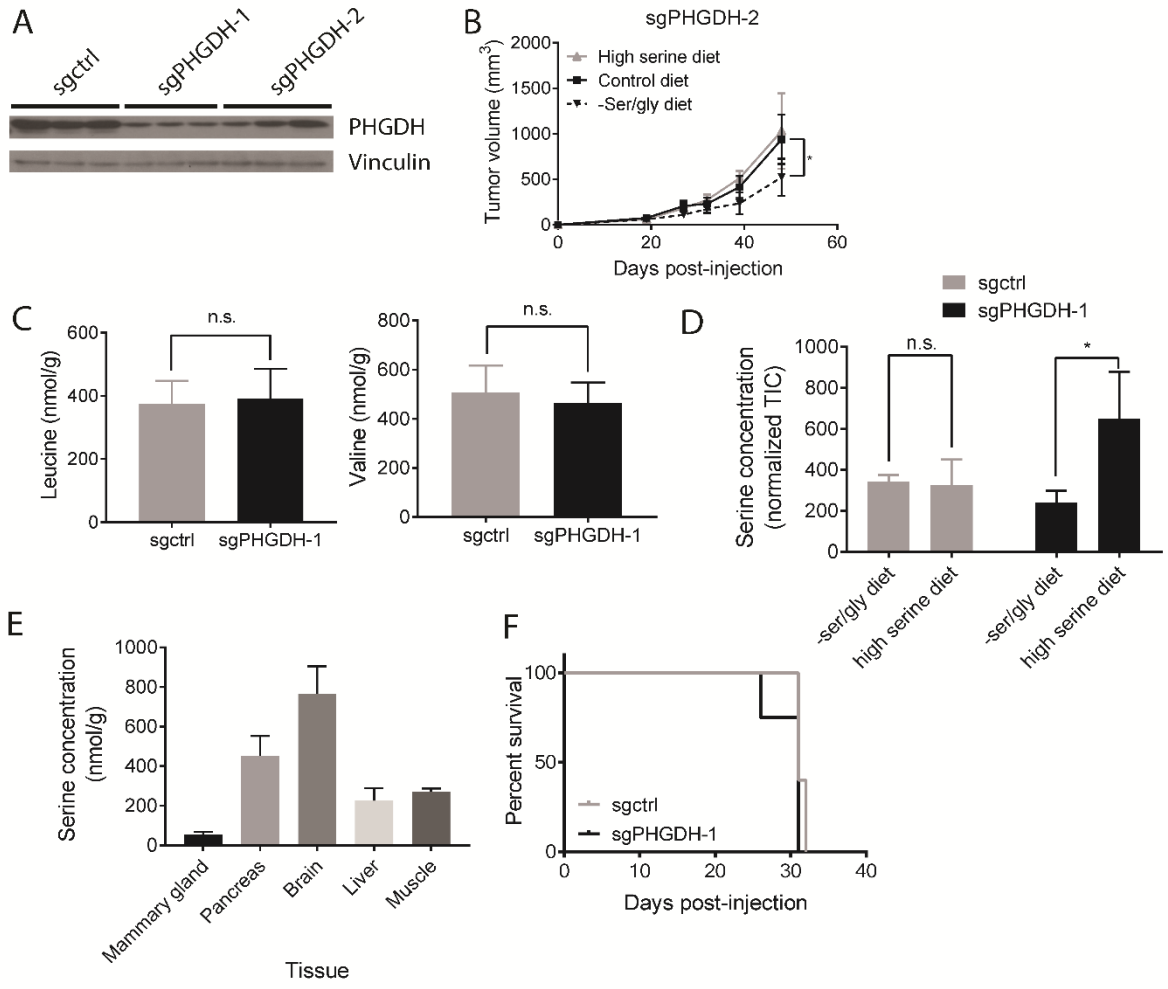
A
sgctrl
sgPHGDH-1
sgPHGDH-2
PHGDH
Vinculin
B
sgPHGDH-2
High serine diet
Control diet
-Ser/gly diet
Tumor volume (mm3)
Days post-injection
C
Leucine (nmol/g)
n.s.
sgctrl
sgPHGDH-1
Valine (nmol/g)
n.s.
sgctrl
sgPHGDH-1
D
sgctrl
sgPHGDH-1
Serine concentration (normalized TIC)
n.s.
*
-ser/gly diet
high serine diet
-ser/gly diet
high serine diet
E
Serine concentration (nmol/g)
Mammary gland
Pancreas
Brain
Liver
Muscle
Tissue
F
Percent survival
sgctrl
sgPHGDH-1
Days post-injection

Figure 6. Intermediate expression of PHGDH results in intermediate dependence on dietary serine for tumor growth. (A) Breast cancer cells from an autochthonous *BRCA*$^{fl/fl}$; *Trp53*$^{+/-}$ *MMTV-Cre* breast tumor with either a non-targeting sgRNA (sgctrl), or an sgRNA targeting PHGDH (sgPHGDH-1, sgPHGDH-2) were injected into the mammary fat pad of female NSG mice. Western blot analysis of PHGDH expression in tumors derived from these mice is shown. **(B)** Measurement of the tumor size over time in mice fed the specified diets, for tumors derived from injecting *BRCA*$^{fl/fl}$; *Trp53*$^{+/-}$ *MMTV-Cre* breast tumor cells with either a non-targeting sgRNA (sgctrl) or an sgRNA targeting PHGDH (sgPHGDH-2) into the mammary fat pad of female NSG mice. There was a statistically significant difference in final tumor volume between mice fed –ser/gly and control diets based on an unpaired, two-tailed Welch's t test which yielded a p value of 0.0345. n=5 mice on each diet. **(C)** Concentration of the essential amino acids leucine and valine in control tumors (sgctrl) compared to PHGDH knockdown tumors (sgPHGDH-1) as measured by GC/MS. There was no statistically significant change in leucine or valine concentration based on an unpaired, two-tailed Welch's t test that produced p values of 0.7919 for leucine and 0.5803 for valine. n=4 tumors for each genotype. **(D)** LC/MS measurement of total ion counts (TIC) of serine normalized to tumor weight in control (sgctrl) and PHGDH knockdown (sgPHGDH-1) mammary fat pad orthotopic tumors formed from murine cell lines in mice fed either a –ser/gly diet or a high serine diet. No statistically significant change in serine levels were detected between sgctrl tumors fed a –ser/gly diet or a high serine diet as determined by an unpaired, two-tailed Welch's t test that yielded a p value of 0.8208. There was a statistically significant difference in serine levels between sgPHGDH-1 tumors in mice fed either a –ser/gly diet or a high serine diet as determined by an unpaired, two-tailed Welch's t test that yielded a p value of 0.0134. n = 4 tumors for each genotype. **(E)** Total serine amount measured in tissues from C57BL/6J mice by GC/MS normalized to tissue weight. n = 4 mice for each tissue. **(F)** Kaplan-Meier plot showing survival of NSG mice for which the same number of control (sgctrl) or PHGDH knockdown (sgPHGDH-1) cells derived from autochthonous breast tumors were implanted into the pancreas. There was no statistically significant difference in survival based on a Mantel-Cox log-rank test with a p-value of 0.1050. n = 5 mice per condition. For all panels, the values represent the mean +/- SD.

To determine whether increased PHGDH expression in human cancer provides a similar advantage, we expressed PHGDH in MDA-MB-231 human triple negative breast cancer cells with low PHGDH expression that approximates levels in normal mammary glands (Figure 7A) (Mattaini et al., 2015; Possemato et al., 2011). Similar to the findings observed in murine breast cancer cells, PHGDH expression increases serine synthesis pathway activity (Figure 7B) and provides a proliferative advantage to MDA-MB-231 cells when serine levels are low (Figure 8A). To determine whether this proliferative advantage is retained in a physiological environment, MDA-MB-231 cells were injected orthotopically into the mammary fat pad of NSG mice. Tumors formed from PHGDH low control cells are sensitive to dietary serine and glycine deprivation, while tumors formed from PHGDH expressing cells better tolerate this condition. Further, PHGDH high cells deprived of dietary serine grow as rapidly as PHGDH low control tumors fed a serine replete diet (Figure 8B). The growth advantage conferred by PHGDH expression is dependent on PHGDH enzymatic activity, as expression of a dehydrogenase-dead R236E mutant of PHGDH does not alter tumor growth (Figure 7D). PHGDH expressing tumors also contained increased amounts of serine, with no significant change in glycine, α-ketoglutarate, or total 2-hydroxyglutarate levels (Figure 8C, Figure 7F-G). These results suggest that serine might be limiting for MDA-MB-231 mammary fat pad tumor growth even on a control diet. Consistent with this hypothesis, control xenografts in mice fed a high serine diet grew more rapidly than xenografts in mice fed a control diet (Figure 8D). Interestingly, PHGDH high xenografts in mice fed a control diet grew at the same rate as PHGDH low xenografts in mice fed a high serine diet, suggesting that either PHGDH expression or a high serine diet may be sufficient to overcome serine limitation. If so, combining PHGDH expression with a high serine

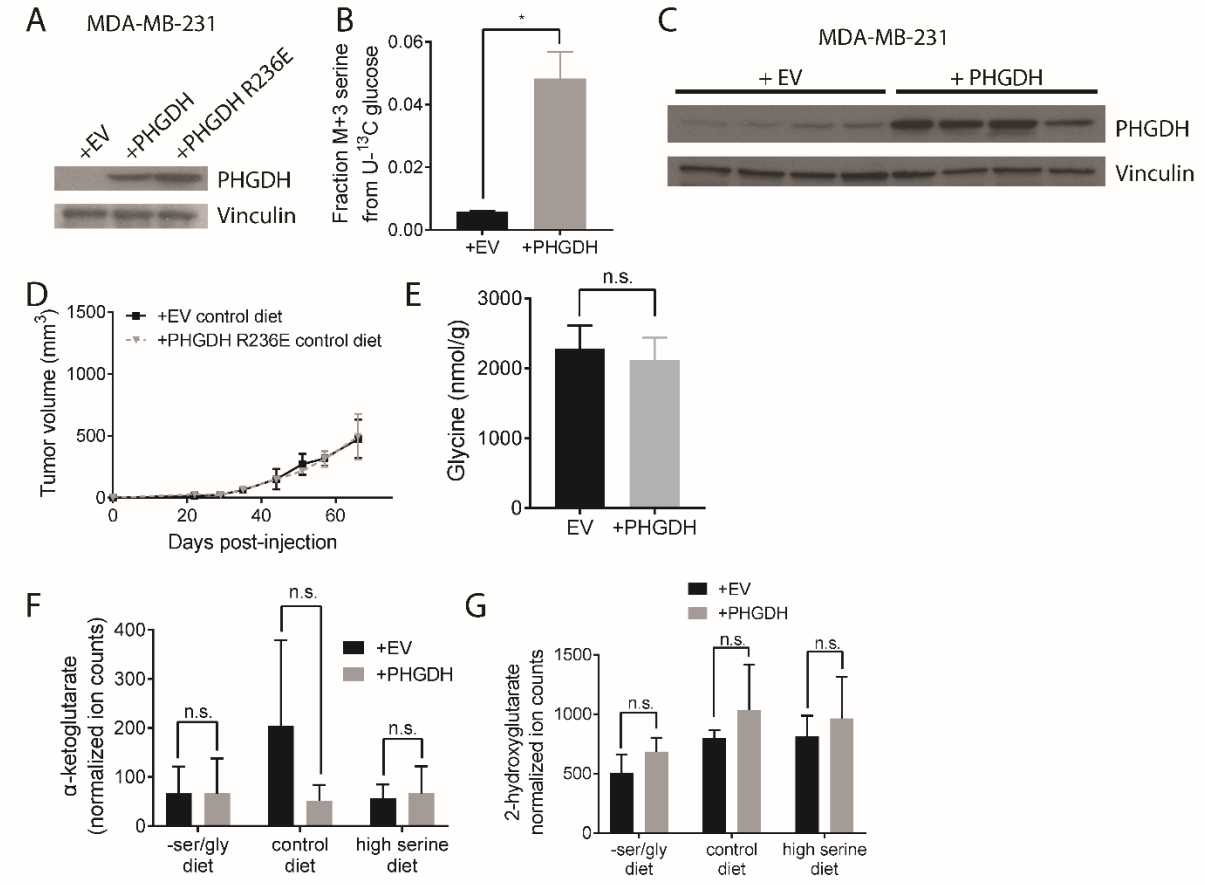
A
MDA-MB-231
+EV
+PHGDH
+PHGDH R236E
PHGDH
Vinculin
B
Fraction M+3 serine from U-13C glucose
0.06
0.04
0.02
0.00
*
+EV
+PHGDH
C
MDA-MB-231
+ EV
+ PHGDH
PHGDH
Vinculin
D
Tumor volume (mm3)
1500
1000
500
0
+EV control diet
+PHGDH R236E control diet
0
20
40
60
Days post-injection
E
Glycine (nmol/g)
3000
2000
1000
0
n.s.
EV
+PHGDH
F
α-ketoglutarate (normalized ion counts)
400
300
200
100
0
n.s.
n.s.
n.s.
+EV
+PHGDH
-ser/gly diet
control diet
high serine diet
G
2-hydroxyglutarate normalized ion counts
1500
1000
500
0
+EV
+PHGDH
n.s.
n.s.
n.s.
-ser/gly diet
control diet
high serine diet

Figure 7. PHGDH catalytic activity is required to increase serine synthesis and proliferation rate of human breast cancer cells. (A) Western blot of MDA-MB-231 breast cancer cell lines with an empty vector control (+EV), PHGDH (+PHGDH), or PHGDH with an R236E mutation (PHGDH R236E) cultured *in vitro*. **(B)** Fraction of ^{13}C-labeled serine (fully labeled, M+3) in in control (+EV) or PHGDH expressing (+PHGDH) MDA-MB-231 cells cultured in U-^{13}C glucose as measured by GC/MS. There is a statistically significant difference in the fraction of glucose-derived serine between the cell types with a p-value of 0.0130 derived from an unpaired, Welch's t test. (**C)** Western blot of PHGDH expression in empty vector control (+EV) and PHGDH expressing (+PHGDH) MDA-MB-231 mammary fat pad orthotopic tumors. **(D)** Empty vector control (+EV) or PHGDH R236E expressing (+PHGDH R236E) MDA-MB-231 breast cancer cells were injected into the mammary fat pad of female NSG mice fed a control diet. Tumor size over time is shown. n=5 mice for each genotype. **(E)** GC/MS measurement of glycine concentration in empty vector control (EV) and PHGDH expressing (+PHGDH) MDA-MB-231 mammary fat pad orthotopic tumors. No statistically significant change in glycine concentration was detected as determined by an unpaired, two-tailed Welch's t test that yielded a p value of 0.7330. **(F)** Amount of α-ketoglutarate in empty vector control (EV) and PHGDH expressing (+PHGDH) MDA-MB-231 mammary fat pad orthotopic tumors in mice fed either a –ser/gly diet, a control diet, or a high serine diet as measured by LC/MS. No statistically significant change in α-ketoglutarate levels were detected between +EV and +PHGDH tumors as determined by unpaired, two-tailed Welch's t tests that yielded p values of 0.9965, 0.1356, and 0.7359, respectively. **(G)** Amount of 2-hydroxyglutarate in empty vector control (EV) and PHGDH expressing (+PHGDH) MDA-MB-231 mammary fat pad orthotopic tumors in mice fed either a –ser/gly diet, a control diet, or a high serine diet as measured by LC/MS. No statistically significant change in 2-hydroxyglutarate levels were detected between +EV and +PHGDH tumors as determined by unpaired, two-tailed Welch's t tests that yielded p values of 0.0726, 0.2707, and 0.4290, respectively. n=5 tumors for each genotype for **(E)**, **(F)**, and **(G)**. For all panels, the values represent the mean +/- SD.

diet would provide no further advantage. Consistent with this hypothesis, PHGDH expressing tumors in mice on a high serine diet grow at the same rate as control xenografts in mice on a high serine diet, or PHGDH expressing tumors in mice on a control diet (Figure 8E). Taken together, these data argue that the benefits of PHGDH and a high serine diet are redundant. This supports the hypothesis that PHGDH promotes increased tumor growth by providing serine to cells in serine-limited tumor environments.

PHGDH supports serine-dependent biosynthetic processes

If tumors encounter serine deprivation under physiological conditions, biosynthetic processes that require serine may be perturbed. Serine is a donor of one-carbon units that are essential for downstream processes including nucleotide synthesis, lipid synthesis, and regeneration of SAM from SAH (Chiang et al., 1996; Lane and Fan, 2015), and all of these serine fates likely contribute to tumor growth. Multiple reactions in purine nucleotide synthesis require one-carbon units; one such reaction is the production of 5-formamidoimidazole-4-carboxamide ribonucleotide (FAICAR) production from 5-aminoimidazole-4-carboxamide ribonucleotide (AICAR) (Figure 8F). Thus, serine limitation in tumors could deplete one-carbon units and increase levels of AICAR relative to FAICAR. Indeed, the relative ratio of AICAR to FAICAR is higher in control MDA-MB-231 xenograft tumors than in tumors with high PHGDH expression (Figure 8G), consistent with the possibility that PHGDH expressing tumors are more capable of generating FAICAR. This effect is present both in mice fed a diet lacking serine and glycine and a control diet (Figure 8G), two contexts in which PHGDH expression promotes tumor growth (Figure 8D).

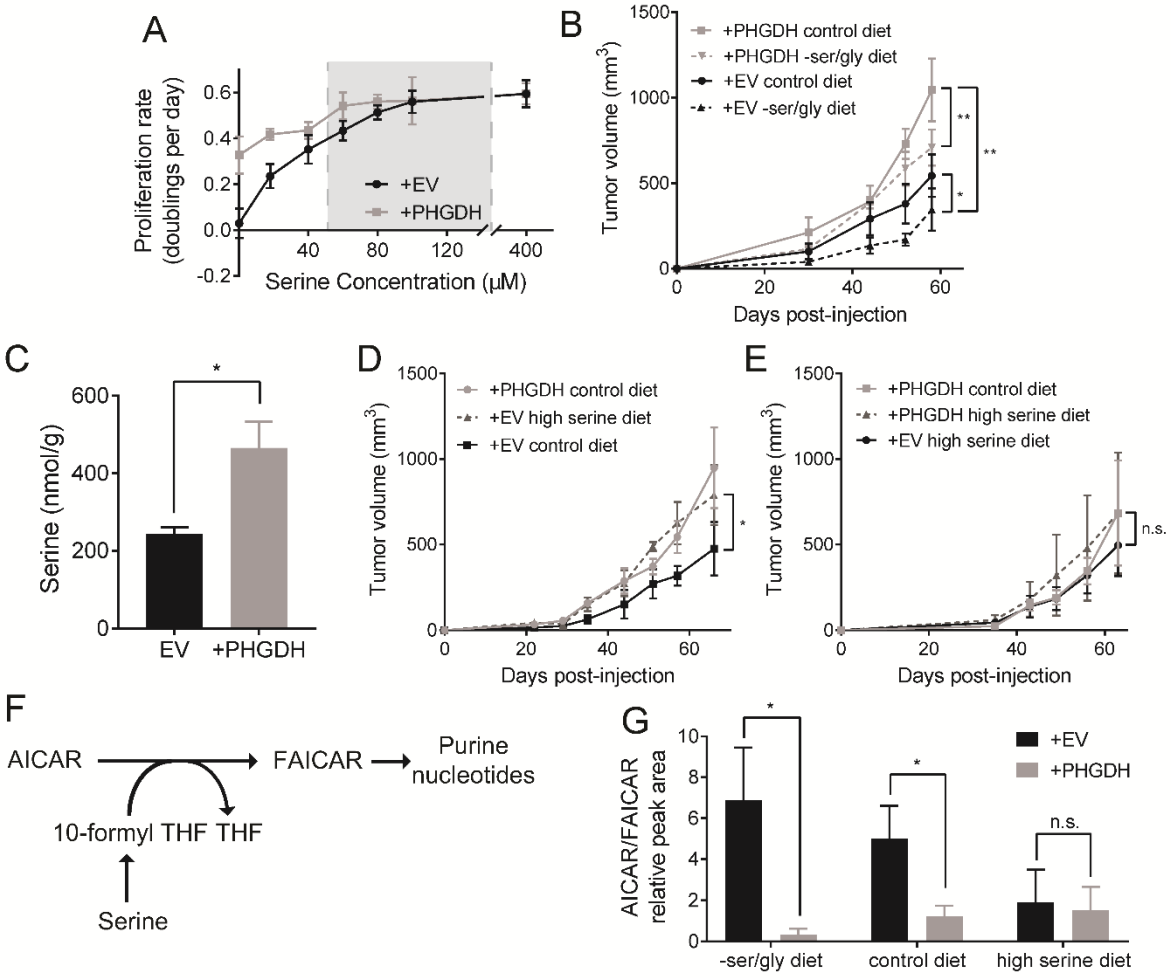
A
Proliferation rate (doublings per day)
0.6
0.4
0.2
0.0
-0.2
40
80
120
400
Serine Concentration (μM)
+EV
+PHGDH
B
Tumor volume (mm3)
1500
1000
500
0
0
20
40
60
Days post-injection
+PHGDH control diet
+PHGDH -ser/gly diet
+EV control diet
+EV -ser/gly diet
**
*
**
C
Serine (nmol/g)
600
400
200
0
*
EV
+PHGDH
D
Tumor volume (mm3)
1500
1000
500
0
0
20
40
60
Days post-injection
+PHGDH control diet
+EV high serine diet
+EV control diet
*
E
Tumor volume (mm3)
1500
1000
500
0
0
20
40
60
Days post-injection
+PHGDH control diet
+PHGDH high serine diet
+EV high serine diet
n.s.
F
AICAR
FAICAR
Purine nucleotides
10-formyl THF
THF
Serine
G
AICAR/FAICAR relative peak area
10
8
6
4
2
0
*
*
n.s.
+EV
+PHGDH
-ser/gly diet
control diet
high serine diet

Figure 8. **PHGDH expression provides serine to promote growth of human breast cancer xenografts. (A)** Proliferation rate of empty vector control (+EV) and PHGDH expressing (+PHGDH) MDA-MB-231 breast cancer cell lines cultured in media containing the indicated amounts of serine. Grey box indicates the reported range of plasma serine concentrations in humans (Trabado et al., 2017). **(B)** Empty vector control (+EV) or PHGDH expressing (+PHGDH) MDA-MB-231 breast cancer cells were injected into mammary fat pads of female NSG mice. Measurement of tumor size over time is shown for tumors derived from the indicated cells in mice fed the indicated diets starting the day that the cells were injected. There is a significant increase in tumor volume at the final time point between +PHGDH and +EV tumors in mice fed either a control diet or a –ser/gly diet based on unpaired, two-tailed Welch's t tests (p=0.0055 and 0.0012, respectively). There is a significant difference in final tumor volume between +EV tumors in mice fed a control diet versus a –ser/gly diet based on an unpaired, two-tailed Welch's t test (p=0.0510). n=5 mice for each combination of genotype and diet. **(C)** Serine concentration in empty vector control (EV) and PHGDH expressing (+PHGDH) MDA-MB-231 mammary fat pad orthotopic tumors. PHGDH expressing tumors displayed a significant increase in serine concentration as determined by an unpaired, two-tailed Welch's t test (p=0.0437). n=5 tumors for each genotype. **(D)-(E)** Empty vector control (+EV) or PHGDH expressing (+PHGDH) MDA-MB-231 breast cancer cells were injected into mammary fat pads of female NSG mice. Measurement of tumor size over time is shown for tumors derived from the indicated cells in mice fed the indicated diets starting the day that the cells were injected. There is a significant increase in tumor volume at the final time point between +EV tumors in mice fed either a control diet or a high serine diet based on an unpaired, two-tailed Welch's t test (p=0.0268). There is no significant difference in tumor volume at the final time point between +PHGDH control diet and +PHGDH high serine diet or between +EV high serine diet and +PHGDH high serine diet based on unpaired, two-tailed Welch's t tests (p=0.9977 and 0.3277, respectively). n=5 mice for each combination of genotype and diet. **(F)** Schematic with select intermediates in *de novo* purine nucleotide biosynthesis. THF: tetrahydrofolate. AICAR: 5-aminoimidazole-4-carboxamide ribonucleotide. FAICAR: 5-formamidoimidazole-4-carboxamide ribonucleotide. **(G)** Ratio of total ion counts of AICAR to FAICAR by LC/MS in empty vector control (EV) and PHGDH expressing (+PHGDH) MDA-MB-231 mammary fat pad orthotopic tumors in mice fed either a diet lacking serine and glycine (-ser/gly), a control diet, or a high serine diet. PHGDH expressing tumors in mice fed a diet lacking serine and glycine and in mice fed a control diet showed a significant decrease in relative AICAR/FAICAR ratio relative to control tumors as determined by an unpaired, two-tailed Welch's t test (p=0.0350 and 0.0419, respectively). There was no significant difference between the relative AICAR/FAICAR ratios in PHGDH expressing and control tumors derived from mice fed a high serine diet by an unpaired, two-tailed Welch's t test (p=0.859). n=4 tumors per genotype.
Mean +/- SD is shown for all panels.

In contrast, mice fed a high serine diet do not display a PHGDH-dependent effect on AICAR/FAICAR ratio (Figure 8G) or a PHGDH-dependent growth advantage (Figure 8E). These results indicate that serine-limited tumors are likely deficient in one-carbon units, which could contribute to slower proliferation. In support of this hypothesis, providing exogenous purines can promote cell proliferation in the absence of serine (Bao et al., 2016). In addition, either PHGDH expression or provision of a high serine diet mitigates alterations in the AICAR/FAICAR ratio, arguing that PHGDH expression benefits tumors by providing serine for biosynthetic processes that otherwise may be limiting for tumor growth.

DISCUSSION

Genetic events to increase PHGDH expression in cancer appear to be selected for because they allow faster cell proliferation in serine-limited tissue environments. Increasing the availability of serine through PHGDH expression or dietary changes provides a proliferative advantage to melanoma and breast cancer, arguing that serine availability may be low in tumors arising in these tissues. Further, though providing serine appears to underlie the benefit of PHGDH in these models, it may be that other tumor types or tumor locations are more limited by other processes; this could explain the serine-independent benefits that PHGDH expression provides in some contexts (Locasale et al., 2011; Mullarky et al., 2016; Pacold et al., 2016; Possemato et al., 2011). Of note, serine availability does not appear to be limiting in all tumors; some breast cancers express serine synthesis pathway enzymes at low levels (Possemato et al., 2011) and are not sensitive to loss of pathway activity (Pacold et al., 2016). Further, dietary serine deprivation does not inhibit mouse pancreatic ductal adenocarcinoma growth (Maddocks et al., 2017) and PHGDH expression does not affect the progression of

tumors derived from breast cells implanted into the pancreas. These observations support a model in which tumor growth in different tissue contexts is limited by the availability of different nutrients.

It is unclear whether serine limitation decreases tumor growth by impairing the activity of a particular biosynthetic pathway. Dissecting this question is complicated by the fact that providing one downstream product of serine metabolism, such as nucleotides or lipids, will allow the serine that would have been used to make these molecules to be available for use in other pathways. As such, each of the biosynthetic fates of serine likely contributes to the serine requirement in tumors. However, deficiency of specific metabolites derived from serine may select for serine synthesis pathway activation. Nucleotide deficiency has been linked to the development of oncogene-induced senescence (Aird et al., 2013), and PHGDH expression may allow cells with oncogene activation to maintain nucleotide levels during periods of serine deprivation and avoid senescence. Indeed, bypass of oncogene-induced senescence can be a barrier to melanoma initiation (Damsky et al., 2015), suggesting one way in which PHGDH expression could cooperate with *Braf* activation to promote melanoma. Serine availability for lipid synthesis may also select for serine synthesis pathway activation. Serine deprivation alters sphingolipid and ceramide metabolism (Gao et al., 2018), and these lipid species can affect cell proliferation and survival. For instance, sphingosine-1-phosphate negatively regulates apoptotic processes (Segui et al., 2006), and low serine can result in production of 1-deoxysphinganine, an error product that induces growth arrest (Esaki et al., 2015; Sayano et al., 2016). The requirement to sustain nucleotide and lipid metabolism may impose a selective pressure to maintain serine availability for cancer cells in certain tissues early in tumor development.

Therefore, cells that upregulate serine synthesis may be more capable of tumor initiation and progression because they can produce the various biomass components derived from serine.

Apart from potential effects on tumor initiation, serine availability may alter the apparent rate of tumor appearance. After tumor initiation, there is a period of proliferation that occurs before tumors are macroscopically detectable (Tubiana, 1989). Even for simultaneously initiated cancers, differences in serine availability could result in altered proliferation rates throughout early tumor progression that affect the time for a cancer to become clinically apparent. Thus, it could appear that higher serine diets promote cancer initiation, when in fact they affect the rate of cancer progression. Many studies to understand how diet affects cancer incidence are interpreted with respect to a risk of developing cancer; however, this study suggests that dietary alterations in nutrients levels could instead shorten the time for a cancer to become clinically apparent.

Serine availability is not the only metabolic parameter that can restrict tumor growth, and other metabolic pathways are likely selected for in response to low availability of microenvironmental nutrients. Which nutrients are most limiting for a given tumor is influenced by vascularization (Farnsworth et al., 2014), metabolic cooperation and competition with surrounding stromal and immune cells (Buck et al., 2017; Gupta et al., 2017), and nutrient scavenging ability (Recouvreux and Commisso, 2017). Furthermore, metabolite competition for membrane transport might affect nutrient uptake. As a consequence, plasma metabolite levels may not fully predict the capacity of tumors to obtain certain nutrients. The complex interplay between each of these factors could result in variability in which nutrients' availability restrains cancer cell proliferation, even within one tissue of origin. Determining which metabolites and

pathways are limiting for tumor growth has the potential to explain how cancer-associated genetic events arise and guide dietary interventions that reduce cancer progression.

MATERIALS AND METHODS

Mouse strains

PHGDH^{tetO} mice were generated as described in (Mattaini et al., 2018), with the *PHGDH^{tetO}* allele targeted to the ColA1 locus. *PHGDH^{tetO}* was expressed using a *R26-M2rtTA* unless otherwise noted. *Braf^{CA}; Tyr-CreER* and *Braf^{CA}; PTEN$^{fl/fl}$; Tyr-CreER* mice are described in (Dankort et al., 2009), and were of mixed C57BL/6J and 129S4/SvJaeJ background. *BRCA$^{fl/fl}$; Trp53$^{+/-}$; MMTV-Cre* mice are described in (Xu et al., 1999). All experiments utilizing *BRCA$^{fl/fl}$Trp53$^{+/-}$* mice also used an *MMTV-rtTA* (Whisenhunt et al., 2006) for mammary specific expression of PHGDH. Female NOD.Cg-*Prkdc^{scid} Il2rg^{tm1Wjl}*/SzJ (NSG) and male C57BL/6J mice were ordered from The Jackson Laboratory and were 12 weeks old at the time of experiments. All experiments were carried out in accordance with MIT Committee on Animal Care guidelines.

Cell lines

Cells were passaged in RPMI-1640 (Corning Life Sciences, Tewksbury, MA) with 10% fetal bovine serum (FBS) that had been heat inactivated for 30 min. at 56˚C (VWR Seradigm, Lot 120B14). All cells were cultured in a Heracell (Thermofisher) humidified incubators at 37˚C and 5% CO_2. MDA-MB-231 cells were obtained from ATCC (Manassas, VA) and are derived from a breast tumor in a female patient. A control autochthonous breast tumor from a female mouse

lacking the *PHGDH^{tetO}* allele was used to generate the murine breast cancer cells, and that cell line was genotyped to ensure that it lacked both *Brca1* and wild type *Trp53*.

Mouse procedures

Mice were housed in SPF facilities kept at 68-72 °F. For all experiments using *PHGDH^{tetO}* and control mice, all mice contained an rtTA and were treated with doxycycline; the only difference between experimental groups was the presence or absence of the *PHGDH^{tetO}* allele. *Braf^{CA};Tyr-CreER* mice were treated on days 3 and 5 after birth with 10 µL of 50 mg/mL 4-hydroxytamoxifen (Cayman Chemical, Ann Arbor, MI, 17308) dissolved in dimethylsulfoxide using a paintbrush to spread the 4-hydroxytamoxifen across the underside of the mouse. *Braf^{CA}; Tyr-CreER* mice were monitored for at least 1 year to determine if tumors developed. *Braf^{CA}; PTEN$^{fl/fl}$; Tyr-CreER* mice were depilated with Nair (Church & Dwight, Ewing Township, NJ) over a 1 cm^2 region in the lower center of the back, then treated the next day with 1 µL of 1.67 mg/mL 4-hydroxytamoxifen dissolved in 100% ethanol. Blood was collected from fed, anesthetized mice by retro-orbital bleeding at 11 AM unless otherwise indicated. Blood was placed directly into EDTA coated collection tubes (Sarstedt, Nümbrecht, Germany, 41.1395.105) and centrifuged 10’ at 845 x g; the supernatant of plasma was transferred to another tube. Mammary fat pad orthotopic injections were performed as described in (Kocaturk and Versteeg, 2015) with the following modifications: for experiments with the cell lines made from autochthonous breast tumors, 100,000 cells were injected in a volume of 100 µL phosphate buffered saline (PBS). For MDA-MB-231 experiments, 500,000 cells were injected in a volume of 100 µL PBS. For the experiment in Figure 8E, 200,000 cells were injected in a volume of 80 µL

PBS. All tumors were monitored by caliper measurements. Mice were de-identified so that caliper measurements were blinded. Tumor volume was calculated using the formula ½ (width^2 x length) and mice were euthanized when total tumor burden reached 1 cm^3. For pancreatic implantation of cells, 100,000 cells were suspended in 100 µL PBS and injected into the pancreas. Mice were euthanized according to institutional guidelines and survival time was recorded.

Diets

Doxycycline hyclate (625 mg/kg) was administered through the diet (Envigo, Huntingdon, United Kingdom, TD.01306), which was changed once per week. Serine and glycine free (TD.160752), control (TD.110839), and high serine (TD.160575) diets were purchased from Envigo. Diet formulations are listed in Table 1.

Western blotting

Tumor pieces were homogenized in 1 mL RIPA buffer [25 mM Tris-Cl, 150 mM NaCl, 0.5% sodium deoxycholate, 1% Triton X-100, 1x cOmplete protease inhibitor (Roche, Basel, Switzerland)] using a GentleMACS tissue homogenizer (Miltenyi Biotec, Bergisch Gladbach, Germany). For tissue culture cells, cells were scraped in 300 µL RIPA buffer. In each case, the resulting lysate was clarified by centrifugation at 21000 x g for 20 min. Protein concentration of the lysate was determined by BCA assay (Thermofisher). Lysates were resuspended at 1 mg/mL in Laemmli SDS-PAGE sample loading buffer (10% glycerol, 2% SDS, 60 mM Tris-Cl pH 6.8, 1% b-mercaptoethanol, 0.01% bromophenol blue) and denatured at 100˚C for 5 min. Extracts (30 µg

of protein) were resolved by SDS-PAGE using 12% acrylamide gels running at 120 V until the dye front left the gel. After SDS-PAGE resolution, protein extracts were transferred to nitrocellulose using an iBlot semi-dry transfer system (Thermofisher). Membranes were blocked in 5% non-fat dry milk, incubated in primary antibodies to PHGDH (Sigma-Aldrich, St. Louis, MO, HPA021241, 1:1000) or vinculin (Abcam, Cambridge, MA, ab18058, 1:250) and detected using HRP-conjugated secondary antibodies and chemiluminescence.

Histology

Tissues were fixed in 10% formalin (VWR, Radnor, PA, 48218-700) for 24 hours at room temperature, then stored in 70% ethanol until embedding in paraffin. For immunohistochemistry, antigen retrieval was performed at 97 °C for 20 minutes using pH 6.0 citrate buffer composed of 10 mM sodium citrate and 0.05% Tween 20. The following antibodies were used for immunohistochemistry: Sox10 (Santa Cruz Biotechnology, Dallas, TX, sc-17342, 1:100), PHGDH (Sigma-Aldrich, HPA021241, 1:2000), Ki67 (BD Biosciences, Franklin Lakes, NJ, 550609, 1:40), and cleaved caspase 3 (Cell Signaling Technology, Danvers, MA 9661S, 1:300). Slides were scanned using an Aperio slide scanner (Leica Biosystems, Wetzlar, Germany), and images were analyzed using Aperio ImageScope. Ki67 and PHGDH staining was quantitated using the Positive Pixel Counter v9 in Aperio ImageScope. For Ki67, a region of each tumor measuring 1.5 mm by 0.7 mm was quantitated at 10x magnification. For PHGDH, 5 mammary glands were quantitated per mouse at 20x magnification using a color threshold of 0.1. Cleaved caspase 3 staining was quantitated by scoring 300 cells per tumor as positive or negative. Samples were de-identified before all staining quantitation.

RT-qPCR

RNA was collected from tumors using Trizol reagent (Thermofisher, Waltham, MA). Tumor pieces were digested in 1 mL of Trizol using a GentleMACS tissue homogenizer and RNA was isolated according to standard protocol (Rio et al., 2010). cDNA was reverse transcribed using an iScript cDNA Synthesis Kit (Bio-Rad, Hercules, CA). RT-qPCR was performed with SYBR Green on a LightCycler 480 II machine (Roche). Primers used are described in (Mattaini et al., 2018).

CRISPR interference

CRISPR interference (Qi et al., 2013) knockdown of PHGDH was performed using the pLV hU6-sgRNA hUbC-dCas9-KRAB-T2a-Puro plasmid described in (Thakore et al., 2015) (Addgene plasmid # 71236). Guides were selected using algorithms developed in (Horlbeck et al., 2016; Sanson et al., 2018) and are listed in the Key Resources Table.

Cell culture and media

All cell lines were regularly tested for mycoplasma contamination using the Mycoprobe mycoplasma detection kit (R and D Systems, Minneapolis, MN). For experiments, cells were grown in RPMI-1640 with the indicated concentrations of serine with 10% FBS that has been dialyzed to remove small molecules. RPMI-1640 with varying levels of serine was made using the method outlined in (Muir et al., 2017). Briefly, enough of all of the components of RPMI-1640 media except for serine were weighed out to make 25 L of media, then the resulting powder was homogenized using an electric blade coffee grinder (Hamilton Beach, Glen Allen,

VA, 80365) that had been washed with methanol then water. The resulting powder was resuspended in water to make RPMI-1640 media lacking serine. Serine was dissolved in water to make 1000-fold concentrated stock solutions, then added back to RPMI-1640 media lacking serine to achieve the indicated concentrations of serine in RPMI. Cellular proliferation rate in different media conditions was determined as previously described (Sullivan et al., 2015). Briefly, cell lines proliferating in log phase in RPMI-1640 medium were trypsinized, counted and plated into six well dishes (Corning Life Sciences) in 2 mL of RPMI-1640 medium and incubated overnight. Initial seeding density was 40,000 cells/well. The next day, a six well plate of cells was trypsinized and counted to provide a number of cells at the start of the experiment. Cells were then washed twice with 2 mL of phosphate buffered saline (PBS), and 8 mL of the indicated media was added. This large volume of media was chosen to prevent nutrient depletion. Cells were then trypsinized and counted 4 days after adding the indicated media. Proliferation rate was determined using the following formula: Proliferation rate in doublings/day = [Log2(Final Day 4 cell count/Initial Day 0 cell count)]/4 days. Cells were counted using a Cellometer Auto T4 Plus Cell Counter (Nexcelom Bioscience, Lawrence, MA).

Generation of mouse tumor cell lines

A control autochthonous breast tumor arising in a female *BRCA*$^{fl/fl}$; *Trp53*$^{+/-}$; *MMTV-Cre* mouse lacking the *PHGDH*^{tetO} allele was disaggregated using dissecting scissors, then resuspended in 5 mL sterile PBS with 3 mg/mL dispase II (Roche), 1 mg/mL collagenase I (Worthington Biochemical, Lakewood, NJ), and 0.1 mg/mL DNase I (Sigma-Aldrich). This solution was incubated at 37 °C for 30 minutes, then EDTA was added to a final concentration of 10 mM to

stop the digestion reaction. The digested tumor was passed through a 70 µm cell strainer then washed twice with sterile PBS and plated in RPMI-1640. Genomic DNA was isolated from the cell line using a DNeasy Blood and Tissue Kit (Qiagen, Hilden, Germany) and genotyped using standard PCR methods (Mattaini et al., 2018; Xu et al., 1999) to ensure that cell lines were derived from tumor cells that had deleted *Brca1* and lacked any wild type *Trp53*.

Metabolite extraction

For analysis of mouse plasma, 5 µL of plasma was mixed with 5 µL of a standard composed of a ^{13}C amino acid mix (Cambridge Isotopes, Tewksbury, MA, MSK-A2-1.2) diluted to a concentration of 200 µM per amino acid in order to allow for absolute quantitation of amino acid levels. 600 µL 80% HPLC grade methanol (Sigma-Aldrich, 646377-4X4L) containing 1 µg norvaline (Sigma-Aldrich, N7627) per sample was added to each tube, vortexed for 10 minutes at 4 °C, then centrifuged at 21000 x g at 4°C for 10 minutes. 400 µL of sample was removed and dried under nitrogen. For analysis of tumor metabolites, tumors were snap-frozen in liquid nitrogen, then ground on liquid nitrogen using a mortar and pestle to obtain a homogenous powder. Approximately 10 mg of tumor powder was weighed, then 5 µL of a standard composed of a ^{13}C amino acid mix (Cambridge Isotopes, MSK-A2-1.2) diluted to a concentration of 200 µM per amino acid, 600 µL HPLC grade methanol, 300 µL HPLC grade water (Sigma-Aldrich), and 400 µL chloroform (Sigma-Aldrich) were added. Samples were vortexed for 10 minutes at 4 °C, then centrifuged at 21000 x g at 4°C for 10 minutes. 400 µL of the aqueous layer was removed and dried under nitrogen.

^{13}C-glucose tracing

For tracing of ^{13}C glucose into serine, 100,000 cells were plated per well in 6-well plates (Corning Life Sciences) and allowed to attach overnight. Cells were then switched to media containing uniformly labeled ^{13}C glucose (U-^{13}C glucose) in place of glucose. Cells were incubated for 24 hours in media containing ^{13}C glucose. On ice, culture media was aspirated and plates were washed three times with 150 mM NaCl. 600 µL of 80:20 HPLC grade methanol:HPLC grade water was added to each well, and cells were scraped using the top end of a pipette tip. The resulting liquid was transferred to an Eppendorf tube, vortexed for 10 minutes at 4 °C, then centrifuged at 21000 x g at 4°C for 10 minutes. 400 µL of the aqueous layer was removed and dried under nitrogen.

GC/MS

Polar metabolites were analyzed by GC-MS as described previously (Lewis et al., 2014). Dried and frozen metabolite extracts were derivatized with 16 mL MOX reagent (Thermofisher, TS-45950) for 60 min. at 37˚C. Samples were then derivatized with N-tertbutyldimethylsilyl-N-methyltrifluoroacetamide with 1% tert-butyldimethylchlorosilane (Sigma-Aldrich) 30 min. at 60˚C. Following derivatization, samples were analyzed by GC/MS, using a DB-35MS column (Agilent Technologies, Santa Clara, CA) installed in an Agilent 7890A gas chromatograph coupled to an Agilent 5997B mass spectrometer. Helium was used as the carrier gas at a flow rate of 1.2 mL/min. One microliter of sample was injected in split mode (all samples were split 1:1) at 270˚C. After injection, the GC oven was held at 100˚C for 1 min. and increased to 300˚C at 3.5 ˚C/min. The oven was then ramped to 320˚C at 20 ˚C/min. and held for 5 min. at this 320˚C. The MS system operated under electron impact ionization at 70 eV and the MS source

and quadrupole were held at 230˚C and 150˚C respectively. The detector was used in scanning mode, and the scanned ion range was 100–650 m/z. Mass isotopomer distributions were determined by integrating appropriate ion fragments for each metabolite (Lewis et al., 2014) using in-house software (Young et al., 2008) that corrects for natural abundance using previously described methods (Fernandez et al., 1996). Absolute quantitation of samples was obtained by comparing peak area for the ^{12}C amino acid with the peak area of the corresponding ^{13}C standard. α-ketoglutarate abundance was quantitated by normalizing the α-ketoglutarate peak area to a norvaline internal standard and to the weight of the tumor that was extracted for analysis.

LC/MS

Dried tumor extracts were resuspended in 100 µL HPLC grade water. LC-MS analysis was performed using a QExactive orbitrap mass spectrometer using an Ion Max source and heated electro- spray ionization (HESI) probe coupled to a Dionex Ultimate 3000 UPLC system (Thermofisher). External mass calibration was performed every 7 days. Samples were separated by chromatography by injecting 10 µL of sample on a SeQuant ZIC-pHILIC 2.1 mm x 150 mm (5 µm particle size) column. Flow rate was set to 150 mL/min. and temperatures were set to 25˚C for the column compartment and 4˚C for the autosampler tray. Mobile phase A was 20 mM ammonium carbonate, 0.1% ammonium hydroxide. Mobile phase B was 100% acetonitrile. The chromatographic gradient was: 0–20 min.: linear gradient from 80% to 20% mobile phase B; 20–20.5 min.: linear gradient from 20% to 80% mobile phase B; 20.5 to 28 min.: hold at 80% mobile phase B. The mass spectrometer was operated in full scan, polarity-switching mode and

the spray voltage was set to 3.0 kV, the heated capillary held at 275˚C, and the HESI probe was held at 350˚C. The sheath gas flow rate was 40 units, the auxiliary gas flow was 15 units and the sweep gas flow was one unit. The MS data acquisition was performed in a range of 70–1000 m/z, with the resolution set set at 70,000, the AGC target at $1x10^6$, and the maximum injection time at 20 msec. Relative quantitation of polar metabolites was performed with XCalibur QuanBrowser 2.2 (Thermo Fisher Scientific) using a 5 ppm mass tolerance and referencing an in-house library of chemical standards. Peak areas were normalized to tumor weight and ^{13}C-leucine standard peak area.

Quantification and statistical analysis

Survival of *Braf^{CA}; PTEN$^{fl/fl}$; Tyr-CreER* mice was compared using a stratified Cox proportional hazards model in order to test whether PHGDH expression scales up the relative hazard ratios in both male and female mice, which have different baseline hazards in this model. Survival of *BRCA$^{fl/fl}$; Trp53$^{+/-}$* mice was compared using a Mantel-Cox log-rank test. Mice were excluded from survival studies if they displayed non-tumor related health problems. No other data was excluded from the study. All further statistical information is described in the figure legends.

ACKNOWLEDGEMENTS

We thank Jen Sinnott for assistance with statistical analysis, and the Koch Institute Swanson Biotechnology Center for technical support, specifically Kathy Cormier. K.R.M. was supported by NSF Graduate Research Fellowship DGE-1122374. K.R.M. and M.R.S. were supported by T32-GM007287, and M.R.S. acknowledges support from an MIT Koch Institute Graduate Fellowship. A.M. was supported by F32CA213810. M.G.V.H. acknowledges support from R21CA198028, R01CA168653, the MIT Ludwig Center, the MIT Center for Precision Cancer Medicine, SU2C, the Lustgarten Foundation, and a Faculty Scholar Grant from HHMI.

AUTHOR CONTRIBUTIONS

Conceptualization, M.R.S., K.R.M., and M.G.V.H.; Methodology, M.R.S., K.R.M., E.A.D., K.M., M.W.B., and C.A.L.; Formal Analysis, M.R.S. and K.R.M.; Investigation, M.R.S., K.R.M., E.A.D, A.A.N., M.F.R., A.M., and A.M.D.; Resources, M.W.B. and C.A.L.; Writing – Original Draft, M.R.S.; Writing – Review & Editing, M.R.S., K.R.M., A.M., A.M.D., C.A.L., M.G.V.H.; Funding Acquisition, M.G.V.H.

REFERENCES

Adams, C.M. (2007). Role of the transcription factor ATF4 in the anabolic actions of insulin and the anti-anabolic actions of glucocorticoids. J Biol Chem *282*, 16744-16753.

Aird, K.M., Zhang, G., Li, H., Tu, Z., Bitler, B.G., Garipov, A., Wu, H., Wei, Z., Wagner, S.N., Herlyn, M.*, et al.* (2013). Suppression of nucleotide metabolism underlies the establishment and maintenance of oncogene-induced senescence. Cell Rep *3*, 1252-1265.

Anlinker, J., and Mayer, J. (1956). An Operant Conditioning Technique for Studying Feeding-Fasting Patterns in Normal and Obese Mice. Journal of Applied Physiology *8*, 667-670.

Bao, X.R., Ong, S.E., Goldberger, O., Peng, J., Sharma, R., Thompson, D.A., Vafai, S.B., Cox, A.G., Marutani, E., Ichinose, F.*, et al.* (2016). Mitochondrial dysfunction remodels one-carbon metabolism in human cells. Elife *5*.

Ben-Sahra, I., Hoxhaj, G., Ricoult, S.J.H., Asara, J.M., and Manning, B.D. (2016). mTORC1 induces purine synthesis through control of the mitochondrial tetrahydrofolate cycle. Science *351*, 728-733.

Buck, M.D., Sowell, R.T., Kaech, S.M., and Pearce, E.L. (2017). Metabolic Instruction of Immunity. Cell *169*, 570-586.

Chen, J.Y., Chung, F., Yang, G.Z., Pu, M.Y., Gao, H., Jiang, W., Yin, H., Capka, V., Kasibhatla, S., Laffitte, B.*, et al.* (2013). Phosphoglycerate dehydrogenase is dispensable for breast tumor maintenance and growth. Oncotarget *4*, 2502-2511.

Chiang, P.K., Gordon, R.K., Tal, J., Zeng, G.C., Doctor, B.P., Pardhasaradhi, K., and McCann, P.P. (1996). S-Adenosylmethionine and methylation. FASEB J *10*, 471-480.

Chin, L. (2003). The genetics of malignant melanoma: lessons from mouse and man. Nat Rev Cancer *3*, 559-570.

Damsky, W., Micevic, G., Meeth, K., Muthusamy, V., Curley, D.P., Santhanakrishnan, M., Erdelyi, I., Platt, J.T., Huang, L., Theodosakis, N.*, et al.* (2015). mTORC1 activation blocks BrafV600E-induced growth arrest but is insufficient for melanoma formation. Cancer Cell *27*, 41-56.

Dankort, D., Curley, D.P., Cartlidge, R.A., Nelson, B., Karnezis, A.N., Damsky, W.E., Jr., You, M.J., DePinho, R.A., McMahon, M., and Bosenberg, M. (2009). Braf(V600E) cooperates with Pten loss to induce metastatic melanoma. Nat Genet *41*, 544-552.

DeNicola, G.M., Chen, P.H., Mullarky, E., Sudderth, J.A., Hu, Z., Wu, D., Tang, H., Xie, Y., Asara, J.M., Huffman, K.E.*, et al.* (2015). NRF2 regulates serine biosynthesis in non-small cell lung cancer. Nat Genet *47*, 1475-1481.

Ding, J., Li, T., Wang, X., Zhao, E., Choi, J.H., Yang, L., Zha, Y., Dong, Z., Huang, S., Asara, J.M.*, et al.* (2013). The histone H3 methyltransferase G9A epigenetically activates the serine-glycine synthesis pathway to sustain cancer cell survival and proliferation. Cell Metab *18*, 896-907.

Esaki, K., Sayano, T., Sonoda, C., Akagi, T., Suzuki, T., Ogawa, T., Okamoto, M., Yoshikawa, T., Hirabayashi, Y., and Furuya, S. (2015). L-Serine Deficiency Elicits Intracellular Accumulation of Cytotoxic Deoxysphingolipids and Lipid Body Formation. J Biol Chem *290*, 14595-14609.

Fan, J., Teng, X., Liu, L., Mattaini, K.R., Looper, R.E., Vander Heiden, M.G., and Rabinowitz, J.D. (2015). Human phosphoglycerate dehydrogenase produces the oncometabolite D-2-hydroxyglutarate. ACS Chem Biol *10*, 510-516.

Farnsworth, R.H., Lackmann, M., Achen, M.G., and Stacker, S.A. (2014). Vascular remodeling in cancer. Oncogene *33*, 3496-3505.

Feng, D., and Lazar, M.A. (2012). Clocks, metabolism, and the epigenome. Mol Cell *47*, 158-167.

Fernandez, C.A., DesRosiers, C., Previs, S.F., David, F., and Brunengraber, H. (1996). Correction of C-13 mass isotopomer distributions for natural stable isotope abundance. Journal of Mass Spectrometry *31*, 255-262.

Gao, X., Lee, K., Reid, M.A., Sanderson, S.M., Qiu, C., Li, S., Liu, J., and Locasale, J.W. (2018). Serine Availability Influences Mitochondrial Dynamics and Function through Lipid Metabolism. Cell Rep *22*, 3507-3520.

Gupta, S., Roy, A., and Dwarakanath, B.S. (2017). Metabolic Cooperation and Competition in the Tumor Microenvironment: Implications for Therapy. Front Oncol *7*, 68.

Hausinger, R.P. (2004). FeII/alpha-ketoglutarate-dependent hydroxylases and related enzymes. Crit Rev Biochem Mol Biol *39*, 21-68.

Horlbeck, M.A., Gilbert, L.A., Villalta, J.E., Adamson, B., Pak, R.A., Chen, Y., Fields, A.P., Park, C.Y., Corn, J.E., Kampmann, M.*, et al.* (2016). Compact and highly active next-generation libraries for CRISPR-mediated gene repression and activation. Elife *5*.

Hosios, A.M., Hecht, V.C., Danai, L.V., Johnson, M.O., Rathmell, J.C., Steinhauser, M.L., Manalis, S.R., and Vander Heiden, M.G. (2016). Amino Acids Rather than Glucose Account for the Majority of Cell Mass in Proliferating Mammalian Cells. Dev Cell *36*, 540-549.

Hwang, I.Y., Kwak, S., Lee, S., Kim, H., Lee, S.E., Kim, J.H., Kim, Y.A., Jeon, Y.K., Chung, D.H., Jin, X.*, et al.* (2016). Psat1-Dependent Fluctuations in alpha-Ketoglutarate Affect the Timing of ESC Differentiation. Cell Metab *24*, 494-501.

Kalhan, S.C., Uppal, S.O., Moorman, J.L., Bennett, C., Gruca, L.L., Parimi, P.S., Dasarathy, S., Serre, D., and Hanson, R.W. (2011). Metabolic and genomic response to dietary isocaloric protein restriction in the rat. J Biol Chem *286*, 5266-5277.

Kocaturk, B., and Versteeg, H.H. (2015). Orthotopic injection of breast cancer cells into the mammary fat pad of mice to study tumor growth. J Vis Exp.

Labuschagne, C.F., van den Broek, N.J., Mackay, G.M., Vousden, K.H., and Maddocks, O.D.K. (2014). Serine, but not glycine, supports one-carbon metabolism and proliferation of cancer cells. Cell Rep *7*, 1248-1258.

Lane, A.N., and Fan, T.W. (2015). Regulation of mammalian nucleotide metabolism and biosynthesis. Nucleic Acids Res *43*, 2466-2485.

Lewis, C.A., Parker, S.J., Fiske, B.P., McCloskey, D., Gui, D.Y., Green, C.R., Vokes, N.I., Feist, A.M., Vander Heiden, M.G., and Metallo, C.M. (2014). Tracing compartmentalized NADPH metabolism in the cytosol and mitochondria of mammalian cells. Mol Cell *55*, 253-263.

Li, S., Swanson, S.K., Gogol, M., Florens, L., Washburn, M.P., Workman, J.L., and Suganuma, T. (2015). Serine and SAM Responsive Complex SESAME Regulates Histone Modification Crosstalk by Sensing Cellular Metabolism. Mol Cell *60*, 408-421.

Locasale, J.W., Grassian, A.R., Melman, T., Lyssiotis, C.A., Mattaini, K.R., Bass, A.J., Heffron, G., Metallo, C.M., Muranen, T., Sharfi, H.*, et al.* (2011). Phosphoglycerate dehydrogenase diverts glycolytic flux and contributes to oncogenesis. Nat Genet *43*, 869-874.

Ma, E.H., Bantug, G., Griss, T., Condotta, S., Johnson, R.M., Samborska, B., Mainolfi, N., Suri, V., Guak, H., Balmer, M.L.*, et al.* (2017). Serine Is an Essential Metabolite for Effector T Cell Expansion. Cell Metab *25*, 345-357.

Maddocks, O.D.K., Athineos, D., Cheung, E.C., Lee, P., Zhang, T., van den Broek, N.J.F., Mackay, G.M., Labuschagne, C.F., Gay, D., Kruiswijk, F.*, et al.* (2017). Modulating the therapeutic response of tumours to dietary serine and glycine starvation. Nature *544*, 372-376.

Maddocks, O.D.K., Berkers, C.R., Mason, S.M., Zheng, L., Blyth, K., Gottlieb, E., and Vousden, K.H. (2013). Serine starvation induces stress and p53-dependent metabolic remodelling in cancer cells. Nature *493*, 542-546.

Mattaini, K.R., Brignole, E.J., Kini, M., Davidson, S.M., Fiske, B.P., Drennan, C.L., and Vander Heiden, M.G. (2015). An epitope tag alters phosphoglycerate dehydrogenase structure and impairs ability to support cell proliferation. Cancer Metab *3*, 5.

Mattaini, K.R., Sullivan, M.R., Lau, A.N., Fiske, B.P., Bronson, R.T., and Vander Heiden, M.G. (2018). Increased PHGDH expression uncouples hair follicle cycle progression and promotes inappropriate melanin accumulation. BioRxiv pre-print. https://doi.org/10.1101/249250

Muir, A., Danai, L.V., Gui, D.Y., Waingarten, C.Y., Lewis, C.A., and Vander Heiden, M.G. (2017). Environmental cystine drives glutamine anaplerosis and sensitizes cancer cells to glutaminase inhibition. Elife *6*.

Mullarky, E., Lucki, N.C., Beheshti Zavareh, R., Anglin, J.L., Gomes, A.P., Nicolay, B.N., Wong, J.C., Christen, S., Takahashi, H., Singh, P.K.*, et al.* (2016). Identification of a small molecule inhibitor of 3-phosphoglycerate dehydrogenase to target serine biosynthesis in cancers. Proc Natl Acad Sci U S A *113*, 1778-1783.

Mullen, T.D., Hannun, Y.A., and Obeid, L.M. (2012). Ceramide synthases at the centre of sphingolipid metabolism and biology. Biochem J *441*, 789-802.

Newman, A.C., and Maddocks, O.D.K. (2017). Serine and Functional Metabolites in Cancer. Trends Cell Biol *27*, 645-657.

Nilsson, L.M., Forshell, T.Z., Rimpi, S., Kreutzer, C., Pretsch, W., Bornkamm, G.W., and Nilsson, J.A. (2012). Mouse genetics suggests cell-context dependency for Myc-regulated metabolic enzymes during tumorigenesis. PLoS Genet *8*, e1002573.

Ou, Y., Wang, S.J., Jiang, L., Zheng, B., and Gu, W. (2015). p53 Protein-mediated regulation of phosphoglycerate dehydrogenase (PHGDH) is crucial for the apoptotic response upon serine starvation. J Biol Chem *290*, 457-466.

Pacold, M.E., Brimacombe, K.R., Chan, S.H., Rohde, J.M., Lewis, C.A., Swier, L.J., Possemato, R., Chen, W.W., Sullivan, L.B., Fiske, B.P.*, et al.* (2016). A PHGDH inhibitor reveals coordination of serine synthesis and one-carbon unit fate. Nat Chem Biol *12*, 452-458.

Pan, M., Reid, M.A., Lowman, X.H., Kulkarni, R.P., Tran, T.Q., Liu, X., Yang, Y., Hernandez-Davies, J.E., Rosales, K.K., Li, H.*, et al.* (2016). Regional glutamine deficiency in tumours promotes dedifferentiation through inhibition of histone demethylation. Nat Cell Biol *18*, 1090-1101.

Pavlova, N.N., and Thompson, C.B. (2016). The Emerging Hallmarks of Cancer Metabolism. Cell Metab *23*, 27-47.

Possemato, R., Marks, K.M., Shaul, Y.D., Pacold, M.E., Kim, D., Birsoy, K., Sethumadhavan, S., Woo, H.K., Jang, H.G., Jha, A.K.*, et al.* (2011). Functional genomics reveal that the serine synthesis pathway is essential in breast cancer. Nature *476*, 346-350.

Qi, L.S., Larson, M.H., Gilbert, L.A., Doudna, J.A., Weissman, J.S., Arkin, A.P., and Lim, W.A. (2013). Repurposing CRISPR as an RNA-guided platform for sequence-specific control of gene expression. Cell *152*, 1173-1183.

Recouvreux, M.V., and Commisso, C. (2017). Macropinocytosis: A Metabolic Adaptation to Nutrient Stress in Cancer. Front Endocrinol (Lausanne) *8*, 261.

Rio, D.C., Ares, M., Jr., Hannon, G.J., and Nilsen, T.W. (2010). Purification of RNA using TRIzol (TRI reagent). Cold Spring Harb Protoc *2010*, pdb prot5439.

Samanta, D., Park, Y., Andrabi, S.A., Shelton, L.M., Gilkes, D.M., and Semenza, G.L. (2016). PHGDH Expression Is Required for Mitochondrial Redox Homeostasis, Breast Cancer Stem Cell Maintenance, and Lung Metastasis. Cancer Res *76*, 4430-4442.

Sanson, K.R., Hanna, R.E., Hegde, M., Donovan, K.F., Strand, C., Sullender, M.E., Vaimberg, E.W., Goodale, A., Root, D.E., Piccioni, F.*, et al.* (2018). Optimized libraries for CRISPR-Cas9 genetic screens with multiple modalities. Nat Commun *9*, 5416.

Sayano, T., Kawano, Y., Kusada, W., Arimoto, Y., Esaki, K., Hamano, M., Udono, M., Katakura, Y., Ogawa, T., Kato, H.*, et al.* (2016). Adaptive response to l-serine deficiency is mediated by p38 MAPK activation via 1-deoxysphinganine in normal fibroblasts. FEBS Open Bio *6*, 303-316.

Segui, B., Andrieu-Abadie, N., Jaffrezou, J.P., Benoist, H., and Levade, T. (2006). Sphingolipids as modulators of cancer cell death: potential therapeutic targets. Biochim Biophys Acta *1758*, 2104-2120.

Sullivan, L.B., Gui, D.Y., Hosios, A.M., Bush, L.N., Freinkman, E., and Vander Heiden, M.G. (2015). Supporting Aspartate Biosynthesis Is an Essential Function of Respiration in Proliferating Cells. Cell *162*, 552-563.

Thakore, P.I., D'Ippolito, A.M., Song, L., Safi, A., Shivakumar, N.K., Kabadi, A.M., Reddy, T.E., Crawford, G.E., and Gersbach, C.A. (2015). Highly specific epigenome editing by CRISPR-Cas9 repressors for silencing of distal regulatory elements. Nat Methods *12*, 1143-1149.

Trabado, S., Al-Salameh, A., Croixmarie, V., Masson, P., Corruble, E., Feve, B., Colle, R., Ripoll, L., Walther, B., Boursier-Neyret, C.*, et al.* (2017). The human plasma-metabolome: Reference values in 800 French healthy volunteers; impact of cholesterol, gender and age. PLoS One *12*, e0173615.

Tubiana, M. (1989). Tumor Cell Proliferation Kinetics and Tumor Growth Rate. Acta Oncologica *28*, 113-121.

Vance, J.E., and Tasseva, G. (2013). Formation and function of phosphatidylserine and phosphatidylethanolamine in mammalian cells. Biochim Biophys Acta *1831*, 543-554.

Vander Heiden, M.G., and DeBerardinis, R.J. (2017). Understanding the Intersections between Metabolism and Cancer Biology. Cell *168*, 657-669.

Whisenhunt, T.R., Yang, X., Bowe, D.B., Paterson, A.J., Van Tine, B.A., and Kudlow, J.E. (2006). Disrupting the enzyme complex regulating O-GlcNAcylation blocks signaling and development. Glycobiology *16*, 551-563.

Xu, X., Wagner, K.U., Larson, D., Weaver, Z., Li, C., Ried, T., Hennighausen, L., Wynshaw-Boris, A., and Deng, C.X. (1999). Conditional mutation of Brca1 in mammary epithelial cells results in blunted ductal morphogenesis and tumour formation. Nat Genet *22*, 37-43.

Ye, D., Guan, K.L., and Xiong, Y. (2018). Metabolism, Activity, and Targeting of D- and L-2-Hydroxyglutarates. Trends Cancer *4*, 151-165.

Young, J.D., Walther, J.L., Antoniewicz, M.R., Yoo, H., and Stephanopoulos, G. (2008). An elementary metabolite unit (EMU) based method of isotopically nonstationary flux analysis. Biotechnol Bioeng *99*, 686-699.

Zambrowicz, B.P., Imamoto, A., Fiering, S., Herzenberg, L.A., Kerr, W.G., and Soriano, P. (1997). Disruption of overlapping transcripts in the ROSA beta geo 26 gene trap strain leads to widespread expression of beta-galactosidase in mouse embryos and hematopoietic cells. Proc Natl Acad Sci U S A *94*, 3789-3794.

CHAPTER THREE: Methionine synthase is essential for cell proliferation in environments with physiological folates

Mark R. Sullivan[1,2], Montana F. Reilly[1,2], Alicia M. Darnell[1,2], Caroline A. Lewis[3], Matthew G. Vander Heiden[1,2,4,5]

[1]Koch Institute for Integrative Cancer Research and [2]Department of Biology, Massachusetts Institute of Technology, Cambridge, Massachusetts 02139, USA
[3]Whitehead Institute for Biomedical Research, Cambridge, MA 02139, USA
[4]Dana-Farber Cancer Institute, Boston, Massachusetts 02215, USA
[5]Broad Institute, Cambridge, Massachusetts 02139, USA

ABSTRACT

Methionine synthase (MTR) has long been recognized as an important enzyme in the maintenance of both methionine metabolism and folate-dependent reactions, and early work suggested that inhibition of MTR could restrain tumor growth. However, a lack of genetic tools and inconsistent use of physiological culture conditions has confounded efforts to understand the effects of inhibiting MTR *in vivo* and has precluded effective targeting of MTR in cancer. Here we demonstrate that MTR is required for proliferation only in cells cultured in media containing the physiological source of folate, 5-methyl tetrahydrofolate. We find that MTR is necessary to maintain intracellular levels of both S-adenosyl methionine (SAM) and nucleotides, but not methionine. Further, MTR is essential for tumor growth in mice because it is required to access circulating folates, highlighting the importance of culturing cells in 5-methyl tetrahydrofolate to accurately model folate and nucleotide metabolism. These results suggest that MTR plays an important cell-autonomous role in maintenance of nucleotide and SAM synthesis and that MTR may represent an effective therapeutic target in tumors.

INTRODUCTION

Folate metabolism is critical for cell survival and proliferation, as one-carbon units carried by folate cofactors are necessary for nucleotide synthesis (Lane and Fan, 2015) as well as various cellular methylation reactions (Chiang et al., 1996). There exist multiple folate species that cells require for biosynthetic reactions (Figure 1A), and each of these molecules can be synthesized within the cell from tetrahydrofolate (THF) (Ducker and Rabinowitz, 2017). In culture, cells are typically provided with folic acid, a form of folate that can be converted to THF through the

enzymatic action of dihydrofolate reductase (DHFR) (Figure 2A). However, in mammals, the predominant circulating form of folate is 5-methyl tetrahydrofolate (5-methyl THF) (Pfeiffer et al., 2015), a reduced form of folate that must be converted into tetrahydrofolate (THF) to be utilized in subsequent biosynthetic reactions (Ducker and Rabinowitz, 2017). As environmental levels of nutrients can strongly influence cellular metabolism (Muir et al., 2018), we sought to understand how culturing cells in the physiological folate source, 5-methyl THF, impacts metabolism.

Conversion of 5-methyl THF to THF is coupled to synthesis of the amino acid methionine from homocysteine, a reaction catalyzed by the vitamin B12 (cobalamin)-dependent enzyme methionine synthase (MTR) (Banerjee and Matthews, 1990; Stover, 2010) (Figure 2A). MTR is the only known enzyme that can regenerate THF from 5-methyl THF. Loss of MTR activity from cobalamin insufficiency causes accumulation of intracellular 5-methyl THF, a situation referred to as the "methyl-folate trap" (Chanarin et al., 1985; Fujii et al., 1982). This irreversible accumulation of 5-methyl THF results in limited THF availability to generate other reduced forms of folate that are required for the biosynthesis of nucleotides. Given this critical role of MTR in processing 5-methyl THF, culturing cells in folic acid might partially mask the necessity of MTR for tumor growth. Indeed, some work has suggested that MTR deficiency causes folate-related perturbations that affect cancer cell growth (McLean et al., 1997; Walker et al., 1997).

The folate source available in the environment may modulate MTR activity in a way that impacts biosynthesis beyond folate metabolism. MTR is important for methionine and S-adenosyl methionine (SAM) metabolism (Boss, 1985; Chanarin et al., 1985; Liteplo et al., 1991; Matthews, 1997) and has been suggested to impair cancer cell growth by interfering with

methionine and SAM synthesis (Liteplo et al., 1991; Matthews, 1997). In animals, MTR is also important for maintaining whole-body methionine and SAM levels (Chanarin et al., 1985; Lumb et al., 1983; Scott et al., 1981; van der Westhuyzen et al., 1982). Thus, the folate source available to cancer cells may not only impact folate metabolism, but also methionine and SAM levels in tumors. Methionine restriction can inhibit tumor growth (Chaturvedi et al., 2018), so understanding the effects of culturing cells in 5-methyl THF on methionine metabolism could also be important for understanding the role that MTR plays in tumor progression.

Multiple studies in humans have suggested that MTR may be important to sustain tumor growth. Cancer progression was observed to be restrained in a human patient with impaired cobalamin metabolism (Corcino et al., 1971). Further, inactivation of cobalamin through administration of nitrous oxide has been shown to inhibit leukemia growth in humans (Eastwood et al., 1963; Ikeda et al., 1989). These studies have utilized inactivation of cobalamin by nitrous oxide and other compounds, which may have secondary effects when administered in patients. Thus, whether specific MTR inhibition restrains tumor progression *in vivo* and the mechanistic effects of MTR inhibition that are most important for tumor growth remain unclear.

We examine the role of MTR in tumor growth by knocking it out using CRISPR-Cas9 in cancer cells and by growing these cells in 5-methyl THF. We find that growth in 5-methyl THF, but not folic acid, imposes an absolute dependence on MTR for proliferation. Intracellular SAM and nucleotide pools are reduced in the absence of MTR. Exogenous nucleotides are sufficient to rescue this proliferation defect while methionine and SAM are not, suggesting that MTR loss functionally inhibits growth through folate insufficiency and impaired nucleotide synthesis. In a

mouse xenograft tumor model, MTR expression is essential for tumor growth, and MTR knockout tumors can be fully rescued by supplementation of excess folic acid. Together, these experiments demonstrate that MTR is critical for tumor growth due to its role in sustaining folate metabolism and underscore the importance of culturing cells in the physiological source of folates.

RESULTS

Cancer cells can be cultured in 5-methyl THF

The predominant folate in circulation in humans is 5-methyl THF (Pfeiffer et al., 2015); this is also true in mice fed a standard mouse chow (Figure 2B). To accurately model folate metabolism in cultured cells, we sought to determine whether adherent cancer cells could be cultured using 5-methyl THF as the sole folate source and to then characterize the effect of different folate sources on cell proliferation. Previous work has shown that leukemia cells can be grown for short periods in 5-methyl THF (Liteplo et al., 1991; Matthews, 1997). To generalize these findings to cancer cells derived from solid tumors, we utilized two cell lines, A549 and T.T, that exhibit average MTR expression levels compared to all cell lines in The Cancer Genome Atlas (Cancer Genome Atlas Research et al., 2013) (Figure 2C). We observed that folate deprivation does not diminish the proliferation rate of either cell line over the course of a 4-day experiment (Figure 2D-E), suggesting that cells may contain excess folate reserves that are sufficient to sustain growth over this period. Additionally, the dialyzed fetal bovine serum used to supplement the culture media contains low levels of both folic acid and 5-methyl THF (Figure 1B), suggesting that cells may be able to proliferate using these trace amounts of folates.

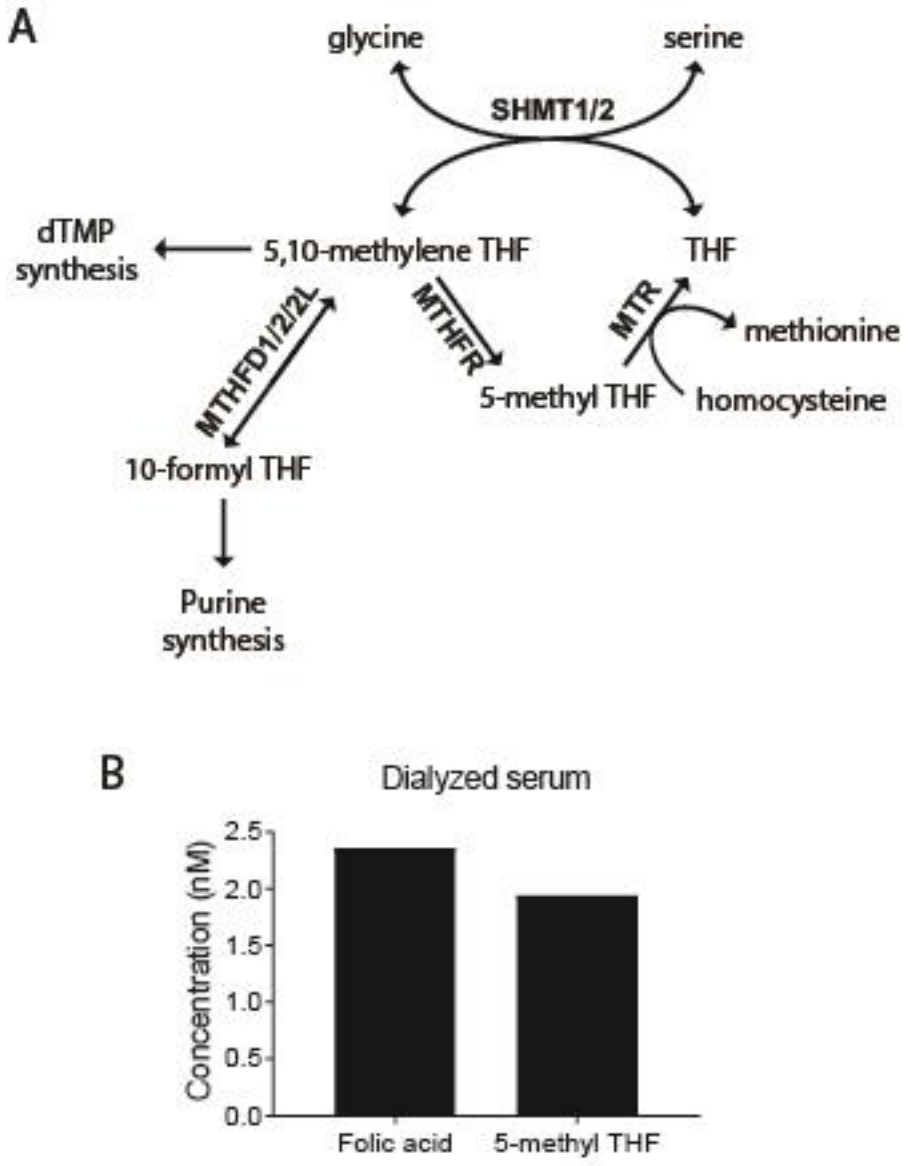

Figure 1. Overview of folate metabolism. (A) Simplified schematic of folate metabolism. SHMT: serine hydroxymethyltransferase. dTMP: deoxythymidine monophosphate. THF: tetrahydrofolate. MTHFD: methylenetetrahydrofolate dehydrogenase. MTHFR: methylenetetrahydrofolate reductase. MTR: methionine synthase. **(B)** LC/MS measurement of folic acid and 5-methyl THF concentrations present in dialyzed fetal bovine serum that is used in culture media.

In order to examine the behavior of cells that only have access to 5-methyl THF as a folate source, we chose to pre-incubate cells in media lacking folic acid for 3 days prior to each experiment. After 3 days of folate deprivation, cells provided with folic acid or 5-methyl THF are able to proliferate at their normal rate. In contrast, cells deprived of folic acid for longer periods display a substantial growth defect, indicating that this pre-starvation effectively depletes intracellular folate stores (Figure 2D-E). Providing 5-methyl THF as the sole folate source does not alter the long-term proliferative capacity of adherent cancer cells, as passaging cells in 5-methyl THF for 3 weeks does not alter their proliferation rate when switched back to standard media containing folic acid as the folate source (Figure 2F). Further, 5-methyl THF sustains proliferation at similar concentrations as folic acid (Figure 2G). Together, these results suggest that 5-methyl THF is sufficient to sustain the growth of adherent cancer cells in the absence of other folate sources. Of interest, the concentration of 5-methyl THF in plasma of mice is 153 nM (Figure 2B), a concentration that is not able to sustain maximal proliferation of A549 cancer cells in culture. This suggests that folate availability may be limiting for rapidly proliferating cells *in vivo*, consistent with reports that folate supplementation can accelerate the growth of some tumors (Farber et al., 1947; Farber et al., 1948; Hansen et al., 2017).

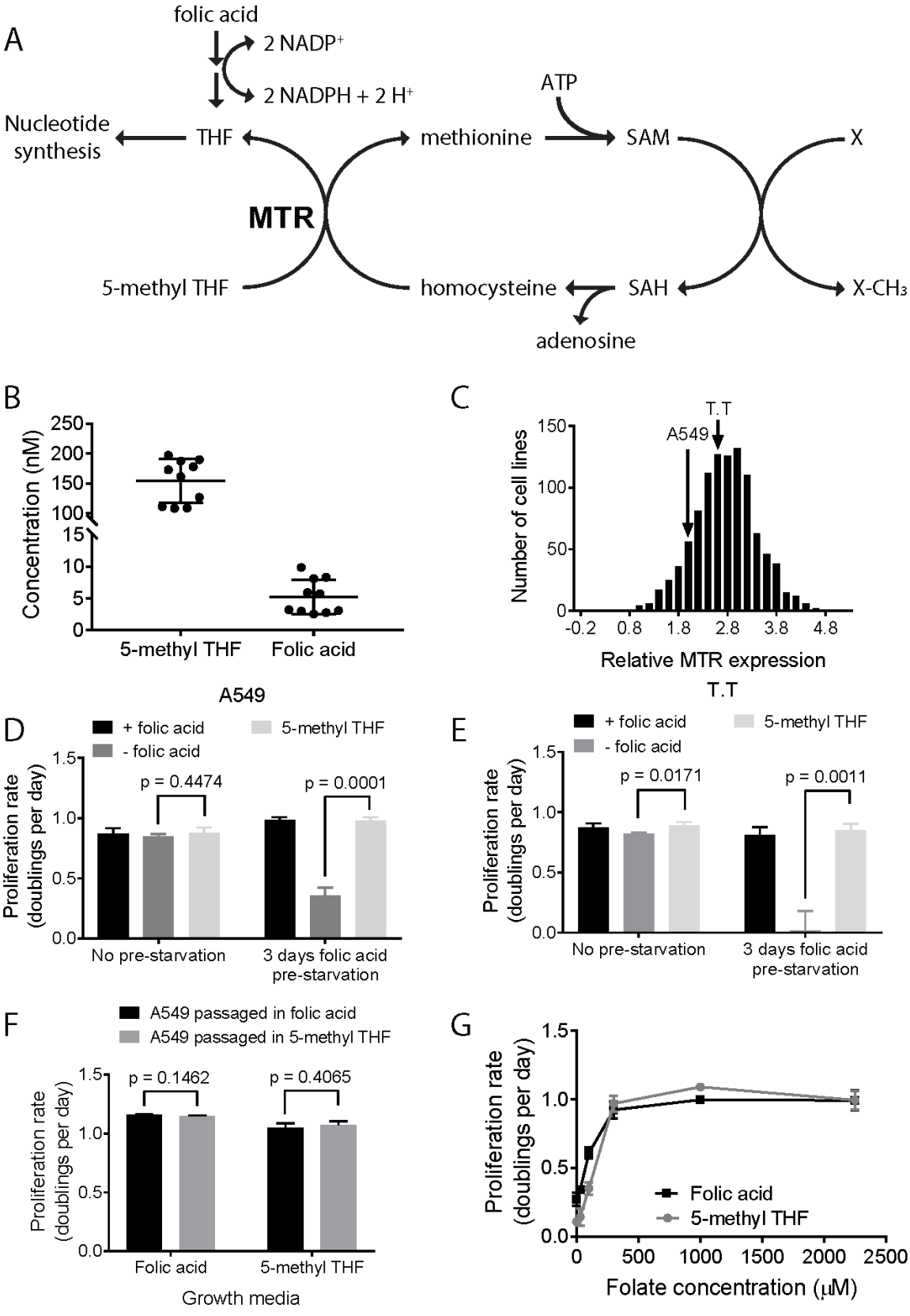
A
folic acid
2 NADP+
2 NADPH + 2 H+
ATP
Nucleotide synthesis
THF
methionine
SAM
X
MTR
5-methyl THF
homocysteine
SAH
X-CH3
adenosine
B
Concentration (nM)
5-methyl THF
Folic acid
A549
C
T.T
A549
Number of cell lines
Relative MTR expression
T.T
D
+ folic acid
- folic acid
5-methyl THF
Proliferation rate (doublings per day)
p = 0.4474
p = 0.0001
No pre-starvation
3 days folic acid pre-starvation
E
+ folic acid
- folic acid
5-methyl THF
Proliferation rate (doublings per day)
p = 0.0171
p = 0.0011
No pre-starvation
3 days folic acid pre-starvation
F
A549 passaged in folic acid
A549 passaged in 5-methyl THF
Proliferation rate (doublings per day)
p = 0.1462
p = 0.4065
Folic acid
5-methyl THF
Growth media
G
Proliferation rate (doublings per day)
Folic acid
5-methyl THF
Folate concentration (μM)

Figure 2. Adherent cells can be cultured in 5-methyl THF. (A) Schematic of folate and methionine metabolism. SAM: S-adenosyl methionine. SAH: S-adenosyl homocysteine. MTR: methionine synthase. **(B)** LC/MS measurement of 5-methyl THF and folic acid concentration in plasma from NSG mice. n = 10 mice. **(C)** Histogram of MTR expression in cell lines in The Cancer Genome Atlas. Proliferation rate of A549 **(D)** and T.T **(E)** cells in the presence of the indicated folate sources after either no pre-starvation or 3 days of folic acid pre-starvation. **(F)** Proliferation rate of A549 cells in the indicated growth media after 3 weeks of passaging in media containing either folic acid or 5-methyl THF as a folate source. **(G)** Proliferation rate of A549 cells in media containing the indicated amounts of either folic acid or 5-methyl THF.
Mean +/- SD is displayed for all panels. p values indicated on all panels are derived from two-tailed, unpaired Welch's t tests.

MTR is necessary for growth in a physiological folate source

As cancer cells are able to proliferate in culture with 5-methyl THF as the sole folate source, we sought to use this system to examine the role of MTR in cancer. To this end, MTR was knocked out in A549 and T.T cells using CRISPR-Cas9 editing (sgMTR), and an sgRNA-resistant version of MTR was added back to each cell line (Figure 3A). In both cell lines, MTR is essential for growth when 5-methyl THF is the sole folate source (Figure 3B-C). Interestingly, sgMTR A549 cells display a proliferative defect even when folic acid is provided (Figure 3B), indicating that these cells either require MTR for another purpose in addition to utilization of exogenous 5-methyl THF or that exogenous folic acid is partially converted to and then trapped as 5-methyl THF in the absence of MTR. However, MTR knockout T.T cells do not display any growth defect when folic acid is provided (Figure 3C), suggesting that the proliferation of these cells is dependent on MTR only for processing of exogenous 5-methyl THF.

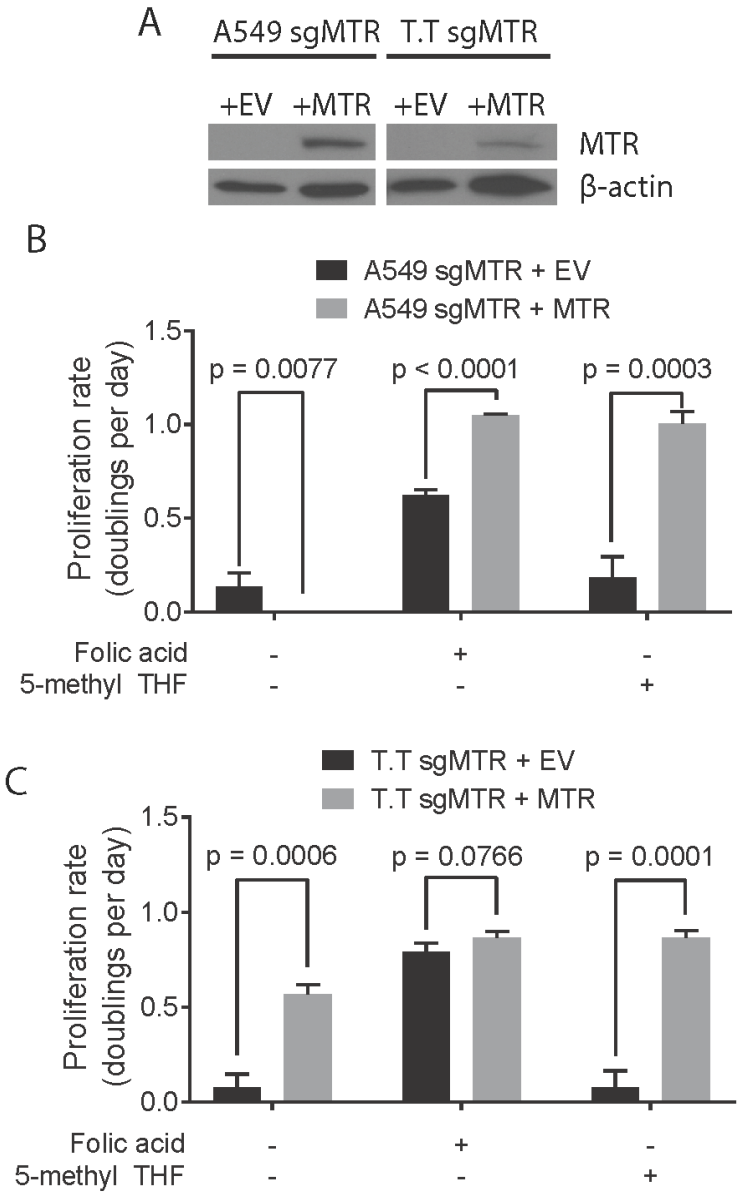

Figure 3. Methionine synthase is essential for growth in 5-methyl THF. (A) Western blot analysis of MTR expression in A549 and T.T cells containing an sgRNA targeting MTR. Cells either contain an empty vector (+EV) or express sgRNA resistant MTR (+MTR). Proliferation rates of A549 **(B)** and T.T **(C)** cells with no MTR expression (+EV) or expression of sgRNA resistant MTR (+MTR). Cells were grown in the indicated folate sources after 3 days of folate pre-starvation.

Mean +/- SD is displayed for all panels. p values indicated on all panels are derived from two-tailed, unpaired Welch's t tests.

MTR expression is not necessary to maintain methionine levels

To understand the physiological role of MTR in supporting proliferation in 5-methyl THF, we examined the metabolic consequences of MTR loss. MTR can support both methionine and folate metabolism, and we sought to determine if metabolism of either is altered in cancer cells upon MTR loss. First we considered methionine metabolism. If failure to synthesize methionine upon MTR loss results in intracellular methionine levels insufficient for growth, addition of exogenous methionine should promote proliferation. RPMI-1640 cell culture media used in this study contains 100 μM methionine, similar to the circulating plasma methionine level in mice (see Chapter 2). Providing additional methionine above that level did not rescue proliferation of MTR knockout cells (Figure 4A, Figure 5A), suggesting that they do not fail to proliferate due to a lack of methionine. Indeed, methionine levels are actually higher within MTR knockout cells than control cells (Figure 4B, Figure 5B). This is likely a non-specific consequence of their reduced proliferation rate, as other nonessential amino acids such as serine and essential amino acids such as lysine accumulate as well (Figure 4B, Figure 5B). Together, these results suggest that MTR knockout cells are not deficient in methionine for growth and that MTR is not required to maintain intracellular methionine pools given physiological levels of exogenous methionine.

MTR deletion perturbs SAM metabolism

Methionine is directly converted to S-adenosylmethionine SAM by addition of an adenosine triphosphate (ATP) molecule. In contrast to methionine, SAM pool sizes are decreased in MTR knockout cells (Figure 4C, Figure 5C). Low SAM levels could affect proliferation by altering the

cellular methylation state (Cho et al., 2012; Su et al., 2016), or by inhibiting activation of mTORC1 kinase (Gu et al., 2017). However, SAM levels are reduced regardless of the exogenous folate source upon loss of MTR (Figure 4C, Figure 5C) and therefore do not correlate with proliferation rate, suggesting that alterations in SAM levels are not responsible for reduced proliferation of MTR knockout cells in 5-methyl THF. Further, similar decreases in levels of the downstream metabolite S-adenosylhomocysteine (SAH) render the SAM/SAH ratio uncorrelated with MTR expression or folate source (Figure 4C, Figure 5C). Together, these experiments suggest that MTR expression is required to maintain SAM and SAH pool sizes, but not the SAM/SAH ratio. Further, depleted SAM/SAH pools do not explain the proliferation defects observed in the absence of MTR. Collectively, this suggests that supporting methionine metabolism is not a critical function of MTR when cells are cultured in physiological folates.

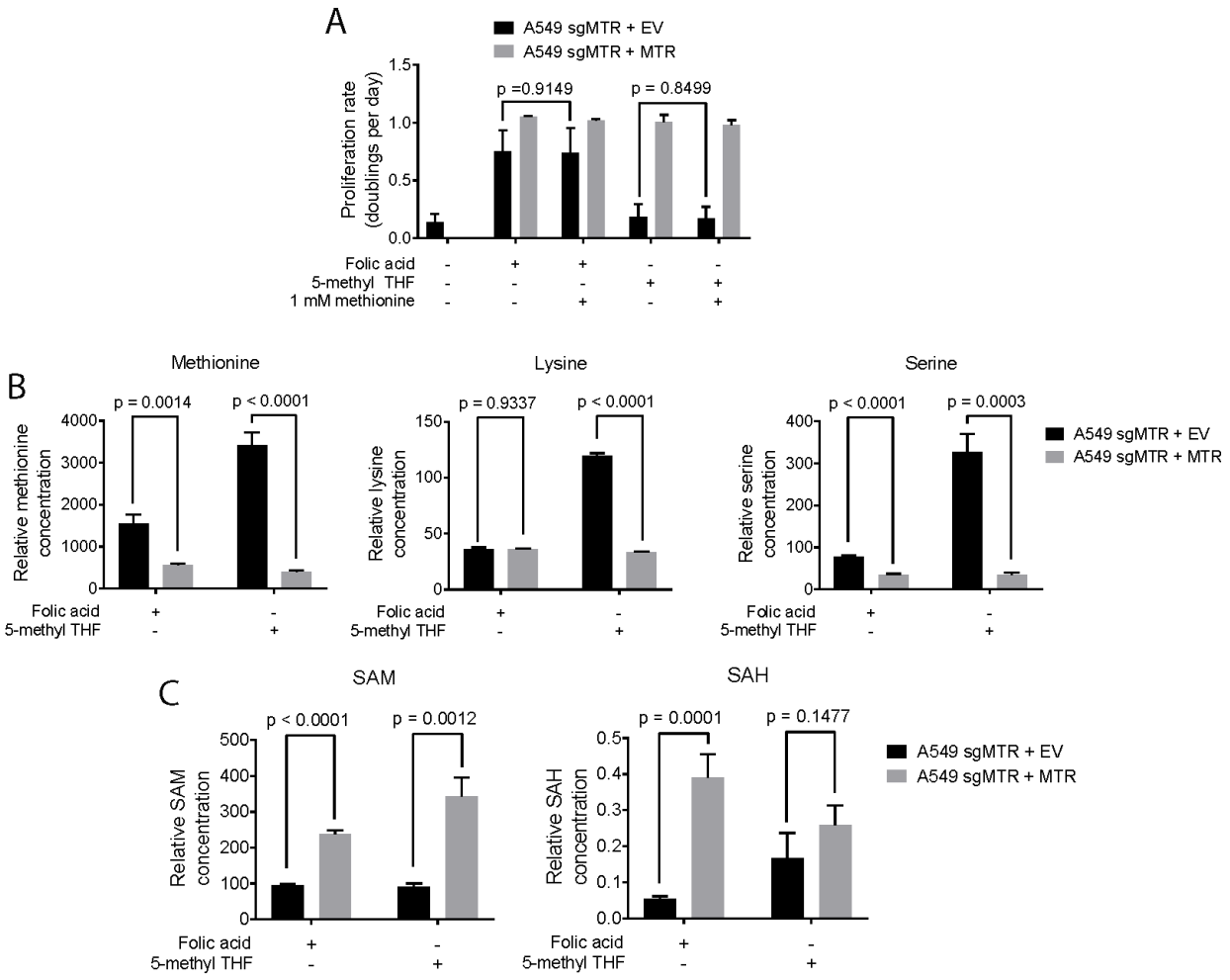

Figure 4. MTR expression affects SAM but not methionine metabolism. (A) Proliferation rates of A549 cells with no MTR expression (+EV) or expression of sgRNA resistant MTR (+MTR) in the indicated folate sources with or without the addition of 1 mM methionine in addition to the 100 µM methionine present in RPMI-1640 culture media. **(B)** LC/MS measurement of intracellular methionine, lysine, and serine levels in A549 cells with no MTR expression (+EV) or expression of sgRNA resistant MTR (+MTR) grown for 4 days in the indicated folate sources. Data are normalized to the total protein content of cells in each condition. **(C)** LC/MS measurement of intracellular SAM and SAH levels in A549 cells with no MTR expression (+EV) or expression of sgRNA resistant MTR (+MTR) grown for 4 days in the indicated folate sources. Data are normalized to the total protein content of cells in each condition.

Mean +/- SD is displayed for all panels. p values indicated on all panels are derived from two-tailed, unpaired Welch's t tests.

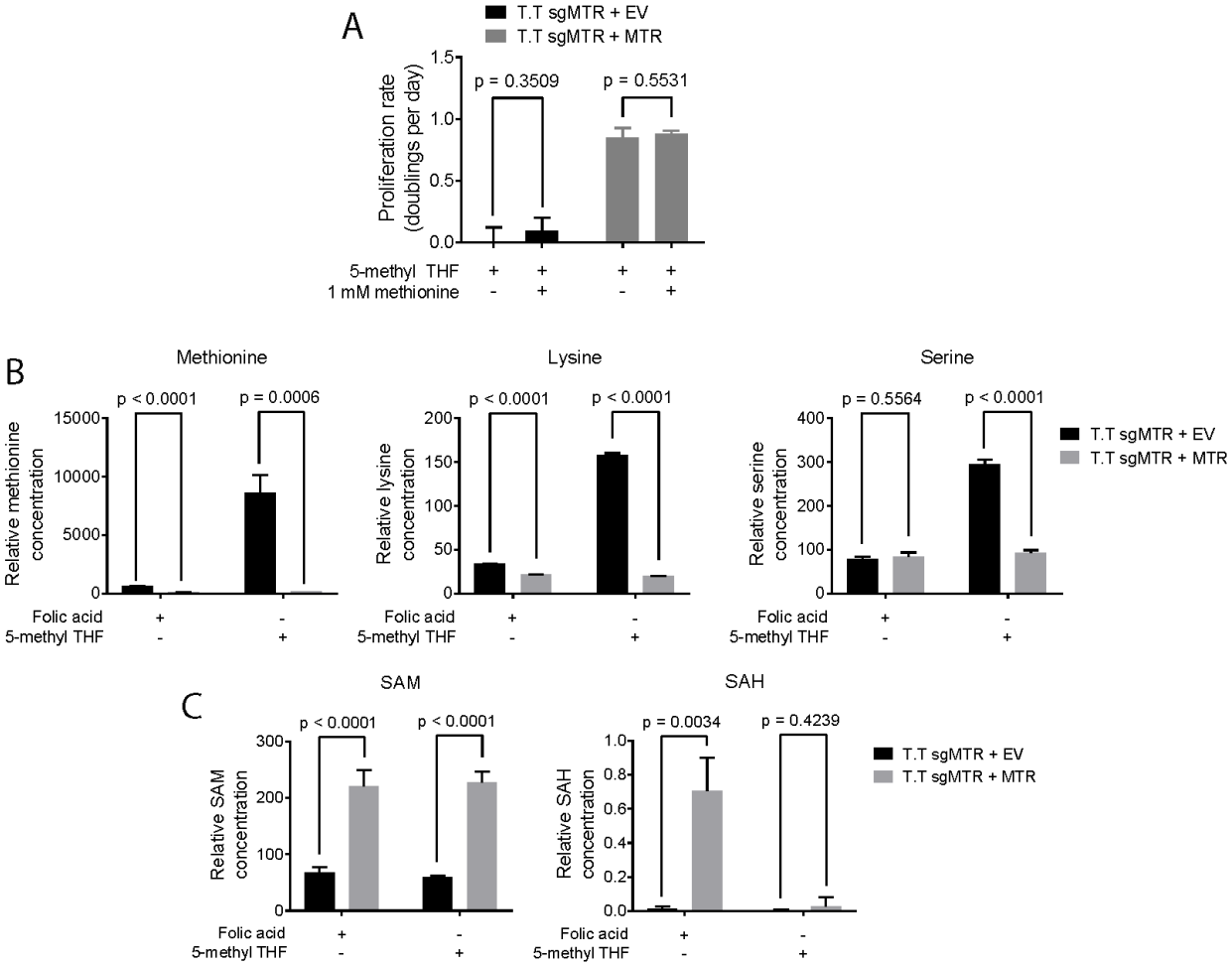

Figure 5. MTR expression affects SAM but not methionine metabolism in T.T cells. (A) Proliferation rates of T.T cells with no MTR expression (+EV) or expression of sgRNA resistant MTR (+MTR) in the indicated folate sources with or without the addition of 1 mM methionine in addition to the 100 µM methionine present in RPMI-1640 culture media. **(B)** LC/MS measurement of intracellular methionine, lysine, and serine levels in T.T cells with no MTR expression (+EV) or expression of sgRNA resistant MTR (+MTR) grown for 4 days in the indicated folate sources. Data are normalized to the total protein content of cells in each condition. **(C)** LC/MS measurement of intracellular SAM and SAH levels in T.T cells with no MTR expression (+EV) or expression of sgRNA resistant MTR (+MTR) grown for 4 days in the indicated folate sources. Data are normalized to the total protein content of cells in each condition.

Mean +/- SD is displayed for all panels. p values indicated on all panels are derived from two-tailed, unpaired Welch's t tests.

MTR is required for nucleotide synthesis

MTR expression is required to convert 5-methyl THF into THF for use in nucleotide synthesis. Thus, nucleotide synthesis may be compromised by loss of MTR. Indeed, levels of adenosine nucleotides are decreased in MTR knockout cells (Figure 6A, Figure 7A). Adenosine nucleotide levels are further decreased in MTR knockout cells grown in 5-methyl THF relative to those grown in folic acid, correlating with the greater reduction in proliferation rate of MTR knockout cells in 5 methyl THF (Figure 6A, Figure 7A). In addition to direct effects on nucleotide synthesis, folate insufficiency may impact SAM synthesis, as the nucleotide ATP is required to synthesize SAM from methionine (Mato et al., 1997). Thus, impaired nucleotide synthesis due to altered folate metabolism could explain the decreased SAM and SAH levels observed in MTR knockout cells, rather than being a result of impaired methionine metabolism.

If nucleotide synthesis is impaired due to a lack of reduced folate species derived from THF, intermediates in nucleotide synthesis prior to steps that utilize folates should accumulate (Labuschagne et al., 2014) (Figure 6B). Consistent with this possibility, levels of two intermediates in purine synthesis upstream of folate-utilizing steps, glycinamide ribonucleotide (GAR) and 5-amino-4-imidazolecarboxamide ribonucleotide (AICAR), are elevated in MTR knockout cells (Figure 6C, Figure 7B). GAR and AICAR levels further increase in MTR knockout cells cultured in 5-methyl THF relative to cells grown in folic acid, suggesting that these cells have particularly impaired purine nucleotide synthesis.

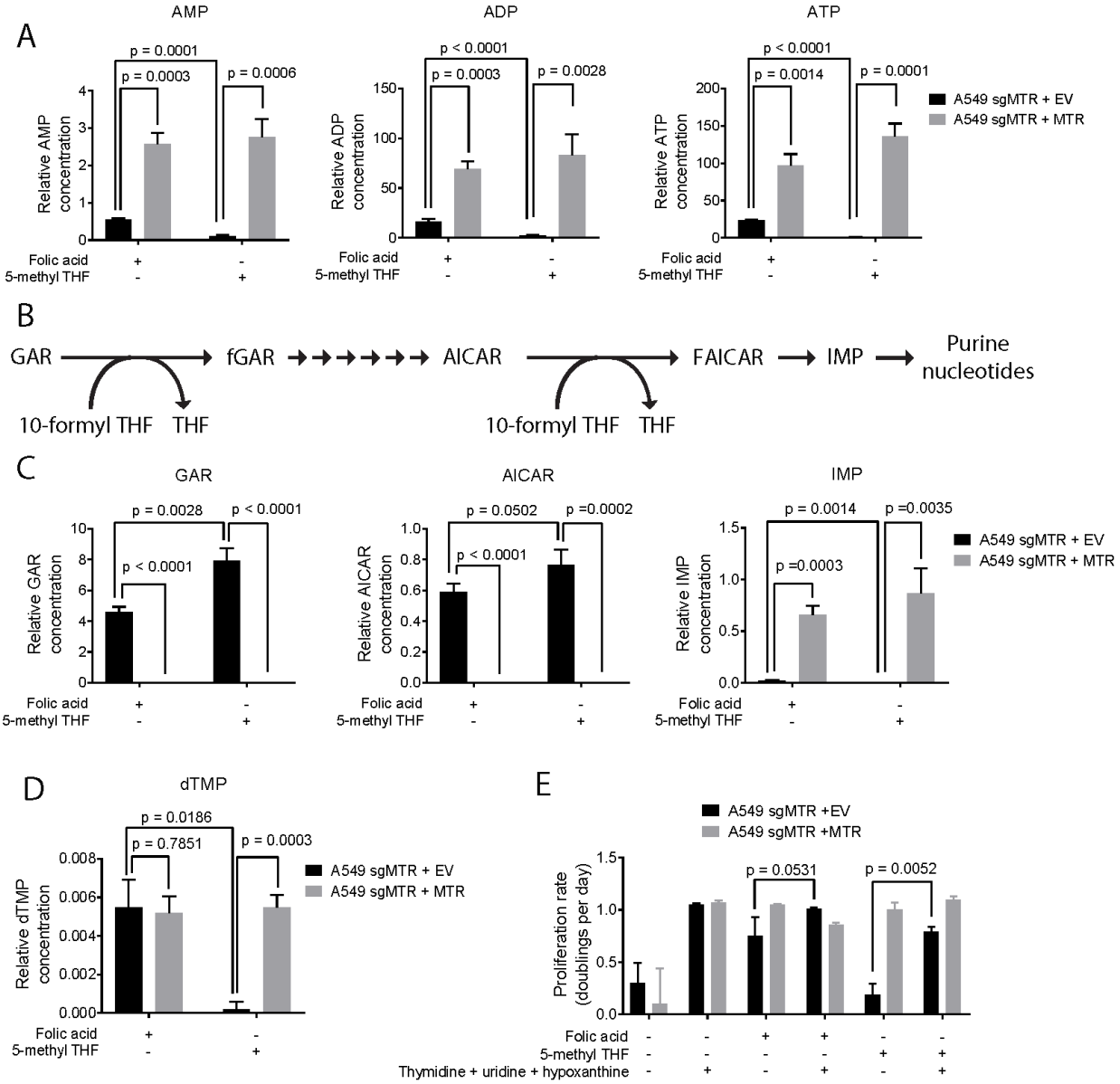
A
AMP
ADP
ATP
p = 0.0001
p = 0.0003
p = 0.0006
p < 0.0001
p = 0.0003
p = 0.0028
p < 0.0001
p = 0.0014
p = 0.0001
Relative AMP concentration
Relative ADP concentration
Relative ATP concentration
A549 sgMTR + EV
A549 sgMTR + MTR
Folic acid
5-methyl THF
B
GAR
fGAR
AICAR
FAICAR
IMP
Purine nucleotides
10-formyl THF
THF
C
GAR
AICAR
IMP
p = 0.0028
p < 0.0001
p < 0.0001
p = 0.0502
p =0.0002
p < 0.0001
p = 0.0014
p =0.0035
p =0.0003
Relative GAR concentration
Relative AICAR concentration
Relative IMP concentration
D
dTMP
p = 0.0186
p = 0.7851
p = 0.0003
Relative dTMP concentration
E
A549 sgMTR +EV
A549 sgMTR +MTR
p = 0.0531
p = 0.0052
Proliferation rate (doublings per day)
Thymidine + uridine + hypoxanthine

Figure 6. MTR knockout results in folate insufficiency and impairs nucleotide synthesis. (A) LC/MS measurement of intracellular AMP, ADP, and ATP levels in A549 cells with no MTR expression (+EV) or expression of sgRNA resistant MTR (+MTR) grown for 4 days in the indicated folate sources. **(B)** Schematic of purine synthesis. GAR: glycinamide ribonucleotide. fGAR: 5'-phosphoribosyl-N-formylglycinamide. AICAR: 5-amino-4-imidazolecarboxamide ribonucleotide. FAICAR: 5-formamidoimidazole-4-carboxamide ribonucleotide. IMP: inosine monophosphate. THF: tetrahydrofolate. **(C)** LC/MS measurement of intracellular GAR, AICAR, and IMP levels in A549 cells with no MTR expression (+EV) or expression of sgRNA resistant MTR (+MTR) grown for 4 days in the indicated folate sources. **(D)** LC/MS measurement of intracellular dTMP levels in A549 cells with no MTR expression (+EV) or expression of sgRNA resistant MTR (+MTR) grown for 4 days in the indicated folate sources. **(E)** Proliferation rates of A549 cells with no MTR expression (+EV) or expression of sgRNA resistant MTR (+MTR) in the indicated folate sources with or without the addition of 100 µM thymidine, 100 µM uridine, and 100 µM hypoxanthine (Thymidine + uridine + hypoxanthine).
Mean +/- SD is displayed for all panels. p values indicated on all panels are derived from two-tailed, unpaired Welch's t tests. For all LC/MS measurements, data are normalized to the total protein content of cells in each condition.

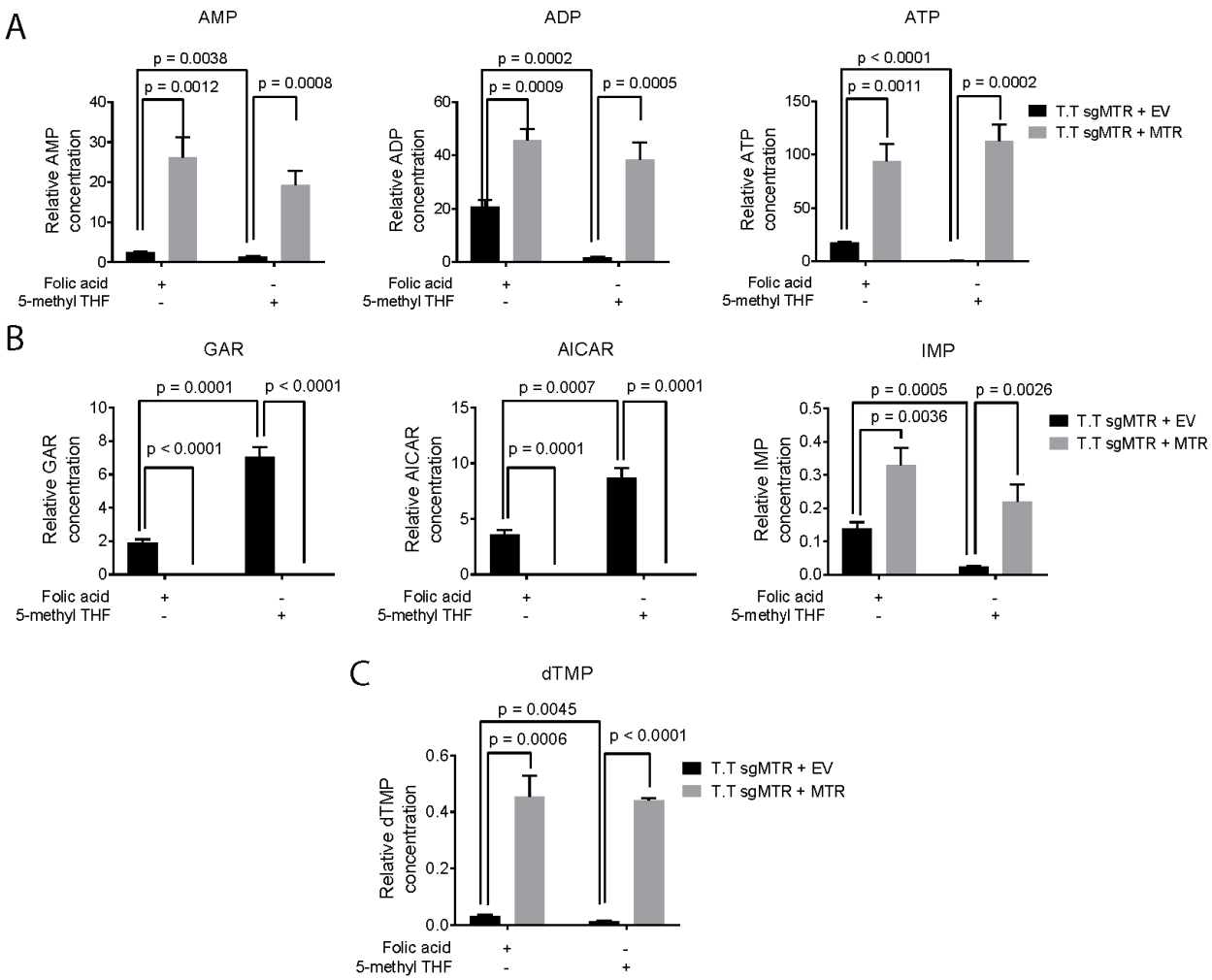

Figure 7. MTR knockout results in folate insufficiency and impairs nucleotide synthesis in T.T cells. (A) LC/MS measurement of intracellular AMP, ADP, and ATP levels in T.T cells with no MTR expression (+EV) or expression of sgRNA resistant MTR (+MTR) grown for 4 days in the indicated folate sources. **(B)** LC/MS measurement of intracellular GAR, AICAR, and IMP levels in T.T cells with no MTR expression (+EV) or expression of sgRNA resistant MTR (+MTR) grown for 4 days in the indicated folate sources. **(C)** LC/MS measurement of intracellular dTMP levels in T.T cells with no MTR expression (+EV) or expression of sgRNA resistant MTR (+MTR) grown for 4 days in the indicated folate sources.

Mean +/- SD is displayed for all panels. p values indicated on all panels are derived from two-tailed, unpaired Welch's t tests. For all LC/MS measurements, data are normalized to the total protein content of cells in each condition.

Further supporting this conclusion, inosine monophosphate (IMP), a purine precursor downstream of GAR and AICAR, is depleted in MTR knockout cells. IMP levels are also further depleted in MTR knockout cells grown in 5-methyl THF (Figure 6C, Figure 7B). If folate metabolism is globally disrupted by MTR knockout, cells should also have impaired pyrimidine synthesis, as deoxythymidine monophosphate (dTMP) synthesis requires a one-carbon unit in its synthesis. Indeed, dTMP levels are depleted in MTR knockout cells grown in 5-methyl THF (Figure 6D, FC). Addition of exogenous nucleosides is able to fully rescue the growth of MTR knockout cells, suggesting that the proliferative defect observed in MTR knockout cells in culture is driven by depleted nucleotide levels (Figure 6E).

MTR is necessary for tumor growth in order to maintain folate metabolism

If MTR is required to support folate metabolism and nucleotide synthesis in cancer cells that are cultured in 5-methyl THF, it should be required for tumor growth *in vivo* as 5-methyl THF is the predominant folate present in human (Pfeiffer et al., 2015) and mouse (Figure 2B) plasma. However, folic acid is also present in the circulation of both humans (Pfeiffer et al., 2015) and mice (Figure 2B), and may be sufficient to sustain tumor growth in the absence of MTR. To address whether MTR is necessary for tumor growth *in vivo*, we injected A549 cells into the flanks of NOD.Cg-*Prkdc*^{scid} *Il2rg*^{tm1Wjl}/SzJ (NSG) mice that were fed a diet containing folic acid at levels consistent with a human diet (Bailey et al., 2010; Reeves, 1997). MTR expression was essential for tumor formation, as no tumors formed in mice injected with MTR knockout cells (Figure 5A). If MTR is essential for tumor growth solely by supporting folate metabolism and not methionine or SAM levels, folic acid supplementation should rescue the growth of MTR knockout cells by providing a folate source that circumvents the need for 5 methyl-THF

conversion to THF by MTR. Provision of folic acid in the drinking water of mice results in increased plasma folic acid levels in some mice (Figure 8B), without altering 5-methyl THF levels in circulation (Figure 8C). The degree of increase in plasma folic acid levels was variable and did not result in a statistically significant increase in average folic acid concentration (Figure 8B); however, folic acid supplementation is sufficient to fully rescue the growth of MTR knockout tumors (Figure 8D), suggesting that MTR is essential for tumor growth due to its role in producing THF.

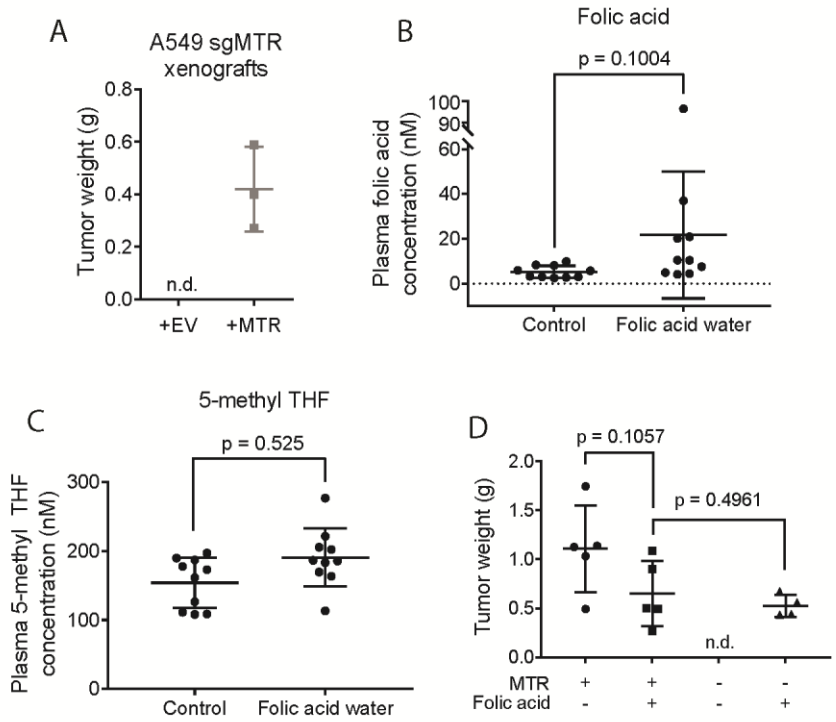

Figure 8. MTR is essential to maintain folate metabolism in tumors. (A) Tumor weight of subcutaneous xenografts formed by injecting 100,000 A549 cells with no MTR expression (+EV) or expression of sgRNA resistant MTR (+MTR) into the flanks of NSG mice. Tumors were harvested 4 months after injection. n.d.: tumors were not detected. Plasma concentration of folic acid **(B)** and 5-methyl THF **(C)** in NSG mice provided with either normal water (Control) or water containing 0.1 g/L folic acid (Folic acid water). **(D)** Tumor weight of subcutaneous xenografts formed by injecting 1,000,000 A549 cells with no MTR expression or expression of sgRNA resistant MTR (+MTR) into the flanks of NSG mice. Mice were provided either with normal water or water containing 0.1 g/L folic acid from the day the cells were injected throughout the experiment. Tumors were harvested 3 months after injection. n.d.: tumors were not detected.

Mean +/- SD is displayed for all panels. p values indicated on all panels are derived from two-tailed, unpaired Welch's t tests.

DISCUSSION

Folate metabolism is inaccurately modeled in standard culture conditions

Commercial culture media formulations typically contain folic acid as the folate source. Though folic acid is fully capable of supporting cancer cell proliferation, it results in improperly modeled metabolism; MTR is dispensable for proliferation in standard culture media but is essential for growth in the physiological folate source 5-methyl THF *in vitro* and *in vivo*. Other enzymes related to MTR are also probably essential under physiological conditions. These enzymes may include those that process and transport cobalamin, as well as methionine synthase reductase (MTRR), which serves to chaperone (Yamada et al., 2006) and regenerate MTR (Olteanu and Banerjee, 2001). The function of other folate-related enzymes is likely altered by the choice of folate source in culture and it will be important for studies of folate metabolism to be carried out using 5-methyl THF rather than folic acid. Studies of anti-folate drugs should also be performed using media containing 5-methyl THF, as many anti-folates reduce the production of THF from folic acid by inhibiting dihydrofolate reductase (DHFR). Thus, these anti-folates would be expected to be more toxic to cells grown in folic acid than those cultured in 5-methyl THF, which is converted to THF without requiring DHFR. Broadly, folate metabolism is intricately linked to many metabolic pathways and cellular processes, and future studies are warranted to determine how cellular metabolism operates when constrained by physiological folates.

SAM and nucleotide levels can be altered without changing proliferation rate

MTR expression appears to be necessary to maintain maximal intracellular nucleotide, SAM, and SAH concentrations even when cells are provided with folic acid in the media, suggesting that cancer cells are not able to efficiently use folic acid as a folate source in the absence of

MTR. However, cells are still able to maintain proliferation even with lower intracellular nucleotide, SAM, and SAH levels; in fact, in the T.T. cell line, proliferation rate is unchanged despite these metabolic alterations. Therefore, cells have a substantial capacity to tolerate decreases in SAM and nucleotide levels. If tumor cells *in vivo* are somewhat limited by folate availability, it may be that cancer cells contain far less SAM and nucleotides *in vivo* than in culture. This would have implications not only for the study of nucleotide metabolism and anti-folates, but also for the design of drugs that compete with nucleotides for binding to target proteins. We note that it may still be true that MTR knockout affects phenotypes other than proliferation rate. For instance, the epigenetic state of cells may be altered by changes in SAM and SAH levels in a manner that is not discernable by measuring growth rate but that is still important for cell function. Further study of the role of MTR in cells that are sensitive to epigenetic changes will yield insight into the role that metabolism plays in cell state.

MTR impacts SAM levels by reducing nucleotide synthesis

On a whole-animal level, MTR contributes to methionine synthesis. However, animals are capable of synthesizing methionine through betaine-homocysteine S-methyltransferase (BHMT) even in the absence of MTR (Chanarin et al., 1985), and we observe that MTR is not critical for maintaining methionine levels in a cancer cell-autonomous fashion. However, despite the presence of sufficient methionine, SAM and SAH levels are depleted in MTR knockout cells. Thus, methionine levels likely are not the critical determinant of SAM levels when MTR is inhibited. Instead, it appears that impaired ATP synthesis due to folate deficiency can lead to depletion of SAM pools in cells lacking MTR activity. Interestingly, depletion of adenosine nucleotides has been demonstrated to hinder cell growth in part through inhibition of mTORC1

signaling (Emmanuel et al., 2017; Hoxhaj et al., 2017). Given that SAM and SAH are sensed by the protein SAMTOR and are necessary to activate mTORC1 signaling (Gu et al., 2017), reduced SAM levels may provide a mechanism by which mTORC1 can sense adenosine availability. Further study of the crosstalk between folate availability, SAM levels, and ATP levels will have implications for understanding metabolic growth signals to the mTORC1 pathway.

MTR represents a therapeutic target in tumors responsive to anti-folates

MTR expression is essential for xenograft growth. However, its potential utility as a therapeutic target in cancer relies upon tumor cells having a higher demand for MTR activity than non-cancer cells. Given that MTR expression appears to be necessary to support tumor folate metabolism rather than methionine or SAM synthesis, tumor types with a high demand for nucleotide synthesis might be expected to respond to inhibition of MTR. Cancers that are responsive to anti-folates might represent one such subset of malignancies. MTR inhibition may have a different therapeutic window than anti-folates; for instance, non-small cell lung cancer (NSCLC) can be treated with pemetrexed, an anti-folate with multiple targets including thymidylate synthase (TS) (Li et al., 2014). However, TS is overexpressed in NSCLC (Otake et al., 1999), suggesting that tumor cells may have some ability to cope with inhibition of TS that normal cells lack. Despite this, pemetrexed still retains a therapeutic window for treatment of NSCLC. Inhibition of MTR or other related enzymes such as MTRR may present an alternative way to inhibit nucleotide synthesis that tumors may not be well-equipped to overcome.

MATERIALS AND METHODS

Cell culture

Cells were passaged in RPMI-1640 (Corning Life Sciences, Tewksbury, MA) with 10% fetal bovine serum (FBS) that had been heat inactivated for 30 min. at 56˚C (VWR Seradigm, Lot 120B14). All cells were cultured in a Heracell (Thermofisher) humidified incubators at 37˚C and 5% CO_2. A549 cells were obtained from ATCC (Manassas, VA). A549 cells are derived from a lung adenocarcinoma in a male patient. T.T cells were derived from an oral metastasis of an esophageal squamous cell carcinoma in a male patient. All cell lines were regularly tested for mycoplasma contamination using the Mycoprobe mycoplasma detection kit (R and D Systems, Minneapolis, MN). For experiments, cells were grown in RPMI-1640 without phenol red with 10% FBS that has been dialyzed to remove small molecules. RPMI-1640 lacking folic acid was made using the method outlined in (Muir et al., 2017). Briefly, enough of all of the components of RPMI-1640 media except for folic acid were weighed out to make 25 L of media, then the resulting powder was homogenized using an electric blade coffee grinder (Hamilton Beach, Glen Allen, VA, 80365) that had been washed with methanol then water. The resulting powder was resuspended in water to make RPMI-1640 media lacking folic acid. Folic acid (Sigma-Aldrich, St. Louis, MO, F8758) or (6S)-5-Methyl-5,6,7,8-tetrahydrofolic acid (5-methyl THF) (Schircks Laboratories, Bauma, Switzerland, 16.236) was dissolved in water to make 1000-fold concentrated stock solutions, then added back to RPMI-1640 media lacking folic acid. For experiments in which excess methionine was added to media, a 100 mM stock of methionine (Sigma-Aldrich) was generated in water and added back to RPMI-1640 media with the indicated folate source.

Proliferation assays

Cellular proliferation rate in different media conditions was determined as previously described (Sullivan et al., 2015). Cell lines were pre-starved of folic acid for 3 days, a time period that was empirically determined to be the longest folic acid starvation that still allowed for full recovery of maximal proliferation rate when cells were provided a folate source. For the 3 day pre-starvation, cells were plated into RPMI-1640 lacking folic acid at a density of 300,000 cells per 10 mL such that the cells were proliferating in log phase after 3 days. Cells were trypsinized, counted and plated into six well dishes (Corning Life Sciences) in 2 mL of RPMI-1640 medium lacking folic acid and incubated overnight. Initial seeding density was 40,000 cells/well. The next day, a six well plate of cells was trypsinized and counted to provide a number of cells at the start of the experiment. Cells were then washed twice with 2 mL of phosphate buffered saline (PBS), and 2 mL of the indicated media was added. For rescue experiments, 1 mM methionine, 1 mM SAM (Sigma-Aldrich, A7007), or the combination of 100 µM each uridine, thymidine, and hypoxanthine were added to the experimental media. Cells were then trypsinized and counted 4 days after adding the indicated media. Proliferation rate was determined using the following formula: Proliferation rate in doublings/day = [Log2(Final Day 4 cell count/Initial Day 0 cell count)]/4 days. Cells were counted using a Cellometer Auto T4 Plus Cell Counter (Nexcelom Bioscience, Lawrence, MA).

Generation of MTR knockout cell lines

MTR knockout using CRISPR-Cas9 was accomplished using the pLenti-CRISPR v2 plasmid (Addgene Plasmid 49535) (Sanjana et al., 2014). sgRNAs were designed based on previously

described algorithms (Hart et al., 2015), and MTR knockout was carried out using the following sgRNA sequence: TGGCATTGATCTCATCCCGC. Cell lines were diluted in 96 well plates to obtain single cell clones, and loss of MTR expression in individual clones was confirmed by western blot. sgRNA resistant cDNA of MTR was ordered from VectorBuilder (Shenandoah, TX) with silent mutations in the region of the gene targeted by the sgRNA.

Western blotting

Cells were scraped in 300 µL – 1 mL RIPA buffer [25 mM Tris-Cl, 150 mM NaCl, 0.5% sodium deoxycholate, 1% Triton X-100, 1x cOmplete protease inhibitor (Roche, Basel, Switzerland), 1x phosSTOP (Sigma-Aldrich)]. The resulting lysate was clarified by centrifugation at 21000 x g for 10 min. Protein concentration of the lysate was determined by BCA assay (Thermofisher). Lysates were resuspended at 1 mg/mL in Laemmli SDS-PAGE sample loading buffer (10% glycerol, 2% SDS, 60 mM Tris-Cl pH 6.8, 1% b-mercaptoethanol, 0.01% bromophenol blue) and denatured at 100˚C for 5 min. Extracts (30 µg of protein) were resolved by SDS-PAGE using 12% acrylamide gels running at 120 V until the dye front left the gel. After SDS-PAGE resolution, protein extracts were transferred to nitrocellulose using an iBlot semi-dry transfer system (Thermofisher). Membranes were blocked in 5% non-fat dry milk, incubated in primary antibodies to MTR (Abcam, Cambridge, UK, ab66039, 1:1000) or β-actin (Cell Signaling Technology, Danvers, MA 8457, 1:1000) and detected using HRP-conjugated secondary antibodies and chemiluminescence.

Metabolite extraction

For analysis of mouse plasma folates, 10 µL of plasma was mixed with 90 µL extraction buffer (80:20 methanol:water with 2.5 mM sodium ascorbate, 25 mM ammonium acetate, 100 nM aminopterin). Samples were vortexed for 10 minutes at 4 °C, then centrifuged at 21000 x g at 4°C for 10 minutes. Supernatant was removed and dried under nitrogen. For cell extraction, 5 µL of a standard composed of a ^{13}C amino acid mix (Cambridge Isotopes, Tewksbury, MA, MSK-A2-1.2) diluted to a concentration of 200 µM per amino acid was added to 600 µL 80% HPLC grade methanol (Sigma-Aldrich, 646377-4X4L) and added to cells. Cells were then scraped, transferred to an Eppendorf tube, vortexed for 10 minutes at 4 °C, then centrifuged at 21000 x g at 4°C for 10 minutes. 400 µL of sample was removed and dried under nitrogen.

LC/MS for polar metabolites

Dried samples were resuspended in 100 µL HPLC grade water. LC-MS analysis was performed using a QExactive orbitrap mass spectrometer using an Ion Max source and heated electro-spray ionization (HESI) probe coupled to a Dionex Ultimate 3000 UPLC system (Thermofisher). External mass calibration was performed every 7 days. Polar metabolite samples were separated by chromatography by injecting 10 µL of sample on a SeQuant ZIC-pHILIC 2.1 mm x 150 mm (5 µm particle size) column. Flow rate was set to 150 mL/min. and temperatures were set to 25˚C for the column compartment and 4˚C for the autosampler tray. Mobile phase A was 20 mM ammonium carbonate, 0.1% ammonium hydroxide. Mobile phase B was 100% acetonitrile. The chromatographic gradient was: 0–20 min.: linear gradient from 80% to 20% mobile phase B; 20–20.5 min.: linear gradient from 20% to 80% mobile phase B; 20.5 to 28

min.: hold at 80% mobile phase B. The mass spectrometer was operated in full scan, polarity-switching mode and the spray voltage was set to 3.0 kV, the heated capillary held at 275˚C, and the HESI probe was held at 350˚C. The sheath gas flow rate was 40 units, the auxiliary gas flow was 15 units and the sweep gas flow was one unit. The MS data acquisition was performed in a range of 70–1000 m/z, with the resolution set set at 70,000, the AGC target at $1x10^6$, and the maximum injection time at 20 msec. Relative quantitation of metabolites was performed with XCalibur QuanBrowser 2.2 (Thermo Fisher Scientific) using a 5 ppm mass tolerance and referencing an in-house library of chemical standards. Peak areas were normalized to cell number and ^{13}C-amino acid standard peak areas.

LC/MS for folate species

Detection of folate species was performed on the same instrumentation described above, as outlined in (Kanarek et al., 2018). In general, instrument settings remained the same unless specified. Samples were resuspended in 100 µL water and 15 µL was injected onto an Ascentis® Express C18 HPLC column (2.7 µm × 15 cm × 2.1 mm; Sigma Aldrich). The column oven and autosampler tray were held at 30°C and 4°C, respectively. The following conditions were used to achieve chromatographic separation: Buffer A was 0.1% formic acid; buffer B was acetonitrile with 0.1% formic acid. The chromatographic gradient was run at a flow rate of 0.250 mL/min as follows: 0-5min.: gradient was held at 5% B; 5-10 min.: linear gradient of 5% to 36% B; 10.1-14.0 min.: linear gradient from 36%-95% B; 14.1-18.0 min.: gradient was returned to 5% B. The mass spectrometer was operated in full-scan, positive ionization mode. MS data acquisition was performed using three narrow-range scans: 438-450 m/z; 452-462 m/z; and 470-478 m/z, with

the resolution set at 70,000, the AGC target at 10e6, and the maximum injection time of 150 msec. Relative quantitation of folate species was performed with XCalibur QuanBrowser 2.2 (Thermo Fisher Scientific) using a 5 ppm mass tolerance. Folate species were identified using chemical standards.

Mouse procedures

Cells were trypsininzed and either 100,000 or 1,000,000 cells were resuspended in 100 µL PBS as indicated on figure legends. Cells were injected into the flanks of NSG mice. Mice were euthanized according to institutional guidelines and tumor weight was recorded. 0.1 g/L folic acid water was prepared by resuspending folic acid in tap water, then filtering the mixture through a 0.22 µm filter to sterilize the water.

Blood collection

Blood was collected from fed, anesthetized mice by retro-orbital bleeding at 11 AM. Blood was placed directly into EDTA coated collection tubes (Sarstedt, Nümbrecht, Germany, 41.1395.105) and centrifuged 10’ at 845 x g; the supernatant of plasma was transferred to another tube.

ACKNOWLEDGEMENTS

We thank Naama Kanarek for her thoughtful comments and technical advice on folate measurements. We acknowledge all of the members of the Vander Heiden lab, as well as Alex Muir, for helpful input and advice on the manuscript. M.R.S. was supported by T32-GM007287 and by an MIT Koch Institute Graduate Fellowship. M.G.V.H. acknowledges support from R21CA198028, R01CA168653, the MIT Ludwig Center, the MIT Center for Precision Cancer Medicine, SU2C, the Lustgarten Foundation, and a Faculty Scholar Grant from HHMI.

AUTHOR CONTRIBUTIONS

Conceptualization, M.R.S., M.G.V.H.; Methodology, M.R.S., M.F.R., C.A.L.; Formal Analysis, M.R.S.; Investigation, M.R.S., M.F.R., A.M.D.; Resources, C.A.L.; Visualization, M.R.S.; Writing – Original Draft, M.R.S.; Writing – Review & Editing, M.R.S., A.M.D., M.G.V.H.; Funding Acquisition, M.G.V.H.

REFERENCES

Bailey, R.L., Dodd, K.W., Gahche, J.J., Dwyer, J.T., McDowell, M.A., Yetley, E.A., Sempos, C.A., Burt, V.L., Radimer, K.L., and Picciano, M.F. (2010). Total folate and folic acid intake from foods and dietary supplements in the United States: 2003-2006. Am J Clin Nutr *91*, 231-237.

Banerjee, R.V., and Matthews, R.G. (1990). Cobalamin-dependent methionine synthase. FASEB J *4*, 1450-1459.

Boss, G.R. (1985). Cobalamin inactivation decreases purine and methionine synthesis in cultured lymphoblasts. J Clin Invest *76*, 213-218.

Cancer Genome Atlas Research, N., Weinstein, J.N., Collisson, E.A., Mills, G.B., Shaw, K.R., Ozenberger, B.A., Ellrott, K., Shmulevich, I., Sander, C., and Stuart, J.M. (2013). The Cancer Genome Atlas Pan-Cancer analysis project. Nat Genet *45*, 1113-1120.

Chanarin, I., Deacon, R., Lumb, M., Muir, M., and Perry, J. (1985). Cobalamin-folate interrelations: a critical review. Blood *66*, 479-489.

Chaturvedi, S., Hoffman, R.M., and Bertino, J.R. (2018). Exploiting methionine restriction for cancer treatment. Biochem Pharmacol *154*, 170-173.

Chiang, P.K., Gordon, R.K., Tal, J., Zeng, G.C., Doctor, B.P., Pardhasaradhi, K., and McCann, P.P. (1996). S-Adenosylmethionine and methylation. FASEB J *10*, 471-480.

Cho, H.S., Shimazu, T., Toyokawa, G., Daigo, Y., Maehara, Y., Hayami, S., Ito, A., Masuda, K., Ikawa, N., Field, H.I.*, et al.* (2012). Enhanced HSP70 lysine methylation promotes proliferation of cancer cells through activation of Aurora kinase B. Nat Commun *3*, 1072.

Corcino, J.J., Zalusky, R., Greenberg, M., and Herbert, V. (1971). Coexistence of Pernicious Anaemia and Chronic Myeloid Leukaemia: An Experiment of Nature Involving Vitamin BI2 Metabolism. Br J Haematol *20*, 511.

Ducker, G.S., and Rabinowitz, J.D. (2017). One-Carbon Metabolism in Health and Disease. Cell Metab *25*, 27-42.

Eastwood, D.W., Green, C.D., Lambdin, M.A., and Gardner, R. (1963). Effect of Nitrous Oxide on the White-Cell Count in Leukemia. New England Journal of Medicine *268*, 297-299.

Emmanuel, N., Ragunathan, S., Shan, Q., Wang, F., Giannakou, A., Huser, N., Jin, G., Myers, J., Abraham, R.T., and Unsal-Kacmaz, K. (2017). Purine Nucleotide Availability Regulates mTORC1 Activity through the Rheb GTPase. Cell Rep *19*, 2665-2680.

Farber, S., Cutler, E.C., Hawkins, J.W., Harrison, J.H., Peirce, E.C., 2nd, and Lenz, G.G. (1947). The Action of Pteroylglutamic Conjugates on Man. Science *106*, 619-621.

Farber, S., Diamond, L.K., Mercer, R.D., Sylvester, R.F., and Wolff, J.A. (1948). Temporary remissions in acute leukemia in children produced by folic acid antagonist, 4-aminopteryl-glutamic acid (aminopterin). New England Journal of Medicine *238*, 787-793.

Fujii, K., Nagasaki, T., and Huennekens, F.M. (1982). Accumulation of 5-methyltetrahydrofolate in cobalamin-deficient L1210 mouse leukemia cells. J Biol Chem *257*, 2144-2146.

Gu, X., Orozco, J.M., Saxton, R.A., Condon, K.J., Liu, G.Y., Krawczyk, P.A., Scaria, S.M., Harper, J.W., Gygi, S.P., and Sabatini, D.M. (2017). SAMTOR is an S-adenosylmethionine sensor for the mTORC1 pathway. Science *358*, 813-818.

Hansen, M.F., Jensen, S.O., Fuchtbauer, E.M., and Martensen, P.M. (2017). High folic acid diet enhances tumour growth in PyMT-induced breast cancer. Br J Cancer *116*, 752-761.

Hart, T., Chandrashekhar, M., Aregger, M., Steinhart, Z., Brown, K.R., MacLeod, G., Mis, M., Zimmermann, M., Fradet-Turcotte, A., Sun, S*., et al.* (2015). High-Resolution CRISPR Screens Reveal Fitness Genes and Genotype-Specific Cancer Liabilities. Cell *163*, 1515-1526.

Hoxhaj, G., Hughes-Hallett, J., Timson, R.C., Ilagan, E., Yuan, M., Asara, J.M., Ben-Sahra, I., and Manning, B.D. (2017). The mTORC1 Signaling Network Senses Changes in Cellular Purine Nucleotide Levels. Cell Rep *21*, 1331-1346.

Ikeda, K., Aosaki, T., Furukawa, Y., Ohta, M., Kano, Y., Tsuboyama, A., Sakamoto, S., Miura, Y., Sakuraya, K., Fuke, N*., et al.* (1989). Antileukemic effect of nitrous oxide in a patient with chronic myelogenous leukemia. Am J Hematol *30*, 114.

Kanarek, N., Keys, H.R., Cantor, J.R., Lewis, C.A., Chan, S.H., Kunchok, T., Abu-Remaileh, M., Freinkman, E., Schweitzer, L.D., and Sabatini, D.M. (2018). Histidine catabolism is a major determinant of methotrexate sensitivity. Nature *559*, 632-636.

Labuschagne, C.F., van den Broek, N.J., Mackay, G.M., Vousden, K.H., and Maddocks, O.D.K. (2014). Serine, but not glycine, supports one-carbon metabolism and proliferation of cancer cells. Cell Rep *7*, 1248-1258.

Lane, A.N., and Fan, T.W. (2015). Regulation of mammalian nucleotide metabolism and biosynthesis. Nucleic Acids Res *43*, 2466-2485.

Li, X., Wei, S., and Chen, J. (2014). Critical appraisal of pemetrexed in the treatment of NSCLC and metastatic pulmonary nodules. Onco Targets Ther *7*, 937-945.

Liteplo, R.G., Hipwell, S.E., Rosenblatt, D.S., Sillaots, S., and Lue-Shing, H. (1991). Changes in cobalamin metabolism are associated with the altered methionine auxotrophy of highly growth autonomous human melanoma cells. J Cell Physiol *149*, 332-338.

Lumb, M., Sharer, N., Deacon, R., Jennings, P., Purkiss, P., Perry, J., and Chanarin, I. (1983). Effects of nitrous oxide-induced inactivation of cobalamin on methionine and S-adenosylmethionine metabolism in the rat. Biochim Biophys Acta *756*, 354-359.

Mato, J.M., Alvarez, L., Ortiz, P., and Pajares, M.A. (1997). S-adenosylmethionine synthesis: molecular mechanisms and clinical implications. Pharmacol Ther *73*, 265-280.

Matthews, J.H. (1997). Cyanocobalamin [c-lactam] Inhibits Vitamin B12 and Causes Cytotoxicity in HL60 Cells: Methionine Protects Cells Completely. Blood *89*, 4600-4607.

McLean, G.R., Pathare, P.M., Wilbur, D.S., Morgan, A.C., Woodhouse, C.S., Schrader, J.W., and Ziltener, H.J. (1997). Cobalamin analogues modulate the growth of leukemia cells in vitro. Cancer Res *57*, 4015-4022.

Muir, A., Danai, L.V., Gui, D.Y., Waingarten, C.Y., Lewis, C.A., and Vander Heiden, M.G. (2017). Environmental cystine drives glutamine anaplerosis and sensitizes cancer cells to glutaminase inhibition. Elife *6*.

Muir, A., Danai, L.V., and Vander Heiden, M.G. (2018). Microenvironmental regulation of cancer cell metabolism: implications for experimental design and translational studies. Dis Model Mech *11*.

Olteanu, H., and Banerjee, R. (2001). Human methionine synthase reductase, a soluble P-450 reductase-like dual flavoprotein, is sufficient for NADPH-dependent methionine synthase activation. J Biol Chem *276*, 35558-35563.

Otake, Y., Tanaka, F., Yanagihara, K., Hitomi, S., Okabe, H., Fukushima, M., and Wada, H. (1999). Expression of thymidylate synthase in human non-small cell lung cancer. Jpn J Cancer Res *90*, 1248-1253.

Pfeiffer, C.M., Sternberg, M.R., Fazili, Z., Lacher, D.A., Zhang, M., Johnson, C.L., Hamner, H.C., Bailey, R.L., Rader, J.I., Yamini, S*., et al.* (2015). Folate status and concentrations of serum folate forms in the US population: National Health and Nutrition Examination Survey 2011-2. Br J Nutr *113*, 1965-1977.

Reeves, P.G. (1997). Components of the AIN-93 Diets as Improvements in the AIN-76A Diet. J Nutr *127*, 838-841.

Sanjana, N.E., Shalem, O., and Zhang, F. (2014). Improved vectors and genome-wide libraries for CRISPR screening. Nat Methods *11*, 783-784.

Scott, J.M., Dinn, J.J., Wilson, P., and Weir, D.G. (1981). Pathogenesis of subacute combined degeneration: a result of methyl group deficiency. Lancet *2*, 334-337.

Stover, P.J. (2010). Vitamin B12 and older adults. Curr Opin Clin Nutr Metab Care *13*, 24-27.

Su, X., Wellen, K.E., and Rabinowitz, J.D. (2016). Metabolic control of methylation and acetylation. Curr Opin Chem Biol *30*, 52-60.

Sullivan, L.B., Gui, D.Y., Hosios, A.M., Bush, L.N., Freinkman, E., and Vander Heiden, M.G. (2015). Supporting Aspartate Biosynthesis Is an Essential Function of Respiration in Proliferating Cells. Cell *162*, 552-563.

van der Westhuyzen, J., Fernandes-Costa, F., and Metz, J. (1982). Cobalamin inactivation by nitrous oxide produces severe neurological impairment in fruit bats : protection by methionine and aggravation by folates. Life Sci *31*, 2001-2010.

Walker, P.R., Smith, B., Carson, C., LeBlanc, J., Sikorska, M., Woodhouse, C.S., and Morgan, A.C. (1997). Induction of apoptosis in neoplastic cells by depletion of vitamin B12. Cell Death Differ *4*, 233-241.

Yamada, K., Gravel, R.A., Toraya, T., and Matthews, R.G. (2006). Human methionine synthase reductase is a molecular chaperone for human methionine synthase. Proc Natl Acad Sci U S A *103*, 9476-9481.

CHAPTER FOUR: Quantification of microenvironmental metabolites in murine cancers reveals determinants of tumor nutrient availability

Mark R. Sullivan[1], Laura V. Danai[1,2], Caroline A. Lewis[3], Sze Ham Chan[3], Dan Y. Gui[1], Tenzin Kunchok[3], Emily A. Dennstedt[1], Matthew G. Vander Heiden[1,4#] and Alexander Muir[1,5#]

[1]Koch Institute for Integrative Cancer Research and Department of Biology, Massachusetts Institute of Technology, Cambridge, MA 02139, USA; [2]Department of Biochemistry and Molecular Biology, University of Massachusetts, Amherst, Amherst, MA 01003, USA; [3]Department of Biology and Whitehead Institute for Biomedical Research and Massachusetts Institute of Technology, Cambridge, MA 02142, USA; [4]Dana-Farber Cancer Institute, Boston, MA 02115, USA; [5]Ben May Department for Cancer Research, University of Chicago, Chicago, IL 60637, USA

A version of this chapter has been published previously and is reprinted with permission from *eLife*:

Sullivan, M.R., Danai, L.V., Lewis, C.A., Chan, S.H., Gui, D.Y., Kunchok, T., Dennstedt, E.A., Vander Heiden, M.G., Muir, A., Quantification of Microenvironmental Metabolites in Murine Cancers Reveals Determinants of Tumor Nutrient Availability. *eLife* 8: e44235. (2019).

ABSTRACT

Cancer cell metabolism is heavily influenced by microenvironmental factors, including nutrient availability. Therefore, knowledge of microenvironmental nutrient levels is essential to understand tumor metabolism. To measure the extracellular nutrient levels available to tumors, we developed a quantitative metabolomics method to measure the absolute concentrations of >118 metabolites in plasma and tumor interstitial fluid, the extracellular fluid that perfuses tumors. Comparison of nutrient levels in tumor interstitial fluid and plasma revealed that the nutrients available to tumors differ from those present in circulation. Further, by comparing interstitial fluid nutrient levels between autochthonous and transplant models of murine pancreatic and lung adenocarcinoma, we found that tumor type, anatomical location and animal diet affect local nutrient availability. These data provide a comprehensive characterization of the nutrients present in the tumor microenvironment of widely used models of lung and pancreatic cancer and identify factors that influence metabolite levels in tumors.

INTRODUCTION

Tumors exhibit altered metabolism compared to non-transformed tissues (DeBerardinis and Chandel, 2016). For example, animal limbs transformed with oncogenic viruses exhibit increased glucose uptake and lactate secretion relative to unaffected limbs (Cori and Cori, 1925). Some aspects of tumor metabolism, including higher rates of glucose fermentation to lactate, are cell-intrinsic features that are retained when cancer cells are isolated from tumors (Koppenol et al., 2011). Indeed, numerous studies have delineated how cell-intrinsic factors

such as oncogenic genetic lesions or epigenetic state alter cellular metabolism, causing phenotypes such as increased glycolysis (Nagarajan et al., 2016).

However, beyond cell-intrinsic alterations, tumors have modified tissue architecture and an altered tissue microenvironment; these cell-extrinsic factors can also impact the metabolism of tumors (Muir et al., 2018). For instance, the metabolic utilization of both glucose and the amino acid glutamine differs between cells growing in culture and murine tumor models. (Davidson et al., 2016; Muir et al., 2017; Sellers et al., 2015; Tardito et al., 2015). Further, the metabolic enzymes that cancer cells rely upon for proliferation in culture are different than those that the same cells utilize to support growth and survival in tumors (Alvarez et al., 2017; Possemato et al., 2011; Yau et al., 2017). Thus, cancer cell metabolism is influenced by microenvironmental cues.

Numerous microenvironmental factors affect cancer cell metabolism (Anastasiou, 2017; Bi et al., 2018; Muir et al., 2018; Wolpaw and Dang, 2018), including the presence of stromal cells (Lyssiotis and Kimmelman, 2017; Morandi et al., 2016), tumor acidity (Corbet and Feron, 2017; Persi et al., 2018), extracellular matrix properties (DelNero et al., 2018; Tung et al., 2015) and tumor nutrient levels (Muir and Vander Heiden, 2018). In particular, environmental nutrient availability is an important regulator of cancer cell metabolism (Cantor et al., 2017; Muir et al., 2017; Schug et al., 2015; Tardito et al., 2015). Nutrient differences between standard cell culture and animal tumor models can drive substantial changes in cancer cell metabolism that alter the response of cancer cells to metabolically targeted drugs (Cantor et al., 2017; Gui et al., 2016; Muir et al., 2017; Palm et al., 2015), such that drugs that inhibit proliferation of cancer cells in culture fail to exhibit efficacy in tumors derived from the same

cells (Biancur et al., 2017; Davidson et al., 2016). Thus, determining the concentrations of nutrients in the tumor microenvironment is important to understand and therapeutically target cancer cell metabolism.

Tumors and tissues are supplied with nutrients through the vasculature, which filters a nutrient rich fluid from the circulation into the interstitial space of a tissue or tumor (Wiig and Swartz, 2012). The interstitial fluid (IF) then perfuses through the tissue or tumor, exchanging nutrients and wastes with cells. IF is then drained from the tissue or tumor via capillaries and the lymphatic system. Thus, cells in tissues or tumors are not necessarily directly exposed to the nutrients in circulating plasma, but instead are exposed to IF nutrient levels. For healthy organs, IF nutrient levels may be similar to circulating nutrient levels, as these tissues are well vascularized, allowing rapid metabolic exchange with the plasma. Indeed, the IF glucose concentration in healthy skin is very similar to that of circulating plasma (Lonnroth et al., 1987). In contrast to the functional vessels found in normal tissues, tumors commonly have an abnormal vasculature with few vessels transporting blood (Fukumura et al., 2010). This may lead to reduced nutrient delivery and waste exchange between tumor cells and the circulation. Thus, tumor interstitial fluid (TIF) is thought to be nutrient depleted and have increased concentrations of metabolic waste products. Indeed glucose levels in the TIF of some tumors are lower than in the circulation, while lactate levels are higher (Burgess and Sylven, 1962; Gullino et al., 1964; Ho et al., 2015). However, despite the importance of nutrient availability in regulating tumor metabolism and drug sensitivity, TIF nutrients beyond glucose and lactate have not been comprehensively measured, and the factors that determine TIF composition have not been characterized.

We sought to systematically measure absolute nutrient concentrations in plasma and TIF. To do so, we have developed a quantitative mass spectrometry-based approach using both external standards and stable isotope dilution of a library of carbon labeled metabolites allowing for quantification of >118 nutrients in any biofluid. We applied this technique to measure nutrient levels in plasma and TIF isolated from autochthonous and transplantation models of murine lung (LUAD) and pancreatic adenocarcinomas (PDAC) driven by activation of Kras and deletion of p53. Interestingly, we found that anatomical location and tumor tissue of origin are both major determinants of TIF nutrient composition. Dietary changes are also reflected in TIF nutrient levels, while introduction of a *Keap1* mutation into LUAD cells had a smaller effect on the composition of the metabolic tumor microenvironment. Collectively, these experiments elucidate the microenvironmental constraints placed upon tumor metabolism by TIF nutrient levels and provide insight into the factors that dictate tumor nutrient availability.

RESULTS

Isolation of TIF from murine PDAC tumors

We first focused on isolating and analyzing TIF nutrient levels in pancreatic ductal adenocarcinoma (PDAC), as this tumor type is known to have inadequate vasculature leading to tumor hypoxia (Koong et al., 2000) and nutrient deprivation (Commisso et al., 2013; Kamphorst et al., 2015; Lyssiotis and Kimmelman, 2017; Sherman et al., 2017; Sousa et al., 2016). End-stage tumors were isolated from the *LSL-Kras$^{G12D/+}$; Trp53$^{flox/flox}$; Pdx-1-Cre*, (KP-/-C) mouse model of PDAC (Bardeesy et al., 2006). This mouse model recapitulates many aspects of the

human disease including dense stroma (Bardeesy et al., 2006) and alterations in systemic metabolism (Danai et al., 2018; Mayers et al., 2014). We applied a previously described method to collect TIF; tumors were placed on a fine mesh and subjected to low speed centrifugation (Figure 1A) (Haslene-Hox et al., 2011). The mesh prevents cells from passing through but allows TIF to flow out of the tumor and into a collection tube. This method has previously been successfully used to study glucose and lactate levels in tumor samples (Ho et al., 2015; Siska et al., 2017). 5-30 µL of TIF was able to be isolated from ~75% (13/17 tumors) of isolated KP-/-C PDAC tumors. The remaining 25% of tumors did not yield any fluid. The amount of fluid collected per tumor weight is consistent with previous reports of TIF isolation from human tumor samples (Haslene-Hox et al., 2011).

Critically, this centrifugation method does not cause lysis of cells when performed on human tumor samples, ensuring that the isolated fluid is interstitial and not intracellular fluid (Haslene-Hox et al., 2011). To determine the extent to which intracellular fluid from lysed cells might contribute to TIF isolated from the KP-/-C PDAC mouse model, we measured the level of activity of the intracellular enzyme lactate dehydrogenase (LDH) in plasma and TIF from mice bearing PDAC tumors (Figure 1B). As LDH is an intracellular enzyme, LDH activity should indicate the extent to which intracellular material is present in the isolated interstitial fluid. The level of LDH activity in the entire volume of collected TIF was less than 1% of that detected in the whole lysed tumor (Figure 1B), suggesting that intracellular fluid is not a major component of TIF isolated using this method. Though levels of LDH activity in the PDAC TIF samples were ~20 fold higher than those found in plasma samples, similar or higher LDH activities were recovered in TIF of solid tumors isolated by orthogonal methods (~60-80 fold higher LDH activity in TIF than

plasma) (Burgess and Sylven, 1962). These data suggest that TIF isolation by centrifugation does not result in gross cell lysis and contamination of interstitial fluid with intracellular material.

Quantification of TIF metabolites

In order to understand the composition of the tumor microenvironment, we sought to measure the absolute concentrations of metabolites present in TIF using liquid chromatography/mass spectrometry (LC/MS). Absolute LC/MS quantification of metabolites in biological samples such as plasma and TIF is complicated by matrix effects, which alter the ionization and detection of metabolites in different sample types (Trufelli et al., 2011). Indeed, when the same amounts of ^{13}C stable isotope labeled metabolites were added to water or mouse plasma, detected levels of these ^{13}C standards varied widely depending on whether the metabolites were dissolved in water or plasma (Figure 1C). This result reaffirms the presence of significant matrix effects that would confound the comparison of metabolite concentrations measured in different sample types. As a result, the use of external standard curves of metabolites suspended in water can result in systematic error when used to quantitate metabolites in complex mixtures such as plasma and TIF. To circumvent this problem, we utilized stable isotope dilution quantification, in which ^{13}C stable isotope labeled metabolites are added to each biological sample in known quantities, and the ratio of $^{12}C/^{13}C$ for each metabolite is used to calculate the concentration of the ^{12}C metabolite (Figure 1D). As both ^{12}C and ^{13}C metabolites are subject to the same sample-dependent ion enhancement or suppression effects, this method limits error from matrix effects in metabolite quantification (Trufelli et al., 2011).

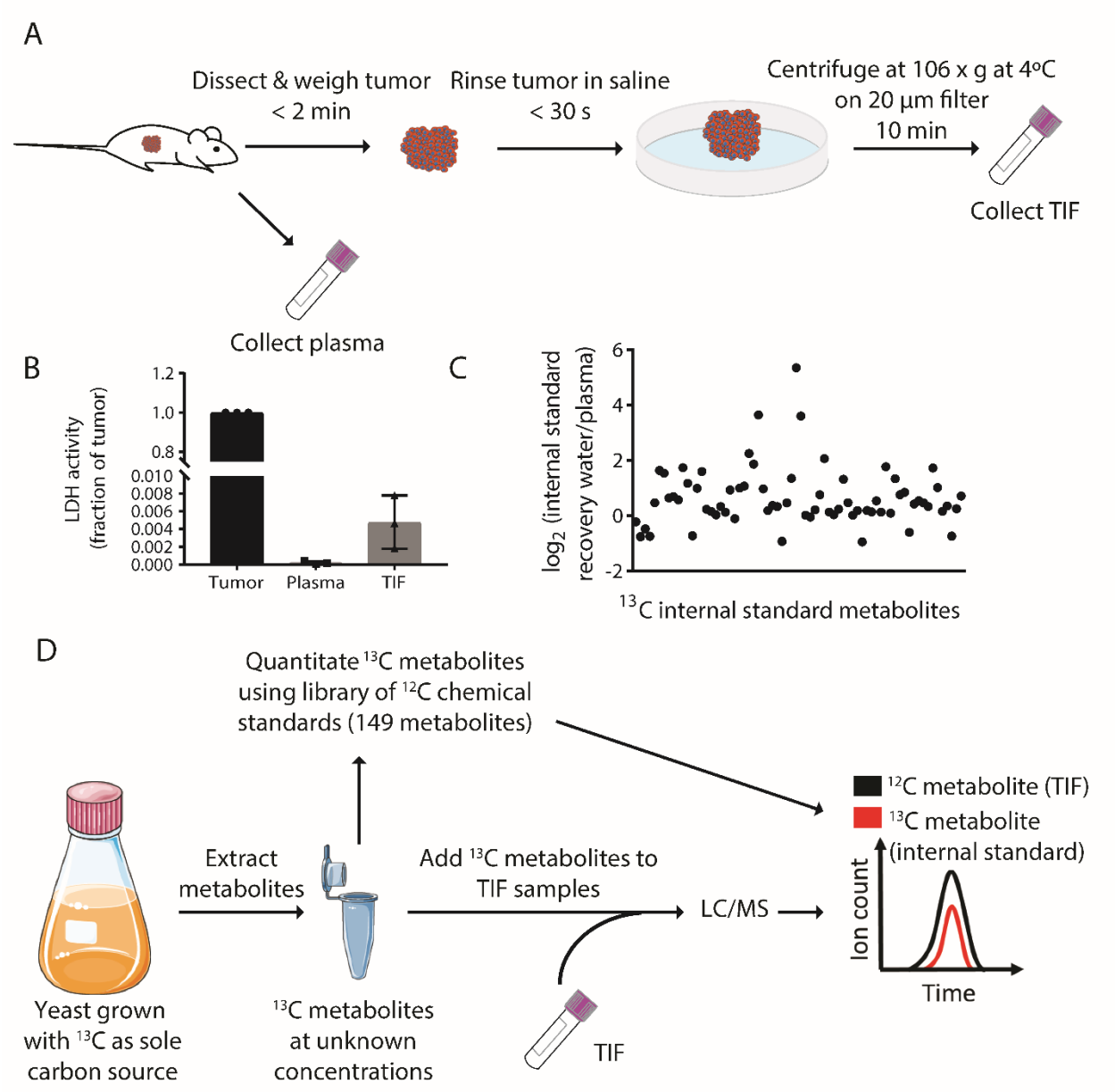

Figure 1. Stable Isotope dilution can be utilized to analyze the composition of TIF. (A) Schematic of TIF isolation. **(B)** LDH activity assay measuring the amount of LDH present in whole tumors, plasma, and TIF from PDAC tumor bearing mice. LDH activity was calculated for the entire volume of TIF isolated from one tumor and plotted as a ratio to the amount of LDH present in the whole tumor lysate. For each TIF sample, an equal volume of plasma was analyzed and compared to the tumor lysate. n = 3 tumors, plasma, and TIF samples each. **(C)** LC/MS measurement of equal concentrations of 70 ^{13}C chemical standards suspended in either water or mouse plasma. Data are plotted as the $\log_2$ fold change between the peak area of the metabolite in water versus in plasma. n = 19 plasma samples and n = 6 water samples. **(D)** Schematic summarizing the TIF quantification method.

To quantitate many metabolites simultaneously using the stable isotope dilution method, we utilized a metabolite extract derived from yeast grown on a ^{13}C carbon substrate in which intracellular metabolites are exhaustively labeled with ^{13}C. Such libraries have been shown to improve the accuracy and precision in metabolite measurements in biological fluids such as plasma (Hermann et al., 2018). In order to use metabolites in the ^{13}C yeast extract as quantitative internal standards, we first quantitated the labeled metabolites in the ^{13}C yeast extract by comparison with external standard curves of 149 polar metabolites detected in previous studies of human plasma metabolite levels (Cantor et al., 2017; Evans et al., 2009; Lawton et al., 2008; Mazzone et al., 2016). 70 metabolites from TIF and plasma samples were quantified by stable isotope dilution using the ^{13}C yeast extract, with lower limits of detection ranging from 100nM to 3µM. The remaining 79 metabolites were not detected in the ^{13}C yeast extract. These metabolites were instead quantified in the TIF and plasma samples by fitting metabolite peak intensity in the samples to the external standard curves (external standard calibration). These measurements are subject to matrix effects of unknown magnitude. We measured the inter-day reproducibility of our method for quantifying metabolites using both stable isotope dilution and calibration to external standard curves in 6 PDAC TIF samples (Figure 2). There was a high degree of correlation across 5 orders of magnitude of metabolite concentrations measured in the TIF samples analyzed by either stable isotope dilution or by calibration to external standards on separate days.

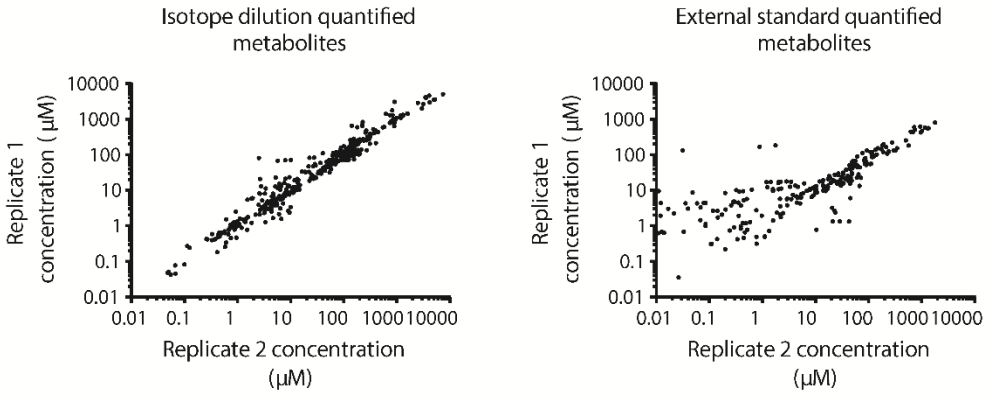

Figure 2. TIF metabolite quantification is reproducible, particularly when using stable isotope dilution. Scatter plots of average LC/MS measurements of metabolite concentrations across two technical replicates of 6 PDAC TIF samples run on different days using either stable isotope dilution (*left*) or calibration to external standard curves (*right*). Each PDAC sample was quantified twice, on different days and using different batches of ^{13}C yeast extract.

Our degree of reproducibility is similar to other quantitative metabolomics studies (Chen et al., 2016). However, particularly for low abundance metabolites (<10μM), metabolites quantified by stable isotope dilution showed greater inter-day reproducibility than those analyzed by external standard calibration. Thus, due to potential matrix effects and lower reproducibility, we consider the concentrations assigned by external standard calibration to be semi-quantitative, in contrast to the quantitative measurements made by stable isotope dilution. By either isotope dilution or external calibration, we measured between 118-136 metabolites in individual experiments analyzing plasma and TIF; low abundance metabolites that were not robustly and reproducibly detected were excluded from individual experiments. Together, this approach allowed us to obtain a combination of quantitative and semi-quantitative measurements of metabolite concentrations in both plasma and TIF.

Pancreatic tumor TIF differs from plasma

To determine if the metabolic composition of TIF differs from that of plasma, we isolated TIF and plasma from PDAC tumor bearing mice. Methods of blood collection that require anesthesia can alter circulating metabolite levels (Overmyer et al., 2015) (Figure 3). Therefore, to ensure that plasma samples would be directly comparable to TIF, plasma samples were isolated from mice via cardiac puncture upon euthanasia.

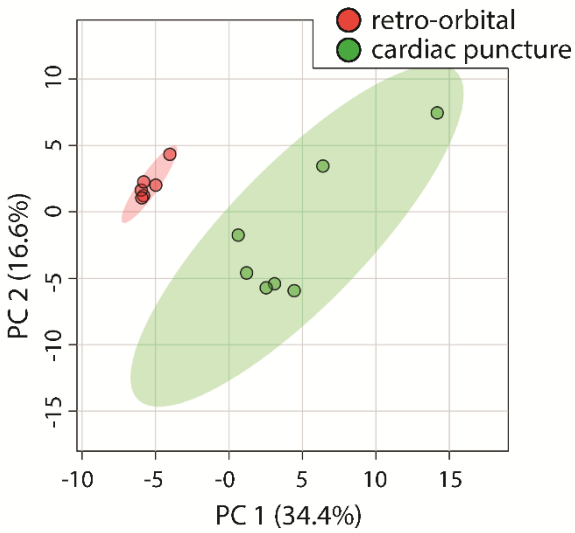

Figure 3. Method of blood collection affects plasma metabolite levels. Principal component analysis of mouse plasma samples based on LC/MS measurements of 117 metabolite concentrations from C57BL/6J mice bearing PDAC tumors. Blood was collected using either retro-orbital bleeding from anesthetized mice or cardiac puncture immediately following cervical dislocation of mice. n = 6 for retro-orbital blood collection, n = 7 for cardiac puncture blood collection.

PDAC TIF and plasma samples were metabolically profiled using the described metabolomics techniques and grouped by either hierarchical clustering (Figure 4A) or principal component analysis (Figure 4B) of metabolite concentrations. By each method, the PDAC TIF samples clustered separately from the plasma samples, suggesting that the metabolic composition of PDAC TIF differs from that of plasma. PDAC TIF and plasma exhibit different matrix effects (Figure 5), which could contribute to the observed global differences in

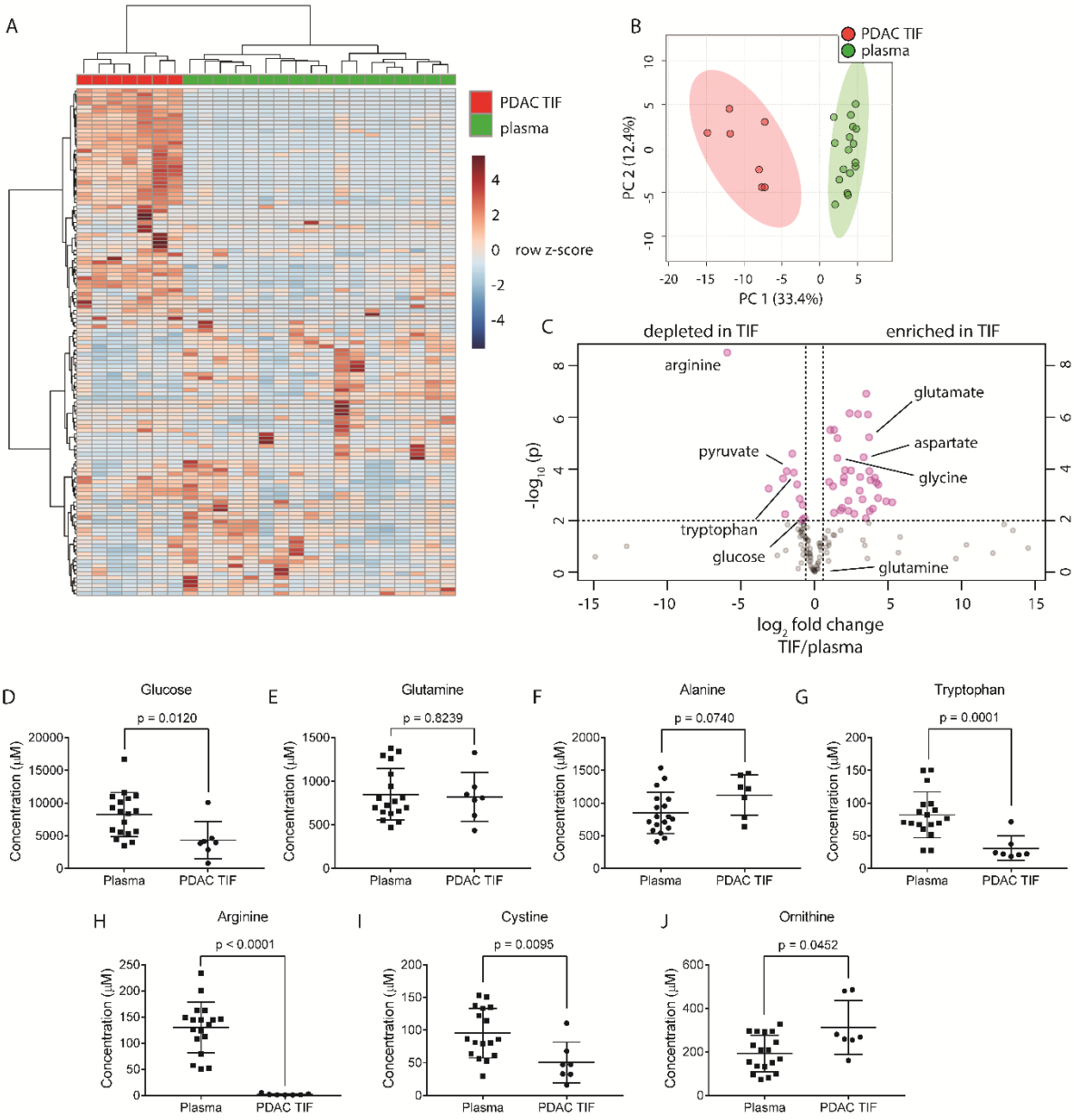

Figure 4. TIF metabolite levels are different than those in plasma. (A) Hierarchical clustering of PDAC TIF and mouse plasma samples based on LC/MS measurements of 136 metabolite concentrations. **(B)** Principal component analysis of PDAC TIF samples and mouse plasma samples based on LC/MS measurements of 136 metabolite concentrations. **(C)** Volcano plot depicting the $\log_2$ fold change in metabolite concentration between PDAC TIF and plasma. A fold change of 1.5 and a raw p-value of 0.01 assuming unequal variance were used to select significantly altered metabolites indicated in pink. LC/MS measurements of glucose **(D)**, glutamine **(E)**, arginine **(F)**, tryptophan **(G)**, alanine **(H)**, cystine **(I)**, and ornithine **(H)** in PDAC TIF and plasma samples. For all panels, n=7 for PDAC TIF and n = 18 for plasma samples.

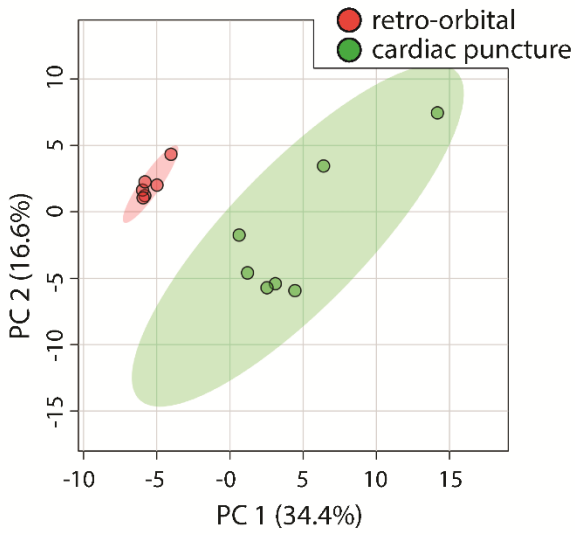

Figure 5. Plasma and TIF exhibit different matrix effects. LC/MS measurement of equal concentrations of 70 ^{13}C chemical standards suspended in either mouse plasma or mouse PDAC TIF. Data are plotted as the $\log_2$ fold change between the peak area of the ^{13}C metabolite in water versus in plasma. n = 19 plasma samples, n = 22 TIF samples.

metabolite levels between TIF and plasma. Therefore, we also conducted a comparison of PDAC TIF and plasma metabolite levels using only metabolites quantified by stable isotope dilution. PDAC TIF is still substantially different from plasma when analysis is limited to only metabolites quantitated using isotopically labeled internal standards (Figure 6), suggesting that the global metabolite composition of TIF differs from that of plasma. The composition of TIF is determined by the summed consumption and excretion rates of nutrients by all cells in the tumor microenvironment and the exchange rate of those metabolites between the TIF and circulation or lymph; thus, TIF composition does not allow for extrapolation of the rates of consumption and excretion of nutrients from tumors. However, if the exchange rate of TIF and the whole-body circulation is slow or compromised, then nutrients that are highly consumed by cells within a tumor may be depleted in the TIF relative to the circulation, while metabolic by-products may accumulate. Therefore, we predicted that nutrients that are highly consumed by tumors and cancer cells in culture may be depleted in TIF, and metabolites excreted by tumors may accumulate in TIF. Consistent with the avid consumption of glucose observed in tumors and cancer cell lines, glucose was depleted in TIF compared to plasma (Figure 4C-D). Amino acids known to be produced by tumors such as glycine and glutamate (Hosios et al., 2016; Jain et al., 2012) were enriched in TIF (Figure 4C). Interestingly, the amino acid glutamine, which is consumed rapidly by cultured cells (Eagle, 1955; Hosios et al., 2016; Jain et al., 2012), was present at similar concentrations in TIF and plasma (Figure 4C,E). We also found that alanine, an amino acid thought to support PDAC cells (Sousa et al., 2016), was abundantly present in both TIF and plasma (Figure 4F).

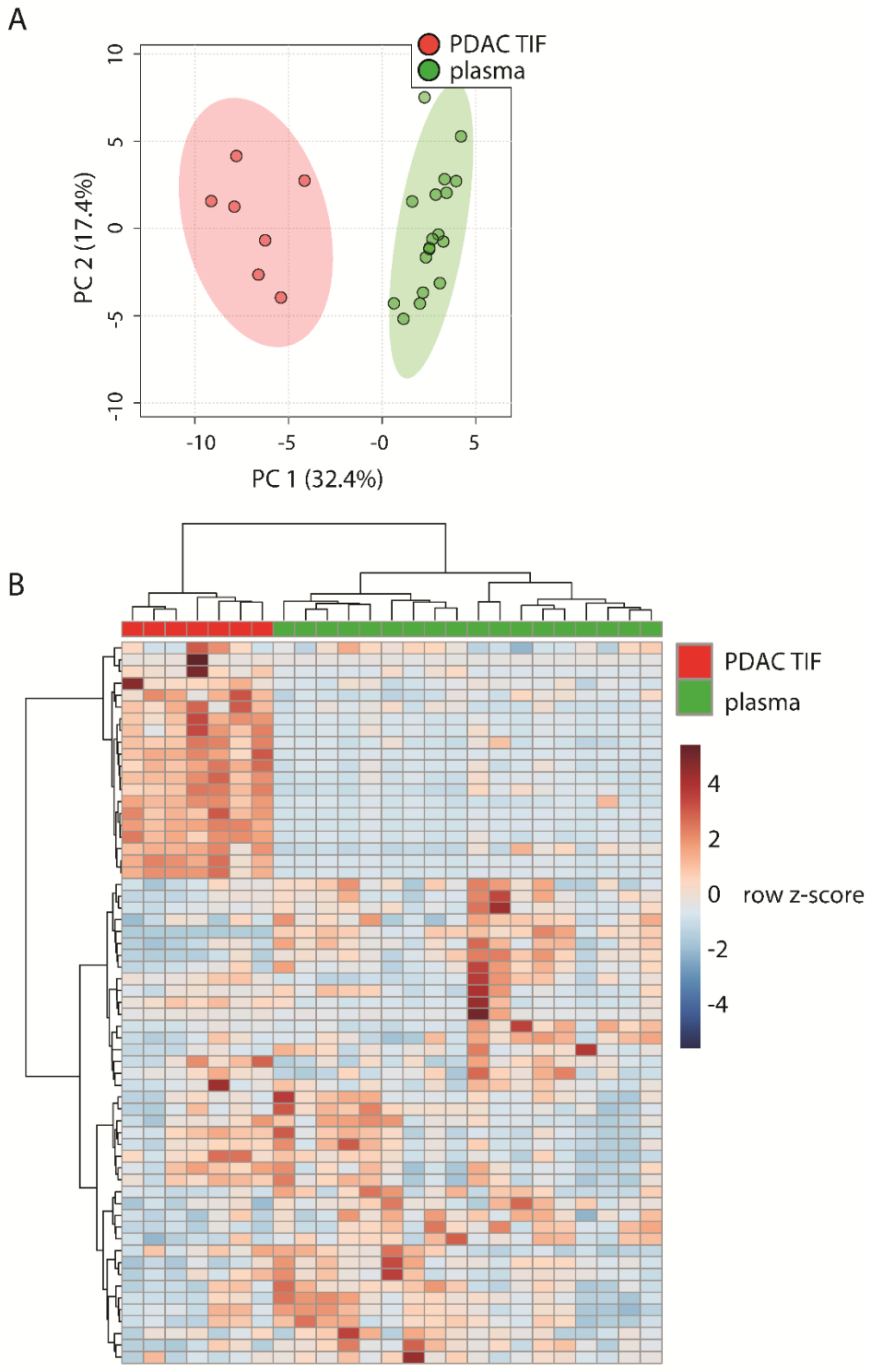

Figure 6. PDAC TIF differs from plasma when comparing only those metabolites quantified using internal isotope-labeled standards. Hierarchical clustering **(A)** and principal component analysis **(B)** of PDAC TIF and mouse plasma samples based on LC/MS measurements of 62 metabolite concentrations using internal standards. For all panels, n=7 for PDAC TIF and n = 18 for plasma samples.

Further, metabolites important for immune cell function such as arginine, tryptophan and cystine (Geiger et al., 2016; Moffett and Namboodiri, 2003; Srivastava et al., 2010) were depleted in PDAC TIF compared to plasma (Figure 4C, G-I). Additionally, levels of ornithine in PDAC TIF increased relative to plasma, suggesting that local arginase activity (Caldwell et al., 2018) may account for PDAC depletion of arginine (Figure 4J). Many metabolites were enriched in TIF (Figure 4C), suggesting that the PDAC tumor microenvironment is not depleted for all nutrients. Instead, PDAC TIF is composed of a complex mix of metabolites that are different from those present in circulation.

Tumor size does not dictate PDAC TIF composition

Having established that PDAC TIF composition is different from that of plasma, we next sought to understand the factors that influence TIF composition. We hypothesized that five factors could influence TIF composition: tumor size, anatomical location, tumor tissue of origin, diet, and tumor genetics. We used mouse models of PDAC and LUAD to systematically test the impact of these factors on TIF nutrient composition. First, we sought to test if the size of tumors influenced the composition of TIF. Since murine PDAC tumors cause morbidity at different times and tumor sizes, we were able to isolate TIF from end stage PDAC tumors of varying sizes (0.31 g – 2.81 g). We tested if tumor size significantly altered TIF composition by comparing TIF metabolite concentrations between large (1.71 – 1.24 g) and small (0.78 – 1.22 g) PDAC tumors (Figure 7). We found that, at least within this size range of tumors, tumor size does not appear to dictate PDAC TIF metabolite levels.

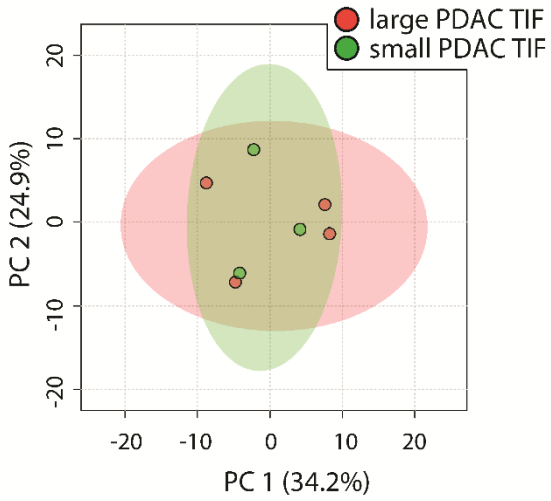

Figure 7. PDAC TIF metabolite levels are not significantly different between large and small tumors. Principal component analysis of TIF samples from large (1.71 – 1.24 g) and small (1.22 – 0.78 g) PDAC tumors based on LC/MS measurements of 136 metabolite concentrations. n=4 for large PDAC tumors and n = 3 for small PDAC tumors.

Tumor location affects the composition of TIF

We hypothesized that PDAC tumors growing in the pancreas, with its diverse set of stromal cells and poor vascularization, might have different TIF composition than the same tumor cells growing in other organs or anatomical locations in the body. To test this hypothesis, we compared the metabolic composition of TIF from autochthonous KP-/-C PDAC tumors to that of tumors derived by subcutaneously injecting PDAC cells isolated from KP-/-C tumors into genetically identical C57BL/6J mice (Figure 8A). Based on measurement of 123 quantitated metabolites that were detectable and quantifiable in this experiment, PDAC TIF was metabolically distinct from TIF derived from isogenic subcutaneous tumors both by principal component analysis (Figure 8B) and by hierarchical clustering (Figure 8C). Interestingly, concentrations of tryptophan, arginine and cystine, which are depleted in autochthonous PDAC TIF, were relatively higher in subcutaneous PDAC TIF (Figure 8D-F). This suggests that

subcutaneous models of PDAC may not mimic the metabolic microenvironment of PDAC tumors. Furthermore, while potentially confounded by comparing transplant and autochthonous PDAC models, these results suggest that the metabolic composition of TIF is not only determined by tumor-intrinsic factors, but potentially also by the anatomical location in which the tumor is growing.

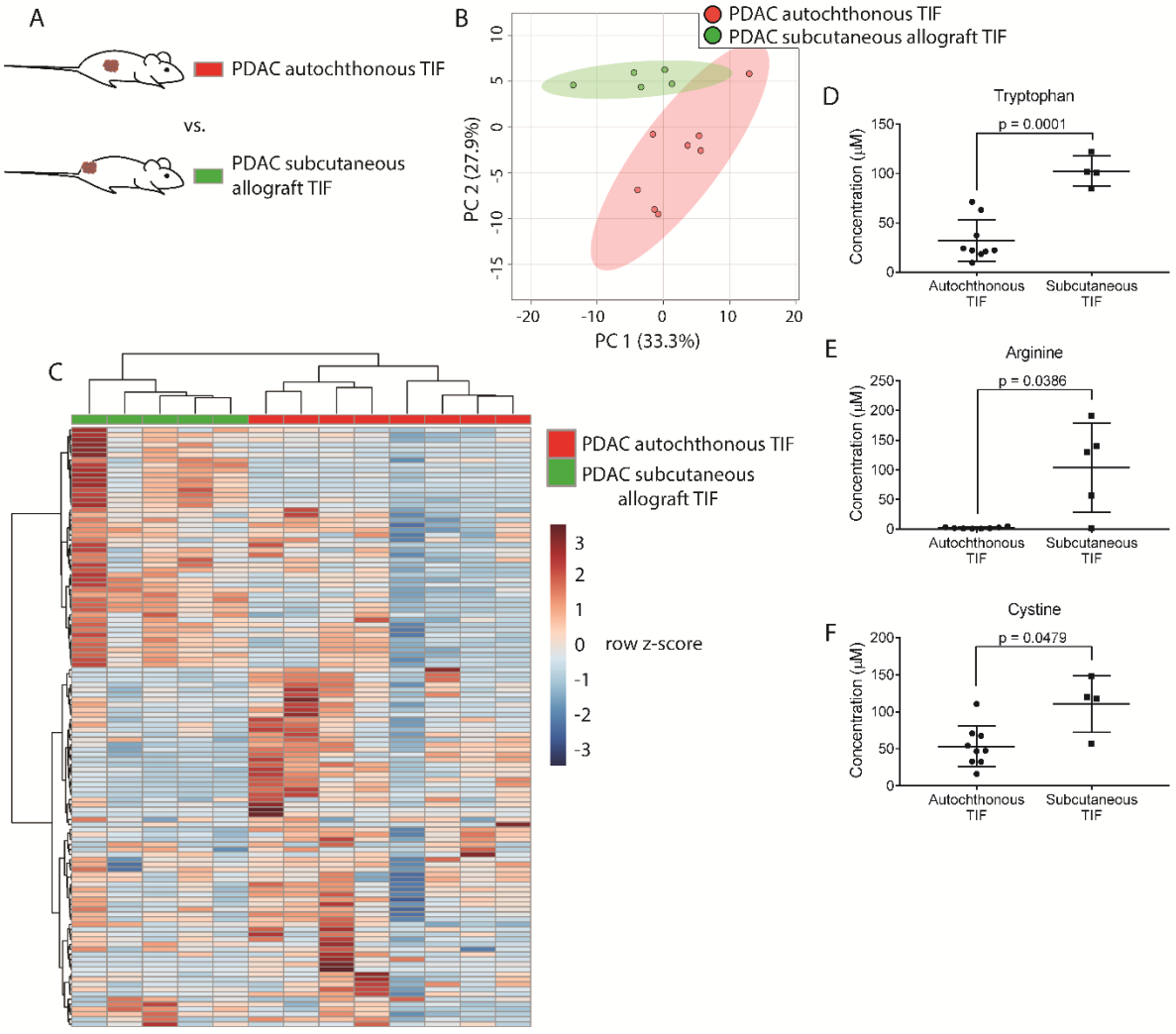

Figure 8. Tumor location dictates metabolic TIF composition. (A) Diagram of experimental models used to test the effect of tumor location on TIF metabolite levels. Principal component analysis **(B)** and hierarchical clustering **(C)** of PDAC TIF and PDAC subcutaneous allograft TIF samples based on LC/MS measurements of 123 metabolite concentrations. LC/MS measurements of tryptophan **(D)**, arginine **(E)**, and cystine **(F)** in PDAC TIF and PDAC subcutaneous allograft TIF. For all panels, n = 7 for PDAC TIF samples and n = 5 for PDAC subcutaneous allografts.

Dietary changes alter TIF composition

Though TIF metabolite levels do not match those found in plasma, factors that influence circulating nutrient levels may be reflected in TIF. One important determinant of plasma metabolite levels is diet; thus, we examined whether dietary changes would alter TIF metabolite levels. For this analysis, we isolated TIF from isogenic PDAC subcutaneous allografts in mice fed either standard mouse chow derived from plant and animal products or a defined diet that replaces whole protein with purified amino acids. This allows us to compare genetically identical tumors growing in the same anatomical location, where only diet is altered. These diets contain many differences in nutrient levels, providing a test case to determine whether significant dietary alterations affect TIF metabolite levels. Based on measurement of 123 metabolites that were detectable and quantifiable in this experiment, TIF from mice fed standard chow differed from TIF from mice fed a defined diet based on principal component analysis (Figure 9B) and hierarchical clustering (Figure 9C).

We next wanted to determine if the changes in TIF composition between diets were primarily due to altered nutrient availability to TIF from circulation, or if other physiological effects of altered diet were affecting TIF. If dietary perturbations primarily affect TIF by simply altering plasma nutrient levels, then the concentration of a metabolite in TIF should correlate with its concentration in plasma to the same degree in both dietary conditions. Thus, if a dietary change increases the plasma level of a metabolite, then the TIF concentration of that metabolite should also increase. Indeed, there is a strong correlation (Pearson r = 0.8927) between TIF to plasma ratio of metabolite concentrations between mice on different diets (Figure 9D).

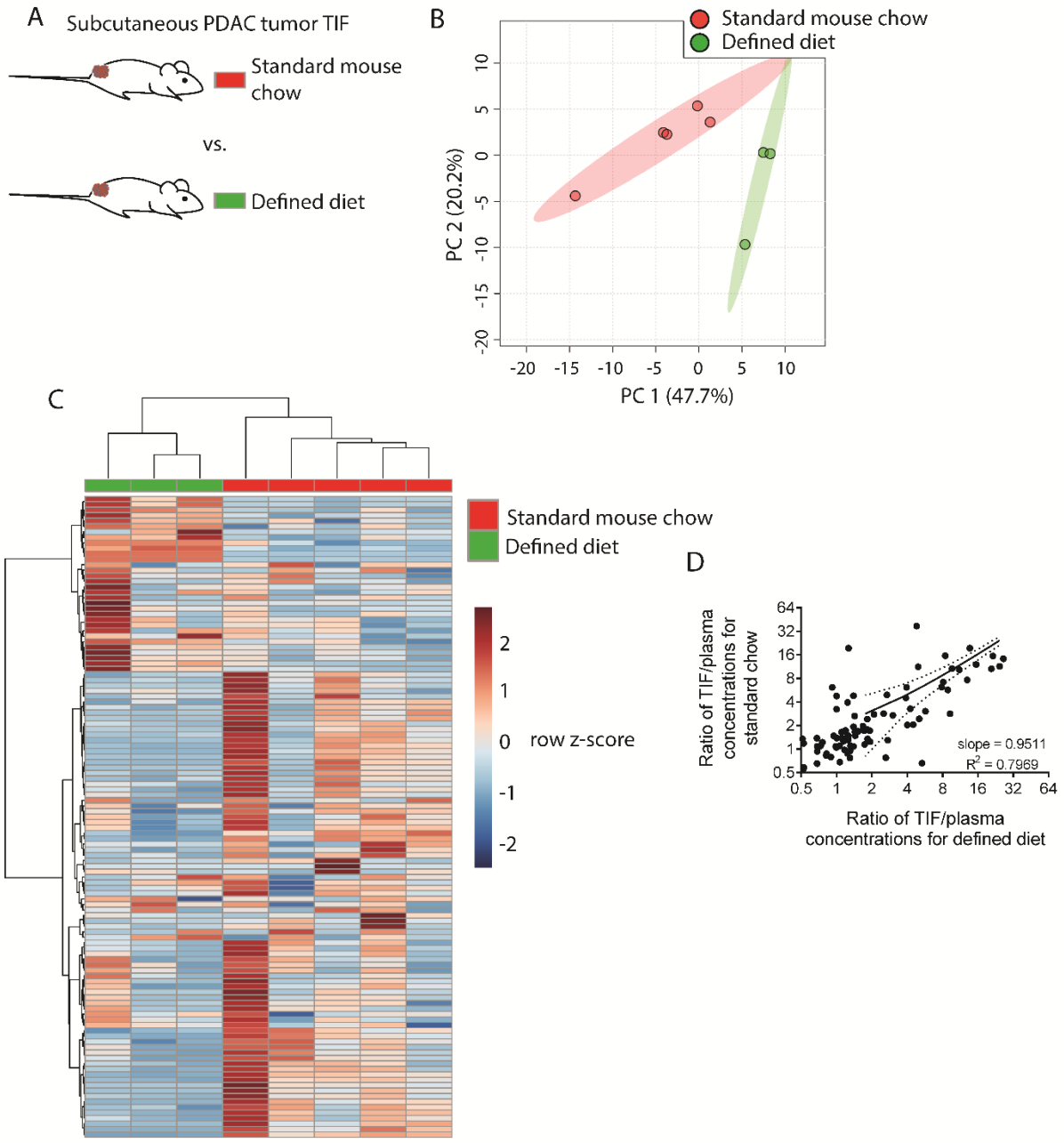

Figure 9. Dietary changes alter TIF composition. (A) Schematic of experimental models used to test the effect of diet on TIF metabolite levels. Principal component analysis **(B)** and hierarchical clustering **(C)** of subcutaneous PDAC allograft TIF samples from mice fed standard mouse chow versus mice fed a defined diet based on LC/MS measurements of 123 metabolite concentrations. **(D)** Ratios of LC/MS measurements of 123 metabolites in TIF versus matched plasma from the same mouse fed standard mouse chow plotted versus the same ratios in mice fed a defined diet. For all panels, n = 5 for TIF from mice fed standard mouse chow and n = 3 for TIF from mice fed a defined diet.

Furthermore, linear regression of TIF to plasma ratios in mice fed different diets nearly yields an identity function (slope = 0.9511, R^2 = 0.7969) (Figure 9D). Thus, while individual TIF metabolite levels are scaled by some factor relative to plasma levels, dietary perturbation does not broadly affect this scaling factor. Thus, in addition to local microenvironmental factors, systemic metabolic changes can affect the composition of TIF by altering circulating nutrient levels.

Tumor tissue of origin affects TIF makeup

Tumor location and circulating metabolite levels are cell-extrinsic factors that influence the TIF composition. However, there exist many cell-intrinsic factors that alter cancer cell metabolism. For instance, the metabolic properties of cancer cells depend upon the tissue from which they originated (Hu et al., 2013; Mayers et al., 2016; Yuneva et al., 2012). To examine whether tissue of origin influences the metabolic makeup of the tumor microenvironment, cancer cells derived from lung (Jackson et al., 2005; Jackson et al., 2001) and PDAC (Bardeesy et al., 2006) tumors both driven by activation of *Kras* and loss of *Trp53* were injected subcutaneously into C57BL/6J mice, such that tumors were established in the same location and with the same genetics, but different tissues of origin (Figure 10A). Based on measurement of 104 metabolites that were detectable and quantifiable in this experiment, TIF from subcutaneous tumors derived from LUAD clustered separately from PDAC subcutaneous allograft TIF by principal component analysis (Figure 10B) and hierarchical clustering (Figure 10C). Similar results were obtained when the analysis was limited to only metabolites quantitated by stable isotope dilution (Figure 11). LUAD and PDAC tumors are known to have different branched-chain amino acid metabolism (Mayers et al., 2016), and levels of branched-chain amino acids and their catabolites were different between LUAD and PDAC tumors (Figure

10D). Additionally, a number of metabolites involved in thiol metabolism are altered between LUAD and PDAC tumors (Figure 10D) (Gall et al., 2010; Irino et al., 2016), suggesting potential differences in sulfur metabolism between these tumors. Collectively, these data suggest that tissue of origin is a determinant of the metabolic composition of TIF.

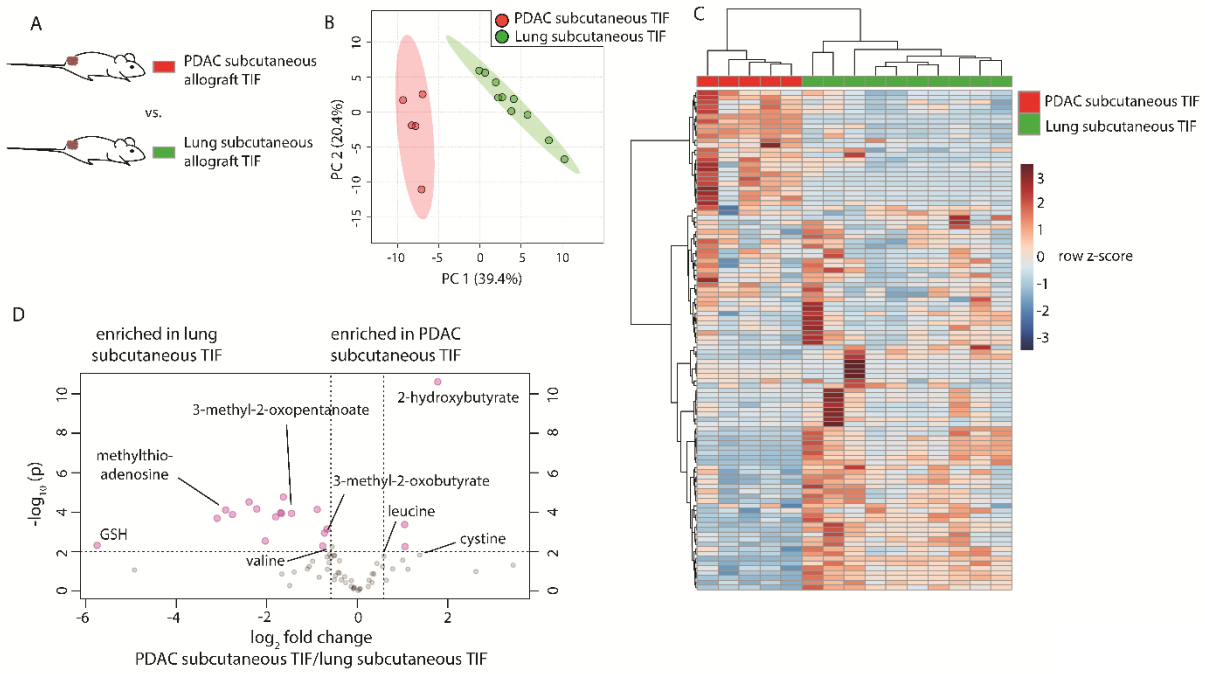

Figure 10. Tumor tissue of origin influences TIF composition independent of tumor location. (A) Diagram of experimental models used to test the effect of tumor tissue of origin on TIF metabolite levels. Principal component analysis **(B)** and hierarchical clustering **(C)** of PDAC subcutaneous allograft TIF and LUAD subcutaneous allograft TIF samples based on LC/MS measurements of 104 metabolite concentrations. **(D)** Volcano plot depicting the $\log_2$ fold change in metabolite concentration between PDAC and LUAD TIF for metabolites measured using stable isotope dilution. A fold change of 1.5 and raw p-value of 0.01 assuming unequal variance were used to select significantly altered metabolites indicated in pink. For all panels, n = 5 for PDAC subcutaneous allograft TIF samples and n = 10 for LUAD subcutaneous allograft TIF samples.

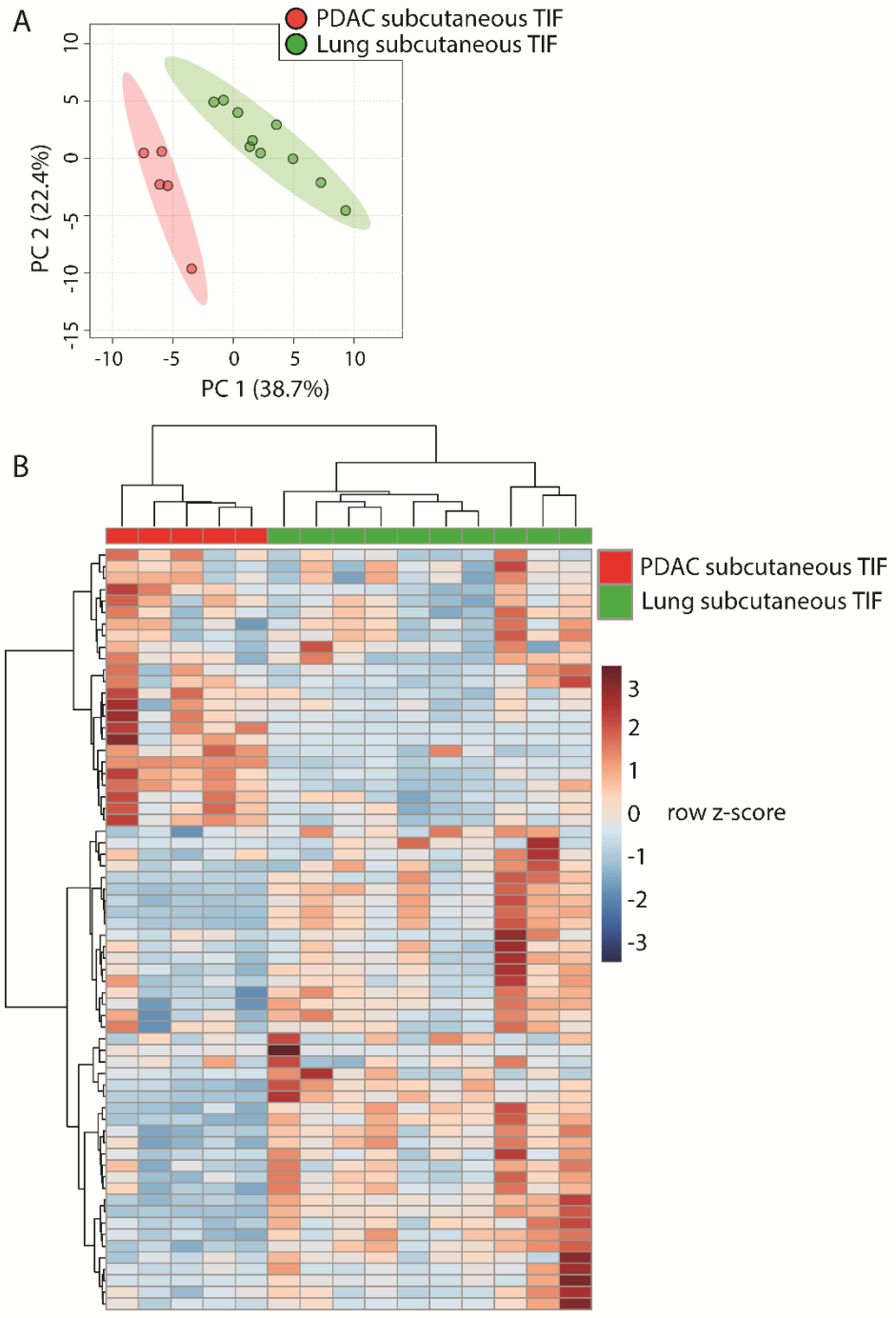

Figure 11. Tumor tissue of origin influences TIF when measured using internal standards only. (A) Diagram of experimental models used to test the effect of tumor tissue of origin on TIF metabolite levels. Principal component analysis **(B)** and hierarchical clustering **(C)** of PDAC subcutaneous allograft TIF and LUAD subcutaneous allograft TIF samples based on LC/MS measurements of 67 metabolites quantified using isotope-labeled internal standards. For all panels, n = 5 for PDAC subcutaneous allograft TIF samples and n = 10 for LUAD subcutaneous allograft TIF samples.

Genetic loss of the tumor suppressor Keap1 has a moderate effect on TIF composition

Genetic alterations can profoundly alter cancer metabolism (Nagarajan et al., 2016). As a test case for whether tumor genetics can influence the metabolism of TIF, we focused on the tumor suppressor *Keap1*. *Keap1* loss is a common occurrence in lung cancer that alters expression of oxidative stress response genes and nutrient transporters, which causes cells to secrete high levels of glutamate and renders tumors highly dependent on glutamine catabolism for growth (Romero et al., 2017; Sayin et al., 2017). Thus, *Keap1* null tumors may possess remodeled metabolism that would be reflected in TIF composition. To test this possibility, we injected previously described LUAD cell lines with wild-type *Keap1* (sgControl) or *Keap1* loss (sg*Keap1*) (Romero et al., 2017) subcutaneously into the flanks of C57BL/6J mice (Figure 12A), and TIF was isolated from these tumors. Based on measurement of 131 metabolites that were detectable and quantifiable in this experiment, TIF samples did not cluster separately based on *Keap1* status by principal component analysis (Figure 12B), but did cluster separately by hierarchical clustering (Figure 12C). Surprisingly, anticipated changes in TIF composition based on alterations to cancer cell metabolism by *Keap1* loss, such as decreased glutamine, glucose and cystine, and increased glutamate and lactate (Romero et al., 2017) were not observed between TIF samples of *Keap1* wild-type and *Keap1* null tumors (Figure 12D-H). Together, these results suggest that genetic *Keap1* status is not a major determinant of metabolic TIF content in subcutaneous lung cancer allografts, and that not all cancer cell-intrinsic perturbations of metabolism cause detectable changes to the tumor nutrient milieu.

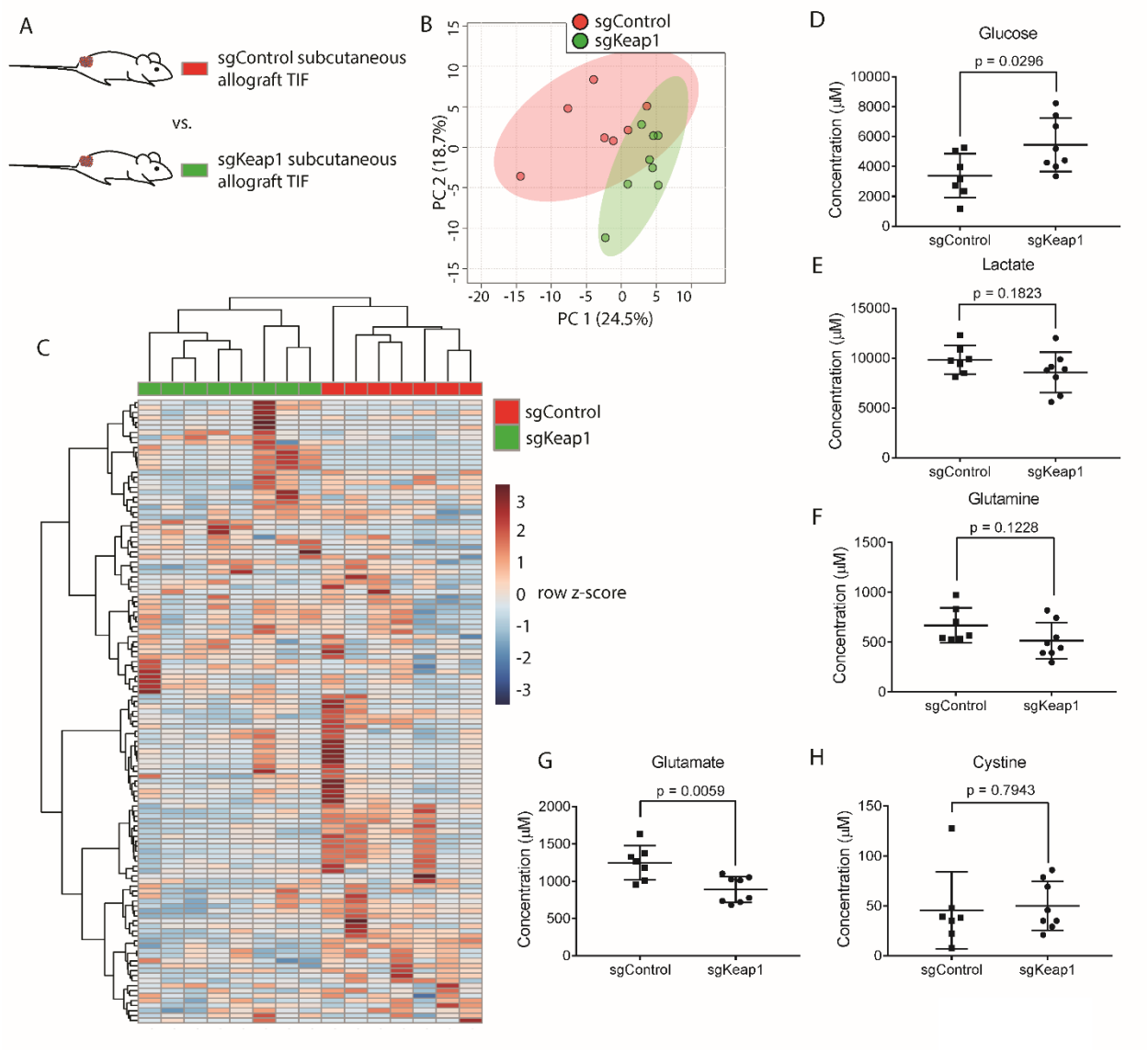

Figure 12. Genetic *Keap1* status is not a major determinant of TIF composition in subcutaneous LUAD allograft tumors. (A) Schematic of experimental models used to test the effect of genetic loss of *Keap1* on TIF metabolite levels. Principal component analysis **(B)** and hierarchical clustering **(C)** of *Keap1* wild-type (sgControl) and *Keap1* null (sgKeap1) subcutaneous LUAD allograft TIF samples based on LC/MS measurements of 131 metabolite concentrations. LC/MS measurements of glucose **(D)**, lactate **(E)**, glutamine **(F)**, glutamate **(G)**, and cystine **(H)** in *Keap1* wild-type (sgControl) and *Keap1* null (sgKeap1) subcutaneous lung allograft TIF samples. For all panels, n = 10 for sgControl subcutaneous lung allograft TIF samples and n = 8 for sgKeap1 subcutaneous LUAD allograft TIF samples.

DISCUSSION

Pancreatic and lung tumors are exposed to nutrient levels different from those in plasma

Intravital imaging of tumors in patients (Fisher et al., 2016) and murine cancer models (Fukumura et al., 2010) has revealed that solid tumors generally have abnormal and dysfunctional vasculature and lymphatic vessels. For example, only ~30% of PDAC blood vessels appear functional (Olive et al., 2009). This is thought to limit nutrient delivery from the circulation to tumors both by reducing blood flow and by inhibiting transcapillary filtration due to increased interstitial pressure (Stylianopoulos et al., 2018). PDAC tumors in particular have striking defects in vasculature with numerous collapsed vessels triggered by increased interstitial pressure (DuFort et al., 2016; Provenzano et al., 2012) or solid stress (Chauhan et al., 2014). In contrast to normal tissues, which, while not in perfect metabolic equilibrium with the circulation (Cengiz and Tamborlane, 2009), tend to have nutrient levels close to what is in the circulation (Lonnroth et al., 1987), it is unlikely that the interstitial environment of tumors is in rapid exchange with the circulation. Coupled with the high metabolic rate of cancer cells, this has led to speculation that tumors will be both nutrient deprived and accumulate metabolic wastes. We find that TIF metabolite levels in the murine cancer models assessed are different from the nutrient levels in plasma. Contrary to many assumptions, not all nutrients are depleted in TIF, with levels of some being higher than what is found in circulation. Thus, our measurements of plasma and TIF nutrient composition are consistent with a model where tumors with abnormal vasculature exist largely as a separate compartment from the bulk circulation, and can have different steady state metabolic microenvironments. This underscores the importance of understanding TIF composition for studies of tumor metabolism.

While we have considered the tumor as a single compartment and analyzed bulk TIF from the entire tumor, it is possible that the tumor actually contains a population of sub-compartments with different perfusion rates (Hensley et al., 2016) and heterogeneous TIF compositions (Wagnerand and Wiig, 2015). Measurements of intratumor metabolites in subsections of tumors suggests that some tumor regions experience different nutrient levels than others (Pan et al., 2016). Thus, while the overall tumor metabolic microenvironment differs from the circulation, an important future challenge will be to understand how compartmentalized nutrient delivery contributes to metabolic heterogeneity observed in solid tumors (Hensley et al., 2016).

Though TIF appears to constitute a separate compartment from plasma, tumor nutrients are ultimately delivered from the circulation. Thus, perturbations to systemic nutrient levels by altering diet affect TIF composition. This relationship between plasma and TIF nutrient levels across different diets suggests that TIF levels of metabolites are derived from plasma metabolite concentrations, and changes in plasma metabolite levels lead to scaled changes in TIF metabolite levels. This argues that a major mechanism by which diet influences tumor nutrient availability is by altering nutrients available in the circulation.

Tumor properties that influence the metabolic microenvironment

Beyond dietary factors, we considered four variables that could influence tumor nutrient availability: tumor size, tissue of origin, tumor anatomical location and tumor genetic make-up. Though we observed that tumor size did not strongly affect the composition of TIF in PDAC tumors, we collected TIF from a relatively small range of sizes of end stage PDAC tumors. Future

work to examine the TIF composition of tumors at various sizes and stages of development may reveal effects of tumor size on TIF nutrient levels.

The finding that PDAC and LUAD tumors have different TIF composition suggests that tissue of origin is a factor that can influence the metabolic microenvironment; however, the mechanism(s) driving this difference remain unclear. Whether cancer cell-intrinsic metabolic differences endowed by the epigenetic memory of the tissue of origin (Hu et al., 2013; Mayers et al., 2016) or other cell-extrinsic differences between PDAC and LUAD, such as differences in non-cancer cells present in the tumor, drive the difference in TIF composition is another important question for future study.

Tumors in different anatomical locations will also contain different stromal cells and different vascularization which could alter the metabolic microenvironment. Comparison of autochthonous and subcutaneous PDAC tumors driven by the same oncogenic driver mutations revealed significant differences in TIF nutrient levels. This suggests that subcutaneous models of PDAC may not fully recapitulate the metabolic microenvironment of this disease, and is in line with observations that subcutaneous models of PDAC fail to recapitulate many aspects of PDAC tumors including marked stromal infiltration and extracellular matrix deposition (Hwang et al., 2016). These observations, along with recent findings that subcutaneous PDAC models do not recapitulate whole body metabolic perturbations observed in autochthonous PDAC models and patients (Danai et al., 2018), suggest subcutaneous models do not recapitulate all metabolic aspects of the disease.

As we compared transplant to autochthonous PDAC models, we cannot distinguish between differences in TIF composition driven by anatomical location versus differences caused

by unique characteristics of transplant and genetically engineered PDAC models. Nevertheless, it is intriguing that autochthonous PDAC tumors have lower levels of arginine, tryptophan and cystine compared to subcutaneous tumors. Stromal myeloid derived cells have been implicated in depleting each of these nutrients from the tumor microenvironment (Kumar et al., 2016), and murine PDAC tumors are known to contain a large number of myeloid lineage cells (Bayne et al., 2012; Goedegebuure et al., 2011; Stromnes et al., 2014; Zhao et al., 2009). Additionally, subcutaneous PDAC tumors are known to have fewer stromal cells (Hwang et al., 2016; Sousa et al., 2016). Thus, it is tempting to speculate that differences in TIF composition between autochthonous and subcutaneous PDAC tumors, including differences in arginine, tryptophan and cystine levels, could be driven by differences in stromal cell populations between anatomical sites. Understanding how anatomical location alters the metabolic microenvironment is critical to determine how local metabolic constraints shape the metabolism of tumors growing in different locations, such as primary and metastatic tumors (Schild et al., 2018).

Lastly, we hypothesized that tumor genetics would also alter TIF composition, and studied the effect of *Keap1* loss because *Keap1* null cancer cells have dramatic alterations in cell-intrinsic metabolism (Best et al., 2018; DeNicola et al., 2015; DeNicola et al., 2011; Mitsuishi et al., 2012; Romero et al., 2017; Sayin et al., 2017). We found moderate differences in TIF composition between tumors formed from otherwise isogenic LUAD cell lines that differed only in *Keap1* loss. These data argue that factors beyond cancer cell-intrinsic metabolism can be dominant in setting nutrient levels in the microenvironment, although future studies are required to determine how other oncogenic alterations alter TIF composition.

Implications of TIF nutrient levels for cellular metabolism and function in the tumor

It is tempting to interpret depletion or accumulation of metabolites as simply being due to rapid cancer cell consumption or release of metabolites without appropriate replenishment or removal from the circulation, allowing cancer cell-intrinsic changes in metabolism to be read out as differences in TIF nutrient levels. However, wild type and *Keap1* null cancer cells have significant changes in metabolism (Best et al., 2018; DeNicola et al., 2015; DeNicola et al., 2011; Mitsuishi et al., 2012; Romero et al., 2017; Sayin et al., 2017), yet tumors derived from cells of these genotypes do not show significant alterations in levels of nutrients whose metabolism is known to be altered by *Keap1* loss. Thus, differences in metabolite concentrations between TIF and plasma cannot be used to extrapolate consumption and release of metabolites by tumors. Instead, future experiments measuring differences in arterial and venous metabolite levels could shed light into quantitative tumor nutrient consumption and release (Gullino et al., 1967; Kallinowski et al., 1988; Sauer et al., 1982).

Nutrient levels in the tumor microenvironment can have profound impacts on the metabolism, growth and drug sensitivity of tumor resident cancer cells (Muir et al., 2018). Our study provides insight into tumor nutrient levels *in vivo* and suggests specific implications for tumor resident cell metabolism. First, we find PDAC tumor interstitial fluid is depleted of some nutrients relative to plasma. Interestingly, these depleted nutrients are not necessarily metabolites predicted to be depleted by cell culture studies. For example, PDAC cells consume large amounts of glucose and glutamine in culture (Son et al., 2013; Ying et al., 2012), and it has been assumed that these nutrients are depleted in the microenvironment (Commisso et al., 2013; Kamphorst et al., 2015; Lyssiotis and Kimmelman, 2017; Sherman et al., 2017; Sousa et

al., 2016). Alanine and branched chain amino acids are also proposed to be limiting for proliferation of PDAC cells in tumors, requiring cancer cells to acquire those nutrients from alternative sources such as stromal cells or extracellular protein (Grankvist et al., 2018; Palm et al., 2015; Sousa et al., 2016). We find that neither glutamine, alanine nor branched-chain amino acids are substantially depleted in PDAC tumors regardless of anatomical site. Further, while glucose is depleted in PDAC TIF relative to circulatory levels, it is still present at millimolar concentration, and glucose deprivation in TIF is not a universal feature of tumors (Siska et al., 2017). Thus, nutrients inferred from cell culture studies to be depleted and limiting in the tumor microenvironment may not be always be key microenvironmental drivers altering PDAC metabolism.

We find that the nutrient most strongly depleted from PDAC TIF is arginine. Arginine supports many aspects of cell physiology (Morris, 2007), raising the question of how PDAC cells adapt to survive and proliferate when levels of this amino acid are so low. Many cell types can synthesize arginine using urea cycle enzymes (Wu et al., 2009), but these metabolic enzymes are silenced by many tumors to enhance nucleotide production (Rabinovich et al., 2015). However, PDAC tumors do not exhibit urea cycle enzyme silencing (Lee et al., 2018; Uhlen et al., 2015) and are reported to have a functional urea cycle (Zaytouni et al., 2017). Perhaps, PDAC cells retain this metabolic pathway to adapt to a tumor microenvironment with limited arginine availability. Additionally, PDAC cells utilize macropinocytosis of environmental protein (Commisso et al., 2013; Kamphorst et al., 2015), and this route of nutrient acquisition may allow PDAC cells to acquire sufficient arginine to support survival and growth.

TIF composition can alter the function of non-cancer cells, such as immune cells, in the tumor microenvironment (Buck et al., 2017). For example, in many tumor types, T lymphocytes can infiltrate and inhibit the progression of tumors, especially when this process is primed with checkpoint blockade treatment (Ribas and Wolchok, 2018). In contrast, PDAC tumors are highly immunosuppressive (Martinez-Bosch et al., 2018) and immunotherapy shows limited efficacy in this disease (Hilmi et al., 2018). Nutrient deprivation in PDAC TIF could contribute to PDAC immunosuppression. Both arginine and tryptophan, which are depleted in the autochthonous PDAC environment, are required for T cell function (Geiger et al., 2016; Moffett and Namboodiri, 2003). Intriguingly, depletion of myeloid cells capable of degrading arginine and tryptophan from PDAC tumors resulted in increased T cell infiltration, proliferation, and activation in PDAC tumors (Bayne et al., 2012; Stromnes et al., 2014; Zhang et al., 2017). Future studies determining how T cell metabolism and function is impacted by tumor nutrient levels could yield insight into how tumors suppress immune rejection (Ecker and Riley, 2018).

Cellular metabolism can respond and adapt to environmental nutrient levels. Indeed, growing cancer cells in media with different nutrient compositions alters their metabolic requirements and response to drugs (Cantor et al., 2017; Muir et al., 2017; Palm et al., 2015; Schug et al., 2015). That metabolism is responsive to environment may underpin the limited ability of *ex vivo* culture models using non-physiological nutrient levels to identify tumor-essential metabolic genes (Horvath et al., 2016; Muir and Vander Heiden, 2018; Ryan et al., 2018). However, given the dearth of information on physiological nutrient levels in solid tumors, it has not been possible to determine the metabolic phenotypes and liabilities of cancer cells in tumor nutrient conditions. By characterizing the polar small molecule nutrients

in PDAC and LUAD tumors, media that better approximates the nutrients available to cancer cells in tumors can be formulated. Examining non-polar and lipid metabolites in the microenvironment will further improve these efforts and lead to cancer models that may better allow us to identify metabolic liabilities of cancer cells that ultimately translate into more effective therapies.

MATERIALS AND METHODS

Animal Studies

All experiments performed in this study were approved by the MIT Committee on Animal Care (IACUC). All mice in this study were fully backcrossed to the C57BL/6J background. Animals were housed on a 12-hour light and 12-hour dark cycle, with ad libitum access to food and water. For studies using *Kras^{G12D} Trp53$^{fl/fl}$ Pdx-1-cre* (KP-/-C) mice (Bardeesy et al., 2006), male and female animals of this genotype were allowed for form end-stage tumors, which occurred approximately 8-10 weeks after birth (Danai et al., 2018). Animals were then euthanized and tumors harvested for TIF isolation as described below. Tumors weighed between 0.31 g – 2.81 g upon harvesting.

For subcutaneous xenograft studies, 12 week old C57BL/6J animals purchased from Jackson Laboratories (IMSR Cat# JAX:000664, RRID:IMSR_JAX:000664) were injected with 100,000 murine PDAC or LUAD cancer cells (suspended in a volume of 100 µL of Matrigel (Corning, 354234) brought to 10 mg/ml with RPMI-1640 (Corning, 50-020-PC) into the subcutaneous space on the flank of the mice. Cell lines used for subcutaneous engraftment in this study are described below. Tumors were then allowed to grow until they reached ~1cm^3 in

volume, which took ~4 weeks after engraftment. Upon the tumor reaching ~1cm^3, animals were euthanized and tumors harvested for TIF isolation as described below.

For dietary studies, C57BL/6J mice were engrafted with murine PDAC cells as described above. On the day of injection, the animals were separated into two cohorts. One group was fed standard mouse chow and the other group was fed a defined amino acid diet. Both groups were fed each diet ad libitum throughout the duration of the experiment. Upon the tumor reaching 1cm^3, animals were euthanized and tumors harvested for TIF isolation as described below.

Cell lines and culture

The murine PDAC cancer cell line (AL1376) used for making subcutaneous grafts was generated as previously described (Mayers et al., 2014) from PDAC tumors from a KP-/-C animal in the C57BL/6J background. The C57BL/6J LUAD cancer cell lines with and without loss of *Keap1* used in tumor grafts in this study were generated previously (Romero et al., 2017) from the *Kras^{G12D} Trp53$^{fl/fl}$ Adenoviral-cre* model of LUAD (Jackson et al., 2005; Jackson et al., 2001). All cell lines were regularly tested for mycoplasma contamination using the Mycoprobe mycoplasma detection kit (R&D Systems). All cells were cultured in a Heracell (Thermofisher) humidified incubators at 37 °C and 5% CO_2. Cell lines were routinely maintained in RPMI-1640 (Corning, 50-020-PC) supplemented with 10% heat inactivated fetal bovine serum (Seradigm, Lot 120B14).

Isolation of tumor interstitial fluid (TIF)

TIF was isolated from tumors using a previously described centrifugal method (Eil et al., 2016; Haslene-Hox et al., 2011; Ho et al., 2015; Wiig et al., 2003). Briefly, tumor bearing animals were euthanized by cervical dislocation and tumors were rapidly dissected from the animals. Dissections took <1 min. to complete. Blood was collected from the same animal via cardiac puncture, and was immediately placed in EDTA-tubes (Sarstedt, North Rhine-Westphalia, Germany) and centrifuged at 845 x g for 10 minutes at 4°C to separate plasma. Plasma was frozen in liquid nitrogen and stored at -80°C until further analysis. Tumors were then weighed and briefly rinsed in room temperature saline (150mM NaCl) and blotted on filter paper (VWR, Radnor, PA, 28298-020). The entire process of preparing the tumor prior to isolation of TIF took ~2 min. The tumors were then put onto 20µm nylon filters (Spectrum Labs, Waltham, MA, 148134) affixed atop 50mL conical tubes, and centrifuged for 10 min. at 4°C at 106 x g. TIF was then collected from the conical tube, frozen in liquid nitrogen and stored at -80°C until further analysis.

Quantification of lactate dehydrogenase activity in TIF, plasma and tumors

To quantitate the amount of LDH activity present in TIF, plasma, and tumors, we utilized the inherent absorbance of NADH at 340 nm to monitor the generation of lactate from pyruvate and NADH. To an assay buffer composed of 50 mM Tris base (Sigma Aldrich, 93362), 100 mM dithiothreitol (Sigma Aldrich, 646563), 180 µM NADH (Sigma Aldrich, N8129), and 500 µM pyruvate (Sigma Aldrich, P5280), we added 20 µL of sample, then monitored the disappearance over time of absorbance of light at 340 nM due to the consumption of NADH. A standard curve

of LDH (Sigma-Aldrich, 10127230001, E.C. 1.1.1.27) was generated with points of 0, 0.005838, 0.007783, 0.011675, 0.02335, and 0.0467 units of LDH activity by diluting LDH in Tris buffered saline composed of 50 mM Tris HCl (VWR, 4103) and 150 mM NaCl (Sigma Aldrich, 746398) pH adjusted to 7.5. Whole tumor samples were prepared by homogenization using a mortar and pestle submerged in liquid nitrogen, and the resulting powder was resuspended at 10 mg/mL in Tris buffered saline. Plasma samples were added undiluted, and TIF samples were diluted 1:10 in Tris buffered saline. Based on the slope of the LDH standard curve, the amount of LDH activity in each sample was calculated and corrected for dilution.

Quantification of metabolite levels in TIF and plasma

In order to quantitate metabolites in TIF and plasma samples, we first constructed a library of 149 chemical standards of plasma polar metabolites. These compounds were selected to encompass a number of metabolic processes and have previously been included in efforts to profile plasma polar metabolites by LC/MS (Cantor et al., 2017; Evans et al., 2009; Lawton et al., 2008; Mazzone et al., 2016). We pooled these metabolites into 7 separate chemical standard pools. To do this, each metabolite in a given pool was weighed and then mixed (6 cycles of 1 min. mixing at 25 Hz followed by 3 min. resting) using a Mixer Mill MM301 (Retsch, Düsseldorf, Germany), and mixed metabolite powder stocks were stored at -20°C prior to resuspension and analysis. Stock solutions of the mixed standards pools containing ~5mM, ~1mM, ~300µM, ~100µM, ~30µM, ~10µM, ~3µM and ~1µM of each metabolite were made in HPLC grade water and were stored at -80°C. We refer to these stock solutions as “external standard pools” throughout. External standard pools were used to confirm the retention time and *m/z* for each

analyte and provide standards to quantitate concentrations of stable isotope labeled internal standards used in downstream analysis, as well as to quantitate metabolite concentrations in TIF and plasma samples directly where internal standards were not available (see below for details).

To extract polar metabolites from plasma, TIF or the external standard pools, 5µL of TIF, plasma or external sample pools was mixed with 45uL of acetonitrile:methanol:formic acid (75:25:0.1) extraction buffer including the following isotopically labeled internal standards: ^{13}C labeled yeast extract (Cambridge Isotope Laboratory, Andover, MA, ISO1), $^{13}C_3$ lactate (Sigma Aldrich, Darmstadt, Germany, 485926), $^{13}C_3$ glycerol (Cambridge Isotope Laboratory, Andover, MA, CLM-1510), $^{13}C_6$ $^{15}N_2$ cystine (Cambridge Isotope Laboratory, Andover, MA, CNLM-4244), $^{2}H_9$ choline (Cambridge Isotope Laboratory, Andover, MA, DLM-549), $^{13}C_4$ 3-hydroxybutyrate (Cambridge Isotope Laboratory, Andover, MA, CLM-3853), $^{13}C_6$ glucose (Cambridge Isotope Laboratory, Andover, MA, CLM-1396), $^{13}C_2$ ^{15}N taurine (Cambridge Isotope Laboratory, Andover, MA, CNLM-10253), $^{2}H_3$ creatinine (Cambridge Isotope Laboratory, Andover, MA, DLM-3653), 8-^{13}C adenine (Cambridge Isotope Laboratory, Andover, MA, CLM-1654), $^{13}C_5$ hypoxanthine (Cambridge Isotope Laboratory, Andover, MA, CLM-8042), 8-^{13}C guanine (Cambridge Isotope Laboratory, Andover, MA, CLM-1019), $^{13}C_3$ serine (Cambridge Isotope Laboratory, Andover, MA, CLM-1574) and $^{13}C_2$ glycine (Cambridge Isotope Laboratory, Andover, MA, CLM-1017). All solvents used in the extraction buffer were HPLC grade. Samples were then vortexed for 10 min. at 4°C and insoluble material was sedimented by centrifugation at 15kg for 10 min. at 4°C. 20µL of the soluble polar metabolite extract was taken for LC/MS analysis.

LC/MS analysis was performed using a QExactive orbitrap mass spectrometer using an Ion Max source and heated electrospray ionization (HESI) probe coupled to a Dionex Ultimate 3000 UPLC system (Thermo Fisher Scientific, Waltham, MA). External mass calibration was performed every 7 days. 2µL of each sample was injected onto a ZIC-pHILIC 2.1 × 150 mm analytical column equipped with a 2.1 × 20 mm guard column (both 5 µm particle size, EMD Millipore). The autosampler and column oven were held at 4°C and 25°C, respectively. Buffer A was 20 mM ammonium carbonate, 0.1% ammonium hydroxide; buffer B was acetonitrile. The chromatographic gradient was run at a flow rate of 0.150 mL/min as follows: 0-20 min: linear gradient from 80% to 20% B; 20-20.5 min: linear gradient from 20% to 80% B; 20.5-28min: hold at 80% B. The mass spectrometer was operated in full scan, polarity-switching mode with the spray voltage set to 3.0 kV, the heated capillary held at 275°C, and the HESI probe held at 350°C. The sheath gas flow rate was set to 40 units, the auxiliary gas flow was set to 15 units, and the sweep gas flow was set to 1 unit. The MS data acquisition was performed in a range of 70-1000 m/z, with the resolution set to 70,000, the AGC target at 1e6, and the maximum injection time at 20 msec.

Metabolite identification and quantification was performed with XCalibur 2.2 software (Thermo Fisher Scientific, Waltham, MA) using a 5ppm mass accuracy and a 0.5 min. retention time window. For metabolite identification, external standard pools were used for assignment of metabolites to peaks at given *m/z* and retention time, and to determine the limit of detection for each metabolite. Metabolite quantification was performed by two separate methods. Where internal standards were available, first, comparison of the peak areas of the stable isotope labeled internal standards with the external standard pools allowed for

quantification of the concentration of labeled internal standards in the extraction buffer. Subsequently, we compared the peak area of a given metabolite in the TIF and plasma samples with the peak area of the internal standard to quantitate the concentration of that metabolite in the TIF or plasma sample. 70 metabolites were quantitated using this internal standard method. For metabolites without internal standards, the peak area of each analyte was normalized to the peak area of a labeled amino acid internal standard that eluted at roughly the same retention time to account for differences in recovery between samples. From the normalized peak areas of metabolites in the external standard pools, we generated a standard curve describing the relationship between metabolite concentration and normalized peak area. The standard curves were linear with fits typically at or above r^2=0.95. Metabolites which did not meet these criteria were excluded from further analysis. These equations were then used to convert normalized peak areas of analytes in the TIF or plasma samples into analyte concentration in the samples. 74 metabolites were quantitated using this method. The relationship between metabolite concentration and normalized peak area is matrix dependent, and the external standards are prepared in water, which is a different matrix than either TIF or plasma. Therefore, we consider metabolite measurements using this external standard method semi-quantitative.

Statistical analysis of TIF and plasma metabolite levels

After determining the concentration of each metabolite in each plasma or TIF sample, all multivariate statistical analysis on the data was performed using Metaboanalyst 4.0 (Chong et al., 2018). All metabolite concentrations were not normalized prior to analysis, but the data was

auto-scaled (mean-centered and divided by the standard deviation of each variable) prior to analysis, as this method of scaling has been shown to perform well with metabolomics data (van den Berg et al., 2006). After scaling the data, we performed principal component analysis and hierarchical clustering with Euclidean distance measurement and clustering by the Ward algorithm. Univariate analysis was performed comparing metabolite levels between groups where metabolite differences of interest were defined by a fold change greater than 1.5 and significance as a FDR-adjusted P-value less than 0.1 assuming unequal group variance. All other statistical analysis and graphical representation of data was performed as described in the **RESULTS** using GraphPad Prism 7 (GraphPad Software, La Jolla, CA).

ACKNOWLEDGEMENTS

We thank Aaron Hosios and all members of the Vander Heiden lab for many useful discussions and experimental advice, and Allison Lau and Sharanya Sivanand for supplying tumor bearing animals used in this work. We thank Sarah Price for assistance with developing data analysis tools. We thank Peggy Hsu, Alicia Darnell, and Allison Lau for comments and help with editing the manuscript. We thank Rodrigo Romero and Tyler Jacks for generously supplying murine LUAD cell lines and providing experimental advice. We thank Susan Kaech, Victor Chubakov and Thomas Roddy for helpful discussions on interstitial fluid isolation and analysis. Lastly, we thank Cambridge Isotope Laboratories for the generous gift of isotopically labeled yeast extract used in this work. This work was supported by grants to M.G.V.H. from the NIH (R01CA168653, R01CA201276, and P30CA1405141), the Lustgarten Foundation, the MIT

Center for Precision Medicine, SU2C, and the Ludwig Center at MIT. A.M. and L.V.D. were supported by NIH Ruth Kirschstein Fellowships, F32CA213810 and F32CA210421 respectively. M.R.S. was supported by T32GM007287 and acknowledges additional support from an MIT Koch Institute Graduate Fellowship. D.Y.G. received support from T32GM007753. M.G.V.H. is a Howard Hughes Medical Institute Faculty Scholar.

AUTHOR CONTRIBUTIONS

Conceptualization, M.R.S., D.Y.G., M.G.V.H., and A.M.; Methodology, M.R.S., L.V.D., C.A.L., S.H.C., T.K., A.M.; Formal Analysis, M.R.S., C.A.L., S.H.C., A.M.; Investigation, M.R.S., L.V.D., C.A.L., S.H.C., D.Y.G., T.K., E.A.D., A.M.; Visualization, M.R.S. and A.M.; Supervision, C.A.L., M.G.V.H., A.M.; Writing – Original Draft, M.R.S. and A.M.; Writing – Review & Editing, M.R.S., L.V.D., C.A.L., D.Y.G., M.G.V.H., A.M.; Funding Acquisition, M.R.S., L.V.D., M.G.V.H., A.M.

REFERENCES

Alvarez, S.W., Sviderskiy, V.O., Terzi, E.M., Papagiannakopoulos, T., Moreira, A.L., Adams, S., Sabatini, D.M., Birsoy, K., and Possemato, R. (2017). NFS1 undergoes positive selection in lung tumours and protects cells from ferroptosis. Nature *551*, 639-643.

Anastasiou, D. (2017). Tumour microenvironment factors shaping the cancer metabolism landscape. Br J Cancer *116*, 277-286.

Bardeesy, N., Aguirre, A.J., Chu, G.C., Cheng, K.H., Lopez, L.V., Hezel, A.F., Feng, B., Brennan, C., Weissleder, R., Mahmood, U.*, et al.* (2006). Both p16(Ink4a) and the p19(Arf)-p53 pathway constrain progression of pancreatic adenocarcinoma in the mouse. Proc Natl Acad Sci U S A *103*, 5947-5952.

Bayne, L.J., Beatty, G.L., Jhala, N., Clark, C.E., Rhim, A.D., Stanger, B.Z., and Vonderheide, R.H. (2012). Tumor-derived granulocyte-macrophage colony-stimulating factor regulates myeloid inflammation and T cell immunity in pancreatic cancer. Cancer Cell *21*, 822-835.

Best, S.A., De Souza, D.P., Kersbergen, A., Policheni, A.N., Dayalan, S., Tull, D., Rathi, V., Gray, D.H., Ritchie, M.E., McConville, M.J.*, et al.* (2018). Synergy between the KEAP1/NRF2 and PI3K Pathways Drives Non-Small-Cell Lung Cancer with an Altered Immune Microenvironment. Cell Metabolism *27*, 935-+.

Bi, J.F., Wu, S.H., Zhang, W.J., and Mischel, P.S. (2018). Targeting cancer's metabolic co-dependencies: A landscape shaped by genotype and tissue context. Bba-Rev Cancer *1870*, 76-87.

Biancur, D.E., Paulo, J.A., Malachowska, B., Del Rey, M.Q., Sousa, C.M., Wang, X., Sohn, A.S.W., Chu, G.C., Gygi, S.P., Harper, J.W.*, et al.* (2017). Compensatory metabolic networks in pancreatic cancers upon perturbation of glutamine metabolism. Nat Commun *8*, 15965.

Buck, M.D., Sowell, R.T., Kaech, S.M., and Pearce, E.L. (2017). Metabolic Instruction of Immunity. Cell *169*, 570-586.

Burgess, E.A., and Sylven, B. (1962). Glucose, lactate, and lactic dehydrogenase activity in normal interstitial fluid and that of solid mouse tumors. Cancer Res *22*, 581-588.

Caldwell, R.W., Rodriguez, P.C., Toque, H.A., Narayanan, S.P., and Caldwell, R.B. (2018). Arginase: A Multifaceted Enzyme Important in Health and Disease. Physiol Rev *98*, 641-665.

Cantor, J.R., Abu-Remaileh, M., Kanarek, N., Freinkman, E., Gao, X., Louissaint, A., Jr., Lewis, C.A., and Sabatini, D.M. (2017). Physiologic Medium Rewires Cellular Metabolism and Reveals Uric Acid as an Endogenous Inhibitor of UMP Synthase. Cell *169*, 258-272 e217.

Cengiz, E., and Tamborlane, W.V. (2009). A tale of two compartments: interstitial versus blood glucose monitoring. Diabetes Technol Ther *11 Suppl 1*, S11-16.

Chauhan, V.P., Boucher, Y., Ferrone, C.R., Roberge, S., Martin, J.D., Stylianopoulos, T., Bardeesy, N., DePinho, R.A., Padera, T.P., Munn, L.L.*, et al.* (2014). Compression of Pancreatic Tumor Blood Vessels by Hyaluronan Is Caused by Solid Stress and Not Interstitial Fluid Pressure. Cancer Cell *26*, 14-15.

Chen, W.W., Freinkman, E., Wang, T., Birsoy, K., and Sabatini, D.M. (2016). Absolute Quantification of Matrix Metabolites Reveals the Dynamics of Mitochondrial Metabolism. Cell *166*, 1324-1337 e1311.

Chong, J., Soufan, O., Li, C., Caraus, I., Li, S., Bourque, G., Wishart, D.S., and Xia, J. (2018). MetaboAnalyst 4.0: towards more transparent and integrative metabolomics analysis. Nucleic Acids Res *46*, W486-W494.

Commisso, C., Davidson, S.M., Soydaner-Azeloglu, R.G., Parker, S.J., Kamphorst, J.J., Hackett, S., Grabocka, E., Nofal, M., Drebin, J.A., Thompson, C.B.*, et al.* (2013). Macropinocytosis of protein is an amino acid supply route in Ras-transformed cells. Nature *497*, 633-+.

Corbet, C., and Feron, O. (2017). Tumour acidosis: from the passenger to the driver's seat. Nat Rev Cancer *17*, 577-593.

Cori, C.F., and Cori, G.T. (1925). The carbohydrate metabolism of tumors. II. Changes in the sugar, lactic acid, and co-combing power of blood passing through a tumor. Journal of Biological Chemistry *65*, 397-405.

Danai, L.V., Babic, A., Rosenthal, M.H., Dennstedt, E.A., Muir, A., Lien, E.C., Mayers, J.R., Tai, K., Lau, A.N., Jones-Sali, P.*, et al.* (2018). Altered exocrine function can drive adipose wasting in early pancreatic cancer. Nature.

Davidson, S.M., Papagiannakopoulos, T., Olenchock, B.A., Heyman, J.E., Keibler, M.A., Luengo, A., Bauer, M.R., Jha, A.K., O'Brien, J.P., Pierce, K.A.*, et al.* (2016). Environment Impacts the Metabolic Dependencies of Ras-Driven Non-Small Cell Lung Cancer. Cell Metab *23*, 517-528.

DeBerardinis, R.J., and Chandel, N.S. (2016). Fundamentals of cancer metabolism. Sci Adv *2*, e1600200.

DelNero, P., Hopkins, B.D., Cantley, L.C., and Fischbach, C. (2018). Cancer metabolism gets physical. Sci Transl Med *10*.

DeNicola, G.M., Chen, P.H., Mullarky, E., Sudderth, J.A., Hu, Z., Wu, D., Tang, H., Xie, Y., Asara, J.M., Huffman, K.E.*, et al.* (2015). NRF2 regulates serine biosynthesis in non-small cell lung cancer. Nat Genet *47*, 1475-1481.

DeNicola, G.M., Karreth, F.A., Humpton, T.J., Gopinathan, A., Wei, C., Frese, K., Mangal, D., Yu, K.H., Yeo, C.J., Calhoun, E.S.*, et al.* (2011). Oncogene-induced Nrf2 transcription promotes ROS detoxification and tumorigenesis. Nature *475*, 106-109.

DuFort, C.C., DelGiorno, K.E., Carlson, M.A., Osgood, R.J., Zhao, C.M., Huang, Z.D., Thompson, C.B., Connor, R.J., Thanos, C.D., Brockenbrough, J.S.*, et al.* (2016). Interstitial Pressure in Pancreatic Ductal Adenocarcinoma Is Dominated by a Gel-Fluid Phase. Biophysical Journal *110*, 2106-2119.

Eagle, H. (1955). Nutrition needs of mammalian cells in tissue culture. Science *122*, 501-514.

Ecker, C., and Riley, J.L. (2018). Translating In Vitro T Cell Metabolic Findings to In Vivo Tumor Models of Nutrient Competition. Cell Metabolism *28*, 190-195.

Eil, R., Vodnala, S.K., Clever, D., Klebanoff, C.A., Sukumar, M., Pan, J.H., Palmer, D.C., Gros, A., Yamamoto, T.N., Patel, S.J.*, et al.* (2016). Ionic immune suppression within the tumour microenvironment limits T cell effector function. Nature *537*, 539-+.

Evans, A.M., DeHaven, C.D., Barrett, T., Mitchell, M., and Milgram, E. (2009). Integrated, nontargeted ultrahigh performance liquid chromatography/electrospray ionization tandem mass spectrometry platform for the identification and relative quantification of the small-molecule complement of biological systems. Anal Chem *81*, 6656-6667.

Fisher, D.T., Muhitch, J.B., Kim, M., Doyen, K.C., Bogner, P.N., Evans, S.S., and Skitzki, J.J. (2016). Intraoperative intravital microscopy permits the study of human tumour vessels. Nat Commun *7*, 10684.

Fukumura, D., Duda, D.G., Munn, L.L., and Jain, R.K. (2010). Tumor Microvasculature and Microenvironment: Novel Insights Through Intravital Imaging in Pre-Clinical Models. Microcirculation *17*, 206-225.

Gall, W.E., Beebe, K., Lawton, K.A., Adam, K.P., Mitchell, M.W., Nakhle, P.J., Ryals, J.A., Milburn, M.V., Nannipieri, M., Camastra, S.*, et al.* (2010). alpha-Hydroxybutyrate Is an Early Biomarker of Insulin Resistance and Glucose Intolerance in a Nondiabetic Population. Plos One *5*.

Geiger, R., Rieckmann, J.C., Wolf, T., Basso, C., Feng, Y., Fuhrer, T., Kogadeeva, M., Picotti, P., Meissner, F., Mann, M.*, et al.* (2016). L-Arginine Modulates T Cell Metabolism and Enhances Survival and Anti-tumor Activity. Cell *167*, 829-842 e813.

Goedegebuure, P., Mitchem, J.B., Porembka, M.R., Tan, M.C., Belt, B.A., Wang-Gillam, A., Gillanders, W.E., Hawkins, W.G., and Linehan, D.C. (2011). Myeloid-derived suppressor cells: general characteristics and relevance to clinical management of pancreatic cancer. Curr Cancer Drug Targets *11*, 734-751.

Grankvist, N., Watrous, J.D., Lagerborg, K.A., Lyutvinskiy, Y., Jain, M., and Nilsson, R. (2018). Profiling the Metabolism of Human Cells by Deep (13)C Labeling. Cell Chem Biol.

Gui, D.Y., Sullivan, L.B., Luengo, A., Hosios, A.M., Bush, L.N., Gitego, N., Davidson, S.M., Freinkman, E., Thomas, C.J., and Vander Heiden, M.G. (2016). Environment Dictates Dependence on Mitochondrial Complex I for NAD+ and Aspartate Production and Determines Cancer Cell Sensitivity to Metformin. Cell Metab *24*, 716-727.

Gullino, P.M., Clark, S.H., and Grantham, F.H. (1964). The Interstitial Fluid of Solid Tumors. Cancer Res *24*, 780-794.

Gullino, P.M., Grantham, F.H., and Courtney, A.H. (1967). Glucose consumption by transplanted tumors in vivo. Cancer Res *27*, 1031-1040.

Haslene-Hox, H., Oveland, E., Berg, K.C., Kolmannskog, O., Woie, K., Salvesen, H.B., Tenstad, O., and Wiig, H. (2011). A new method for isolation of interstitial fluid from human solid tumors applied to proteomic analysis of ovarian carcinoma tissue. PLoS One *6*, e19217.

Hensley, C.T., Faubert, B., Yuan, Q., Lev-Cohain, N., Jin, E., Kim, J., Jiang, L., Ko, B., Skelton, R., Loudat, L.*, et al.* (2016). Metabolic Heterogeneity in Human Lung Tumors. Cell *164*, 681-694.

Hermann, G., Schwaiger, M., Volejnik, P., and Koellensperger, G. (2018). (13)C-labelled yeast as internal standard for LC-MS/MS and LC high resolution MS based amino acid quantification in human plasma. J Pharm Biomed Anal *155*, 329-334.

Hilmi, M., Bartholin, L., and Neuzillet, C. (2018). Immune therapies in pancreatic ductal adenocarcinoma: Where are we now? World J Gastroenterol *24*, 2137-2151.

Ho, P.C., Bihuniak, J.D., Macintyre, A.N., Staron, M., Liu, X.J., Amezquita, R., Tsui, Y.C., Cui, G.L., Micevic, G., Perales, J.C.*, et al.* (2015). Phosphoenolpyruvate Is a Metabolic Checkpoint of Anti-tumor T Cell Responses. Cell *162*, 1217-1228.

Horvath, P., Aulner, N., Bickle, M., Davies, A.M., Nery, E.D., Ebner, D., Montoya, M.C., Ostling, P., Pietiainen, V., Price, L.S*., et al.* (2016). Screening out irrelevant cell-based models of disease. Nat Rev Drug Discov *15*, 751-769.

Hosios, A.M., Hecht, V.C., Danai, L.V., Johnson, M.O., Rathmell, J.C., Steinhauser, M.L., Manalis, S.R., and Vander Heiden, M.G. (2016). Amino Acids Rather than Glucose Account for the Majority of Cell Mass in Proliferating Mammalian Cells. Dev Cell *36*, 540-549.

Hu, J., Locasale, J.W., Bielas, J.H., O'Sullivan, J., Sheahan, K., Cantley, L.C., Vander Heiden, M.G., and Vitkup, D. (2013). Heterogeneity of tumor-induced gene expression changes in the human metabolic network. Nat Biotechnol *31*, 522-529.

Hwang, C.I., Boj, S.F., Clevers, H., and Tuveson, D.A. (2016). Preclinical models of pancreatic ductal adenocarcinoma. J Pathol *238*, 197-204.

Irino, Y., Toh, R., Nagao, M., Mori, T., Honjo, T., Shinohara, M., Tsuda, S., Nakajima, H., Satomi-Kobayashi, S., Shinke, T*., et al.* (2016). 2-Aminobutyric acid modulates glutathione homeostasis in the myocardium. Sci Rep *6*, 36749.

Jackson, E.L., Olive, K.P., Tuveson, D.A., Bronson, R., Crowley, D., Brown, M., and Jacks, T. (2005). The differential effects of mutant p53 alleles on advanced murine lung cancer. Cancer Research *65*, 10280-10288.

Jackson, E.L., Willis, N., Mercer, K., Bronson, R.T., Crowley, D., Montoya, R., Jacks, T., and Tuveson, D.A. (2001). Analysis of lung tumor initiation and progression using conditional expression of oncogenic K-ras. Gene Dev *15*, 3243-3248.

Jain, M., Nilsson, R., Sharma, S., Madhusudhan, N., Kitami, T., Souza, A.L., Kafri, R., Kirschner, M.W., Clish, C.B., and Mootha, V.K. (2012). Metabolite profiling identifies a key role for glycine in rapid cancer cell proliferation. Science *336*, 1040-1044.

Kallinowski, F., Vaupel, P., Runkel, S., Berg, G., Fortmeyer, H.P., Baessler, K.H., Wagner, K., Mueller-Klieser, W., and Walenta, S. (1988). Glucose uptake, lactate release, ketone body turnover, metabolic micromilieu, and pH distributions in human breast cancer xenografts in nude rats. Cancer Res *48*, 7264-7272.

Kamphorst, J.J., Nofal, M., Commisso, C., Hackett, S.R., Lu, W., Grabocka, E., Vander Heiden, M.G., Miller, G., Drebin, J.A., Bar-Sagi, D*., et al.* (2015). Human pancreatic cancer tumors are nutrient poor and tumor cells actively scavenge extracellular protein. Cancer Res *75*, 544-553.

Koong, A.C., Mehta, V.K., Le, Q.T., Fisher, G.A., Terris, D.J., Brown, J.M., Bastidas, A.J., and Vierra, M. (2000). Pancreatic tumors show high levels of hypoxia. Int J Radiat Oncol *48*, 919-922.

Koppenol, W.H., Bounds, P.L., and Dang, C.V. (2011). Otto Warburg's contributions to current concepts of cancer metabolism. Nat Rev Cancer *11*, 325-337.

Kumar, V., Patel, S., Tcyganov, E., and Gabrilovich, D.I. (2016). The Nature of Myeloid-Derived Suppressor Cells in the Tumor Microenvironment. Trends Immunol *37*, 208-220.

Lawton, K.A., Berger, A., Mitchell, M., Milgram, K.E., Evans, A.M., Guo, L., Hanson, R.W., Kalhan, S.C., Ryals, J.A., and Milburn, M.V. (2008). Analysis of the adult human plasma metabolome. Pharmacogenomics *9*, 383-397.

Lee, J.S., Adler, L., Karathia, H., Carmel, N., Rabinovich, S., Auslander, N., Keshet, R., Stettner, N., Silberman, A., Agemy, L.*, et al.* (2018). Urea Cycle Dysregulation Generates Clinically Relevant Genomic and Biochemical Signatures. Cell *174*, 1559-+.

Lonnroth, P., Jansson, P.A., and Smith, U. (1987). A Microdialysis Method Allowing Characterization of Intercellular Water Space in Humans. Am J Physiol *253*, E228-E231.

Lyssiotis, C.A., and Kimmelman, A.C. (2017). Metabolic Interactions in the Tumor Microenvironment. Trends Cell Biol *27*, 863-875.

Martinez-Bosch, N., Vinaixa, J., and Navarro, P. (2018). Immune Evasion in Pancreatic Cancer: From Mechanisms to Therapy. Cancers *10*.

Mayers, J.R., Torrence, M.E., Danai, L.V., Papagiannakopoulos, T., Davidson, S.M., Bauer, M.R., Lau, A.N., Ji, B.W., Dixit, P.D., Hosios, A.M.*, et al.* (2016). Tissue of origin dictates branched-chain amino acid metabolism in mutant Kras-driven cancers. Science *353*, 1161-1165.

Mayers, J.R., Wu, C., Clish, C.B., Kraft, P., Torrence, M.E., Fiske, B.P., Yuan, C., Bao, Y., Townsend, M.K., Tworoger, S.S.*, et al.* (2014). Elevation of circulating branched-chain amino acids is an early event in human pancreatic adenocarcinoma development. Nat Med *20*, 1193-1198.

Mazzone, P.J., Wang, X.F., Beukemann, M., Zhang, Q., Seeley, M., Mohney, R., Holt, T., and Pappan, K.L. (2016). Metabolite Profiles of the Serum of Patients with Non-Small Cell Carcinoma. J Thorac Oncol *11*, 72-78.

Mitsuishi, Y., Taguchi, K., Kawatani, Y., Shibata, T., Nukiwa, T., Aburatani, H., Yamamoto, M., and Motohashi, H. (2012). Nrf2 redirects glucose and glutamine into anabolic pathways in metabolic reprogramming. Cancer Cell *22*, 66-79.

Moffett, J.R., and Namboodiri, M.A. (2003). Tryptophan and the immune response. Immunol Cell Biol *81*, 247-265.

Morandi, A., Giannoni, E., and Chiarugi, P. (2016). Nutrient Exploitation within the Tumor-Stroma Metabolic Crosstalk. Trends Cancer *2*, 736-746.

Morris, S.M. (2007). Arginine metabolism: Boundaries of our knowledge. J Nutr *137*, 1602s-1609s.

Muir, A., Danai, L.V., Gui, D.Y., Waingarten, C.Y., Lewis, C.A., and Vander Heiden, M.G. (2017). Environmental cystine drives glutamine anaplerosis and sensitizes cancer cells to glutaminase inhibition. Elife *6*.

Muir, A., Danai, L.V., and Vander Heiden, M.G. (2018). Microenvironmental regulation of cancer cell metabolism: implications for experimental design and translational studies. Dis Model Mech *11*.

Muir, A., and Vander Heiden, M.G. (2018). The nutrient environment affects therapy. Science *360*, 962-963.

Nagarajan, A., Malvi, P., and Wajapeyee, N. (2016). Oncogene-directed alterations in cancer cell metabolism. Trends Cancer *2*, 365-377.

Olive, K.P., Jacobetz, M.A., Davidson, C.J., Gopinathan, A., McIntyre, D., Honess, D., Madhu, B., Goldgraben, M.A., Caldwell, M.E., Allard, D.*, et al.* (2009). Inhibition of Hedgehog signaling enhances delivery of chemotherapy in a mouse model of pancreatic cancer. Science *324*, 1457-1461.

Overmyer, K.A., Thonusin, C., Qi, N.R., Burant, C.F., and Evans, C.R. (2015). Impact of anesthesia and euthanasia on metabolomics of mammalian tissues: studies in a C57BL/6J mouse model. PLoS One *10*, e0117232.

Palm, W., Park, Y., Wright, K., Pavlova, N.N., Tuveson, D.A., and Thompson, C.B. (2015). The Utilization of Extracellular Proteins as Nutrients Is Suppressed by mTORC1. Cell *162*, 259-270.

Pan, M., Reid, M.A., Lowman, X.H., Kulkarni, R.P., Tran, T.Q., Liu, X.J., Yang, Y., Hernandez-Davies, J.E., Rosales, K.K., Li, H.Q.*, et al.* (2016). Regional glutamine deficiency in tumours promotes dedifferentiation through inhibition of histone demethylation. Nature Cell Biology *18*, 1090-1101.

Persi, E., Duran-Frigola, M., Damaghi, M., Roush, W.R., Aloy, P., Cleveland, J.L., Gillies, R.J., and Ruppin, E. (2018). Systems analysis of intracellular pH vulnerabilities for cancer therapy. Nature Communications *9*.

Possemato, R., Marks, K.M., Shaul, Y.D., Pacold, M.E., Kim, D., Birsoy, K., Sethumadhavan, S., Woo, H.K., Jang, H.G., Jha, A.K.*, et al.* (2011). Functional genomics reveal that the serine synthesis pathway is essential in breast cancer. Nature *476*, 346-350.

Provenzano, P.P., Cuevas, C., Chang, A.E., Goel, V.K., Von Hoff, D.D., and Hingorani, S.R. (2012). Enzymatic targeting of the stroma ablates physical barriers to treatment of pancreatic ductal adenocarcinoma. Cancer Cell *21*, 418-429.

Rabinovich, S., Adler, L., Yizhak, K., Sarver, A., Silberman, A., Agron, S., Stettner, N., Sun, Q., Brandis, A., Helbling, D.*, et al.* (2015). Diversion of aspartate in ASS1-deficient tumours fosters de novo pyrimidine synthesis. Nature *527*, 379-+.

Ribas, A., and Wolchok, J.D. (2018). Cancer immunotherapy using checkpoint blockade. Science *359*, 1350-+.

Romero, R., Sayin, V.I., Davidson, S.M., Bauer, M.R., Singh, S.X., LeBoeuf, S.E., Karakousi, T.R., Ellis, D.C., Bhutkar, A., Sanchez-Rivera, F.J.*, et al.* (2017). Keap1 loss promotes Kras-driven lung cancer and results in dependence on glutaminolysis. Nat Med *23*, 1362-1368.

Ryan, C.J., Bajrami, I., and Lord, C.J. (2018). Synthetic Lethality and Cancer - Penetrance as the Major Barrier. Trends in Cancer *4*, 671-683.

Sauer, L.A., Stayman, J.W., 3rd, and Dauchy, R.T. (1982). Amino acid, glucose, and lactic acid utilization in vivo by rat tumors. Cancer Res *42*, 4090-4097.

Sayin, V.I., LeBoeuf, S.E., Singh, S.X., Davidson, S.M., Biancur, D., Guzelhan, B.S., Alvarez, S.W., Wu, W.L., Karakousi, T.R., Zavitsanou, A.M.*, et al.* (2017). Activation of the NRF2 antioxidant program generates an imbalance in central carbon metabolism in cancer. Elife *6*.

Schild, T., Low, V., Blenis, J., and Gomes, A.P. (2018). Unique Metabolic Adaptations Dictate Distal Organ-Specific Metastatic Colonization. Cancer Cell *33*, 347-354.

Schug, Z.T., Peck, B., Jones, D.T., Zhang, Q., Grosskurth, S., Alam, I.S., Goodwin, L.M., Smethurst, E., Mason, S., Blyth, K.*, et al.* (2015). Acetyl-CoA synthetase 2 promotes acetate utilization and maintains cancer cell growth under metabolic stress. Cancer Cell *27*, 57-71.

Sellers, K., Fox, M.P., Bousamra, M., 2nd, Slone, S.P., Higashi, R.M., Miller, D.M., Wang, Y., Yan, J., Yuneva, M.O., Deshpande, R.*, et al.* (2015). Pyruvate carboxylase is critical for non-small-cell lung cancer proliferation. J Clin Invest *125*, 687-698.

Sherman, M.H., Yu, R.T., Tseng, T.W., Sousa, C.M., Liu, S.H., Truitt, M.L., He, N.H., Ding, N., Liddle, C., Atkins, A.R.*, et al.* (2017). Stromal cues regulate the pancreatic cancer epigenome and metabolome. P Natl Acad Sci USA *114*, 1129-1134.

Siska, P.J., Beckermann, K.E., Mason, F.M., Andrejeva, G., Greenplate, A.R., Sendor, A.B., Chiang, Y.J., Corona, A.L., Gemta, L.F., Vincent, B.G.*, et al.* (2017). Mitochondrial dysregulation and glycolytic insufficiency functionally impair CD8 T cells infiltrating human renal cell carcinoma. JCI Insight *2*.

Son, J., Lyssiotis, C.A., Ying, H.Q., Wang, X.X., Hua, S.J., Ligorio, M., Perera, R.M., Ferrone, C.R., Mullarky, E., Shyh-Chang, N.*, et al.* (2013). Glutamine supports pancreatic cancer growth through a KRAS-regulated metabolic pathway (vol 496, pg 101, 2013). Nature *499*.

Sousa, C.M., Biancur, D.E., Wang, X., Halbrook, C.J., Sherman, M.H., Zhang, L., Kremer, D., Hwang, R.F., Witkiewicz, A.K., Ying, H.*, et al.* (2016). Pancreatic stellate cells support tumour metabolism through autophagic alanine secretion. Nature *536*, 479-483.

Srivastava, M.K., Sinha, P., Clements, V.K., Rodriguez, P., and Ostrand-Rosenberg, S. (2010). Myeloid-Derived Suppressor Cells Inhibit T-Cell Activation by Depleting Cystine and Cysteine. Cancer Research *70*, 68-77.

Stromnes, I.M., Brockenbrough, J.S., Izeradjene, K., Carlson, M.A., Cuevas, C., Simmons, R.M., Greenberg, P.D., and Hingorani, S.R. (2014). Targeted depletion of an MDSC subset unmasks pancreatic ductal adenocarcinoma to adaptive immunity. Gut *63*, 1769-1781.

Stylianopoulos, T., Munn, L.L., and Jain, R.K. (2018). Reengineering the Physical Microenvironment of Tumors to Improve Drug Delivery and Efficacy: From Mathematical Modeling to Bench to Bedside. Trends in Cancer *4*, 292-319.

Tardito, S., Oudin, A., Ahmed, S.U., Fack, F., Keunen, O., Zheng, L., Miletic, H., Sakariassen, P.O., Weinstock, A., Wagner, A.*, et al.* (2015). Glutamine synthetase activity fuels nucleotide biosynthesis and supports growth of glutamine-restricted glioblastoma. Nat Cell Biol *17*, 1556-1568.

Trufelli, H., Palma, P., Famiglini, G., and Cappiello, A. (2011). An overview of matrix effects in liquid chromatography-mass spectrometry. Mass Spectrom Rev *30*, 491-509.

Tung, J.C., Barnes, J.M., Desai, S.R., Sistrunk, C., Conklin, M.W., Schedin, P., Eliceiri, K.W., Keely, P.J., Seewaldt, V.L., and Weaver, V.M. (2015). Tumor mechanics and metabolic dysfunction. Free Radic Biol Med *79*, 269-280.

Uhlen, M., Fagerberg, L., Hallstrom, B.M., Lindskog, C., Oksvold, P., Mardinoglu, A., Sivertsson, A., Kampf, C., Sjostedt, E., Asplund, A.*, et al.* (2015). Tissue-based map of the human proteome. Science *347*.

van den Berg, R.A., Hoefsloot, H.C.J., Westerhuis, J.A., Smilde, A.K., and van der Werf, M.J. (2006). Centering, scaling, and transformations: improving the biological information content of metabolomics data. Bmc Genomics *7*.

Wagnerand, M., and Wiig, H. (2015). Tumor interstitial fluid formation, characterization, and clinical implications. Front Oncol *5*.

Wiig, H., Aukland, K., and Tenstad, O. (2003). Isolation of interstitial fluid from rat mammary tumors by a centrifugation method. Am J Physiol Heart Circ Physiol *284*, H416-424.

Wiig, H., and Swartz, M.A. (2012). Interstitial Fluid and Lymph Formation and Transport: Physiological Regulation and Roles in Inflammation and Cancer. Physiol Rev *92*, 1005-1060.

Wolpaw, A.J., and Dang, C.V. (2018). Exploiting Metabolic Vulnerabilities of Cancer with Precision and Accuracy. Trends Cell Biol *28*, 201-212.

Wu, G.Y., Bazer, F.W., Davis, T.A., Kim, S.W., Li, P., Rhoads, J.M., Satterfield, M.C., Smith, S.B., Spencer, T.E., and Yin, Y.L. (2009). Arginine metabolism and nutrition in growth, health and disease. Amino Acids *37*, 153-168.

Yau, E.H., Kummetha, I.R., Lichinchi, G., Tang, R., Zhang, Y., and Rana, T.M. (2017). Genome-Wide CRISPR Screen for Essential Cell Growth Mediators in Mutant KRAS Colorectal Cancers. Cancer Res *77*, 6330-6339.

Ying, H.Q., Kimmelman, A.C., Lyssiotis, C.A., Hua, S.J., Chu, G.C., Fletcher-Sananikone, E., Locasale, J.W., Son, J., Zhang, H.L., Coloff, J.L*., et al.* (2012). Oncogenic Kras Maintains Pancreatic Tumors through Regulation of Anabolic Glucose Metabolism. Cell *149*, 656-670.

Yuneva, M.O., Fan, T.W.M., Allen, T.D., Higashi, R.M., Ferraris, D.V., Tsukamoto, T., Mates, J.M., Alonso, F.J., Wang, C.M., Seo, Y*., et al.* (2012). The Metabolic Profile of Tumors Depends on Both the Responsible Genetic Lesion and Tissue Type. Cell Metabolism *15*, 157-170.

Zaytouni, T., Tsai, P.Y., Hitchcock, D.S., DuBois, C.D., Freinkman, E., Lin, L., Morales-Oyarvide, V., Lenehan, P.J., Wolpin, B.M., Mino-Kenudson, M*., et al.* (2017). Critical role for arginase 2 in obesity-associated pancreatic cancer. Nat Commun *8*, 242.

Zhang, Y., Velez-Delgado, A., Mathew, E., Li, D., Mendez, F.M., Flannagan, K., Rhim, A.D., Simeone, D.M., Beatty, G.L., and Pasca di Magliano, M. (2017). Myeloid cells are required for PD-1/PD-L1 checkpoint activation and the establishment of an immunosuppressive environment in pancreatic cancer. Gut *66*, 124-136.

Zhao, F., Obermann, S., von Wasielewski, R., Haile, L., Manns, M.P., Korangy, F., and Greten, T.F. (2009). Increase in frequency of myeloid-derived suppressor cells in mice with spontaneous pancreatic carcinoma. Immunology *128*, 141-149.

CHAPTER FIVE: Discussion and Future Directions

SUMMARY

Nutrient availability has the potential to impact tumor growth. Whether tumor cells are able to access sufficient quantities of a nutrient depends upon cancer cell-intrinsic properties that alter nutrient demand and the cell's capacity to acquire nutrients, as well as upon cell-extrinsic factors that determine the accessibility of a metabolite in the environment of a cancer cell. In this dissertation, I have examined multiple cell-intrinsic and cell-extrinsic factors that impact nutrient availability for cancer cells.

Given recent interest in the role of the amino acid serine (Maddocks et al., 2017; Maddocks et al., 2013) and the serine synthesis pathway (DeNicola et al., 2015; Locasale et al., 2011; Possemato et al., 2011) in cancer, we first examined whether increased serine synthesis promotes tumor growth. We found that both increasing serine availability through synthesis or by changing serine levels in the environment of tumors is sufficient to accelerate tumor progression in breast cancer and melanoma. Our results suggest that the mammary fat pad is an environment in which serine levels may be low, and that breast tumors might upregulate serine synthesis pathway activity in order to compensate for the low availability of serine. These findings illustrate a specific context in which tumor growth is limited by an inability to acquire sufficient serine and highlight the role that environmental nutrients can play in determining the vulnerabilities of cancer cells.

To further examine the role of environmental nutrients in shaping amino acid and nucleotide metabolism, we studied the effects of culturing cancer cells in the physiological form of folate present in circulation in mammals. Previous work suggested that the folate source available to cells would affect the activity of the enzyme methionine synthase, which is required both for methionine and folate metabolism (Chanarin et al., 1985). We found that under physiological conditions, methionine synthase becomes essential for tumor growth due to its role in promoting folate metabolism. This work demonstrates the therapeutic potential of targeting methionine synthase to inhibit cancer growth and further underscores the importance of studying cancer metabolism in a physiological setting.

Given the critical importance of environmental nutrient levels in determining metabolic phenotypes, we chose to quantitate the absolute levels of metabolites present in the local tumor environment. Prior to this work, the levels of nutrients directly available to the tumor had not been determined. To address this question, we isolated interstitial fluid from tumors, as interstitial fluid represents the medium through which nutrients are directly exchanged with cancer cells. We then quantitated the concentration of numerous metabolites in tumor interstitial fluid to determine the exact nutrient accessibility that cancer cells experience. We also compared the composition of interstitial fluid between various tumor types and found that tumor location, tumor tissue of origin, diet, and tumor genetics all play some role in determining the nutrient availability in interstitial fluid.

Together, the results described in this dissertation demonstrate the critical role that the nutrient environment plays in shaping cancer metabolism and provide a basis for future work to examine how metabolism supports tumor growth in different contexts.

DISCUSSION

Limiting nutrients as therapeutic targets

The goal of this thesis work has been to identify sources of nutrient limitation for tumors with the hope that characterizing the metabolites that are most difficult for tumors to obtain in sufficient quantities would illuminate metabolic pathways that might serve as therapeutic targets. We believe that nutrients that are limiting for tumor growth might represent therapeutic targets because cancer is unable to fully meet its demands for these metabolites. In contrast, normal tissues are likely not limited for nutrients under basal conditions; for instance, a muscle cell or brain cell in a healthy adult would not be more functional if provided with an excess of serine or folates. As a result, we suspect that cancer will be more susceptible than normal tissues to treatments that reduce the availability of some limiting nutrients. This is of critical importance, as cancer therapies are only effective if they are more harmful to tumors than to normal tissues.

Methods of identifying limiting metabolites and metabolic pathways

If limiting metabolites represent potential therapeutic targets, then identifying all of the nutrients that are limiting for various tumor types will be important. In this dissertation, we have utilized multiple different approaches to identify limiting metabolites. First, we inferred that serine might be a limiting metabolite because certain tumors upregulate serine synthesis pathway enzymes. Thus, finding metabolic enzymes that are expressed at higher levels in certain tumors may identify metabolic pathways that are highly active in order to compensate

for low nutrient availability. Second, we studied the essentiality of a gene, methionine synthase, under physiological nutrient conditions. Studying the altered metabolic requirements imposed upon cells by growth in physiological nutrient conditions can potentially reveal limiting nutrients or metabolic pathways that might be important for tumor growth *in vivo*. Finally, we directly profiled the accessibility of nutrients in the tumor microenvironment. This analysis identified multiple nutrients that are less abundant in the tumor interstitial fluid than in bulk circulation, suggesting that tumors may have less access to those metabolites than normal tissues. By directly measuring which nutrients are lacking in the tumor microenvironment, we can identify metabolic pathways that may be essential for tumors to cope with their environmental nutrient levels but non-essential for non-cancerous tissues.

Limiting nutrients may be variable across cancers

A key conclusion from this dissertation is that the sources of nutrient limitation for tumors can vary dramatically depending on the environment. Environmental factors can be as simple as the presence or absence of a single nutrient, like serine or 5-methyl THF, in the extracellular milieu. These environmental features can also be more complex, encompassing the summed effects of tumor location, cancer tissue of origin, interactions with immune cells, and many additional factors. We have begun to characterize the metabolic tumor environment in pancreatic and lung cancer driven by specific oncogenes. In this process, we have determined that different tumor types may have unique metabolic vulnerabilities. For instance, we note the relative lack of arginine in the pancreatic tumor microenvironment, suggesting that pancreatic tumors might be particularly dependent on the *de novo* synthesis of arginine. This potential vulnerability is

not shared across any of the other tumor types that we tested, suggesting that further study of nutrient limitation may require the examination of specific tumors in their endogenous niches.

Studies of cancer metabolism require biological context

Many of the reactions that comprise the cellular metabolic network have long been understood. Each of the enzymatic reactions discussed in this dissertation were discovered more than 60 years ago (du Vigneaud et al., 1939; Ichihara and Greenberg, 1955). However, we still lack knowledge of the behavior of these enzymes in specific contexts in living organisms. We have long understood that serine (Davis et al., 1970; Snell, 1984) and folates (Farber et al., 1947; Farber et al., 1948) can be important for the proliferation of tumors. However, in many cases, we do not have a comprehensive grasp of which tissues require those nutrients at which times. This understanding is required to determine which metabolic pathways might serve as effective therapeutic targets in particular tumor types. Our lack of contextual understanding persists on a molecular level, as well; for instance, we have discovered many substrates that can move through cell-surface transporters, but our understanding of the actual fluxes through those transporters in tumors or normal tissues is far from complete (Cesar-Razquin et al., 2015). Attempting to understand how metabolism operates under biologically relevant conditions is challenging; it often requires an understanding of nuanced interactions between many pathways. However, it will be important to attempt to model the complexities present in physiological metabolism to advance our understanding of these pathways.

Examination of conditionally essential metabolic pathways can yield therapeutic targets

Given our incomplete understanding of the contextual importance of metabolic pathways, it may be important to focus additional attention on pathways that are non-essential or conditionally essential for cancer cell growth. For instance, serine is a non-essential amino acid that can be synthesized by many cells, yet its availability can dramatically influence tumor growth. Similarly, methionine synthase is a non-essential enzyme for cancer cells in standard culture media, yet it is completely essential in more physiological media and in animals. The concept that non-essential genes can actually be important for growth likely extends beyond cancer metabolism, as many non-essential genes can be made essential depending on culture conditions (Rancati et al., 2018). Many of the screening approaches used in studying cancer biology rely upon finding genes that are necessary for rapid proliferation in culture; however, the proteins that may make the most effective therapeutic targets could function to allow cancer cell survival under very specific stress conditions or in particular environments. For instance, proteins necessary for a cancer cell to survive the stresses associated with metastasis or chemotherapy treatment could be completely irrelevant to normal growth and survival in culture or even in a primary tumor in an animal model of cancer. Thus, deriving a more complete understanding of the roles that non-essential genes play in cancer and designing screening techniques to study specific stress conditions or environmental niches could be critical to developing more effective cancer therapies.

FINAL PERSPECTIVE

Metabolism plays a role in most cellular processes in some form. Protein synthesis requires amino acids; transcription and DNA replication require the synthesis of nucleotides. In this way,

metabolism can influence almost any part of biology. As a result, it will be important to continue to develop our understanding of how metabolism interfaces with the many biological processes that occur within cells. To do this effectively, we must grow our understanding of how metabolism works in biologically relevant contexts. Many of the enzymatic reactions that comprise metabolism have been thoroughly described, but without proper context, our understanding of what these enzymes are capable of can provide a misleading depiction of what actually occurs within cells in animals. Given how sensitive metabolic processes are to cell-extrinsic environmental factors, the continuing development of better tools to assay cell metabolism in biologically relevant contexts will be critical. These improved tools may take the form of more physiological culture media based on measurements of the physical parameters and nutrient content of the *in vivo* environment, or may require further advances in the techniques used to model metabolism computationally or study metabolic processes in animals.

In this dissertation, we have provided a quantitative description of the nutrient composition of the tumor microenvironment that can serve as a basis to build tools and techniques that more accurately model metabolism in cancer. Using the approach of studying metabolism in biologically relevant contexts, we have also characterized specific situations in which cancer is sensitive to availability of the amino acid serine, and we have identified a potential therapeutic target in methionine synthase that is only important for cancer cell growth under physiological nutrient conditions. We feel that the insights that we have provided into the composition of the metabolic environment in tumors and into the metabolic

requirements of cancer cells in physiologically relevant contexts will serve as a framework for future work in cancer metabolism.

REFERENCES

Cesar-Razquin, A., Snijder, B., Frappier-Brinton, T., Isserlin, R., Gyimesi, G., Bai, X., Reithmeier, R.A., Hepworth, D., Hediger, M.A., Edwards, A.M.*, et al.* (2015). A Call for Systematic Research on Solute Carriers. Cell *162*, 478-487.

Chanarin, I., Deacon, R., Lumb, M., Muir, M., and Perry, J. (1985). Cobalamin-folate interrelations: a critical review. Blood *66*, 479-489.

Davis, J.L., Fallon, H.J., and Morris, H.P. (1970). Two enzymes of serine metabolism in rat liver and hepatomas. Cancer Res *30*, 2917-2920.

DeNicola, G.M., Chen, P.H., Mullarky, E., Sudderth, J.A., Hu, Z., Wu, D., Tang, H., Xie, Y., Asara, J.M., Huffman, K.E.*, et al.* (2015). NRF2 regulates serine biosynthesis in non-small cell lung cancer. Nat Genet *47*, 1475-1481.

du Vigneaud, V., Chandler, J.P., Moyer, A.W., and Keppel, D.M. (1939). The effect of choline on the ability of homocystine to replace methionine in the diet. J Biol Chem, 57-76.

Farber, S., Cutler, E.C., Hawkins, J.W., Harrison, J.H., Peirce, E.C., 2nd, and Lenz, G.G. (1947). The Action of Pteroylglutamic Conjugates on Man. Science *106*, 619-621.

Farber, S., Diamond, L.K., Mercer, R.D., Sylvester, R.F., and Wolff, J.A. (1948). Temporary remissions in acute leukemia in children produced by folic acid antagonist, 4-aminopteryl-glutamic acid (aminopterin). New England Journal of Medicine *238*, 787-793.

Ichihara, A., and Greenberg, D.M. (1955). Pathway of Serine Formation from Carbohydrate in Rat Liver. Proc Natl Acad Sci U S A *41*, 605-609.

Locasale, J.W., Grassian, A.R., Melman, T., Lyssiotis, C.A., Mattaini, K.R., Bass, A.J., Heffron, G., Metallo, C.M., Muranen, T., Sharfi, H.*, et al.* (2011). Phosphoglycerate dehydrogenase diverts glycolytic flux and contributes to oncogenesis. Nat Genet *43*, 869-874.

Maddocks, O.D.K., Athineos, D., Cheung, E.C., Lee, P., Zhang, T., van den Broek, N.J.F., Mackay, G.M., Labuschagne, C.F., Gay, D., Kruiswijk, F.*, et al.* (2017). Modulating the therapeutic response of tumours to dietary serine and glycine starvation. Nature *544*, 372-376.

Maddocks, O.D.K., Berkers, C.R., Mason, S.M., Zheng, L., Blyth, K., Gottlieb, E., and Vousden, K.H. (2013). Serine starvation induces stress and p53-dependent metabolic remodelling in cancer cells. Nature *493*, 542-546.

Possemato, R., Marks, K.M., Shaul, Y.D., Pacold, M.E., Kim, D., Birsoy, K., Sethumadhavan, S., Woo, H.K., Jang, H.G., Jha, A.K.*, et al.* (2011). Functional genomics reveal that the serine synthesis pathway is essential in breast cancer. Nature *476*, 346-350.

Rancati, G., Moffat, J., Typas, A., and Pavelka, N. (2018). Emerging and evolving concepts in gene essentiality. Nat Rev Genet *19*, 34-49.

Snell, K. (1984). Enzymes of serine metabolism in normal, developing and neoplastic rat tissues. Adv Enzyme Regul *22*, 325-400.

APPENDIX A: Increased PHGDH expression uncouples hair follicle cycle progression and promotes inappropriate melanin accumulation

Katherine R. Mattaini[1,2,6], Mark R. Sullivan[1,2,6], Allison N. Lau[1,2], Brian P. Fiske[1,2], Roderick T. Bronson[3], Matthew G. Vander Heiden[1,2,4,5]

[1]Koch Institute for Integrative Cancer Research and [2]Department of Biology, Massachusetts Institute of Technology, Cambridge, Massachusetts 02139, USA
[3]Rodent Histopathology Core, Harvard Medical School, Boston, Massachusetts 02111, USA
[4]Dana-Farber Cancer Institute, Boston, Massachusetts 02215, USA
[5]Broad Institute, Cambridge, Massachusetts 02139, USA

[6]These authors contributed equally to this chapter

A version of this chapter has been submitted for publication.

ABSTRACT

Copy number gain of the *PHGDH* gene, which encodes the first enzyme in serine biosynthesis, is found in some human cancers including a subset of melanomas. In order to study the effect of increased *PHGDH* expression in tissues *in vivo*, we generated mice harboring a *PHGDH*^{tetO} allele that allows tissue-specific, doxycycline-inducible PHGDH expression. Tissues and cells derived from *PHGDH*^{tetO} mice exhibit increased serine biosynthesis. Histological examination of skin tissue from *PHGDH*^{tetO} mice reveals the presence of melanin granules in anagen II hair follicles, despite the fact that in wild type mice melanin synthesis is closely coupled to the hair follicle cycle and does not begin until later in the cycle. This phenotype occurs in the absence of any global change in hair follicle cycle timing. The inappropriate presence of melanin early in the hair follicle cycle following PHGDH expression is also accompanied by increased melanocyte abundance in anagen II skin. Together, these data may provide insight into how PHGDH expression impacts normal melanocyte biology to promote melanoma.

INTRODUCTION

D-3-phosphoglycerate dehydrogenase (PHGDH) is the first enzyme in the *de novo* serine biosynthesis pathway. Flux through this pathway can be important for the proliferation of some cancer cells, and the *PHGDH* gene is located in a region of focal genomic copy number gain that is associated with subsets of breast cancer and melanoma as well as cell lines derived from other cancer types (Locasale et al., 2011, Possemato et al., 2011). *PHGDH*-amplified cells are dependent on expression of catalytically active enzyme to proliferate (Mattaini et al., 2015),

and high PHGDH expression is associated with negative clinical outcomes in breast cancer (Locasale et al., 2011, Pollari et al., 2011, Possemato et al., 2011), glioma (Liu et al., 2013) and cervical cancer (Jing et al., 2013). In addition to gene amplification, PHGDH expression can be upregulated through transcriptional and epigenetic mechanisms (Adams, 2007, Ding et al., 2013, Nilsson et al., 2012). As discussed in Chapter 2, PHGDH expression can serve to promote breast cancer and melanoma. In the autochthonous models described in Chapter 2, PHGDH overexpression occurs first in non-cancerous melanocytes and mammary epithelial cells. Thus, it is of interest to understand how PHGDH expression affects these normal tissues.

Because *PHGDH* gene copy number gain is observed with higher frequency in melanoma compared to other cancers (Locasale et al., 2011, Possemato et al., 2011), the effect of PHGDH expression on melanocyte biology is of particular interest. Melanocytes are the main pigment-producing cells in mammals. In mice, cutaneous melanocytes in truncal skin are exclusively follicular. Melanogenesis in follicular melanocytes is closely coupled to hair follicle (HF) cycling. Once a HF and the first hair are formed during morphogenesis, the entire base of the HF, the cycling portion, undergoes programmed cell death during a period known as catagen. The HF then enters a "resting" phase, telogen, before the anagen period (Chase, 1954, Fuchs, 2007) during which the entire lower portion of the HF is repopulated from epithelial and melanocyte stem cells located in the bulge region (Cotsarelis et al., 1990, Nishimura et al., 2002). Initiation of melanogenesis is tightly coupled to anagen progression (Slominski and Paus, 1993), with the first melanin granules visible in the HF during the anagen IIIa stage, when the hair follicle bulb extends to the border of the dermis and subcutis (Muller-Rover et al., 2001). Though serine biosynthesis is not obviously connected to HF cycling, serine biosynthesis pathway enzymes

may affect differentiation of survival of stem cells (Hwang et al., 2016, Samanta et al., 2016), which could potentially perturb HF cycle progression.

To study how increased PHGDH expression affects normal tissue function in mice, we developed a transgenic mouse harboring a human PHGDH cDNA under the control of a doxycycline-inducible promoter. We found that expression of PHGDH results in premature appearance of melanin in HFs as well as an increased number of melanocytes in whole skin, suggesting that PHGDH expression affects melanocyte proliferation and/or differentiation, which may contribute to selection for increased PHGDH expression in cancer.

RESULTS

Generation of a *PHGDH^{tetO}* allele

In order to model the consequences of *PHGDH* copy number gain observed in cancer and study the effect of increased PHGDH expression in tissues, a transgenic mouse was engineered to enable tissue-directed PHGDH expression using a previously described system (Beard et al., 2006). A human PHGDH cDNA under the control of the tetracycline operator minimal promoter (tetO) was introduced into embryonic stem (ES) cells containing a reverse tetracycline transactivator (*M2rtTA*) allele under the control of the endogenous Rosa26 promoter that is active in most tissues, and these ES cells were used to generate mice with the *PHGDH^{tetO}* allele (Figure 1A-D).

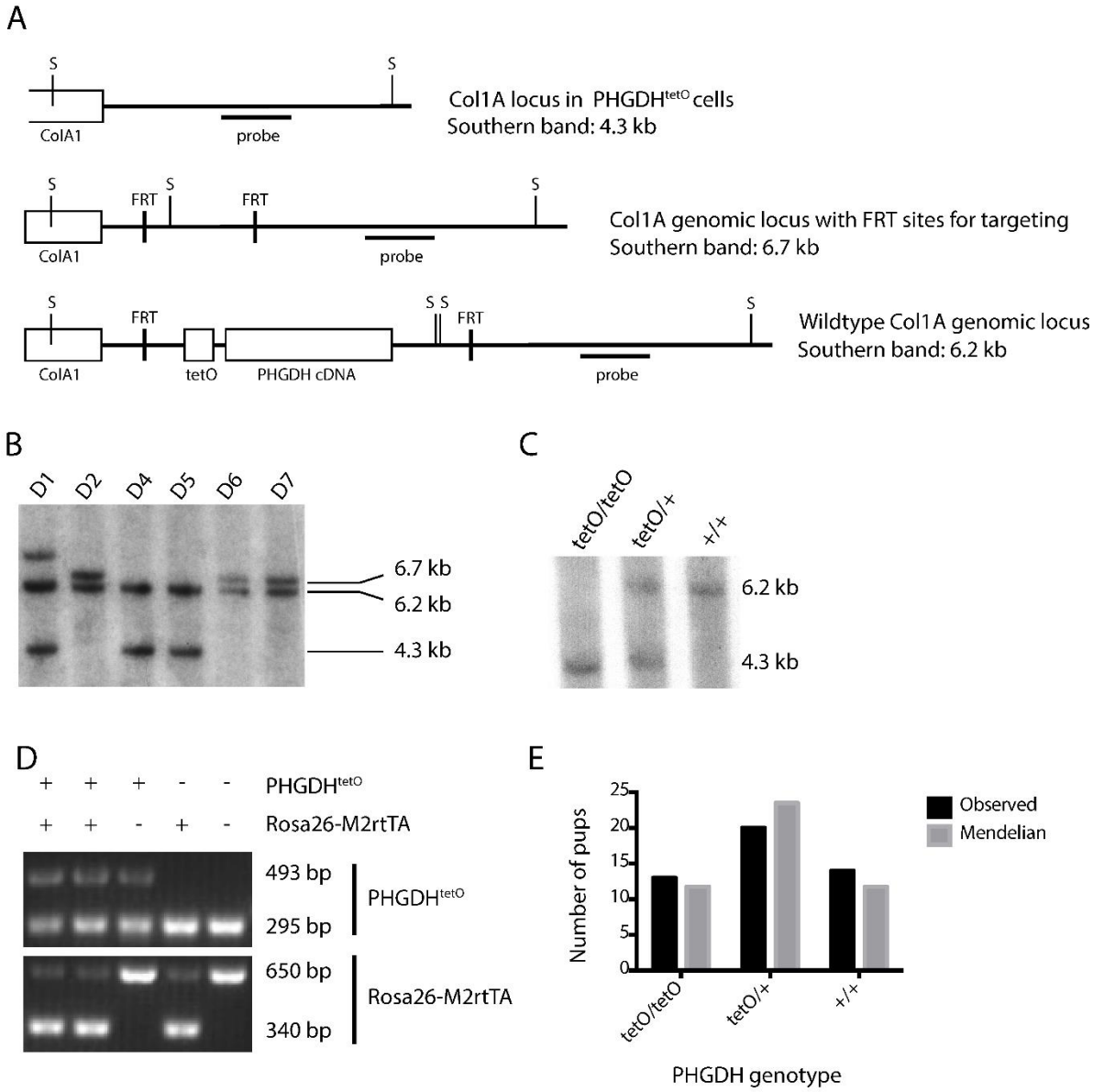
A
S
S
Col1A
probe
Col1A locus in PHGDH^tetO cells
Southern band: 4.3 kb
FRT
FRT
Col1A genomic locus with FRT sites for targeting
Southern band: 6.7 kb
tetO
PHGDH cDNA
Wildtype Col1A genomic locus
Southern band: 6.2 kb
B
D1
D2
D4
D5
D6
D7
6.7 kb
6.2 kb
4.3 kb
C
tetO/tetO
tetO/+
+/+
6.2 kb
4.3 kb
D
PHGDH^tetO
Rosa26-M2rtTA
493 bp
295 bp
650 bp
340 bp
E
Number of pups
Observed
Mendelian
PHGDH genotype
F
human rPHGDH
mouse rPHGDH
ng protein
PHGDH

Figure 1. Generation of the PHGDH^{tetO} allele

(A) Schematic of the Col1A locus in wildtype mouse cells (top), the modified locus in KH2 ES cells (middle) and the locus after targeting to introduce the PHGDH^{tetO} allele (bottom). The PHGDH cDNA introduced into the Col1A locus is the human sequence. The expected band sizes when the indicated probe is used for Southern blot analysis as in (B) and (C)] are indicated. Also shown are the location of the SpeI sites (marked "S") in each locus used to digest genomic DNA for Southern blot analysis. FRT, flippase recognition target site; tetO, tetracycline operator minimal promoter. (B) Southern blot analysis of SpeI-digested genomic DNA from six PHGDH^{tetO}-targeted ES cells. Clones D4 and D5 exhibit proper targeting of the Col1A locus and an unaffected wild-type allele. (C) Southern blot analysis of SpeI-digested genomic DNA from mice of the indicated genotypes. (D) PCR-based genotyping of the PHGDH^{tetO} and Rosa26-M2rtTA alleles. In the PHGDH^{tetO} reaction, the presence of the transgene is indicated by the upper band; in the Rosa26-M2rtTA reaction, the presence of the transgene is indicated by the lower band. (E) The number of offspring of each genotype observed when mice hemizygous for the PHGDH^{tetO} allele exposed to a doxycycline diet were mated. The observed distribution of genotypes in the offspring did not differ significantly from expected Mendelian ratios, with p=0.58 by the $\chi 2$ goodness-of-fit test. (F) Western blot analysis of PHGDH protein using the indicated amount of recombinant human or mouse PHGDH to test antibody specificity.

Characterization of *PHGDH^{tetO}* mice

PHGDH is only expressed in tissues from mice with both the *PHGDH^{tetO}* and the *Rosa26-M2rtTA* alleles and only upon exposure of tissues to doxycycline (dox) (Figure 2A). To test whether increased PHGDH expression affects viability, breeding pairs of *PHGDH^{tetO}* hemizygotes were continually fed a diet containing dox to induce PHGDH expression in most mouse tissues. Offspring from these crosses were born in expected Mendelian ratios (Figure 1E). Expression from the Rosa26 promoter is active by the blastocyst stage of the developing embryo (Zambrowicz et al., 1997), and dox readily crosses the placenta to regulate transgene expression in the developing embryo (Fedorov et al., 2001, Perl et al., 2002a, Perl et al., 2002b, Shin et al., 1999). Thus, this result suggests that increased PHGDH expression in the embryo does not prevent mouse development or viability.

Embryonic fibroblasts (MEFs) derived from *PHGDH^{tetO};Rosa26-M2rtTA* mice display dose-dependent, dox-inducible PHGDH expression (Figure 2B). The antibody used throughout this study recognizes both human and mouse PHGDH proteins with similar affinities by Western blot (Figure 1F); thus, PHGDH expression observed in *PHGDH$^{+/+}$* MEFs and in conditions without dox-induced transgene activation reflect mouse PHGDH protein expressed from the endogenous locus. In previous studies examining a variety of cell lines and tissues, expression of PHGDH at the protein level correlates with serine biosynthesis pathway flux (Davis and Fallon, 1970, Locasale et al., 2011, Possemato et al., 2011). Similar results are obtained following transgene expression, as dox-treated *PHGDH^{tetO};Rosa26-M2rtTA* MEFs show a dose-dependent increase in both PHGDH protein and the concentration of the unique serine biosynthesis

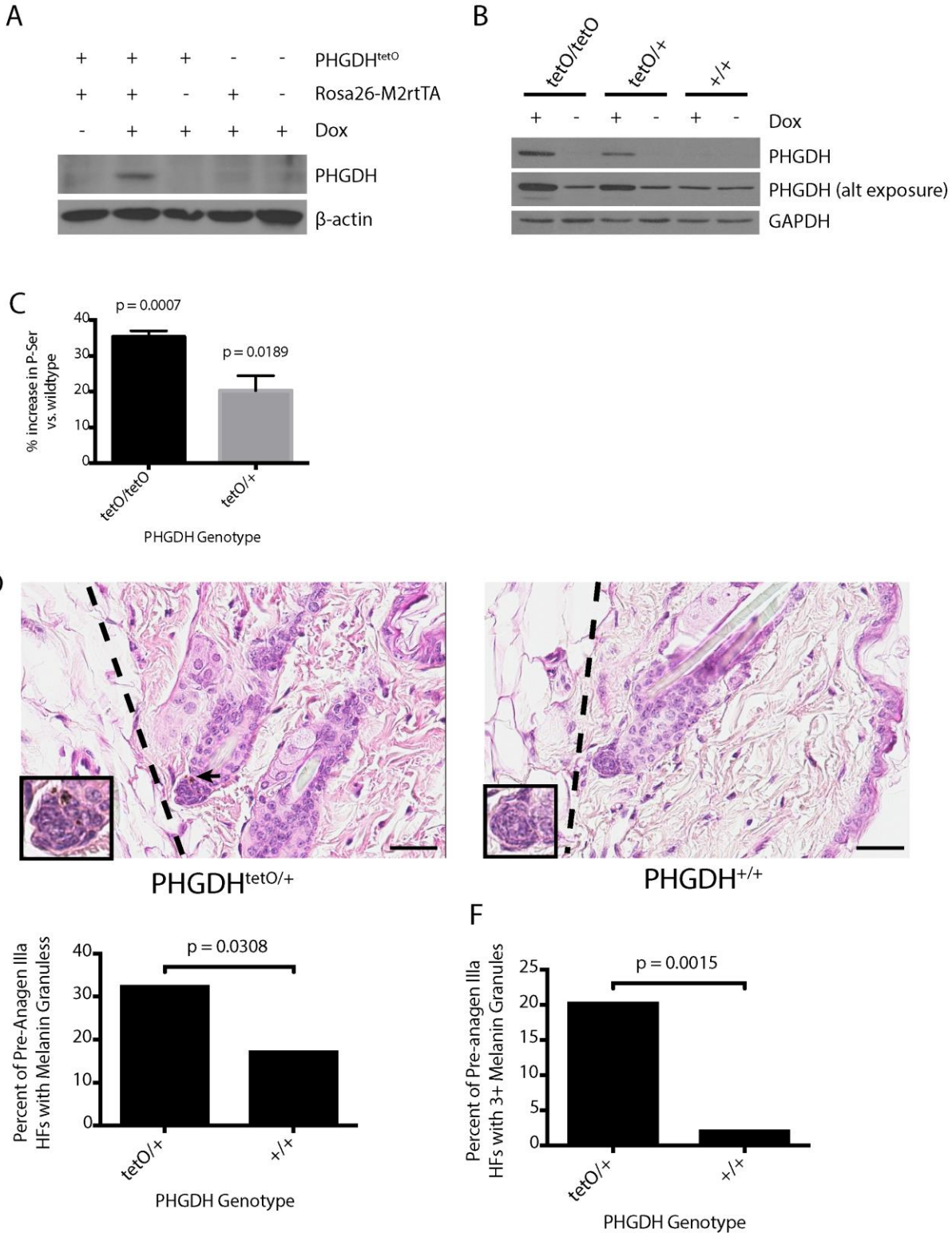
A
+ + + - - PHGDH^tetO
+ + - + - Rosa26-M2rtTA
- + + + + Dox
PHGDH
β-actin
B
tetO/tetO
tetO/+
+/+
+ - + - + - Dox
PHGDH
PHGDH (alt exposure)
GAPDH
C
p = 0.0007
p = 0.0189
% increase in P-Ser vs. wildtype
40
30
20
10
0
tetO/tetO
tetO/+
PHGDH Genotype
D
PHGDH^tetO/+
PHGDH^+/+
E
p = 0.0308
Percent of Pre-Anagen IIIa HFs with Melanin Granuless
40
30
20
10
0
tetO/+
+/+
PHGDH Genotype
F
p = 0.0015
Percent of Pre-anagen IIIa HFs with 3+ Melanin Granules
25
20
15
10
5
0
tetO/+
+/+
PHGDH Genotype

Figure 2. Introducing a *PHGDH^{tetO}* allele into mice increases PHGDH expression and results in the aberrant appearance of melanin granules

(A) Western blot analysis to assess PHGDH expression in liver lysates from mice harboring the indicated alleles and were exposed to a doxycycline containing diet (Dox) or a control diet for 5 days. β-actin expression was also assessed as a loading control. **(B)** Western blot analysis to assess PHGDH expression in MEFs derived from mice with the *Rosa26-M2rtTA* allele and the indicated number of *PHGDH^{tetO}* (tetO) alleles that were cultured in media with or without doxycycline (Dox) as for 72 hours as indicated. Both a light and dark exposure (alt exposure) is shown, as is GAPDH expression as a loading control. **(C)** The percent increase in the concentration of intracellular phosphoserine (P-ser) in MEFs derived from mice described in (B) harboring one (tetO/+) or two (tetO/tetO) transgene alleles relative to levels found in MEFs derived from wildtype mice is shown. All MEFs were cultured for 4 days in media with doxycycline prior to measurement of P-Ser levels by LC-MS. Data shown represent the mean (+/- SEM). The increase is statistically significant with p values from two-tailed Student's T test. **(D)** Representative H&E staining of skin sections from 3.5-month-old mice of the indicated genotypes that had been exposed to a doxycycline-containing diet for 9 days. Dotted lines delineate the border between the dermis and the subcutis. Arrow indicates melanin granules in the hair follicles (HFs) of the *PHGDH^{tetO};Rosa26-M2rtTA* mouse. All hair follicle shown are pre-anagen IIIa as they are contained completely within the dermis. Images were obtained at 40x magnification. Scale bar = 30 μm. Inset images are magnified 80X. **(E)** Quantitation of the percent of pre-anagen IIIa hair follicles (HF) in each genotype that contain any melanin granules. Data shown represent the % observed when analyzing 167 HFs from one PHGDH^{tetO};*Rosa26-M2rtTA* mouse and 46 HFs from one wild type mouse. **(F)** Quantitation of the percent of pre-anagen IIIa hair follicles (HF) in each genotype with three or more melanin granules. Data shown represent the % observed when analyzing 167 HFs from one PHGDH^{tetO};*Rosa26-M2rtTA* mouse and 46 HFs from one wild type mouse. The percent increase in hair follicles with melanin granules shown in (E) and (F) is statistically significant with p values derived from one-tailed Fisher's exact test.

pathway intermediate phosphoserine compared to dox-treated wild type MEFs (Figure 2B-C). These data suggest the transgene expression can increase serine biosynthesis in cells.

Mice with long-term PHGDH overexpression are grossly normal

PHGDH^{tetO};Rosa26-M2rtTA mice were exposed to dox diet beginning at 6 weeks of age and maintained on this diet for 16-18 months. During this time, mice were monitored weekly without evidence of any obvious abnormalities while alive and at necropsy. Liver and skin samples were analyzed by Western blot for PHGDH protein expression. Some samples showed less PHGDH expression than expected after 16-18 months of dox exposure (Figure 3), but liver and skin samples from the same individual showed consistent expression levels suggesting that differences in transgene silencing might underlie the variability in expression between mice. Histological analysis of skin, brain, white and brown fat, mammary gland, pancreas, liver, spleen, kidney, colon, lung and heart tissue in this cohort from control mice and *PHGDH^{tetO};Rosa26-M2rtTA* mice with high PHGDH expression by Western blot was unremarkable, suggesting that mice with long-term increased PHGDH expression are grossly normal.

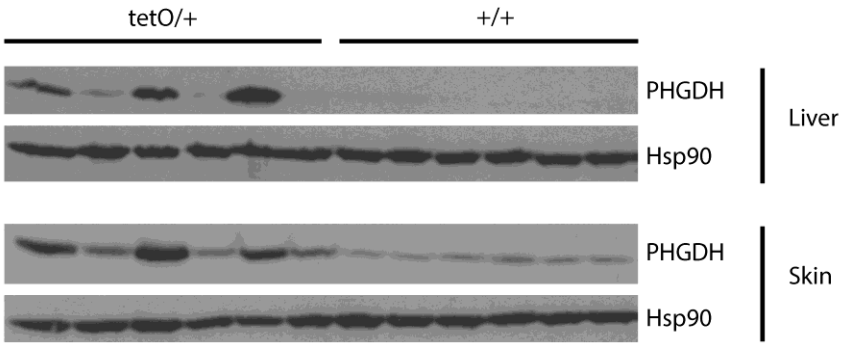

Figure 3. Tissues from mice with long-term exposure to doxycycline diet show variable PHGDH expression. Western blot analysis for PHGDH expression in liver and skin from PHGDH^{tetO};Rosa26-M2rtTA (tetO/+) and wildtype (+/+) mice that were exposed to doxycycline diet for 16-18 months. Hsp90 expression is also shown as a loading control.

Pre-anagen IIIa hair follicles in *PHGDH^{tetO}* mice inappropriately contain melanin granules

Given the high frequency of *PHGDH* gene copy number gain observed in melanoma compared to other cancers (Locasale et al., 2011, Possemato et al., 2011), we sought to examine the effect of PHGDH expression on melanocyte biology. When examining the skin of 3.5 month-old mice treated with dox for 9 days, an anomaly in follicular melanin was observed (Figure 2D). The bulbs of the HFs pictured in Figure 2D are surrounded entirely by dermis, identifying them as pre-anagen IIIa; however, in *PHGDH^{tetO}*;*Rosa26-M2rtTA* HFs melanin granules are visible. Ordinarily, during catagen, all cells from the cycling portion of the HF undergo apoptosis, including the melanocytes. Any melanin they have produced is passed to the keratinocytes that make up the hair itself, so that melanin is no longer present in the bulb before new melanin is produced in anagen IIIa of the next HF cycle. Occasionally, melanin granules produced in a previous HF cycle will not be extruded with the hair shaft and are visible

in the dermal papilla in telogen, anagen I, or anagen II (Tobin et al., 1998). However, the *PHGDH*^{tetO};*Rosa26-M2rtTA* skin had a significantly greater proportion of pre-anagen IIIa HFs displaying melanin than the wildtype skin (Figure 2E). Furthermore, although some pre-anagen IIIa HFs in the wildtype skin displayed one or two melanin granules, almost none had three or more (Figure 2F). In contrast, many melanin-containing follicles in the *PHGDH*^{tetO};*Rosa26-M2rtTA* skin had as many as 5-10 granules.

PHGDH expression does not globally affect timing of the hair follicle cycle

To further characterize this phenotype, HF cycling was synchronized by plucking hair from a region of skin to induce HFs in that region to enter a new cycle. Skin was then harvested at defined time points to examine a desired cycle stage (Muller-Rover et al., 2001). In order to determine the effect of PHGDH overexpression on follicular melanin throughout the HF cycle, two approaches were used: one set of mice was fed dox diet for two days before plucking (red bar) and the other set for thirty days before the HF cycle was synchronized by plucking (blue bar) (Figure 5A). The first few HF cycles following birth are relatively synchronous across individuals (Muller-Rover et al., 2001). Therefore, a 30-day pre-induction with dox followed by plucking at 49 days of age allows PHGDH overexpression during the entire cycle preceding plucking, from telogen to telogen. Conversely, the 2-day pre-induction only allowed PHGDH overexpression during the very end of the HF cycle preceding synchronization. By using two different pre-induction times, we aimed to determine whether the melanin phenotype required PHGDH overexpression in only the current HF cycle or if expression in the preceding cycle was required for melanin accumulation.

Examination of skin at various time points after HF synchronization in mice exposed to dox for thirty days prior to plucking suggested PHGDH overexpression does not globally affect timing of the HF cycle (Figure 4A). HFs in synchronized skin from both control and *PHGDH*^{tetO};*Rosa26-M2rtTA* mice were found in the expected stages for their collection days. Additionally, no perceptible differences visible by H&E staining were evident in any HF stage other than anagen II. The fact that the phenotype is anagen II-specific likely explains why it was not detected in the cohort of aged mice. Anagen II is relatively short compared to the entire HF cycle; thus, anagen II HFs are not abundant in mice of any age. Furthermore, HF cycling becomes more asynchronous as mice age (Paus and Foitzik, 2004), so that the likelihood of collecting a skin sample by chance with an abundance of anagen II HFs is further decreased.

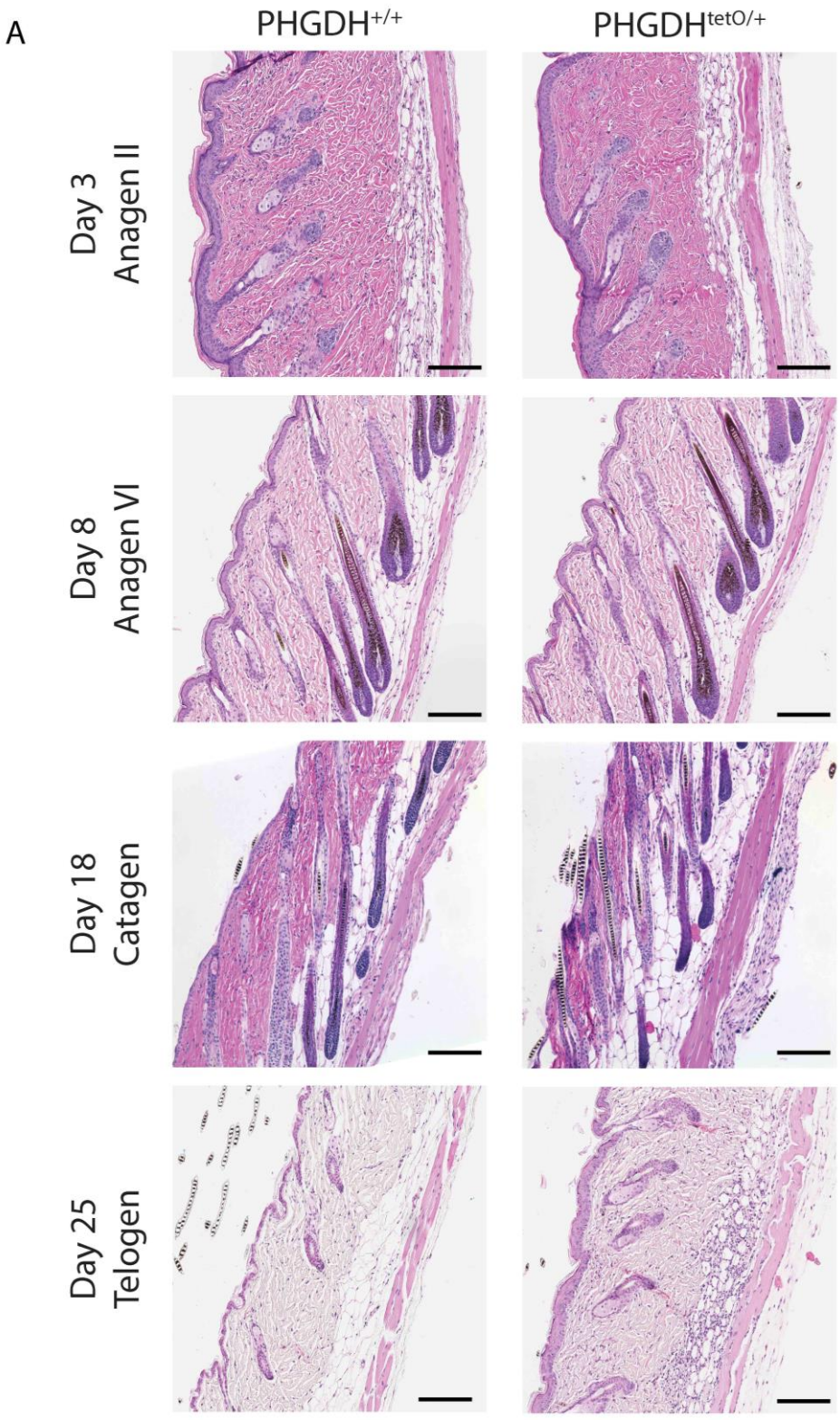
A
PHGDH+/+
PHGDHtetO/+
Day 3
Anagen II
Day 8
Anagen VI
Day 18
Catagen
Day 25
Telogen

B

PHGDH$^{+/+}$

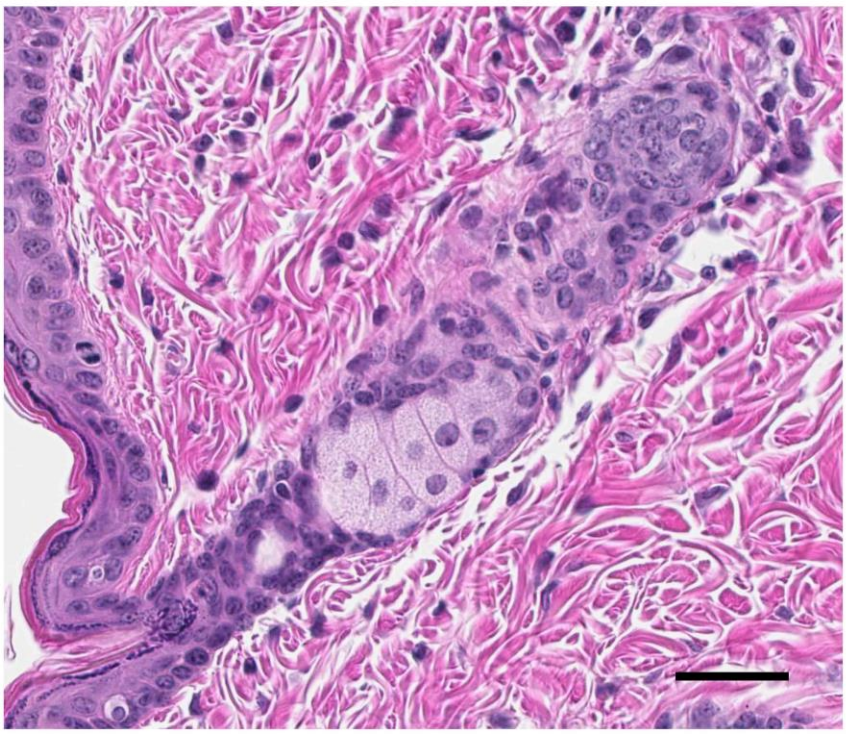

PHGDH$^{tetO/+}$

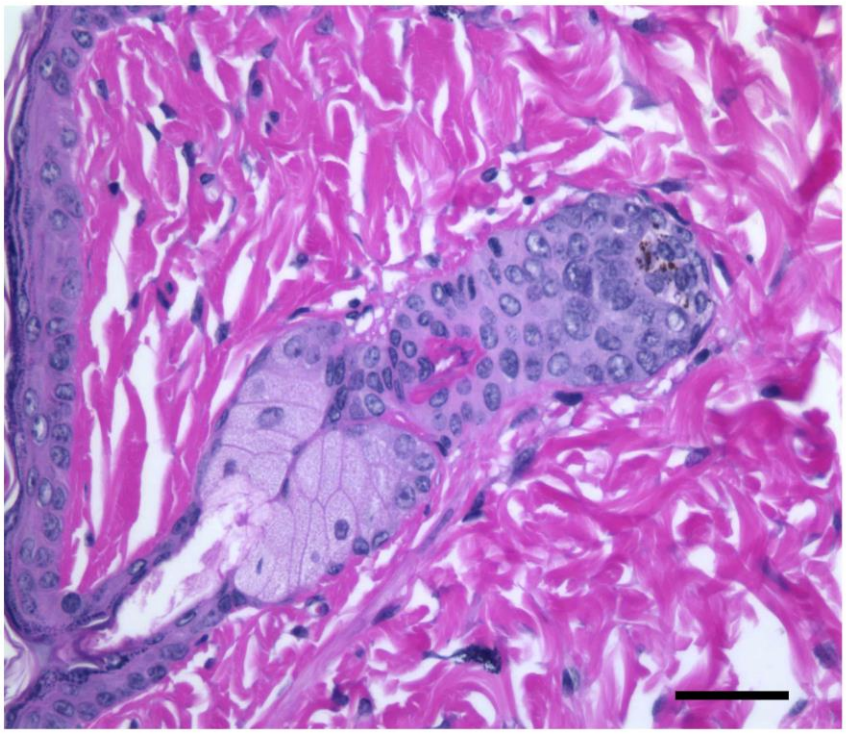

Figure 4. PHGDH expression leads to melanin accumulation in pre-anagen IIIa hair follicles but does not globally affect timing of the hair follicle cycle.

(A) A region of hair was plucked from 49 day-old mice (at the second telogen) to synchronize the hair follicle cycle, and skin samples were collected at defined days thereafter. Data were collected from PHGDH^{tetO};Rosa26-M2rtTA or control (+/+) mice that were exposed to doxycycline (Dox) for 30 days prior to synchronization. Representative H&E staining of skin sections from mice of the indicated genotypes is shown. Images were obtained at 4x magnification. Scale bar = 1 mm. (B) Representative H&E staining of skin from a control (PHGDH$^{+/+}$) and PHGDH^{tetO};R26-M2rtTA (PHGDH$^{tetO/+}$) mouse showing anagen II hair follicles (HFs) that contain zero and multiple melanin granules, respectively. Images were obtained at 40x magnification. Scale bar = 30 µm.

Anagen II hair follicles in synchronized *PHGDH^{tetO}* skin contain melanin granules

Anagen II follicles in synchronized skin of *PHGDH^{tetO}*;*Rosa26-M2rtTA* mice with only a 2-day dox pre-induction show the presence of inappropriate melanin granules, but neither the proportion of HFs with melanin (Figure 5B) nor the fraction of HFs with three or more melanin granules (Figure 5C) is significantly different than in wild-type mice. Analyzing skin by Western blot shows that 2-day pre-induction is sufficient to moderately increase PHGDH levels in some mice; however, the change in expression is higher in the skin of mice exposed to dox diet for 30 days (Figure 5D), raising the possibility that the absence of a melanin phenotype after 2 days of dox pre-induction is due to the latency of PHGDH expression.

Examination of anagen II skin from mice with a 30-day pre-induction showed inappropriate melanin accumulation to a degree that reproduced the initial phenotype observed (Figure 4B). The anagen II HFs from the skin of *PHGDH^{tetO}*;*Rosa26-M2rtTA* mice more frequently contained melanin (Figure 5E) and were more likely to have a high number of melanin granules (Figure 5F) than their wild-type counterparts. The percentages observed in this experiment were similar to those observed in the initial unsynchronized experiment (Figure 2D-F). To confirm that melanin accumulation is associated with increased PHGDH expression from the transgene, we designed qPCR primers specific for human or mouse PHGDH cDNA (Figure 6A-D) and found that in synchronized *PHGDH^{tetO}*;*Rosa26-M2rtTA* skin, expression of human PHGDH was increased while expression of mouse PHGDH was unchanged (Figure 5G).

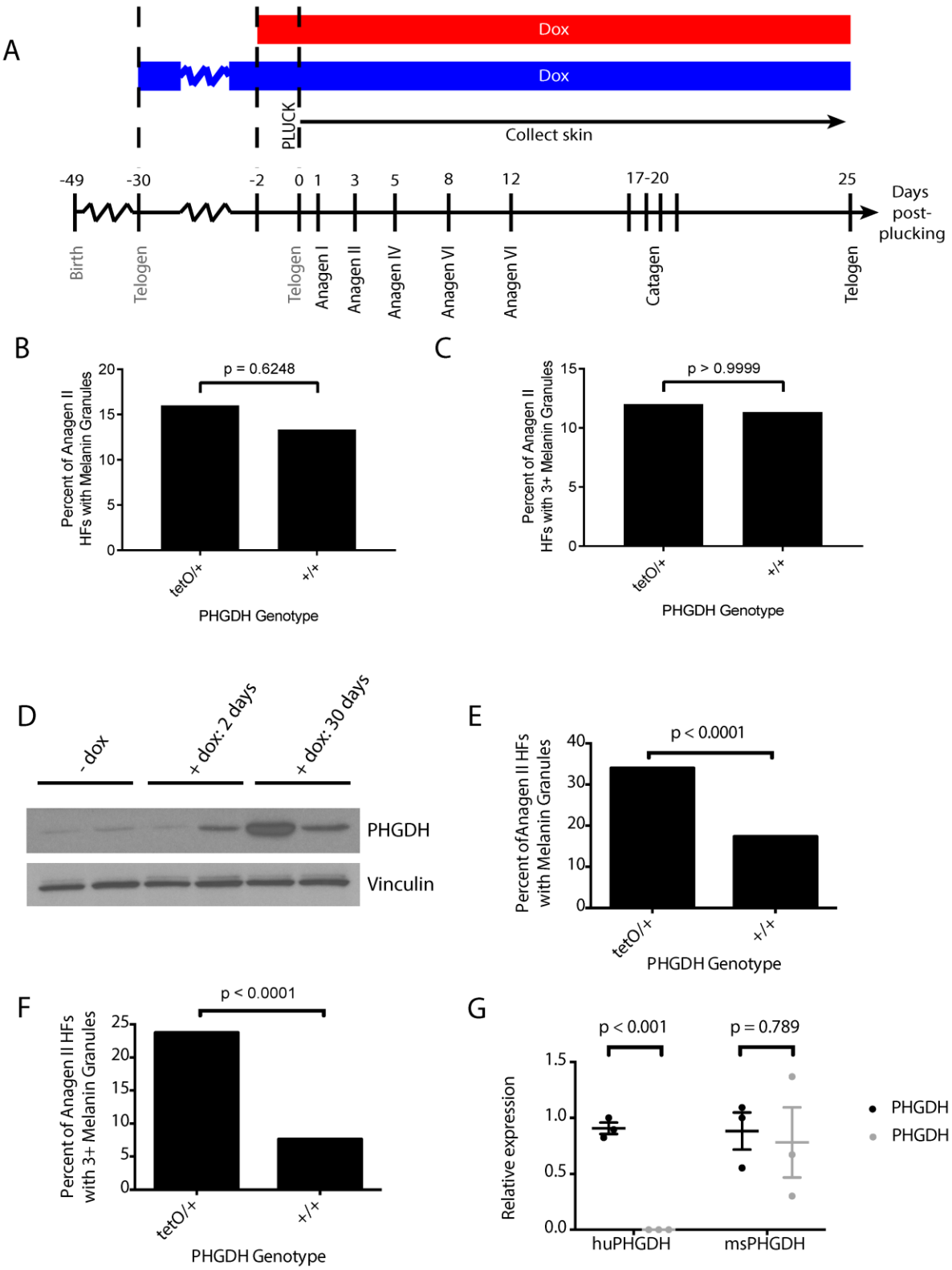
A
Dox
Dox
PLUCK
Collect skin
-49
-30
-2
0
1
3
5
8
12
17-20
25
Days post-plucking
Birth
Telogen
Telogen
Anagen I
Anagen II
Anagen IV
Anagen VI
Anagen VI
Catagen
Telogen
B
p = 0.6248
Percent of Anagen II HFs with Melanin Granules
tetO/+
+/+
PHGDH Genotype
C
p > 0.9999
Percent of Anagen II HFs with 3+ Melanin Granules
tetO/+
+/+
PHGDH Genotype
D
- dox
+ dox: 2 days
+ dox: 30 days
PHGDH
Vinculin
E
p < 0.0001
Percent ofAnagen II HFs with Melanin Granules
tetO/+
+/+
PHGDH Genotype
F
p < 0.0001
Percent of Anagen II HFs with 3+ Melanin Granules
tetO/+
+/+
PHGDH Genotype
G
p < 0.001
p = 0.789
Relative expression
huPHGDH
msPHGDH
PHGDH tetO/+
PHGDH +/+

Figure 5. PHGDH expression during the previous hair follicle cycle leads to increased melanin accumulation. **(A**) A region of hair was plucked from 49 day-old mice (at the second telogen) to synchronize the hair follicle cycle, and skin samples were collected at defined days thereafter. Data were collected from *PHGDH^{tetO}*;*Rosa26-M2rtTA* (tetO/+) or control (+/+) mice that were exposed to doxycycline (Dox) for either 2 days or 30 days prior to synchronization. Shown is a schematic of the experiment, with the red bar depicting mice exposed to doxycycline diet for 2-days before synchronization, and the blue bar depicting mice exposed to doxycycline for 30-days before synchronization. **(B)** Quantitation of the percent of anagen II hair follicles (HFs) containing any melanin granules in *PHGDH^{tetO}*;*Rosa26-M2rtTA* (tetO/+) or control (+/+) mice exposed to doxycycline for 2 days prior to synchronization. Data shown represent the % observed when analyzing 50 HFs per mouse from 3 mice of each genotype **(C)** Quantitation of the percent of anagen II hair follicles with three or more melanin granules in *PHGDH^{tetO}*;*Rosa26-M2rtTA* (tetO/+) or control (+/+) mice exposed to doxycycline for 2 days prior to synchronization. Data shown represent the % observed when analyzing 50 HFs per mouse from 3 mice of each genotype. No statistically significant increase in hair follicles with melanin granules were observed in (B) or (C) with p-values derived from two-tailed Fisher's exact test. **(D)** Western blot analysis for PHGDH expression in skin from *PHGDH^{tetO}*;*Rosa26-M2rtTA* mice never exposed to doxycycline-containing diet (-dox) or fed a doxycycline-containing diet for 2 or 30 days as indicated. Vinculin expression is also shown as a loading control. **(E)** Quantitation of the percent of anagen II hair follicles (HFs) containing any melanin granules in *PHGDH^{tetO}*;*Rosa26-M2rtTA* (tetO/+) or control (+/+) exposed to doxycycline for 30 days prior to synchronization. Data shown represent the % observed when analyzing 50 HFs per mouse from 3 mice of each genotype. **(F)** Quantitation of the percent of anagen II hair follicles with three or more melanin granules *PHGDH^{tetO}*;*Rosa26-M2rtTA* (tetO/+) or control (+/+) mice exposed to doxycycline for 30-days prior to synchronization. Data shown represent the % observed when analyzing 50 HFs per mouse from 3 mice of each genotype. The increase in hair follicles with melanin granules shown in (E) and (F) is statistically significant with p-values derived from two-tailed Fisher's exact test. **(G)** qPCR to assess species-specific PHGDH expression in anagen II skin isolated from *PHGDH^{tetO}*;*Rosa26-M2rtTA* (tetO/+) or control (+/+) mice exposed to doxycycline for 30-days prior to synchronization. An increase in human PHGDH (huPHGDH), but not mouse PHGDH (msPHGDH) expression is statistically significant with p values derived from unpaired Student's t test. Data shown represent the mean (+/- SD).

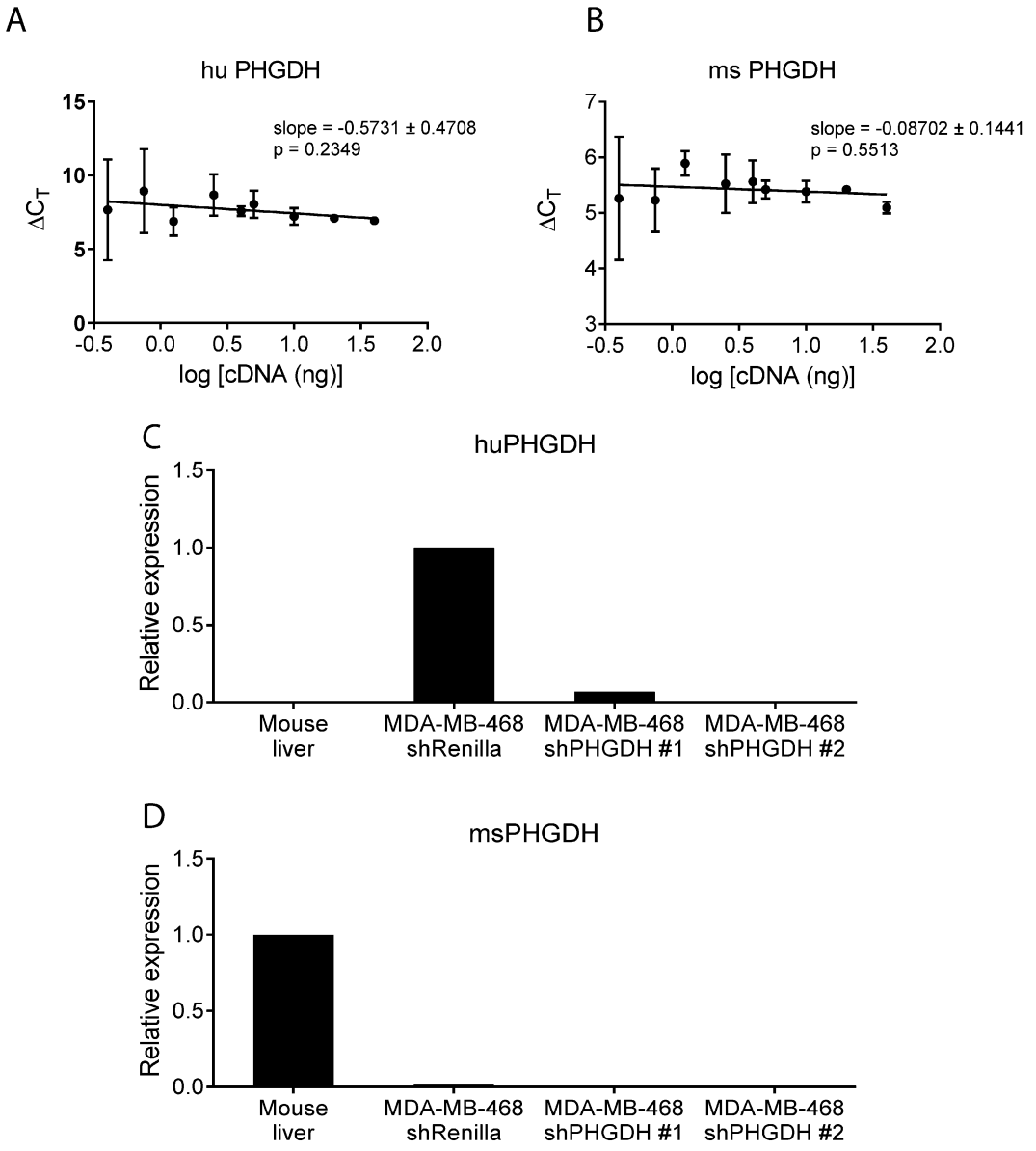

Figure 6. Validation of species-specific PHGDH qPCR primers

qPCR primers specific to (A) human (hu PHGDH) and(B) mouse (ms PHGDH) PHGDH were tested for linearity and relative quantitation compared to 18S rRNA. The slope of each line does not significantly differ from 0, with p-values derived from an F test. The same human (C) and mouse (D) PHGDH primers were examined for an ability to amplify PHGDH cDNA derived from mouse liver or the human cell line MDA-MB-468 infected with a control shRNA (shRenilla) or one of two hairpins targeting PHGDH (shPHGDH).

Melanin accumulation in *PHGDH^{tetO}* mice is caused by cell autonomous PHGDH expression

In order to determine whether the melanin phenotype observed in the *PHGDH^{tetO}*;*Rosa26-M2rtTA* mice is cell autonomous, we crossed *PHGDH^{tetO}* mice to mice harboring a *Dct-rtTA* allele that allows melanocyte-specific transgene expression (Zaidi et al., 2011a, Zaidi et al., 2011b). With a 30-day pre-induction, skin from *PHGDH^{tetO}*;*Dct-rtTA* mice displayed melanin granules in anagen II HFs with similar percentages as those observed in mice with a *Rosa26-M2rtTA* allele (Figure 7A-B), suggesting that the PHGDH-dependent presence of melanin in anagen II HFs is a melanocyte-autonomous event.

Melanin accumulation can be caused by acute PHGDH overexpression

To evaluate whether PHGDH expression is required in the previous HF cycle for this phenotype, we used a 2-day pre-induction with dox. Though a 2-day pre-induction led to only weak PHGDH expression when driven by *Rosa26-M2rtTA*, the melanocyte specific *Dct-rtTA* is predicted to promote higher PHGDH expression in these cells. Indeed, we found that with a 2 day pre-induction, skin from *PHGDH^{tetO}*;*Dct-rtTA* mice displayed melanin granules in anagen II HFs at a higher rate than skin from wildtype mice (Figure 7C-D). The presence of the melanin phenotype with a 2-day pre-induction suggests that the phenotype does not depend on PHGDH overexpression during the previous catagen. This argues against PHGDH promoting survival of melanocytes that would normally die during the previous catagen phase. Instead, the effect of PHGDH expression on uncoupling melanin appearance with normal HF cycle progression only requires the presence of PHGDH during the earliest phases of the HF cycle.

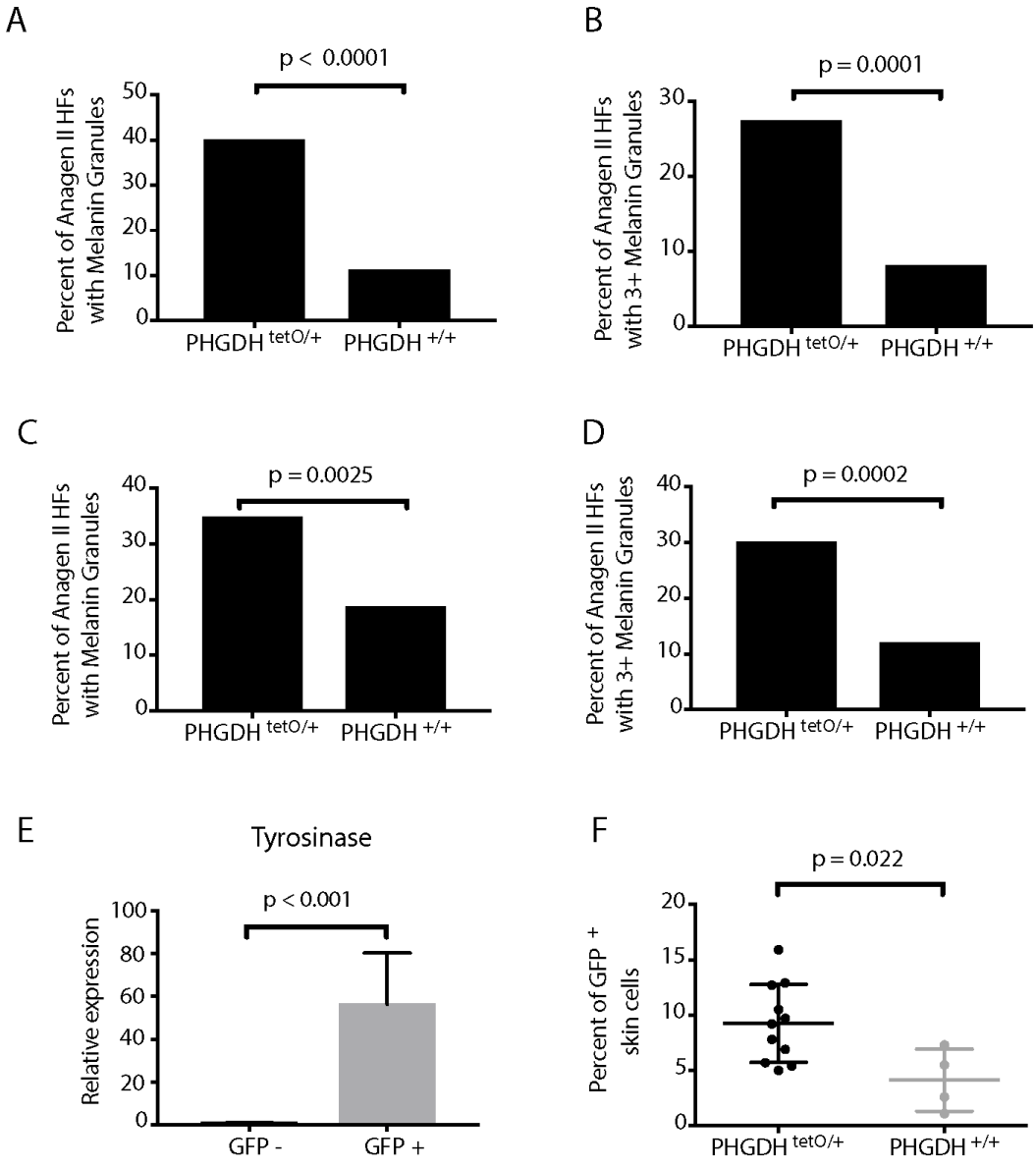
A
p < 0.0001
Percent of Anagen II HFs with Melanin Granules
50
40
30
20
10
0
PHGDH tetO/+
PHGDH +/+
B
p = 0.0001
Percent of Anagen II HFs with 3+ Melanin Granules
30
20
10
0
PHGDH tetO/+
PHGDH +/+
C
p = 0.0025
Percent of Anagen II HFs with Melanin Granules
40
30
20
10
0
PHGDH tetO/+
PHGDH +/+
D
p = 0.0002
Percent of Anagen II HFs with 3+ Melanin Granules
40
30
20
10
0
PHGDH tetO/+
PHGDH +/+
E
Tyrosinase
p < 0.001
Relative expression
100
80
60
40
20
0
GFP -
GFP +
F
p = 0.022
Percent of GFP + skin cells
20
15
10
5
0
PHGDH tetO/+
PHGDH +/+

Figure 7. Increased PHGDH expression in melanocytes drives melanin accumulation in anagen II hair follicles and increases melanocyte abundance.

(A) *PHGDH^{tetO}* mice were crossed to *Dct-rtTA* mice to drive increased PHGDH expression solely in melanocytes. Quantitation of the percent of anagen II hair follicles (HFs) containing any melanin granules in skin from *Dct-rtTA* mice with the indicated *PHGDH^{tetO}* genotype exposed to doxycycline for 30 days prior to hair follicle synchronization as described in Figure 5. Data shown represent the % observed when analyzing 50 HFs per mouse from 3 mice of each genotype. **(B)** Quantitation of the percent of anagen II hair follicles (HFs) with three or more melanin granules in in skin from mice described in (A) exposed to doxycycline for 30 days prior to hair follicle synchronization. Data shown represent the % observed when analyzing 50 HFs per mouse from 3 mice of each genotype. **(C)** Quantitation of the percent of anagen II hair follicles (HFs) containing any melanin granules in skin from mice described in (A) exposed to doxycycline for 2 days prior to hair follicle synchronization. Data shown represent the % observed when analyzing 50 HFs per mouse from 3 mice of each genotype **(D)** Quantitation of the percent of anagen II hair follicles (HFs) with three or more melanin granules in skin from mice described in (A) exposed to doxycycline for 2 days prior to hair follicle synchronization. Data shown represent the % observed when analyzing 50 HFs per mouse from 3 mice of each genotype. The increase in hair follicles with melanin granules shown in (A-D) is statistically significant with p-values derived from two-tailed Fisher's exact test. **(E)** *PHGDH^{tetO}*; *Dct-rtTA* mice were crossed to *H2B-GFP^{tetO}* mice such that melanocytes would express both PHGDH and GFP. qPCR to assess tyrosinase expression (a melanocyte-specific enzyme) in GFP- and GFP+ cells isolated from *PHGDH^{tetO};Dct-rtTA; H2B-GFP^{tetO}* mice exposed to doxycycline for 30 days prior to hair follicle synchronization. Data shown represent the mean (+/- SD). The increase in tyrosinase expression is significant with p-values derived from an unpaired Student's t test. **(F)** Mice described in (E) with or without a *PHGDH^{tetO}* allele we exposed to doxycycline for 30-days prior to hair follicle synchronization and subsequent collection of anagen II skin samples. Cells isolated from skin were analyzed by flow cytometry to assess GFP+ melanocyte abundance. Data shown represent the mean (+/- SD). The increase in GFP+ melanocytes from PHGDH$^{tetO/+}$ mice is statistically significant with p-values derived from an unpaired Student's t test.

Increased PHGDH expression in melanocytes increases melanocyte abundance in anagen II skin

To determine whether the presence of excess melanin granules in anagen II HFs is related to a change in melanocyte number, we quantified melanocyte abundance using flow cytometry. To quantify melanocytes *PHGDH*^{tetO}; *Dct-rtTA* mice were crossed to *H2B-GFP*^{tetO} mice (Tumbar et al., 2004, Zaidi et al., 2011a, Zaidi et al., 2011b) so that melanocytes would express both PHGDH and GFP. The resulting mice were then exposed to a dox diet for 30 days, plucked, and skin was collected in anagen II. Adapting previously described protocols (Joshi et al., 2017, Zaidi et al., 2011a), this skin was then dissociated into single-cell suspension and sorted by flow cytometry into GFP-positive and GFP-negative populations in order to quantitate the effect of PHGDH expression on the relative abundance of GFP-positive melanocytes (Figure 8A). In order to validate that the GFP-positive cells were indeed melanocytes, we performed qPCR for tyrosinase, a melanocyte marker, which was present in GFP-positive cells, and nearly undetectable in GFP-negative cells (Figure 7E). Conversely, expression of KPRP, a keratinocyte marker, and AdipoQ, an adipocyte marker, were restricted to the GFP-negative cells (Figure 8B-C). The proportion of GFP-positive cells was significantly higher in anagen II skin from mice with the *PHGDH*^{tetO};*Rosa26-M2rtTA* alleles (Figure 7F), suggesting that melanocytes are more abundant in anagen II skin when PHGDH is overexpressed.

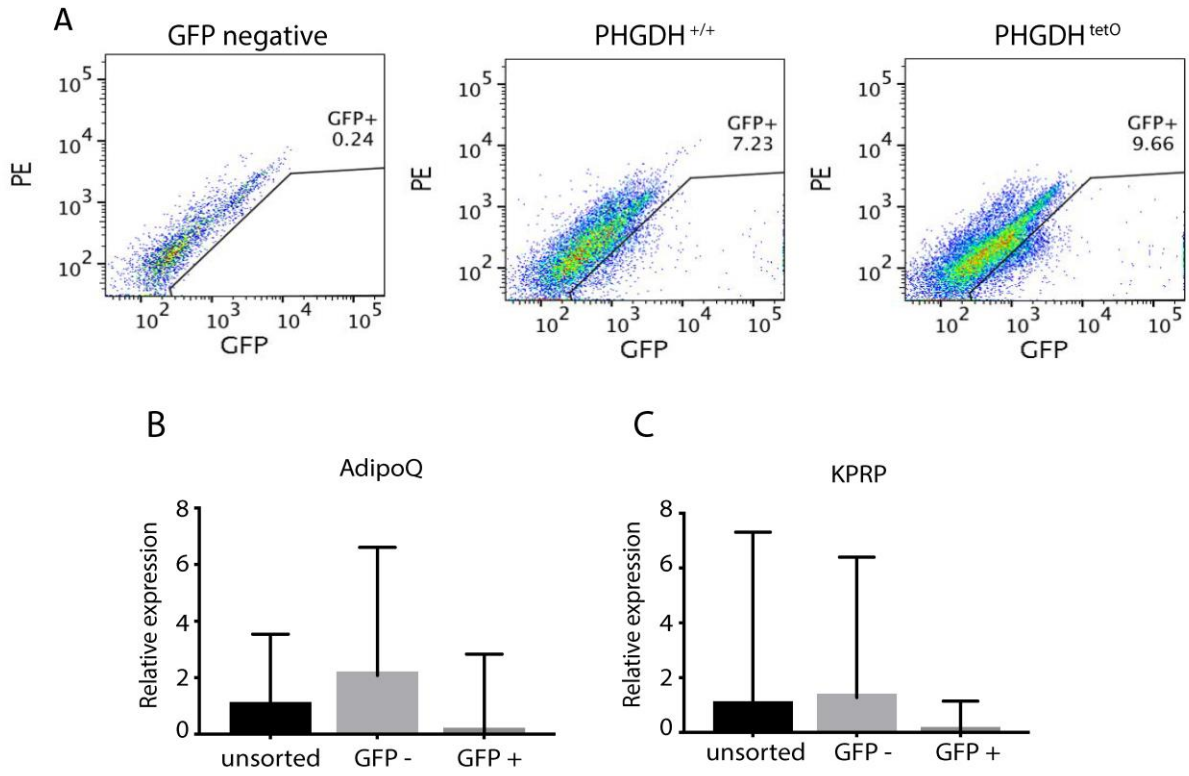

Figure 8. Evidence that adipocytes and keratinocytes sort into the GFP- fraction when cells are isolated from the skin of PHGDH^{tetO}; Dct-rtTA; H2B-GFP^{tetO} mice.

(A) PHGDH^{tetO}; Dct-rtTA; H2B-GFP^{tetO} mice with melanocytes that express both PHGDH and GFP, along with control mice with melanocytes that express GFP were exposed to doxycycline for 30 days prior to hair follicle synchronization. Anagen II skin samples were isolated, and GFP+ and GFP- cells were isolated via FACS. Cells were gated on the single cell, live (DAPI-) population. GFP+ cells were identified based on signal in a GFP channel compared to autofluorescence as measured by signal in a PE channel using a skin sample from a mouse that did not contain H2B-GFP^{tetO} (GFP negative) as a negative control. Representative FACS plots from a PHGDHtetO mouse and a wildtype (PHGDH+/+) mouse are shown. (B) qPCR analysis of cDNA isolated from unsorted, GFP-, and GFP+ cells isolated from the skin of PHGDH^{tetO}; Dct-rtTA; H2B-GFP^{tetO} mice described in Figure 4E. Primers were used to amplify the keratinocyte-specific gene KPRP, and (C) the adipocyte-specific gene AdipoQ as indicated. Data shown represent the mean (+ SD).

DISCUSSION

High *PHGDH* expression is observed in select cancer cells and in some cases is necessary for proliferation and survival (Locasale et al., 2011, Possemato et al., 2011). Genomic copy number gain involving *PHGDH* is observed with higher frequency in melanoma than in other cancers (Locasale et al., 2011), and in this regard it is interesting that increased PHGDH expression driven by a ubiquitous promoter in mice results in a phenotype involving melanocytes such that progression of the hair follicle cycle is uncoupled from melanin appearance. This effect on normal melanocyte biology may provide insight into how PHGDH expression contributes to melanoma.

A key unanswered question is why hair follicles in *PHGDH*^{tetO} mice display an increased number of melanin granules and melanocytes early in the HF cycle. Melanogenesis involves the production, survival and differentiation of melanocytes (Tobin, 2008), functional melanosome biogenesis (Schiaffino, 2010), appropriate transcription, translation, modification, and activity of synthetic enzymes such as tyrosinase (Videira et al., 2013, Wang and Hebert, 2006), input from autocrine and paracrine signals (Hsiao and Fisher, 2014), and availability of substrate and appropriate chemical conditions for melanogenesis, including pH and redox state (Hearing, 2011, Schallreuter et al., 2008). Increased serine synthesis might affect one or more of these processes in melanocytes or melanocyte stem cells. Alterations in redox state may be relevant to PHGDH expression, as increased serine synthesis is associated with resistance to oxidative stress in melanoma and breast cancer (Piskounova et al., 2015, Samanta et al., 2016). PHGDH could also affect follicular melanogenesis by promoting inappropriate differentiation of melanocytic stem cells into melanocytes or increased melanocyte proliferation. Further

examination of the role of PHGDH in these processes may provide insight into how PHGDH expression promotes tumor formation.

MATERIALS AND METHODS

All mouse studies were performed in accordance with institutional guidelines and approved by the MIT Committee on Animal Care.

Generation of PHGDH^{tetO} Mice

A previously described system was used to generate *PHGDH^{tetO}* mice (Beard et al., 2006). Briefly, human PHGDH cDNA with GenBank Accession BC011262.1 from Open Biosystems (MHS1010-73507) was amplified with the following primers:

PHGDH MfeI F: 5'-CAATTGGCCACCATGGCTTTTGCAAATCTGCGGAAAGT-3'

PHGDH Mfe R: 5'-CAATTGTTAGAAGTGGAACTGGAAGGCTTCAG-3'

This insert was digested with MfeI from NEB (R0589) and cloned into the EcoRI sites in the pgk-ATG-frt plasmid from Addgene (#20734) to generate a targeting plasmid using standard molecular biology techniques. Sequencing was used to screen for the correct insert orientation and confirm cDNA sequence. The targeting plasmid was co-electroporated with pCAGGS-flpE plasmid (Addgene, # 20733) into F1 C57BL/6 x 129S4 hybrid KH2 ES cells. The KH2 cells as well as pgk-ATG-frt and pCAGGS-flpE-puro were kind gifts from Rudolf Jaenisch (plasmids via Addgene). Clonal selection of ES cells was performed with 150 ug/ml hygromycin B for 9 days, and 8 individual clones were screened by Southern blot as described below. Two ES clones with a properly integrated PHGDH transgene in the Col1a1 locus were injected independently into

C57BL/6 blastocysts to produce chimeric mice. The chimeric C57BL/6 x 129S4 *PHGDH*^{tetO} transgene founder mice were mated to C57BL/6 background and some showed germline transmission. Before this study and over the course of these experiments, the mice were continually backcrossed onto the C57BL/6 background.

Southern Blotting

Genomic DNA was digested with SpeI from NEB (R0133). Digested DNA was then separated on an agarose gel, and neutral transfer was performed overnight using Hybond-XL membrane from GE Healthcare Biosciences (RPN303S). Membrane was crosslinked using a Stratalinker UV Crosslinker from Stratagene. The membrane was incubated with Stratagene QuickHyb Hybridization Solution from Agilent (201220). The probe was prepared from the Col1a-3'probe plasmid from Addgene (#20731) by digesting with XbaI and PstI from NEB (R0145 and R0140) and gel purifying the released probe. Purified probe was denatured, then labeled using α-^{32}P-dCTP from PerkinElmer Life Sciences (BLU013H) and the Rediprime II DNA Labeling System from GE Healthcare Life Sciences (RPN1633) according to kit instructions. Labeled probe was then purified with Micro Bio-Spin P-6 Gel Columns from Bio-Rad (#732-6200) according to company instructions. Purified, labeled probe was mixed with salmon sperm DNA from Stratagene (201190). Immediately before using, probe was denatured. The probe was then incubated with the membrane and hybridization solution for 1 hr at 68°C. The membrane was washed, then exposed to autoradiography film with an intensifier screen before developing.

PCR Genotyping

PCR genotyping was performed using standard molecular biology techniques under conditions described below.

Allele	Primers	Annealing temp., °C	Wild type allele band size, bp	Transgene allele band size, bp
PHGDH^{tetO}	oIMR6724: 5'- CCCTCCATGTGTGACCAAGG -3' oIMR6725: 5'- GCACAGCATTGCGGACATGC -3' oIMR6726: 5'- GCAGAAGCGCGGCCGTCTGG -3' (Sequences from Jackson Laboratory)	65	295	493
Rosa26-M2rtTA	oIMR8545: 5'-AAAGTCGCTCTGAGTTGTTAT-3' oIMR8546: 5'-GGAGCGGGAGAAATGGATATG-3' oIMR8052: 5'-GCGAAGAGTTTGTCCTCAACC-3' (Sequences from Jackson Laboratory)	65	~650	340
Dct-rtTA	Y104: 5'-ACTAAGTAAGGATCAATTCAG -3' Y105: 5'-TGTACTAGGCAGACTGTG-3' (Sequences from NCI Mouse Repository)	55	(No band)	370
H2B-GFP	Y106: 5'-GCCACAAGTTCAGCGTGTCC-3' Y107: 5'-GATGCCCTTCAGCTCGATGC-3' (Sequences from NCI Mouse Repository)	60	(No band)	314

Western Blotting

Western blots were performed using standard techniques with primary antibodies against PHGDH (Sigma, HPA021241), β-actin (abcam, ab1801), GAPDH (Cell Signaling Technology, 2118S), Hsp90 (Cell Signaling Technology, #4877), or vinculin (abcam, ab18058) and detected using HRP-conjugated secondary antibodies and chemiluminescence.

Generation of Embryonic Fibroblasts & Cell Culture

MEFs were prepared from E13.5 *PHGDH*$^{tetO/tetO}$, *PHGDH*$^{tetO/+}$ or *PHGDH*$^{+/+}$ embryos with the *Rosa26-M2rtTA* allele using standard protocols. MEFs were maintained in DMEM with pyruvate, 10% tet-free FBS, 2 mM glutamine, penicillin/streptomycin and 3.5 µl beta-mercaptoethanol per 500 ml DMEM.

Mass Spectrometry

MEFs were grown in medium supplemented with 1 µg/ml doxycycline for 4 days before extraction. Cells were extracted in ice cold 1:4:5 water:methanol:chloroform with valine-D8 as an internal standard. The aqueous layer was dried under N_2 and resuspended in 1:1 water:acetonitrile. Samples were analyzed by LC/MS using a QExactive benchtop orbitrap mass spectrometer equipped with a heated electrospray ionization (HESI) probe, coupled to a Dionex UltiMate 3000 UPLC system (Thermo Fisher Scientific, San Jose, CA). Samples were separated by injecting 10 µl of each sample onto a ZIC-pHILIC 2.1 x 150 mm (5 µm particle size) column (EMD). Flow rate was set to 100 µL/min, column compartment was set to 25°C, and autosampler sample tray was set to 4°C. Mobile Phase A consisted of 20 mM ammonium

carbonate, 0.1% ammonium hydroxide. Mobile Phase B was 100% acetonitrile. The mobile phase gradient (%B) was as follows: 0 min 80%, 5 min 80%, 30 min 20%, 31 min 80%, 42 min 80%. All mobile phase was introduced into the ionization source set with the following parameters: sheath gas = 40, auxiliary gas = 15, sweep gas = 1, spray voltage = -3.1kV or +3.0kV, capillary temperature = 275°C, S-lens RF level = 40, probe temperature = 350°C. Metabolites were monitored using a targeted selected ion monitoring (tSIM) method in negative mode with the quadrupole centered on the M-H ion m+1.5, m+2.5, or m+3.5 mass with a 8 amu isolation window, depending on the number of carbons in the target metabolite. Resolution was set to 70,000, full-scan AGC target was set to 106 ions, and tSIM AGC target was set to 105 ions. Relative quantitation of polar metabolites was performed with XCalibur QuanBrowser 2.2 (Thermo Fisher Scientific) using a 5 ppm mass tolerance and referencing an in-house library of chemical standards. Concentration was normalized to cell number.

Histology

Tissues were fixed overnight to 24 hrs in formalin and stained with hematoxylin and eosin using standard techniques.

Hair Follicle Synchronization and Quantitation of Melanin in Hair Follicles

To synchronize HFs, mice were anesthetized and skin was plucked over two $1cm^2$ areas halfway down the back of mice equidistant from the spine. After the procedure, mice were given carprofen at 3 mg/kg once per day for 3 days as an analgesic. HFs with the bulb located entirely in the dermis were considered to be pre-anagen IIIa. HFs with a lower bulb were not included in

the analysis. Only HFs with a fully visible bulb were included in the analysis and all sections were de-identified for blinded quantitation. Each HF assessed for the presence of melanin granules was classified as “none,” “one,” “two” or “three or more”, and each distinct granule was counted as one regardless of size.

RT-qPCR

RNA was collected from skin using Trizol reagent (Ambion). Skin samples were digested in 1 mL of Trizol using a GentleMACS tissue homogenizer and RNA was isolated according to standard protocol. RNA from FACS samples was isolated using the RNAqueous Micro Kit (Ambion). cDNA was reverse transcribed using an iScript cDNA Synthesis Kit. RT-qPCR was performed with SYBR Green on a LightCycler 480 II machine from Roche. Primers were used at a final concentration of 1 µM. The primers used are listed in the table below.

Target	**Forward Primer**	**Reverse Primer**
Human PHGDH	CTGCGGAAAGTGCTCATCAGT	TGGCAGAGCGAACAATAAGGC
Mouse PHGDH	ATGGCCTTCGCAAATCTGC	AGTTCAGCTATCAGCTCCTCC
Tyrosinase	CACCATGCTTTTGTGGACAG	GGCTTCTGGGTAAACTTCCAA
AdipoQ	TGTTCCTCTTAATCCTGCCCA	CCAACCTGCACAAGTTCCCTT
KPRP	AACCCGTTCGTTGTCCCAG	TTGGGTGAAGTTATATGAGCCAC
F4/80	TGACTCACCTTGTGGTCCTAA	CTTCCCAGAATCCAGTCTTTCC
GAPDH	TGTAGACCATGTAGTTGAGGTCA	AGGTCGGTGTGAACGGATTTG

Flow cytometry

Synchronized skin was dissected from mice, then cut into small pieces in a Petri dish using dissecting scissors. The skin was resuspended in 5 mL sterile PBS with 3 mg/mL dispase II (Roche), 1 mg/mL collagenase I (Worthington Biochemical), and 0.1 mg/mL DNase I (Sigma-Aldrich). This solution was incubated at 37 °C for 30 minutes, then EDTA was added to a final concentration of 10 mM to stop the digestion reaction. The digested skin was passed through a 70 μm cell strainer then washed twice with sterile PBS. Cells were stained with 1 μg/mL DAPI for 15 minutes as a live-dead marker, then analyzed for GFP expression on BD FACSAria III flow cytometer.

ACKNOWLEDGEMENTS

We thank Lauren Surface and Laurie Boyer for their advice generating the *PHGDH*^{tetO} mice. We also thank Roberta Ferretti, Jackie Lees, and Marcus Bosenberg for advice on skin sectioning for hair follicle analysis, the Koch Institute Swanson Biotechnology Center for technical support, specifically Aurora Connor and Noranne Enzer at the Mouse ES Cell and Transgenics Core Facility, Kathy Cormier at the Hope Babette Tang (1983) Histology Facility and Scott Malstrom at the Animal Imaging and Preclinical Testing facility. We thank the NCI Mouse Repository for providing us with the iDCT-GFP (01XT4) mice. We acknowledge Michael Pacold for providing recombinant mouse PHGDH enzyme. LC/MS was performed at the Whitehead Institute Metabolite Profiling Core Facility. We thank Jordan Bartlebaugh for performing Western blot analysis. Generation of the *PHGDH*^{tetO} mice was supported in part by the MIT Cancer Center support grant (P30-CA14051). K.R.M. acknowledges support from the NSF Graduate Research

Fellowship Program, DGE-1122374. A.N.L. is a Robert Black Fellow of the Damon Runyon Cancer Research Foundation, DRG-2241-15. K.R.M. and M.R.S. were supported by T32-GM007287, and M.R.S. acknowledges additional support from an MIT Koch Institute Graduate Fellowship. M.G.V.H. acknowledges support from R21-CA198028, R01-CA168653, the Ludwig Center at MIT, the MIT Center for Precision Cancer Medicine, SU2C, and a Faculty Scholar Grant from the Howard Hughes Medical Institute.

AUTHOR CONTRIBUTIONS

Conceptualization, K.R.M., M.R.S., and M.G.V.H.; Methodology, K.R.M., M.R.S., A.N.L.; Formal Analysis, M.R.S. and K.R.M.; Investigation, K.R.M., M.R.S., A.N.L., B.P.F., R.T.B.; Writing – Original Draft, K.R.M. and M.R.S.; Writing – Review & Editing, M.R.S., K.R.M., M.G.V.H.; Funding Acquisition, K.R.M., M.R.S., M.G.V.H.

REFERENCES

Adams CM. Role of the transcription factor ATF4 in the anabolic actions of insulin and the anti-anabolic actions of glucocorticoids. J Biol Chem 2007;282(23):16744-53.

Beard C, Hochedlinger K, Plath K, Wutz A, Jaenisch R. Efficient method to generate single-copy transgenic mice by site-specific integration in embryonic stem cells. Genesis 2006;44(1):23-8.

Chase HB. Growth of the hair. Physiological reviews 1954;34(1):113-26.

Cotsarelis G, Sun TT, Lavker RM. Label-retaining cells reside in the bulge area of pilosebaceous unit: implications for follicular stem cells, hair cycle, and skin carcinogenesis. Cell 1990;61(7):1329-37.

Davis JL, Fallon HJ. Studies on the role of 3-phosphoglycerate dehydrogenase in the regulation of serine biosynthesis in rat liver. The Journal of biological chemistry 1970;245(21):5838-46.

Ding J, Li T, Wang X, Zhao E, Choi JH, Yang L, et al. The histone H3 methyltransferase G9A epigenetically activates the serine-glycine synthesis pathway to sustain cancer cell survival and proliferation. Cell Metab 2013;18(6):896-907.

Fedorov LM, Tyrsin OY, Krenn V, Chernigovskaya EV, Rapp UR. Tet-system for the regulation of gene expression during embryonic development. Transgenic research 2001;10(3):247-58.

Fuchs E. Scratching the surface of skin development. Nature 2007;445(7130):834-42.

Hearing VJ. Determination of melanin synthetic pathways. The Journal of investigative dermatology 2011;131(E1):E8-E11.

Hsiao JJ, Fisher DE. The roles of microphthalmia-associated transcription factor and pigmentation in melanoma. Archives of biochemistry and biophysics 2014;563:28-34.

Hwang IY, Kwak S, Lee S, Kim H, Lee SE, Kim JH, et al. Psat1-Dependent Fluctuations in alpha-Ketoglutarate Affect the Timing of ESC Differentiation. Cell Metab 2016;24(3):494-501.

Jing Z, Heng W, Aiping D, Yafei Q, Shulan Z. Expression and clinical significance of phosphoglycerate dehydrogenase and squamous cell carcinoma antigen in cervical cancer. International journal of gynecological cancer : official journal of the International Gynecological Cancer Society 2013;23(8):1465-9.

Joshi SS, Tandukar B, Castaneda M, Jiang S, Diwakar G, Hertzano RP, et al. Characterization of a new, inducible transgenic mouse model with GFP expression in melanocytes and their precursors. Gene Expr Patterns 2017;27:76-84.

Liu J, Guo S, Li Q, Yang L, Xia Z, Zhang L, et al. Phosphoglycerate dehydrogenase induces glioma cells proliferation and invasion by stabilizing forkhead box M1. Journal of neuro-oncology 2013;111(3):245-55.

Locasale JW, Grassian AR, Melman T, Lyssiotis CA, Mattaini KR, Bass AJ, et al. Phosphoglycerate dehydrogenase diverts glycolytic flux and contributes to oncogenesis. Nat Genet 2011;43(9):869-74.

Mattaini KR, Brignole EJ, Kini M, Davidson SM, Fiske BP, Drennan CL, et al. An epitope tag alters phosphoglycerate dehydrogenase structure and impairs ability to support cell proliferation. Cancer Metab 2015;3:5.

Muller-Rover S, Handjiski B, van der Veen C, Eichmuller S, Foitzik K, McKay IA, et al. A comprehensive guide for the accurate classification of murine hair follicles in distinct hair cycle stages. The Journal of investigative dermatology 2001;117(1):3-15.

Nilsson LM, Forshell TZ, Rimpi S, Kreutzer C, Pretsch W, Bornkamm GW, et al. Mouse genetics suggests cell-context dependency for Myc-regulated metabolic enzymes during tumorigenesis. PLoS Genet 2012;8(3):e1002573.

Nishimura EK, Jordan SA, Oshima H, Yoshida H, Osawa M, Moriyama M, et al. Dominant role of the niche in melanocyte stem-cell fate determination. Nature 2002;416(6883):854-60.

Paus R, Foitzik K. In search of the "hair cycle clock": a guided tour. Differentiation; research in biological diversity 2004;72(9-10):489-511.

Perl AK, Tichelaar JW, Whitsett JA. Conditional gene expression in the respiratory epithelium of the mouse. Transgenic research 2002a;11(1):21-9.

Perl AK, Wert SE, Nagy A, Lobe CG, Whitsett JA. Early restriction of peripheral and proximal cell lineages during formation of the lung. Proceedings of the National Academy of Sciences of the United States of America 2002b;99(16):10482-7.

Piskounova E, Agathocleous M, Murphy MM, Hu Z, Huddlestun SE, Zhao Z, et al. Oxidative stress inhibits distant metastasis by human melanoma cells. Nature 2015;527(7577):186-91.

Pollari S, Kakonen SM, Edgren H, Wolf M, Kohonen P, Sara H, et al. Enhanced serine production by bone metastatic breast cancer cells stimulates osteoclastogenesis. Breast cancer research and treatment 2011;125(2):421-30.

Possemato R, Marks KM, Shaul YD, Pacold ME, Kim D, Birsoy K, et al. Functional genomics reveal that the serine synthesis pathway is essential in breast cancer. Nature 2011;476(7360):346-50.

Samanta D, Park Y, Andrabi SA, Shelton LM, Gilkes DM, Semenza GL. PHGDH Expression Is Required for Mitochondrial Redox Homeostasis, Breast Cancer Stem Cell Maintenance, and Lung Metastasis. Cancer Res 2016;76(15):4430-42.

Schallreuter KU, Kothari S, Chavan B, Spencer JD. Regulation of melanogenesis--controversies and new concepts. Exp Dermatol 2008;17(5):395-404.

Schiaffino MV. Signaling pathways in melanosome biogenesis and pathology. The international journal of biochemistry & cell biology 2010;42(7):1094-104.

Shin MK, Levorse JM, Ingram RS, Tilghman SM. The temporal requirement for endothelin receptor-B signalling during neural crest development. Nature 1999;402(6761):496-501.

Slominski A, Paus R. Melanogenesis is coupled to murine anagen: toward new concepts for the role of melanocytes and the regulation of melanogenesis in hair growth. The Journal of investigative dermatology 1993;101(1 Suppl):90S-7S.

Tobin DJ. Human hair pigmentation--biological aspects. International journal of cosmetic science 2008;30(4):233-57.

Tobin DJ, Hagen E, Botchkarev VA, Paus R. Do hair bulb melanocytes undergo apoptosis during hair follicle regression (catagen)? The Journal of investigative dermatology 1998;111(6):941-7.

Tumbar T, Guasch G, Greco V, Blanpain C, Lowry WE, Rendl M, et al. Defining the epithelial stem cell niche in skin. Science 2004;303(5656):359-63.

Videira IF, Moura DF, Magina S. Mechanisms regulating melanogenesis. Anais brasileiros de dermatologia 2013;88(1):76-83.

Wang N, Hebert DN. Tyrosinase maturation through the mammalian secretory pathway: bringing color to life. Pigment cell research / sponsored by the European Society for Pigment Cell Research and the International Pigment Cell Society 2006;19(1):3-18.

Zaidi MR, Davis S, Noonan FP, Graff-Cherry C, Hawley TS, Walker RL, et al. Interferon-gamma links ultraviolet radiation to melanomagenesis in mice. Nature 2011a;469(7331):548-53.

Zaidi MR, Hornyak TJ, Merlino G. A genetically engineered mouse model with inducible GFP expression in melanocytes. Pigment Cell Melanoma Res 2011b;24(2):393-4.

Zambrowicz BP, Imamoto A, Fiering S, Herzenberg LA, Kerr WG, Soriano P. Disruption of overlapping transcripts in the ROSA beta geo 26 gene trap strain leads to widespread expression of beta-galactosidase in mouse embryos and hematopoietic cells. Proc Natl Acad Sci U S A 1997;94(8):3789-94.